Study of a green process forthe production of furfural from hemicellulosic residues of biomass

Kritsana Namhaed

RÉPUBLIQUE FRANÇAISE
Liberté Égalité Fraternité

Université de Toulouse

Doctorat de l'Université de Toulouse

préparé à Toulouse INP

Étude d'un procédé durable de production de furfural à partir des résidus hémicellulosiques issus de la biomasse

---

Thèse présentée et soutenue, le 23 septembre 2024 par

Kritsana NAMHAED

École doctorale
MEGEP - Mécanique, Energétique, Génie civil, Procédés

Spécialité
Génie des Procédés et de l'Environnement

Unité de recherche
LGC - Laboratoire de Génie Chimique

Thèse dirigée par
Patrick COGNET et Thibaut TRIQUET

Composition du jury
M. François JÉRÔME, Rapporteur, Université de Poitiers - IC2MP
M. Lionel ESTEL, Rapporteur, INSA Rouen
Mme Karine VIGIER DE OLIVEIRA, Examinatrice, Université de Poitiers
Mme Sophie THIEBAUD-ROUX, Examinatrice, Toulouse INP
M. Worapon KIATKITTIPONG, Examinateur, Université de Silpakorn
M. Patrick COGNET, Directeur de thèse, Toulouse INP

Membres invités
M. Michel DELMAS, Université de Toulouse
M. Thibaut TRIQUET, INP Toulouse LGC

Acknowledgement

Tout d’abord, je tiens à exprimer ma profonde gratitude à monsieur Estel Lionel et à monsieur Jérôme François, les rapporteurs, pour avoir accepté d’évaluer mon travail de thèse et m’avoir permis de la soutenir. Je remercie également madame Vigier de Oliveira Karine et madame Thiébaud-Roux Sophie d’avoir accepté d’être mes examinatrices et pour le temps précieux que vous m’avez consacré.

Je souhaite également exprimer ma sincère reconnaissance à mes anciens encadrants de stage de master, madame Roux-de Balmann Hélène et monsieur Sylvain Galier, pour leur soutien dans ma candidature à cette thèse. Leur aide a été cruciale, notamment dans l'encadrement du stagiaire de master qui a contribué à la phase finale de mon projet.

Je souhaite exprimer mes plus vifs remerciements à mes encadrants de thèse : monsieur Cognet Patrick et madame Pérès Yolande, pour m’avoir offert cette opportunité de thèse et pour m’avoir chaleureusement accueilli au sein du laboratoire LGC. En travaillant avec leurs côtés, j’ai pu m’épanouir pleinement dans mes missions tout au long de ces trois années. Ils m’ont permis de me guider et me rassurer dans les moments de doute et me recadrer si nécessaire mais tout en me faisant confiance en mon travail en laissant autonome dans mes choix scientifiques. Cela a été une aide véritablement précieuse.

Je souhaite remercier monsieur Triquet Thibaut d’avoir accepté d’être mon co-directeur de thèse et d’avoir consacré son temps et ses efforts pour s’investir pleinement dans un projet qui ne relève pas de son domaine d’expertise. Il m’a guidé et conseillé, m’aidant à surmonter de nombreuses difficultés. Je lui suis reconnaissant pour son soutien, sa disponibilité, sa bienveillance et le partage constant de son expertise.

Je voudrais remercier madame Séverine Camy pour avoir assuré le dépannage de son réacteur pendant près d’un an et demi. Je lui suis reconnaissant pour son soutien, son encadrement et son aide précieuse à la rédaction de mon premier article. Sa disponibilité et son dévouement ont été d’une valeur inestimable.

Je voudrais également remercier messieurs Michel Delmas et Guo-Hua Delmas pour leur implication dans le suivi de mes travaux, en particulier dans la partie du traitement du mélange réel. Je les remercie pour les nombreux échanges que nous avons eus, qui se sont révélés souvent très productifs et instructifs pour moi.

Je souhaite remercier les membres de l'équipe analytique notamment : Laure Latapie, Agathe Juppeau, Aaïs Vandenbossche et Marie-Line de Solan Bethmale. Sans leur expertise dans les techniques analytiques tels que la HPLC, la GC, la chromatographie ionique et l'ICP, je n'aurais pas pu interpréter l'ensemble de mes résultats. Merci pleinement pour votre patience, votre pédagogie et votre intérêt pour mon projet.

Je tiens également à remercier le personnel technique qui a contribué à la réussite de mes expériences. Tout particulièrement, je remercie Etienne Prévot, le premier technicien qui a assemblé le réacteur à double enveloppe pour la première campagne d'expériences de ma thèse. Je suis reconnaissant envers Bruno Broyer pour son accompagnement technique tout au long de ces trois années, ainsi que pour la conception et le montage du pilote de réacteur à haute pression. Mes remerciements vont également à Jean-pierre Escafit et Maiko Riodel pour leur aide précieuse dans la réalisation de mes montages expérimentaux. Je suis reconnaissant envers Alec Maunoury pour ses astuces techniques et nos échanges enrichissants sur les procédés. Enfin, je tiens à remercier Lahcen Farhi et Quentin Ribière pour leur aide technique précieuse en informatique.

Merci à tout le personnel du LGC avec lequel j'ai eu l'occasion d'interagir à plusieurs reprises pour diverses démarches administratives et autres. Je souhaite particulièrement remercier Claudine Lorenzon, Daniele Bouscary, Corinne Lebreton, Philippe Destrac et Jeanluc Labeyrie pour leur aide précieuse et leur gentillesse. Un grand merci à Alain Philip pour sa sympathie et sa capacité à apporter de la bonne humeur au sein de mon laboratoire dans toutes les circonstances.

Je souhaite maintenant adresser mes remerciements à tous mes collègues doctorants et autres que j'ai eu la chance de côtoyer au laboratoire. Tout d'abord, à Erwann, mon précieux collègue avec qui je partage le bureau et le laboratoire. Sans lui, j'aurais eu du mal à m'en sortir avec toutes les démarches administratives. Je te remercie pour tes précieux conseils, ton aide et tes propositions. Je tiens également à exprimer ma gratitude envers Ana et Daniele, mes amies brésiliennes, pour nos déjeuners partagés et les moments inoubliables passés ensemble, ainsi que pour ne jamais m'avoir laissé seul. À Mukhlis et Feby, mes amis asiatiques à l'INP Toulouse, pour leurs efforts pour me sortir de chez moi et faire des activités en dehors du laboratoire. À Sara, mon amie iranienne, pour son soutien et ses conseils. Un immense merci à Gregory Ribeiro, le véritable génie de la simulation logicielle, pour son aide précieuse dans la simulation de l'étude cinétique. Je suis reconnaissant envers Axel, Eva, Célia, Michèle, Edoardo et Abby, avec qui j'ai partagé des moments de détente, de rires et de joie.

Je n’oublie pas mes stagiaires, Adrien et Erwan, pour leur travail rigoureux et acharné afin que je puisse obtenir tous les résultats fiables et nécessaires dans les délais impartis. Merci à vous tous pour votre contribution et votre présence qui ont enrichi mon expérience au laboratoire.

Je tiens également à exprimer ma gratitude envers mes amis en dehors de l’INP Toulouse, notamment Manon, Lisa, Aurélien, Manuel, Christian et Sharath, pour leur soutien et leur aide précieuse dans la résolution de problèmes académiques, linguistiques et quotidiens. Merci à vous pour tous les moments inoubliables partagés à Toulouse et en France.

Enfin, je tiens à exprimer ma profonde gratitude envers mes parents, ma tante, ma grand-mère et mes cousins thaïlandais en France pour leur soutien indéfectible dans toutes mes décisions, mes choix et mes aspirations. Merci du fond du cœur pour tout. À tous, je suis fier de faire partie de votre famille et je vous aime énormément.

Scientific productions

Scientific article

- Elsa Cousin, Kritsana Namhaed, Yolande Pérès, Patrick Cognet, Michel Delmas, Heri Hermansyah, Misri Gozan, Peter Adeniyi Alaba, Mohamed Kheireddine Aroua. Towards efficient and greener processes for furfural production from biomass: A review of the recent trends, *Science of the Total Environment journal*, 847 (2022) 157599.
- Kritsana Namhaed, Yolande Pérès, Worapon Kiatkittipong, Thibaut Triquet, Séverine Camy, Patrick Cognet. Integrated supercritical carbon dioxide extraction for efficient furfural production from xylose using formic acid as a catalyst, The *Journal of Supercritical Fluids*, 210 (2024) 106274.
- Kritsana Namhaed, Worapon Kiatkittipong, Thibaut Triquet, Patrick Cognet. Dehydration of pentose to furfural catalyzed by formic acid – Kinetics and application to real biomass hydrolysates, The *Journal of Environmental Chemical Engineering*, 12 (2024) 113431.

International congress presentation

- Kritsana Namhaed, Patrick Cognet, Thibaut Triquet, Yolande Pérès, Worapon Kiatkittipong. The production of xylose using formic acid as a catalyst in batch and continuous extraction processes, 18th International Conference on Quality in Research, 23 October 2023, Bali, Indonesia [Oral presentation]

National congress presentations

- Kritsana Namahed, Patrick Cognet, Yolande Pérès, Michel Delmas, Guo-Hau Delmas, Laure Latapie, Anaïs Vandenbossche. Etude d'un procédé durable de production de furfural à partir des résidus hémicellulosique issus de la biomasse, 18ème congrès de la Société Française de Génie des Procédés (SFGP 2022), 10 Novembre 2022, Toulouse, France [Oral présentation].
- Sylvain Galier, Kritsana Namhaed, Hélène Roux-de Balmann. Intégration de la nanofiltration pour la production de furfural à partir de biomasse, 18ème congrès de la Société Française de Génie des Procédés (SFGP 2022), 10 Novembre 2022, Toulouse, France [Oral présentation].

Contents

List of figures

List of tables

Nomenclature

Abbreviation

Aq	Aqueous phase	HemiCel	Hemicellulose
Ara	Arabinose	5-HMF	5-(hydroxymethyl)furfural
Atm	Atmosphere	IL	Ionic liquid
BA	Brønsted acid	J	Joule ($kg.m^2.s^{-2}$)
°C	Degree Celsius	k	Kinetic constant
C_5	Pentose sugar	K	Kelvin
C_6	Hexose sugar	LA	Lewis acid
CIMV	Compagnie industrielle de la matière végétale	LEEBio	Low energy extraction of biomass
Conc	Concentration	m	mass
Conv	Conversion	M	Molar (mol/L)
CO_2	Carbon dioxide	Mann	Mannose
CPME	Cyclopentyl methyl ether	min	Minute
d_{ex}	External diameter	MTC	Multi-turbine-column process
d_{in}	Internal diameter	n	number of mole
DES	Deep eutectic solvent	NF	Nanofiltration
DSTR	Discontinuous stirred tank reactor	N_2	Nitrogen gaz
E	Activation energy	Op. Cond.	Operational conditions
FA	Formic acid	Org.	Organic phase
Fur	Furfural	P	Pressure
Fruc	Fructose	PER	Plug flow reactor
Galac	Galactose	pKa	Acid dissociation constant at logarithmic scale
Glu	Glucose	rmp	Round per minute
h	Hour	Sc-CO_2	Supercritical carbon dioxide
H	Hight	T	Temperature
t	Time	V	Volume
USD	U.S. dollar	w/w	Weight in weight

Roman letters

Å	Angström	ρ	Density
β	Béta	γ	Gamma
c	Centi	Ω	Ohm
k	Kilo	μ	Micro
M	Mega	χ	Dry mass content
m	Mili	τ	Separation efficiency
p	para-position		

Subscripts

b	Boiling	n	Number of monomer
c	Critical state	R	Retention

Résumé

Avec l'épuisement des réserves fossiles et les préoccupations environnementales, l'utilisation de la biomasse lignocellulosique renouvelable apparaît comme une voie prometteuse pour la production de produits chimiques non dérivés du pétrole. L'un de ces produits chimiques intéressants est le furfural, qui constitue un substitut viable aux biocarburants et aux additifs. Le furfural peut être généré efficacement par la déshydratation acide des sucres C_5 présents dans les hémicelluloses des biomasses lignocellulosiques. L'objectif principal de cette étude est de développer un procédé durable de conversion des sucres C_5, présents dans les hydrolysats de la biomasse (via le procédé LEEBio^{TM}), en furfural en utilisant l'acide formique comme catalyseur. L'acide formique est très prometteur en raison de sa double fonction : il sert à la fois de solvant dans l'hydrolyse de la biomasse, produisant des hydrolysats riches en sucre, et de catalyseur efficace pour la déshydratation des sucres C_5 en furfural. L'étude a examiné l'impact de divers paramètres opératoires sur la production de furfural, afin d'identifier les conditions optimales par le biais d'expériences en système discontinu utilisant des solutions synthétiques. Les conditions optimales ont été déterminées et consistent en un fonctionnement isotherme à 170 °C pendant 40 min, avec 10 g/L de xylose et 10 % en poids d'acide formique. Dans ces conditions, un rendement en furfural de 58% et une sélectivité de 62% ont été obtenus. Trois méthodes d'extraction - stripping à la vapeur, solvants organiques dans les systèmes biphasiques et extraction au dioxyde de carbone supercritique (Sc-CO_2) - ont été exploitées pour extraire le furfural du milieu réactionnel, empêchant ainsi sa dégradation et améliorant à la fois le rendement et la sélectivité. Un rendement maximal en furfural de 68,5 % avec une sélectivité de 71,4 % a été obtenu par extraction au Sc-CO_2 après 5 h à 140°C et 20 MPa, avec un débit constant de 5 g/min. Ces procédés d'extraction ont facilité la récupération de tout le furfural produit dans l'extrait, tout en minimisant les concentrations de xylose et de furfural dans le réacteur. De plus, un modèle cinétique complexe a été mis au point afin de prédire et modéliser les performances d'un procédé complexe sur la conversion des sucres C_5 en furfural catalysée par l'acide formique. Ce modèle s'est avéré très précis, prédisant les rendements maximaux réalisables avec une précision de plus de 90 %. Cependant, la présence de composés supplémentaires, tels que des éléments inorganiques et des sucres hexosés, a affecté la précision du modèle. Néanmoins, le modèle est resté applicable pour optimiser la production de furfural à partir de matières premières telles que les xylanes et les hydrolysats de biomasse réels. Enfin, le potentiel de l'acide formique en tant que solvant de fractionnement et catalyseur pour la conversion des sucres C_5 en furfural a été exploré en

utilisant des hydrolysats obtenus à partir du fractionnement de la biomasse via le procédé LEEBio^{TM}. Dans des conditions optimisées, les rendements en furfural obtenus à partir d'hydrolysats de biomasse réelle ont dépassé ceux rapportés dans la littérature pour tous les systèmes étudiés. Dans cette étude, le rendement maximal en furfural, de 83 %, a été obtenu à partir de l'hydrolysat de grappes de fruits vides de palmiers à huile dans le système biphasique.

Mots clés : furfural, xylose, acide formique, procédés d'extraction

Abstract

Along with the depletion of fossil reserves and environmental concerns, the utilization of renewable lignocellulosic biomass stands out as a promising avenue for the production of non-petroleum-derived chemicals. One such chemical of interest is furfural, which serves as a viable substitute for biofuels and additives. Furfural can be efficiently generated through the acid dehydration of C_5 sugars found in hemicelluloses within lignocellulosic materials. The primary objective of this study is to develop a sustainable process for converting C_5 sugars, present in hydrolysates from biomass hydrolysis (via the LEEBio^{TM} process), into furfural using formic acid as a catalyst. Formic acid exhibits considerable promise due to its dual functionality: serving as both a solvent in biomass hydrolysis, yielding sugar-rich hydrolysates, and as an effective catalyst for the dehydration of C_5 sugars into furfural. The study investigated the impact of various operating parameters on furfural production, aiming to identify optimal conditions through batch system experiments utilizing synthetic solutions. The optimal conditions were identified as 170 °C for 40 min, with 10 g/L xylose and 10 wt% formic acid. Under these conditions, a furfural yield of 58% and a selectivity of 62% were achieved. Three extraction methods - steam stripping, biphasic organic solvent systems, and supercritical carbon dioxide (Sc-CO_2) extraction - were employed to extract furfural from the reaction medium, thereby preventing furfural degradation and enhancing both yield and selectivity. A maximum furfural yield of 68.5% with 71.4% selectivity was achieved using Sc-CO_2 extraction. This was accomplished after 5 h at 140°C and 20 MPa with a constant flow rate of 5 g/min. These extraction processes facilitated the recovery of all produced furfural in the extract, while minimizing concentrations of xylose and furfural in the reactor. Additionally, a complex kinetic model was developed to predict and model the performances of a complex process for the conversion of C_5 sugars into furfural catalyzed by formic acid. This model proved highly accurate, predicting maximum achievable yields with over 90% precision. However, the presence of additional compounds, such as inorganic elements and hexose sugars, did affect the model's accuracy. Nonetheless, the model remained instrumental in optimizing furfural production from raw materials like xylans and real biomass hydrolysates. Furthermore, the potential of formic acid as a fractionation solvent and catalyst for the conversion of C_5 sugars into furfural was explored using hydrolysates obtained from biomass fractionation via the LEEBio^{TM} process. Under optimized conditions, furfural yields from real biomass hydrolysates surpassed those reported in the literature for all investigated systems. In this study,

the maximum furfural yield of 83% was obtained from the hydrolysate of empty oil palm fruit bunches in the biphasic system.

Keywords: furfural, xylose, formic acid, extraction processes

General introduction

In the current context where traditional chemistry tends to convert into sustainable chemistry, “green chemistry”, the production of bio-based products, waste recovery, circular economy and preservation of natural resources are becoming fundamental values. This shift is necessitated by concerns over the decrease of fossil fuel reserves and increasing environmental concerns, which are compelling industry to decrease their dependence on petroleum-based products and adopt renewable alternatives (Mardani et al., 2015). Thus, lignocellulosic biomass is regarded as a sustainable source material owing to its renewable nature, plentiful availability, and widespread occurrence in the natural world (Ge et al., 2018). The composition of this substance primarily consists of three components: hemicellulose, cellulose, and lignin (Dodds and Gross, 2007; Vispute et al., 2010). Hemicellulose is the second most prevalent polysaccharide in plant cell walls, making around 15 to 30% of the bulk of lignocellulosic compounds (Tayyab, 2018). Due to its amorphous structure, it is easier to hydrolyze than crystalline cellulose, giving mainly C_5 monosaccharides, namely xylose. The utilization of xylose has been given much attention with the development of high-value utilization of biomass. It can be converted into many beneficial chemical compounds such as xylitol, furfural, and xylaric acid (Narisetty et al., 2022). Among these, furfural and its derivatives are very interesting, as pointed out in different recent reviews (Dashtban, 2012; Eseyin and Steele, 2015; Machado et al., 2016; Delbecq et al., 2018).

Furfural, or furfuraldehyde, was recognized as one of the top 10 high-value bio-based chemicals (Bozell and Petersen, 2010). Furfural is widely utilized and in high demand in various industries, such as oil refining for lubricating oils and biofuels, plastics for resins and synthetic fibers, pharmaceuticals, agrochemical industries for herbicides, fungicides, and insecticides, and food for flavoring agents. To our knowledge, there has been no synthetic route available for furfural production in the chemical industry. The only way for furfural synthesis involves the acid-catalyzed dehydration of C_5 sugars derived from hemicellulose (W. Yang et al., 2012). The industrial production of furfural dates back to its discovery by Quaker Oats in 1921. The original process involved acid-catalyzed hydrolysis of hemicellulose and subsequent dehydration of pentosans in lignocellulosic feedstocks (Brownlee and Miner, 1948). The current commercial method for furfural production uses mineral acid solutions, such as sulfuric acid (H_2SO_4) or phosphoric acid (H_3PO_4), and involves high-pressure reactions with biomass. However, this method has numerous disadvantages, including significant corrosion risks,

safety concerns, extensive side reactions, and challenging separation processes, which result in substantial volumes of acid waste.

Consequently, alternative organic acids have garnered attention to address these issues and align with the principles of "green chemistry". Among these, formic acid has emerged as a prominent choice for furfural production. W. Yang et al. (2012) showed that formic acid produced a greater amount of furfural compared to H_2SO_4 and H_3PO_4 because strong mineral acids caused undesirable side reactions such as resinification. Through experimental optimization, furfural yields of up to 74% and selectivity of 78% were reached. Tongtummachat et al. (2022) further optimized furfural production from xylose utilizing formic acid and aluminum chloride catalysts in an organic solvent-free system, achieving a remarkable maximum furfural yield of 92.2% in a continuous setup. Moreover, formic acid has found successful application in biorefining processes such as hemicellulose fractionation and hydrolysis (Dussan et al., 2015). Notably, BioEB's LEEBio^{TM} biorefining process employs formic acid for treating cereal straw or hardwood at low temperature and atmospheric pressure, facilitating the extraction of a lignin- and cellulose-free hemicellulose fraction, suitable for further applications such as furfural synthesis (Delmas, 2021). Thus, the recovered sugar-rich juices already contain formic acid which serves as solvents for deconstructing lignocellulosic biomass and can catalyze the dehydration of xylose into furfural under these conditions. Moreover, cellulose and lignin, which are isolated without degradation, can be used to produce other highly usable products, thereby maximizing the use of biomass.

Despite being industrially recognized since 1921, the yield obtained from commercial processes of furfural production has been roughly 40–50% of the theoretical yield of 72.7%, based on the pentosanes content of the starting material (Kamm et al., 2013). The low furfural yield was mainly attributed to undesired reactions, including furfural condensation between xylose or intermediates and furfural, furfural resinification, and decomposition or fragmentation of furfural (Yan et al., 2014). In order to enhance the yield and selectivity of furfural, it is necessary to rapidly extract the generated furfural from the reaction solution to prevent its degradation caused by secondary loss reactions (Yang et al., 2013).

Current furfural production procedures are being developed in such a way as to minimize side reactions in the liquid phase. Techniques such as elevating temperatures (above 230°C) in processes like Supratherm and Stake, or employing adiabatic flash distillation for furfural isolation (SupraYield), are being explored (Zeitsch, 2000; Marcotullio and De Jong, 2010). W. Yang et al. (2012) investigated the stream stripping process to recover furfural from

the reaction zone in a semi-batch mode, achieving the highest furfural yield of 74% with a selectivity of 78%. Notably, (Agirrezabal-Telleria et al., 2011) found that nitrogen (N_2) acted as a more effective stripping agent than steam, removing 65% of furfural produced from xylose in the vapor phase with a selectivity close to 100%. Another promising approach involves utilizing a biphasic solvent system to enhance furfural yield and selectivity. In this system, furfural is extracted by the organic phase after being generated in the aqueous phase. This leads to the inhibition of furfural degradation reactions that occur in the aqueous phase (L. Zhang et al., 2018). Rong et al. (2012) developed a strategy to produce furfural from xylose at atmospheric pressure, utilizing H_2SO_4 as a catalyst and NaCl as a promoter. With toluene as the organic extraction solvent, the greatest furfural yield of 83% was attained in a biphasic system. Recently, Gómez Millán et al. (2019) evaluated the furfural production from xylose in auto-catalyzed conditions using a biphasic system including water-immiscible solvents, namely isophorone, 2-methyltetrahydrofuran (2-MTHF), and cyclopentyl methyl ether (CPME). Among them, CPME afforded the highest furfural yield of 78% for 93% selectivity at an organic solvent to aqueous solution volume ratio of 1:1. Nevertheless, there has been no research conducted on these extraction systems specifically for the purpose of furfural synthesis utilizing formic acid as a catalyst (organic acid). Furthermore, based on our research, there are limited investigations where these extraction techniques have been used for furfural synthesis from raw biomass.

Despite its disadvantages, including expensive setup, high energy usage, and safety issues, extraction with supercritical carbon dioxide (Sc-CO_2) has recently emerged as an interesting alternative process to efficiently separate the highly reactive product from the reaction mixture. This process improves both the selectivity and the yield of the reaction (Oriez et al., 2023; Shi et al., 2023). CO_2, when in its supercritical phase (T_c =31.1 °C and P_c = 7.4 MPa) is advantageous as a neutral, non-toxic, non-combustible “green” solvent. As a result, it is commonly employed for chemical extraction (Gurgenova et al., 2013). Furthermore, CO_2 exhibits utility as an acid catalyst, particularly in enhancing acid-catalyzed reactions by acting as a Lewis acid due to its polar characteristics (Beckman, 2004). Moreover, its solubility in water enhances water acidity through the formation of carbonic acid, functioning as a Brønsted acid and thereby expediting dehydration reactions (Magalhães da Silva et al., 2014). Gairola and Smirnova (2012) investigated the hydrothermal conversion of xylose to furfural with simultaneous Sc-CO_2 extraction, achieving a maximum furfural production of 68% at 230 °C and 12 MPa. Sangarunlert et al. (2007) optimized furfural production from rice husk via

sulfuric acid hydrolysis accompanied by Sc-CO_2 extraction, attaining a highest furfural yield of 90% using a two-stage process (i.e., pre-hydrolysis and dehydration) with Sc-CO_2. More recently, Sato et al. (2019) explored xylose conversion to furfural using solid catalysts, such as an ion-exchange resin (Amberlyst-70) and zeolites (M-20 and H-ZSM-5), in batch and semi-batch processes with Sc-CO_2 extraction. The most favorable furfural yield, reaching 52.3%, was achieved with Amberlyst-70 in a semi-batch reactor system over 16 h at 150 °C. While Sc-CO_2 extraction has been used alongside mineral acids, solid acid catalysts, and under catalyst-free conditions, no research has yet explored the use of organic acid catalysts, specifically formic acid, in combination with Sc-CO_2 extraction for the furfural production from xylose and raw biomass.

In the process of furfural production from raw biomass, the pretreatment of lignocellulosic material for xylose production often requires high concentrations of formic acid, such as the 85 wt% used in the LEEBio^{TM} process, to effectively break down hemicellulose into xylose (Zhu et al., 2014). Typically, the concentration of xylose obtained is lower than that of formic acid; for instance, the syrup from the LEEBio^{TM} process typically yields 10–30 g/L of xylose for a formic acid concentration of 15 wt%. However, the conversion of xylose to furfural through acid catalysis necessitates only modest concentrations of formic acid. In fact, increasing formic acid concentrations, especially at high temperatures, significantly reduce both yield and selectivity. Ideal conditions for maximizing furfural yields (>70%) and selectivity (>75%) were proposed by W. Yang et al. (2012), involving xylose concentrations ranging from 40 g/L to 120 g/L, formic acid concentrations between 5 g/L and 15 g/L, and reaction temperatures between 170°C and 190°C. Therefore, enhancing furfural production requires a pretreatment step aimed at adjusting the xylose-to-formic acid ratio. Nanofiltration (NF) is particularly notable among membrane processes due to its cost competitiveness, low energy consumption, operational stability, and ease of scale-up (Pinelo et al., 2009; Zhou et al., 2013). Considering the molecular weights of formic acid (46.03 g/mol) and xylose (150.13 g/mol), NF shows promise in adjusting the xylose/formic acid concentration ratio, especially under acidic conditions where both substances remain uncharged, primarily determined by size exclusion. Wang (2010) demonstrated the feasibility of separating xylose from acetic acid using the Desal-5DK membrane, achieving a maximum separation factor of 5.4. This membrane was also effective in separating furans and carboxylic acids in hydrolysates obtained from the dilute acid hydrolysis of rice straw, with a maximum separation factor of 52 (Weng et al., 2010). With numerous references confirming its efficiency

in separating organic acids from sugars, NF emerges as a promising tool for adjusting the concentration ratio of sugars to formic acid in hydrolysates before furfural production.

Although there are many studies on the conversion of xylose into furfural catalyzed by formic acid, few have investigated this process using raw biomass, which typically results in low furfural yield. Therefore, this work aims to develop a sustainable process for transforming pentose sugars contained in the hydrolysate from the hydrolysis of lignocellulosic biomass using the LEEBio^{TM} process to produce furfural with formic acid. Additionally, two extraction methods were investigated to enhance furfural yield and selectivity: steam stripping in a semi-batch system and employing organic solvents in a biphasic system for homogeneously catalyzed reactions. To meet green chemistry requirements and align with sustainable development principles, supercritical carbon dioxide was explored as an alternative extraction agent for the dehydration of xylose into furfural. Furthermore, heterogeneous catalysts, which offer the advantage of being reusable, were examined to improve the catalytic performance of formic acid in converting pentose into furfural. Despite experimental studies, few have identified a preferred reaction mechanism, and predicting results via models remains challenging. This thesis also aims to propose a representative and predictive model of process performance for furfural production from raw materials of varying purity levels.

The first chapter will provide a literature review on furfural production, specifically highlighting several methods to improve the reaction yield and different kinetic model mechanisms for the acid-catalyzed dehydration of xylose into furfural. In the second chapter, the experimental strategy used in this work to answer of all objectives will be presented. The third chapter is dedicated to optimizing operating parameters and simultaneously extracting furfural through steam stripping and biphasic systems for furfural production from xylose and real biomass hydrolysate. In addition, this chapter presents a comparison between furfural production conducted at high pressure and that carried out under normal atmospheric pressure. The fourth chapter exclusively discusses the development of greener routes for furfural production. This involves incorporating supercritical carbon dioxide extraction to improve production efficiency and use a heterogeneous catalyst in combination with formic acid as a catalytic system for furfural production. Finally, in the last chapter, we provide a comprehensive analysis of the kinetic modeling of xylose dehydration into furfural catalyzed by formic acid, along with its application to biomass hydrolysate.

I. Chapter 1

Literature review

This section provides an overview of furfural production from lignocellulosic biomass, encompassing various aspects. Initially, it delves into the starting material for furfural production, its physico-chemical properties, applications, and derivatives. Following this, it thoroughly examines industrial processes and technologies involved in furfural production, including the mechanism and kinetics of the process. Additionally, it explores factors influencing furfural production, such as catalyst selection, reaction medium type, and operating parameters. The paragraph also discusses potential methods for furfural recovery and concludes by addressing the feasibility of furfural production from lignocellulosic biomass, highlighting different technologies aimed at enhancing biomass utilization in furfural production.

I.1 Properties and applications of furfural from lignocellulosic biomass

I.1.1 Valorization of lignocellulosic biomass in furfural

I.1.1.1 Biorefinery concept

Nowadays, the production of chemicals and energy from renewable resources tends to become unavoidable due to declining reserves and rising fossil fuel prices along with environmental concerns (Cherubini and Jungmeier, 2010). In this context, biomass—renewable organic matter derived from biological sources—has emerged as a promising alternative to fossil resources for the production of energy carriers and chemicals. It is the only carbon-rich material source available on Earth (Cherubini, 2010; Shen et al., 2020).

The biorefinery concept encompasses a variety of technologies that can transform biomass resource into their building blocks, which can further be turned into value-added products, biofuels, and chemicals (Figure I-1) (Berntsson et al., 2012).

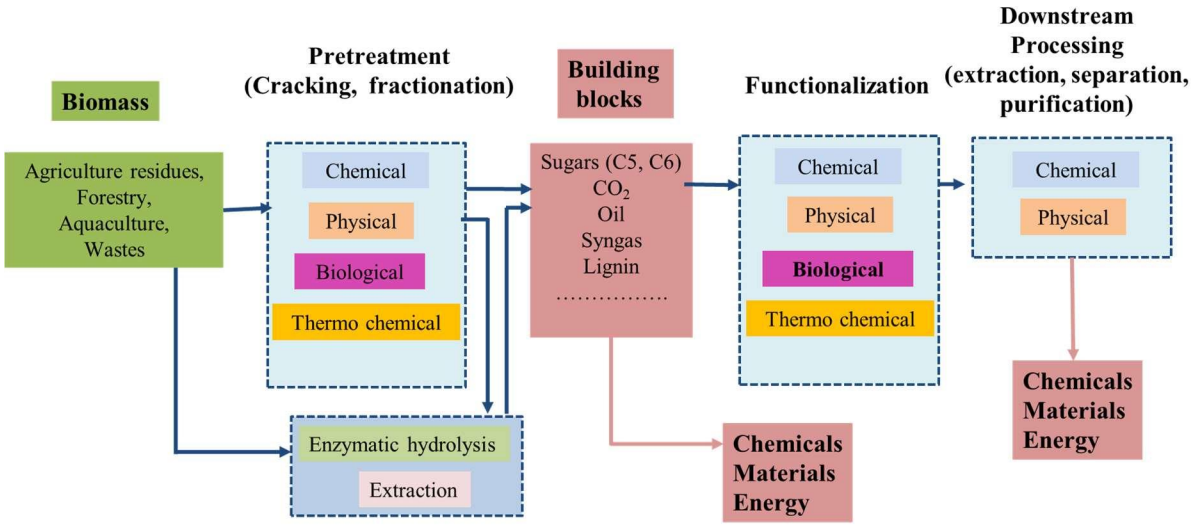

Figure I-1: Diagram of the general biorefinery concept.

Biorefineries can be divided into three generations based on the raw materials used to produce biofuels and bio-based products. As a result, typical agricultural biomass, such as corn, maize, sugarcane, or soybean, is known as raw materials in first-generation biorefineries. The lignocellulosic feedstock which is mainly made up of cellulose, hemicellulose, and lignin, is used by second generation type. The third generation includes industrial facilities in which agricultural residues, forestry, petroleum, and urban trash as feedstock biomass are found, as well as microalgae (Julio et al., 2017).

It is worth noting that the choice of raw materials is crucial since it influences the selection of ultimately generated products as well as their composition due to numerous variations, resulting in a variety of products (Figure I-2) (Cherubini, 2010).

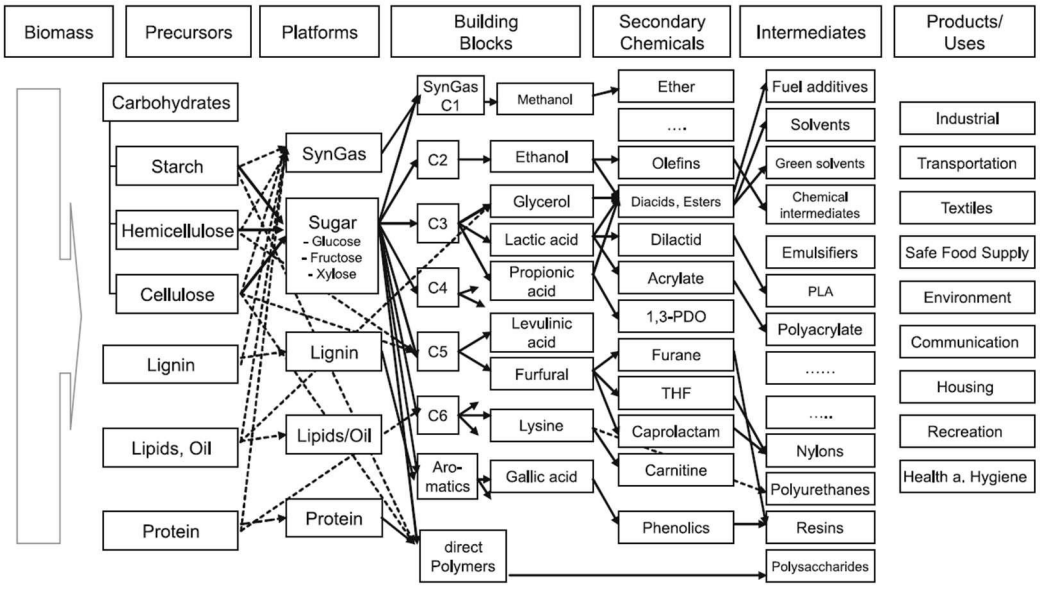

Figure I-2: Model of a biobased product flow-chart for biomass feedstock (Ulber and Sell, 2007).

With an annual global production of around 181.5 billion tones, lignocellulosic material, the feedstock utilized in the second generation of biorefineries, is the most abundant biomass on Earth (Dahmen et al., 2019). Furthermore, because it competes less directly with land usage for food or feed animal production, it is considered as the most important type of biomass feedstock for use in biorefineries (Berntsson et al., 2012).

I.1.1.2 Lignocellulosic Biomass (LB)

Lignocellulosic biomass is composed of cellulose, hemicellulose, and lignin, which together represent 75-85 wt% of the dry matter. It also contains proteins, carbohydrates, and inorganic components, which are considered as ash (Dey et al., 1997) (Figure I-3). The proportion of these components depends not only on the type of biomass (Kenney et al., 2013) but also other factors such as local agronomic conditions (Templeton et al., 2009), drought (Emerson et al., 2014), harvest season and year (Lemus et al., 2002), as well as method of harvesting of biomass (Eisenbies et al., 2015). The composition of various lignocellulosic biomass is shown in Table I-1.

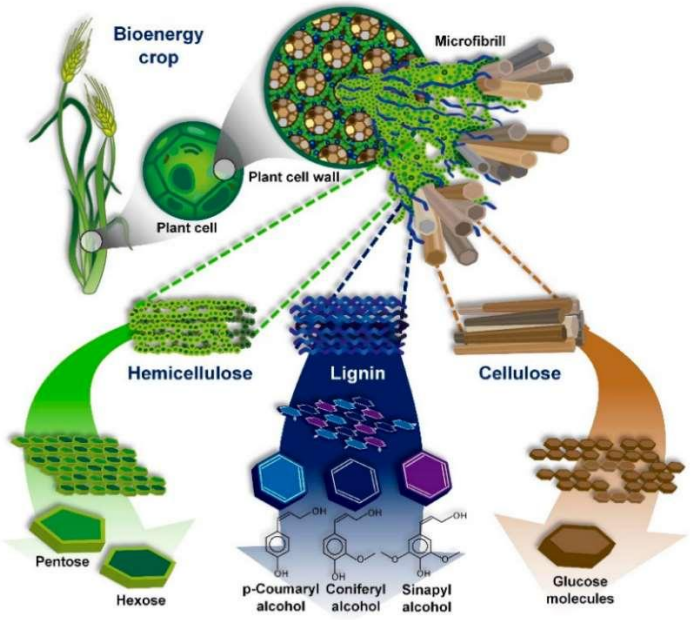

Figure I-3: Structure of lignocellulosic biomass and its biopolymers (Hernández-Beltrán et al., 2019).

Table I-1: Composition of various lignocellulosic biomass (Tayyab, 2018).

Biomass	Lignin (%)	Hemicellulose (%)	Cellulose (%)	Ash (%)	Ref.
Wheat straw	17-19	26-32	33-38	3.74	Rabemanolontsoa and Saka (2013) ; Saini et al. (2015)
Rice straw	12-14	23-28	28-36	9.8	Qu et al. (2011) ; Saini et al. (2015)
Sugarcane bagasse	20-42	19-25	42-48	-	Kim and Day (2011); Saini et al. (2015)
Corn cob	14-15	35-39	42-45	3.53	Rabemanolontsoa and Saka (2013)
Bamboo	20.81	19.49	39.80	1.21	Rabemanolontsoa and Saka (2013)
Switchgrass	10-40	30-50	5-20	5-6	Lynd et al. (1999); McKendry (2002)

Cellulose $(C_6H_{10}O_5)_n$ is a crystalline structure made up of closely packed glucose monomers connected together by β-1,4 glycosidic bonds to create tight polymer chains. Its lateral fibers have a high amount of hydroxyl groups, which increase hydrogen bonding, making it more durable and hence difficult to biodegrade (Abraham et al., 2020). It accounts for 30-50% of lignocellulosic biomass (Haq et al., 2021).

Hemicellulose $(C_5H_8O_4)_n$ is an amorphous, branching polysaccharide with a low degree of polymerization. Because of this, it is easier to degrade than cellulose by microorganisms or by thermochemical and physical processes (Haq et al., 2021). The major structural unit is xylan,

which is made up of randomly dispersed C_5 (xylose and arabinose) or C_6 (glucose, mannose and galactose) sugars (Seidl and Goulart, 2016). Hemicellulose, like cellulose, is typically found in plant cell walls (Abraham et al., 2020). The average hemicellulose concentration of lignocellulosic biomass is 15–35%.

Lignin is a heteropolymer made up of three major phenolic components, namely coniferyl, p-coumaryl, and sinapyl alcohols (Rubin, 2008). It functions as a glue, filling the spaces between cellulose and hemicellulose fibers in lignocellulosic biomass, resulting in a 3D cross-linked, stable molecular structure (Vanholme et al., 2010). It is rigid and resistant to degradation because of its stability (Abraham et al., 2020). Lignocellulosic biomass has a lignin content of 10-20%.

Due to its strong native recalcitrance, the complete utilization of the lignocellulosic biomass feedstock is still challenged to compete economically with petroleum refineries (Sun et al., 2016). Accordingly, a pre-treatment process is required prior to the conversion step to (1) maximize sugar yields, (2) treat a wide range of lignocellulosic feedstocks, (3) ensure lignin recovery for combustion, and, as a result, (4) produce a few inhibitors or co-products, and (5) reduce operational costs and energy consumption (Prasad et al., 2016).

Various pre-treatment technologies have recently been developed which can be divided into four main categories: physical, chemical, physico-chemical, and biological processes. The characteristics, major advantages, and disadvantages of different pre-treatment processes for pre-treating lignocellulosic biomass are summarized in Table I-2. Moreover, the combination of these pre-treatment processes, where their advantages are combined, can enhance the bio-digestibility and facilitate the recovery of isolated biomass components for producing high value-added products as shown in Figure I-4 (Jones et al., 2013; Han et al., 2015).

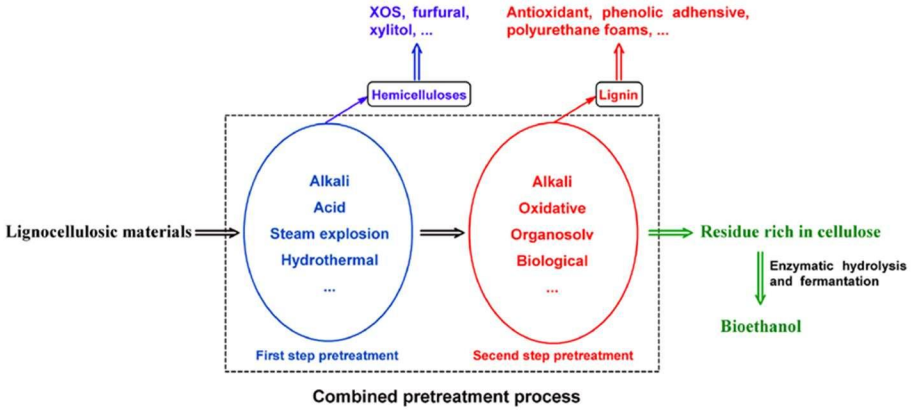

Figure I-4: Schematic diagram of combined pre-treatment strategies to maximize the utilization of lignocellulosic materials (Sun et al., 2016).

Table I-2: Different pre-treatment processes for pretreating lignocellulosic (Taherzadeh and Karimi, 2008; Taha et al., 2016; Sun et al., 2016; Rabemanolontsoa and Saka, 2016).

Pre-treatment	Energy source	Effect	Advantages/disadvantages
Physical	- Wet milling - Dry milling (grinding) - Comminution (ball mill, colloid, hammer, compression) - Irradiation (electron beam, gamma-ray, microwave) - Electric (pulsed electrical field) - Sonication	Increase in accessible surface area and pore size and crystallinity	- No requirement of chemicals and no toxic waste and inhibitors from these processes - Most of the methods are highly energy demanding
Chemical	- Acid and alkaline hydrolysis - Organosolvent using different solvents - Ionic liquids (ILs) - Oxidation using oxidising agents	Digests lignin matrix and makes cellulose and hemicellulose more accessible	- High in delignification and saccharification and economic only when solvents are recycled - High pollution and high chemical recovery cost
Physio-chemical	- Steam explosion - Supercritical and subcritical water (liquid hot water) - CO_2 explosion - Ammonia-fiber expansion (AFEX) - Ammonia recycle percolation (ARP).	Decrease in degrees of polymerization and improve the efficiency of downstream processing	- Direct utilization of wet or fresh lignocellulosic materials and short process time - High energy, chemical consumption and requires specific costly equipment
Biological	- Microbial delignification (bacteria, fungi and actinomycetes) - Enzymatic delignification processes	Disturbing the three components and alter or remove of hemicellulose and lignin	- Environmentally friendly and low energy consumption - Long pre-treatment period

I.1.2 Applications of Hemicellulose from lignocellulosic biomass

As previously detailed, lignocellulosic biomass consists of three main fractions: cellulose, lignin, and hemicellulose, with varying content depending on the biomass type. This section focuses specifically on the hemicellulose fraction, which contains the C_5 sugars, the starting compound for furfural production.

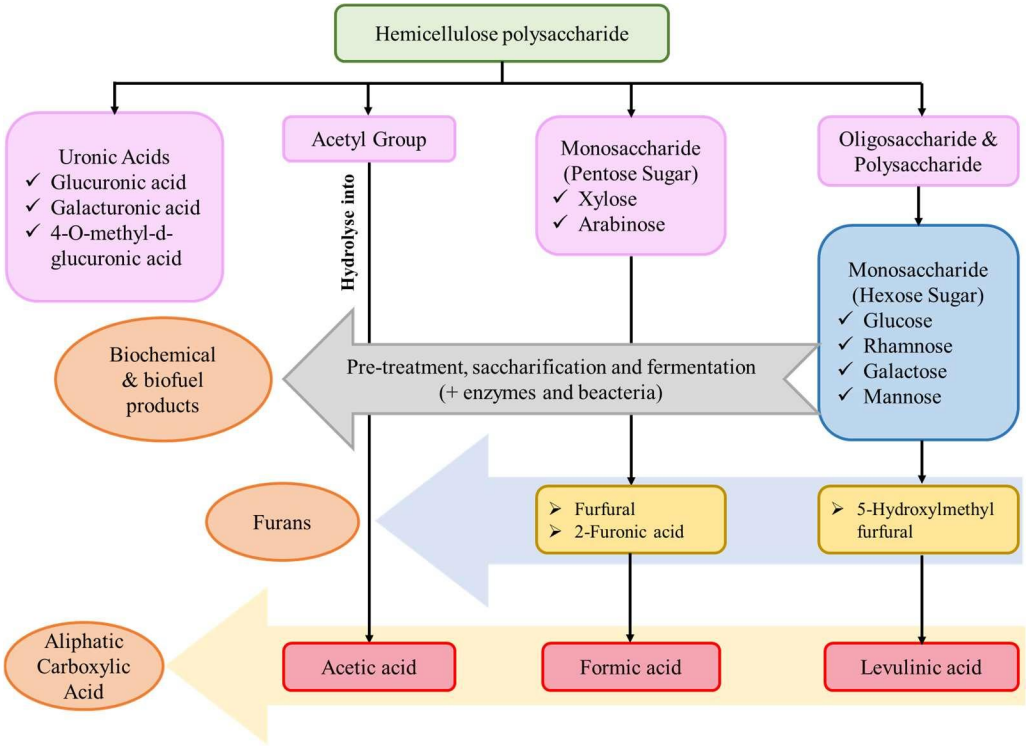

Figure I-5: Degradation products from hemicelluloses derived from acid pretreatments (Rodrigues et al., 2023).

Hemicellulose, after cellulose, is the second most abundant polysaccharide in the plant cell walls of nearly all terrestrial plants. It has diverse molecular structures with polar hydroxyl groups, which result in excellent processability, including easy hydrolysis, biodegradation, and chemical modification (Lu et al., 2021). Efficient extraction of hemicelluloses enables their conversion into a variety of products for the food, pharmaceutical, cosmetics, and textile industries (Figure I-5) (Rodrigues et al., 2023). The composition, chemical structure, and quantity of hemicellulose can vary depending on the plant biomass source. For instance, the dominant hemicellulose in hardwood is xylan (glucuronoxylan), while in softwood, it is primarily mannan (glucomannans and galactoglucomannans). In lignocellulosic biomass, xylan hemicelluloses are present in large quantities, which is the main focus of this work. Due to its amorphous structure, xylan is easier to hydrolyze than crystalline cellulose, yielding mainly C5 monosaccharides, such as xylose (pentoses). The utilization of xylose has received

considerable attention in the development of high-value biomass applications (Chen and Wang, 2017). Xylose can be converted into various valuable chemical compounds, with furfural being the primary molecule of interest in this study. It is thus important to examine the properties of the target molecule, furfural, and its industrial applications to better understand and optimize its production process.

I.1.3 Physico-chemical properties, applications and derivatives of furfural

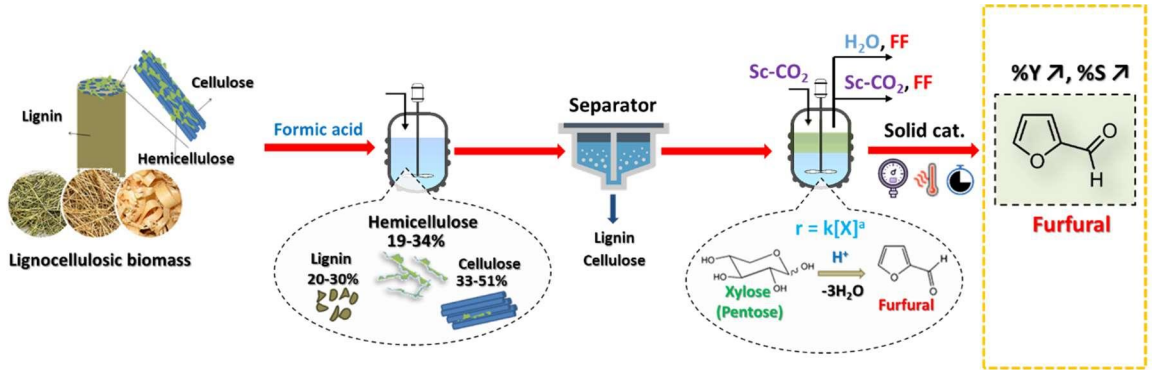

Furfural or furan-2-carboxaldehyde is an organic compound (heterocyclic aldehyde) with empirical formula $C_5H_4O_2$ and a molecular weight of 96.08 g/mol. It is a physically colorless oily liquid with a pure almond odor, but it quickly turns yellow on contact with air. Excellent physical properties of Furfural make it an excellent selective extractant for (1) removing aromatics from lubricating oils to enhance the relationship of viscosity vs. temperature; (2) removing aromatics from diesel fuels to improve ignition properties; and (3) forming cross-linked polymers (Yan et al., 2014).

Furfural contains two strong and functional groups: a C=O aldehyde and a C=C–C=C conjugated system that can undergo a variety of reactions for producing various chemical compounds (Figure I-6). Furfural aldehyde group can be subjected to acetalisation, acylation, aldol and Knoevenagel condensations, reduction to alcohols, reductive amination to amines, decarbonylation, oxidation to carboxylic acids, and Grignard reactions. Moreover, hydrogenation, oxidation, halogenation, open-ring, and nitration processes can all be performed on the furan ring system (C=C–C=C). As a result, furfural and two of its derivatives, furan dicarboxylic acid and levulinic acid, were selected among the top 10 chemicals by the US Department of Energy (DOE) to find the most promising platform chemicals (Bozell and Petersen, 2010).

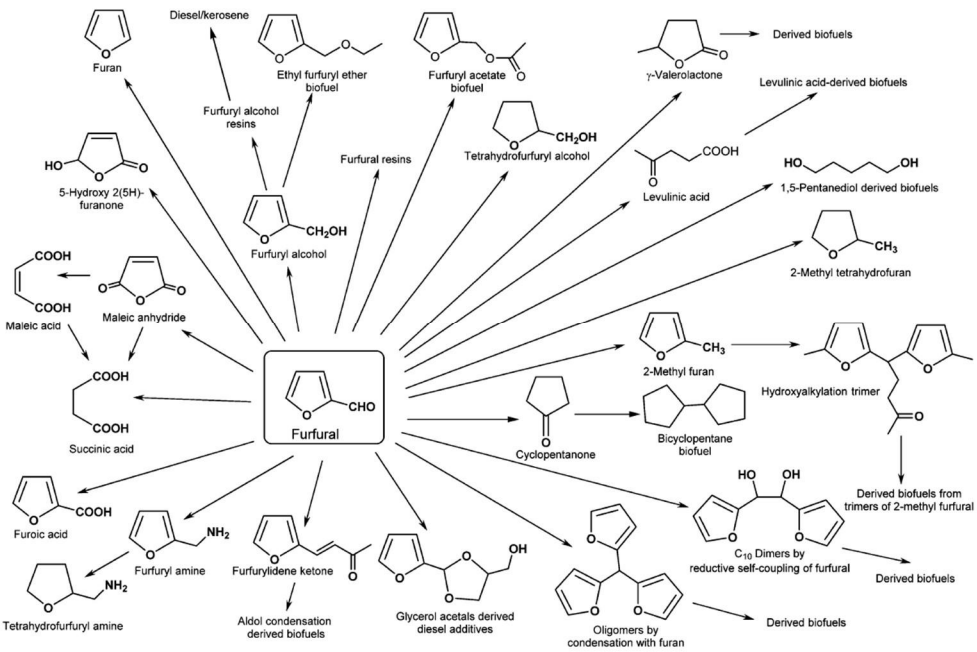

Figure I-6: Summary of the furfural-derived chemicals and biofuels (Mariscal et al., 2016).

Furfural serves as a natural precursor to a diverse array of furan-based compounds and solvents, which have found extensive application across various sectors including plastics, pharmaceuticals, and agrochemicals (Bohre et al., 2015; Eseyin and Steele, 2015). Its versatility extends to the global production of inks, antacids, fungicides, fertilizers, plastics, adhesives, nematicides, and flavoring compounds. Notably, furfuryl alcohol emerges as the most prominent derivative, constituting 80% of the overall consumption of furfural. It is widely utilized as a solvent in petrochemical refining and in the manufacture of furan resins and foundry sand binders. Data Bridge Market Research predicts a strong growth trajectory for the furfural market, with a purity level of over 98.5%. The market is expected to reach USD 900.84 million by 2030, compared to USD 556.74 million in 2022. This reflects a compound annual growth rate (CAGR) of 6.20% from 2023 to 2030 (“Furfural Market Size, Share, Growth & Trends Report, 2030,”). Various drivers propel this growth, including the increasing demand for furfuryl alcohol, pivotal in resin and plastic industries, the expanding utility of furfural as an insecticide, nematicide, and fungicide in agrochemical applications, alongside its efficacy as a weed killer in horticulture. Furthermore, the rising need for furfural as a solvent across a spectrum of end-use industries such as paints and coatings, agriculture, chemicals, refineries, foundries, pharmaceuticals, automotive, and construction, underscores its significance in the global market landscape (Wood, 2019).

I.2 Furfural production

Until now, there has been no synthetic route available for furfural production in the chemical industry (W. Yang et al., 2012). Furfural is typically synthesised from lignocellulosic biomass by dehydrating pentosan (mostly xylan), which is abundant in the hemicellulose of various agricultural residues. The main route for furfural production consists of two steps as mentioned earlier: pentosan sugars in hemicellulose are hydrolysed to obtain xylose, which is then dehydrated to generate furfural. Besides xylose, arabinose which accounts for the second largest proportion of the pentose units in biomass, can also be dehydrated to produce furfural. However, arabinose is less reactive than xylose because of the different steric positioning of the hydroxyl groups (Garrett and Dvorchik, 1969). The overall reaction can be written as follows:

$$\underset{\textit{pentosanes}}{(C_5H_8O_4)_n} + nH_2O \rightarrow \underset{\textit{n-pentoses}}{n(C_5H_{10}O_5)} \rightarrow \underset{\textit{furfural}}{n(C_5H_4O_2)} + 3nH_2O$$

So, the theoretical furfural yield is 72.7 wt% from pentosan and 64 wt% from pentose on a weight-based basis (Zeitsch, 2000).

The first step proceeds rapidly with a high yield (Mansilla et al., 1998). The second step is highly complex because of the occurrence of side reactions. These reactions can be categorized as either resinification (self-polymerization) between furfural and itself, or condensation (cross-polymerization) between furfural and intermediates of xylose-to-furfural. The latter reaction produces black insoluble carbonaceous compounds or humine. Additionally, fragmentation reactions also take place, resulting in a low yield of furfural (Figure I-7) (Jing and Lü, 2007a). The principal furfural destruction reaction product is formic acid, which originates from the hydrolysis of the furfural aldehyde group (Marcotullio and De Jong, 2010).

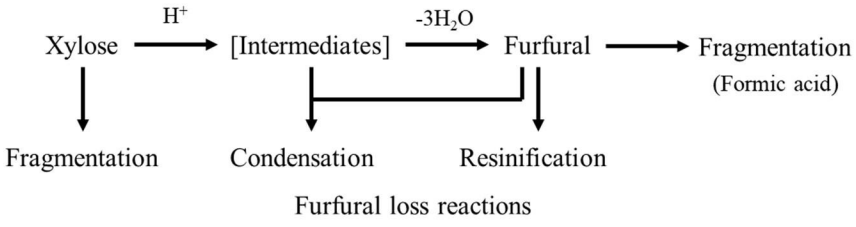

Figure I-7: Simplified scheme of the possible reaction in the xylose-to-furfural process (W. Yang et al., 2012).

Regarding the intermediates susceptible to be produced during the acid-catalyzed dehydration of xylose into furfural, two primary compounds have been identified. Firstly, lyxose, as reported by Antal et al. (1991a), manifests rapidly from open-chain xylose and gradually transforms into furfural and other byproducts. Secondly, xylulose, observed in various literature sources, was detected by Aida et al. (2010) during investigations into xylose reaction pathways under high-pressure sub- and supercritical water conditions (above 40 MPa). However, Enslow and Bell (2015) highlighted that xylulose arises from sugar isomerization reactions catalyzed by Lewis acids or bases rather than Brønsted acids like sulfuric acid, a finding corroborated by Choudhary et al. (2011), who examined xylose isomerization to xylulose and subsequent dehydration to furfural in aqueous media. Both lyxose and xylulose have been identified as intermediates during xylose dehydration catalyzed by Sn-beta zeolite, functioning as a Lewis acid. These intermediates undergo rapid dehydration to furfural through Brønsted acid catalysis. The formation of xylulose and lyxose, a ketopentose, necessitates either functional group rearrangement or a configuration change around the carbon atom linked to the hydroxyl group of the xylose molecule, facilitated by Sn^{4+} (Choudhary et al., 2011) or Cr^{3+} (Choudhary et al., 2012).

Concerning furfural production technologies, two distinct approaches are commonly employed. The first, known as the one-step technology, involves the simultaneous hydrolysis of pentosans to pentose sugars (xylose and arabinose) and the concurrent dehydration of pentose sugars into furfural within a single reactor. Conversely, the two-step process divides the process into distinct stages: initial pentosan hydrolysis under mild conditions, followed by the subsequent dehydration reaction in separate reactors. Notably, the two-stage technology offers several advantages. Firstly, it leaves the residual lignocellulose essentially unaltered, paving the way for its utilization in subsequent phases for the production of valuable chemicals such as phenol, ethanol, and glucose. Moreover, due to the significant increase in furfural yield, the two-stage approach is favored for furfural production (Riansa-ngawong and Prasertsan, 2011; W. Yang et al., 2012; Suxia et al., 2012).

Due to the advantages of a two-step process, different components of lignocellulosic biomass can be utilized separately, thereby maximizing the use of raw biomass. Additionally, by extracting the hemicellulose fraction separately, side reactions between the formed furfural and other substances in the reaction medium can be limited. This approach results in a high furfural yield with high purity. In this work, the concept of a two-step process is applied through the LEEBio™ process, which is detailed at the end of this chapter.

I.2.1 Industrial process for furfural manufacturing

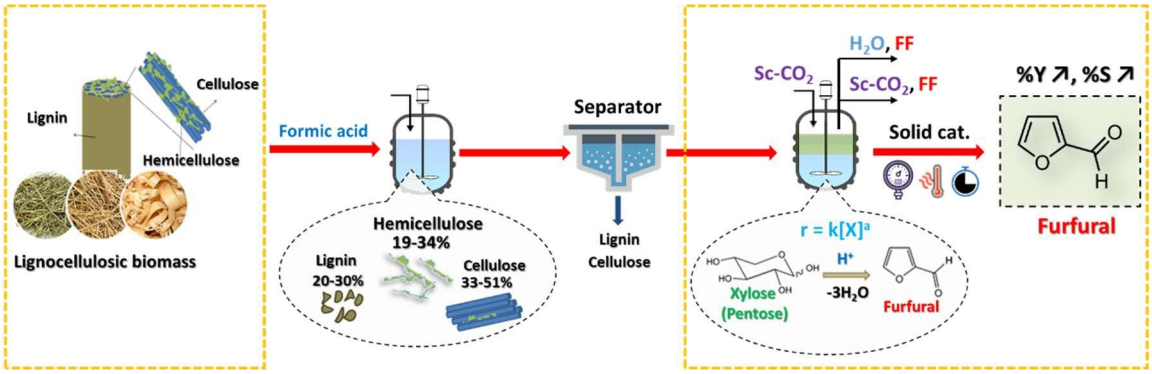

Quaker Oats invented the first known furfural production process, which involved cereal production old cookers. The dried oat hulls were heated with continuous steam injection after being digested with sulfuric acid at 153 °C for 5 h. Steam provided sufficient heat for the process while also removing the furfural from the reaction media, avoiding its self-thermal degradation (Zeitsch, 2000). Other novel processes, such as the Agrifurane, Rosenlew, Escher Wyss, and Batch processes in China, used this expertise. The main differences between the methods, as stated in Table I-3, are the operational mode (batch or continuous process) and reaction temperature (< 200 °C). Based on the pentosanes content of the starting material, the yield obtained from these procedures was roughly 40-50% of the theoretical yield of 72.7 %w/w (Kamm et al., 2013).

Further furfural production procedures are being developed, with a focus on higher reaction temperatures (> 200 °C) and novel separation processes targeted at reducing side reactions in the liquid phase. The “entropy effect” is achieved by running at a high temperature, which limits the furfural condensation reaction (Kamm et al., 2013). The Supratherm process, created by Krupp, the Stakes method, developed by Stake Technologies in Canada, and Suprayield process, currently under study in Australia, are three examples of these technologies.

The current furfural research is divided into two areas of activity: process optimization and the search for new catalytic systems. The Biofine, Vedernikors, CIMV, and MTC methods, all of which have been published and patented in the field of furfural synthesis, have demonstrated promising results in the conversion of hemicellulose to furfural (Wertz and Bédué, 2013; Fang et al., 2017).

Table I-3: Industrial processes for the production of furfural

Process	Reactor	Reaction condition	Fur yield	Ref.
Quaker Oats (1922)	Batch	H_2SO_4, Stripping (153 °C) at high pressure at 5 bar	40-52 %	Brownlee and Miner (1948)
Quaker Oats (1997)	Continuous	H_2SO_4, 184 °C at 11 bar	55%	Zeitsch (2000)
Agrifurane	Batch	H_2SO_4, 177-161 at 6-9 bar	/	Zeitsch (2000)
Escher Wyss	Continuous	H_2SO_4, 170 °C	/	Zeitsch (2000)
Rosenlew	Continuous	Acids formed *in situ,* 180 °C at 10 bar	60%	Kiminki et al. (1977)
Supratherm (1988)	Continuous	H_2SO_4, 200-240 °C	/	Zeitsch (2004)
Stake	Continuous	Acids formed *in situ,* 230 °C at 27.7 bar	66%	Zeitsch (2000)
SupraYield (1990)	Batch	H_3PO_4/CH_3COOH,170-230 °C at high pressure	70%	Zeitsch (2008)
Biofine	Continuous	H_2SO_4, 220 °C at 25 bar	70%	Fitzpatrick (1990)
Vedernikov's	Batch	H_2SO_4	55-75%	Gravitis et al. (2001)
CIMV (2010)	Continuous	HCOOH/CH_3COOH, 230 °C, pressurized	/	Kamm et al. (2013)
MTC (2012)	Continuous	H_2SO_4/NaCl, Stripping (200 °C)	83%	Kamm et al. (2013)

Multiple methodologies at various stages of development are available for the synthesis of furfural. Nevertheless, achieving higher yields under milder process conditions remains challenging. Despite the differences in these procedures, the reaction processes and kinetics involved are generally quite similar. Consequently, it is crucial to monitor and anticipate these mechanisms using models to optimize furfural production in terms of both yield and process investment.

I.2.2 Mechanism and kinetics for the synthesis of furfural

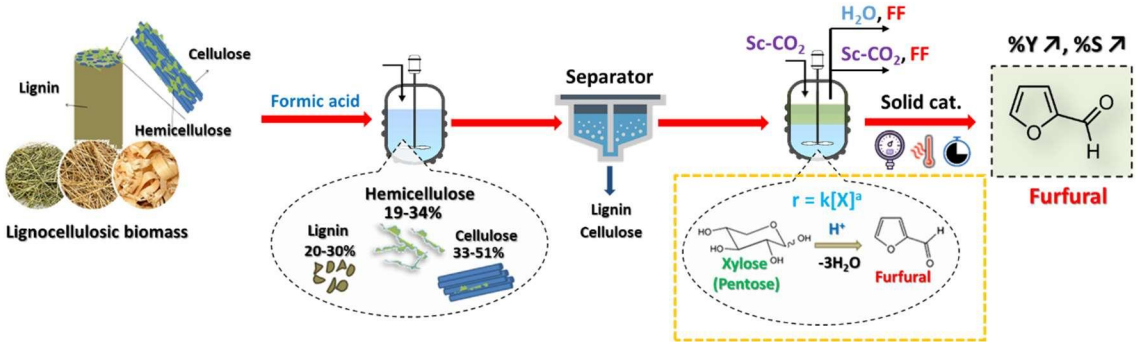

I.2.2.1 Mechanism of cyclodehydration of xylose to furfural

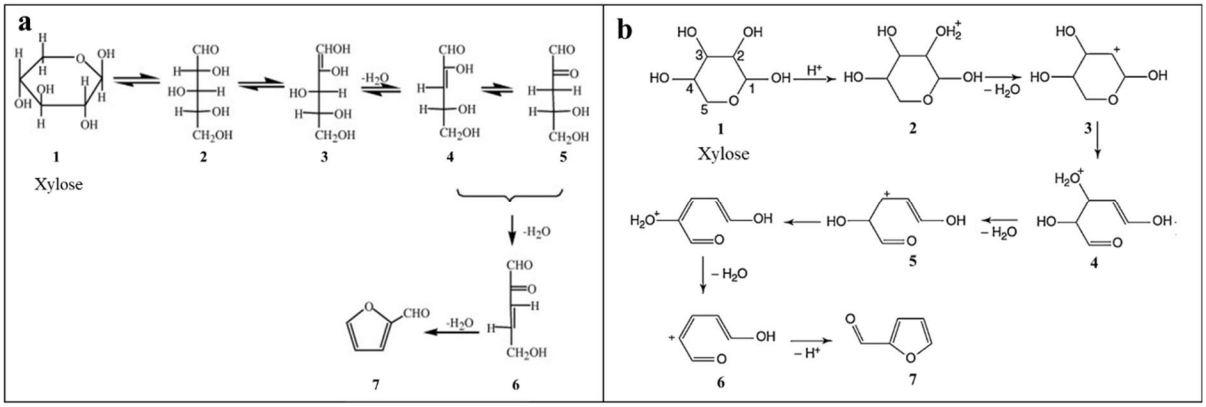

Figure I-8: Mechanism (a) and (b) of the furfural formation from xylose (W. Yang et al., 2012; Agirrezabal-Telleria et al., 2014a).

The mechanism of furfural formation has been the subject of many studies in recent years. However, the exact mechanism has not been established (Feather et al., 1972). Different hypotheses for the mechanism of dehydration of xylose to furfural are proposed among which mechanisms (a) and (b) shown in Figure I-8 are mostly recorded in the literature, and thus will be detailed here (W. Yang et al., 2012).

Mechanism (a) involves the reactions getting along with open-chain intermediates. According to Feather et al. (1972), aldose **(2),** which is in equilibrium with structure **(1)**, converts reversibly to 1,2-enediol **(3)**. The latter is then dehydrated to enolic **(4)** of a 3-deoxyglycosulose **(5)**, which further dehydrates to structure **(6)** and then to the furfural **(7).**

Since the amount of open-chain aldehyde form is less than that of the ring form (less than 1% of the total pentose present), the mechanism seems to start with a cyclic form of xylose

(mechanism (b)). Furthermore, this mechanism is in agreement with kinetic studies (Antal et al., 1991) and NMR studies (Drew et al., 1998) of the conversion of xylose into furfural.

The mechanism (b) involves two 1,2-eliminations and one 1,4-elimination of water. In more detail, an acid catalyst's hydrogen ion first attacks a lone (nonbonding) electron pair of a hydroxyl oxygen, forming a trivalent positively charged oxygen atom **(2)**. The positive charge (electron deficiency) undergoes a fission of the C-O bond, leading to a positively charged fragment **(3)** and to the liberation of water molecule. An intermediate having a double bond will be formed by two electrons from a neighbouring C-X bond, causing a fission of the latter and thus releasing a hydrogen atom **(4)**. This hydrogen atom will attack another lone electron pair of hydroxyl oxygen to generate another liberation of water **(5)**. In the last step, which is 1,4-elimination, the trivalent positively charged carbon atom forms a ring instead of a double bond formation **(6)**. This is sterically facilitated by its planar structure, characterized by a bond angle of 120° (plane trigonal orbital). After the 1,4-elimination, the hydrogen ion is removed to provide furfural **(7)** (Zeitsch, 2000).

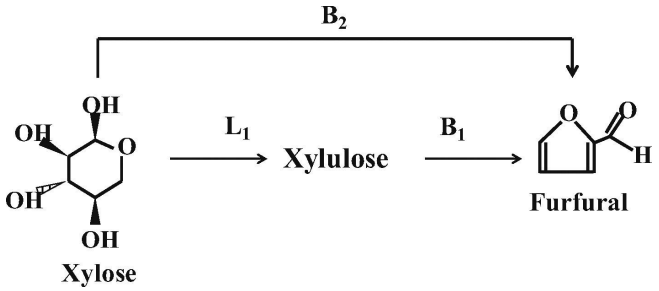

Figure I-9: The isomerization of xylose to xylulose and the dehydration to furfural L: Lewis acid; B: Brønsted acid (Agirrezabal-Telleria et al., 2014a).

Recently, it was found that the mechanism can be modified depending on the type of acidic catalyst. Furfural can be formed directly from xylose using Brønsted acids, as shown above. Lewis acids, on the other hand, produce furfural via the intermediate xylulose as mentioned previously, which can be converted to furfural quickly in the presence of Brønsted-acid catalysts (Figure I-9) (Agirrezabal-Telleria et al., 2014a). When Lewis acid sites were present, the xylose conversion rate was shown to be faster than when Brønsted sites were present. However, a Brønsted site is necessary to produce a large increase in furfural yield (Choudhary et al., 2012).

For this work, the manuscript will primarily focus on reaction mechanism 3, which is the most complex as it considers all possible reactions occurring during furfural production.

However, studying all available mechanisms will enable the reaction mechanism for furfural production to be validated and/or modified.

I.2.2.2 Kinetic modeling

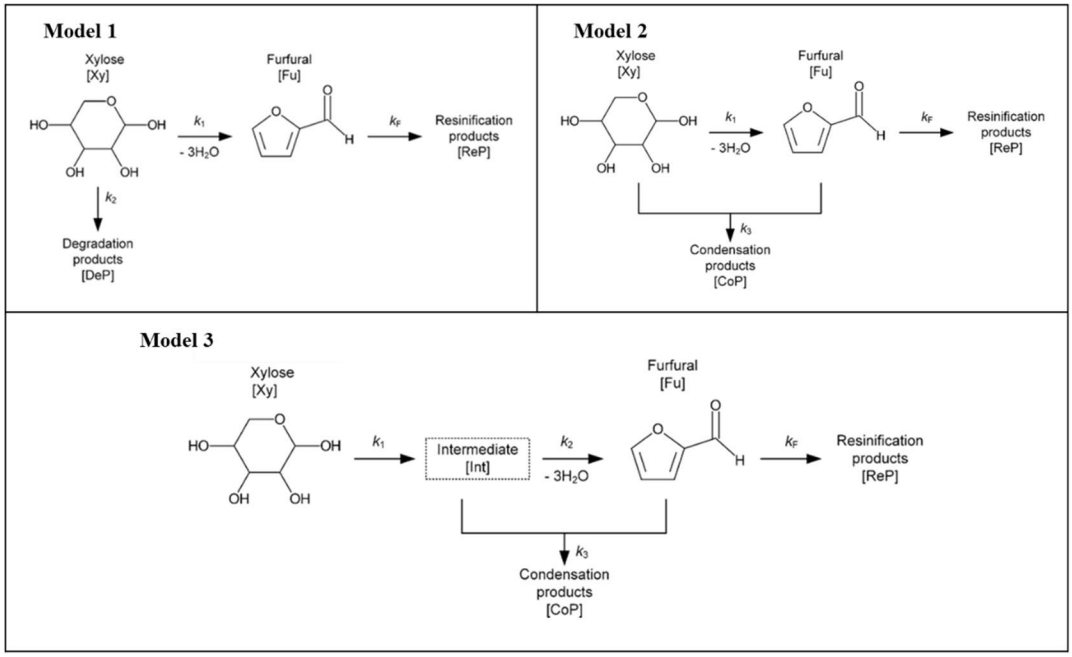

Figure I-10: Reaction mechanisms of xylose conversion into furfural and side products for kinetic modeling (Köchermann et al., 2018).

Several kinetic models for Brønsted acid-catalyzed furfural synthesis have been described in the literature (Lamminpää et al., 2012; Dussan et al., 2015; Köchermann et al., 2018). However, kinetic models commonly include different side reactions when describing the dehydration of xylose to furfural (Weingarten et al., 2010; Chen et al., 2015; Dussan et al., 2015; Köchermann et al., 2018). Figure I-10 depicts all of the models, which differ mostly in terms of their side effects. Model 1 has a first-order reaction kinetic, in which furfural is only degraded by self-polymerization and xylose is directly decomposed. Furfural degradation is also regulated by cross-polymerization between xylose and furfural in Model 2. furfural dehydration via an intermediate species and its cross-polymerization with furfural is considered in Model 3. Models 2 and 3 have a second-order reaction kinetic for cross-polymerization (Köchermann et al., 2018).

The furfural degradation reaction, being a common reaction in all models, has its constant (k_F) and activation energy (E_F) computed independently from other reactions. Furfural undergoes degradation through three distinct loss reactions: (1) furfural resinification,

involving self-polymerization; (2) furfural condensation, where it interacts with xylose or xylose intermediates leading to cross-polymerization; and (3) furfural fragmentation, resulting in the breakdown into smaller molecules such as formic acid. Various studies on furfural degradation have effectively modeled the furfural loss reaction as a first-order process, as noted by Root (1956); Rose et al. (2000); Marcotullio and De Jong (2010) and Jing and Lü (2007a). However, Lamminpää et al. (2014)'s investigation into the kinetics of furfural destruction in a formic acid medium revealed a significant finding: the overall reaction order shifts with the concentration of formic acid catalyst. At higher acid concentrations (30 wt%), the apparent reaction order exceeds one, while at lower concentrations (2 wt%), it falls below one. In terms of the mechanism of furfural resinification, it is conceivable that the polymer-forming reaction scheme begins with a second-order reaction involving two furfural molecules reacting with one another. From there, the polymer chain is extended by adding one furfural molecule at a time. The overall reaction would be close to one if the growth of polymers predominates over the initiation step. When treating furfural loss as a first-order reaction, Lamminpää et al. (2012) and Köchermann et al. (2018) observed a dependency of the rate constant on both temperature and acid concentration. Particularly noteworthy is the significant impact of temperature elevation on the reaction rate, with acid concentration exhibiting a pronounced effect under such conditions.

Experimental data collected by various researchers indicates that Models 1 and 3 offer superior accuracy in predicting furfural synthesis across diverse scenarios. Nevertheless, Dussan et al. (2015)'s findings revealed a limitation in Model 1, as it tended to overestimate furfural formation. This discrepancy arises from the absence of undesired side reactions between xylose and furfural in Model 1's reaction mechanism, which could initiate early in the reaction process. With regard to model 2, the experimental data obtained in the presence of furfural were higher than the concentrations of xylose predicted by this kinetic model. Due to the assumption made in the kinetic model derived from Mechanism 2 that xylose was consumed from the beginning of the reaction subsequent to a second-order reaction involving furfural and xylose, the conversion of xylose was overestimated in this instance. The lack of observed impact on xylose conversion when substantial quantities of furfural are present during the initial stages of the reaction provides support for the hypothesis that furfural exclusively reacts with the intermediate formed from xylose in order to produce condensation products (Lamminpää et al., 2012; Dussan et al., 2015). Furthermore, Antal et al. (1991a) proposed that the various forms of xylose (acyclic, furanose, and pyranose rings) undergo distinct reactions

leading to the conversion into furfural. Consequently, Model 3 emerged as the most suitable choice to elucidate the acid-catalyzed dehydration reaction of xylose to furfural. This is affirmed by studies from Lamminpää et al. (2012); Dussan et al. (2015) and Köchermann et al. (2018) for the following reasons: (1) Model 3 is the most complex, considering all reaction intermediates whose concentrations must be determined to accurately ascertain the kinetic parameters, and (2) it accounts for all possible reactions occurring during the dehydration of xylose into furfural.

Based on kinetic modeling, the rate of xylose conversion and the synthesis of furfural were shown to be impacted by acid concentration, with higher acid concentrations resulting in faster xylose conversion, especially at high temperatures (Dussan et al., 2015). Furthermore, the activation energy for by-product formation from xylose is higher than all other activation energies, indicating that the kinetics of this reaction are temperature sensitive (Jing and Lü, 2007a). Rising temperatures enhanced the decomposition of both xylose and furfural (Lamminpää et al., 2012; Köchermann et al., 2018). Table I-4 and Table I-5 summarize the rate constants and kinetic characteristics of the related reaction mechanism for xylose conversion to furfural, respectively.

Considering that furfural can also be derived from Ara, another pentose sugar present in hemicellulose, Gairola and Smirnova (2012) delved into the dehydration of arabinose to furfural under hydrothermal conditions. According to Mechanism 1, the activation energy and kinetic parameters closely align with those obtained for Ara degradation by Carvalheiro et al. (2008) and are similar to values reported for xylose by various authors, including Jing and Lü (2007a) and Oefner et al. (1992). Contrary to expectations based on the same mechanism, Danon et al. (2014) and Dussan et al. (2015), in their studies on the kinetics of arabinose dehydration in an acidic medium, discovered that the kinetic parameters and activation energy of xylose were greater than those of arabinose. From their findings, it can be inferred that xylose undergoes dehydration more rapidly and yields higher furfural quantities in an acidic medium compared to arabinose. The kinetic characteristics of the related reaction mechanism for arabinose conversion to furfural based on mechanism 1 are presented in Table I-6.

Table I-4: Rate constants of the related reaction mechanism for xylose conversion to furfural.

Ref.	Solvent	Initial concentration (M)			Reactor	T (°C)	Rate constants: k			
		Xyl	Fur	Catalyst			k_1 (1/s)	k_2 (1/s)	k_3 (1/M/s)	k_F (1/s)
Jing and Lü (2007a)	H_2O	0.072	0.034	none	DSTR	180[a]	$5.4x10^{-5}$	$2.1x10^{-5}$	/	$5.5x10^{-6}$
Weingarten et al. (2010)	H_2O	0.002-0.25	0.156	0.1 HCl	DSTR	170[b]	$2.1x10^{-10}$	/	$9.8x10^{-7}$	$4.1x10^{-7}$
Lamminpää et al. (2012)	H_2O	0.067-0.2	0.05-0.16	0.12 HCOOH	Sealed tubes	180[a]	0.13	0.06	/	$2.5x10^{-3}$
Dussan et al. (2015)	H_2O	0.1	0.1	6.5-13.9 HCOOH	Sealed tubes	170[c]	$2.2x10^{-3}$	$5.8x10^{-4}$	$6.4x10^{-3}$	$2.6x10^{-5}$
Köchermann et al. (2018)	H_2O	0.37	0.1	18 H_2SO_4	DSTR	180[c]	$1.1x10^{-3}$	$4.6x10^{-3}$	$1.3x10^{-2}$	$6.8x10^{-5}$

[a]Based on mechanism 1. [b]Based on mechanism 2. [c]Based on mechanism 3.

Table I-5: kinetic characteristics of the related reaction mechanism for xylose conversion to furfural.

Ref.	Solvent	Initial concentration (M)			Reactor	T (°C)	Activation energy: E (kJ/mol)			
		Xyl	Fur	Catalyst			E_1	E_2	E_3	E_F
Jing and Lü (2007a)	H_2O	0.072	0.034	none	DSTR	180-220	111.5[a]	143.1[a]	/	58.8[a]
Weingarten et al. (2010)	H_2O	0.002-0.25	0.156	0.1 (HCl)	DSTR	130-170	123.9[b]	/	72.5[b]	67.6[b]
Lamminpää et al. (2012)	H_2O	0.067-0.2	0.05-0.16	1.5-6.5 (HCOOH)	Sealed tubes	130-200	152.0[a]	161.0[a]	/	75.5[a]
Dussan et al. (2015)	H_2O	0.1	0.1	6.5-13.9 (HCOOH)	Sealed tubes	130-170	140.3[c]	82.9[c]	91.5[c]	81.7[c]
Köchermann et al. (2018)	H_2O	0.37	0.1	18 (H_2SO_4)	DSTR	160-200	86.5[c]	91.8[c]	19.8[c]	44.16[c]

[a]Based on mechanism 1. [b]Based on mechanism 2. [c]Based on mechanism 3.

Table I-6: kinetic characteristics of the related reaction mechanism for arabinose conversion to furfural based on mechanism 1.

Ref.	Solvent	Initial concentration		Reactor	T (°C)	Activation energy: E (kJ/mol)		
		Ara	Catalyst			E_1	E_2	E_F
Gairola and Smirnova (2012)	H_2O	0.2-5 wt%	none	Sealed tubes	180-260	112	121	110
Carvalheiro et al. (2008)	H_2O	-	-	DSTR	150-190	114	117	103
Danon et al. (2014)	H_2O	0.05 M	0.05 M (HCl)	DSTR	160-200	133.3	125.8	102.1
Z. Chen et al. (2015)	H_2O	0.033 M	-	Sealed tubes	210-250	130-135	-	-
Dussan et al. (2015)	H_2O	0.02 M	6.5-13.9 HCOOH	Sealed tubes	130-170	130.2	125.8	81.7

Three models have been developed in the literature, with two of them appearing more suitable for modeling kinetics. However, most existing studies typically focus on a single condition. The aim of this work is to evaluate the accuracy of these models in predicting

furfural yield and to propose kinetic constants applicable to more complex systems beyond single-parameter conditions.

While various kinetic models and processes for furfural production exist, it is worthwhile to explore different synthetic solutions to establish a viable production process. However, using real biomass, which consists of multiple components, complicates the modeling of kinetic equations, making it challenging to identify the effect of each component on the kinetics of xylose conversion into furfural.

I.3 Setting up the furfural production process

I.3.1 Reactor types for furfural production

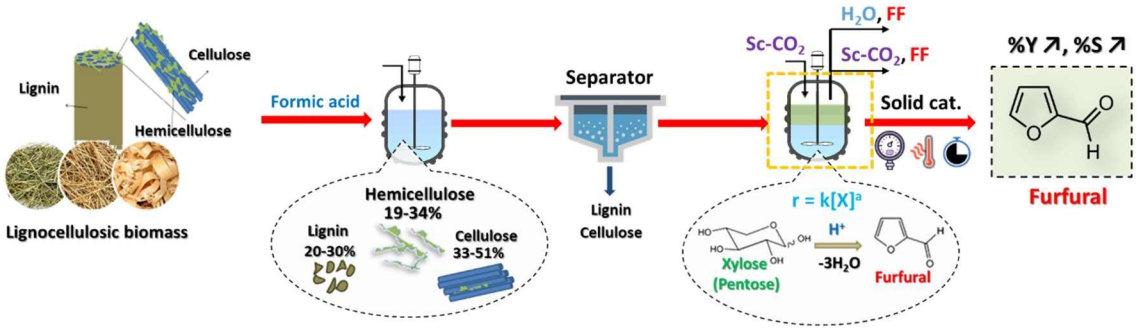

The reactors used for furfural production are divided into two types: autoclaves or batch reactor (with or without continuous distillation of vapors formed) and continuous reactors, such as continuously stirred tank reactors (CSTR) or plug flow reactors (PFR) (Carrasco, 1993). The characteristics of each reactor as well as their application toward furfural synthesis will be detailed in this section.

I.3.1.1 Batch process

The batch process, where no feed is added or product withdrawn during reaction time, is the most commonly used industrial procedure for producing furfural since 1921 in Quaker Oats process (X.-L. Li et al., 2015). The batch dehydration of raw lignocellulosic materials using sulphuric acid provided typically 40-60% of the theoretical value and 50-80% when furfural is rapidly removed from the reaction medium (Zeitsch, 2000). Beside the simplicity and minimal attention required (Liu, 2017), batch reactor systems offer the possibility of testing different parameters at the same time, especially when working with small volumes in laboratory-scale operations (Keskin et al., 2019). Most of the studies in the literature on the production of furfural from either xylose or raw materials appear to use batch systems as shown above.

Moreover, kinetics of furfural formation using both homogeneous (Lamminpää et al., 2012; Z. Chen et al., 2015) and heterogeneous catalysts (O'Neill et al., 2009) in different solvent systems (Weingarten et al., 2010; Gairola and Smirnova, 2012) are mainly carried out in batch reactor.

I.3.1.2 Continuous process

In a continuous process (i.e., continuously stirred tank reactors (CSTR) or plug flow reactors (PFR)), a chemical reaction is run in a constantly flowing stream and all fluid elements have the same reactor residence time (Medeiros and Burnett, 1985). Continuous processes, as opposed to batch processes, have reduced costs in operating and separation operations and are better suited to large-scale manufacturing (Aellig et al., 2015; Li et al., 2015). Indeed, because of the short residence times associated with this process, extended contact between reactants and products could be avoided, resulting in increased product selectivity (Medeiros and Burnett, 1985). Thus, the development of continuous process is of great significance (X.-L. Li et al., 2015).

In recent years, Li et al. (2015) examined the reaction efficiency of xylose conversion to furfural in biphasic systems using a solid acid tantalum-based catalyst in batch and fixed bed reactors. The continuous process, as expected, produced a greater furfural yield of 59% for 96% xylose conversion, whereas the batch process produced a 48% furfural yield with 54% selectivity under comparable conditions. In 1983, Kanzler and Schedler (1983) developed a two-phase continuous reactor using sulfites to form furfural, formic acid, and acetic acid by coupling the separation of products from acidic hydrolysates of vegetable materials. Similarly, Lessard et al. (2010) used a biphasic plug flow reactor to develop selective catalytic processes combining xylose dehydration to furfural and separation. This process allowed to reuse organic solvent and catalyst, thus avoiding the problem of waste generation. The results indicated that using toluene as the extracting solvent for 3 min at 260 °C, xylose can be dehydrated to furfural with a very high yield and selectivity (98%) over (H^+) mordenite.

Later, Aellig et al. (2015) showed interest in fixed bed reactors by combining a biphasic solvent system with a heterogeneous catalyst. The high interfacial area created in the reactor by the Taylor flow of liquids allowed for efficient furfural extraction into the organic phase while limiting side reactions. In addition, because the bed catalyst has less contact with water, it is less susceptible to metal leaching, resulting in stable operation for 24h on stream. By optimizing operating variables, furfural yields of 72% and 69% were achieved from xylose and

xylan, respectively. Additionally, Papaioannou et al. (2019) demonstrates the use of a milli-reactor as an intensified technology for the continuous production of furfural via acid dehydration of xylose in a biphasic medium. Fast mass transfer rates offered by Taylor flow enabled for a very quick extraction of furfural, preventing furfural degradation. Accordingly, by operating at increased temperatures (i.e., 150-190 °C), it is able to retain high furfural selectivity (about 70%) at high xylose conversion (around 80%) and very short residence times (up to 2.5 min).

Batch reactors have proven their worth in determining optimal operating parameters, kinetics, and reaction mechanisms. Therefore, they will also be used in this study to enhance the current understanding of these subjects. Once a thorough investigation is conducted using the batch system to achieve a deep comprehension of the reaction, the process can be tested in a continuous system. Comparing the results from both systems will provide valuable information for designing the process on a larger scale. However, due to the complex setup and high investment required, this study will not investigate furfural production in a continuous system.

I.3.2 Factors influencing furfural production

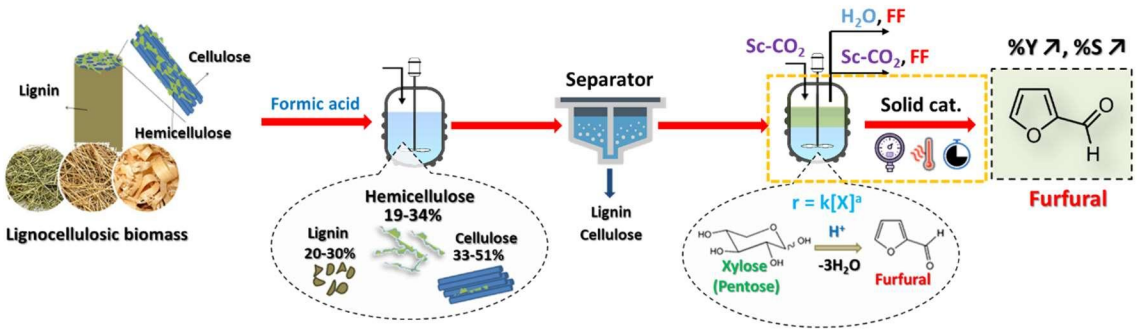

Catalyst compositions, solvent systems and reaction conditions are all factors that influence the conversion of biomass to furfural. Since the furfural synthesis involves a catalytic reaction, catalyst choice is one of the important research approaches to achieve high biomass conversion. The selection of a solvent system is another effective approach for increasing the selectivity of furfural from biomass as it invariably affects the reaction's thermodynamics and kinetics. Also, the reaction conditions must usually be optimized according to the characteristics of the catalytic reaction system (Luo et al., 2019; Zhao et al., 2021a).

I.3.2.1 Catalyst categories

Since furfural is synthesized through a catalytic conversion, the high activity and catalyst acidity, which varies depending on the catalyst type, are required to obtain the high yield of furfural. Thus, the catalyst categories are important aspects to consider in order to achieve an efficient and straightforward procedure for furfural production.

All catalysts are generally divided into two categories: homogeneous and heterogeneous catalysts. This section will focus on the utilization of each type of catalyst for furfural production.

Homogeneous catalysts

Homogeneous catalysts that can be dissolved in the reacting system facilitate the leaching of hemicellulose from solid biomass and promote furfural formation (Carà et al., 2013; Finore et al., 2016). They can be classified into three types: mineral acids, organic acids, and metal salts.

Mineral acid catalyst

Mineral acids such as sulfuric acid, phosphoric acid or superphosphate were the first homogeneous catalyst used for furfural production in traditional method established by Quaker Oats (Brownlee and Miner, 1948). These catalysts are effective, yielding furfural yields of 40%–60% (Zeitsch, 2000), and are still used in a variety of industrial processes as well as on a laboratory scale (Mazar et al., 2017). Table I-7 summarizes the reported furfural yield values testing different mineral acids for furfural production.

Table I-7: Overviews of mineral acids for furfural production

T (°C)	Substrate	Solvent	Catalyst	Fur yield (%)	Ref.
140	Xylose	DMSO/DCM or DMSO/MIBK, 2-butanol	H_2SO_4	91	Chheda et al. (2007)
170	Xylose	Water/MIBK	HCl	85	Weingarten et al. (2010)
180	Xylose	Water	HCl	38	Yemiş and Mazza (2011)
180	Xylan	Water	HCl	34	
170	Xylose	Water/CPME	H_2SO_4, NaCl	80	Campos Molina et al. (2012)
-	Xylose	Water/toluene	H_2SO_4	83	Rong et al. (2012)
170	HemiCel	Water/sec-butylphenol	HCl	78	Alonso et al. (2013)
150	Biomass	Water/toluene	H_2SO_4	70	Burket and Sabesan (2013)
200	Xylose	Water	HCl	64	Vaz Jr. and Donate (2015)
170	Xylose	Water/MIBK	H_2SO_4	80	Mittal et al. (2017)
240	Wood chip	Water	H_2SO_4	76	Mazar et al., (2017)

Organic acids

Since mineral acids have many drawbacks, such as acid corrosiveness and high pollution emissions, alternative, organic acids, have been developed to overcome these issues (Mamman et al., 2008). However, in order to achieve the same conversion as mineral acid, higher acid concentration and/or the presence of other acids are required (Zhao et al., 2021).

Among various organic acids, formic acid is mostly used for the furfural production (Lamminpää and Tanskanen, 2009; W. Yang et al., 2012; Yang et al., 2013; Delbecq et al., 2016). In addition, formic acid is produced during furfural production via decomposition reactions of hemicellulose and furfural, leading to catalyst system self-production and a reduction in production costs (W. Yang et al., 2012).

To our knowledge, the first use of formic acid as a catalyst for furfural formation was reported by Lamminpää and Tanskanen (2009). At the given optimum conditions, a maximum furfural selectivity of 70% and a yield of 60% were achieved by using xylose a starting material at 200 °C for 20 min. Later, W. Yang et al. (2012) demonstrated that formic acid gave the highest yield of furfural than H_2SO_4 and H_3PO_4 since strong mineral acids provoked side reactions (i.e., resinification). By optimizing experimental conditions, the maximum achieved furfural yield and selectivity were 74% and 78%, respectively.

Lately, Delbecq et al. (2016) accomplished 76% and 80% of furfural yield from xylan and xylose, respectively, by using betaine and formic acid mixture in a cyclopentyl methyl ether (CPME)-water biphasic system under microwave irradiation. Since resulted furfural was extracted into CPME, the aqueous layer that contained the catalyst can be recovered and reused at least ten cycles without significant drop of furfural yield. This paves the way for the reuse of homogeneous catalysts in biphasic systems to meet the green chemistry concept.

In order to make the processes more environmentally friendly, various biobased acids produced from degradation of biomass have been investigated as acid catalysts. Rackemann et al. (2014) explored methanesulfonic acid (MSA) as a catalyst for furfural production from xylose. They obtained the highest furfural yield of 65% for 15 min at 180 °C. This result was similar to that obtained using H_2SO_4 under the same operating conditions. Seemala et al. (2016) investigated the use of levulinic acid (LA) as a catalyst in a biphasic solvent system. Pinewood sawdust was found to yield higher amounts of furanic products than eucalyptus sawdust (565 mg/L at 180°C for 15 min vs. 643 mg/L at 200°C for 60 min) due to their different composition of hemicellulose.

Maleic acid is another biobased acid catalyst used for furfural production from in a two-step reaction under microwave heating (Kim et al., 2012). The furfural yield ranging from 29%

to 61% was obtained with poplar, switchgrass, pine and corn stover at 200 °C for 28 min. The recycling of the maleic acid was also investigated after the furfural extraction with dichloromethane. The results showed that xylose conversion was retained while a slightly decrease in furfural yield and selectivity was observed with additional reusable runs.

Metal salts

Metal salts, especially metal chloride, have gained prominence (Catrinck et al., 2020). Zhang et al. (2013) examined the catalytic performance of various metal chloride ($CrCl_3$, $CuCl_2.2H_2O$, LiCl, $FeCl_3.6H_2O$, CuCl, $AlCl_3$) and mineral acids (H_2SO_4, HCl, and H_3PO_4) for furfural production in 1-butyl-3-methylimidazolium chloride ([Bmim]Cl) under microwave irradiation. They found that $AlCl_3$ resulted in the highest furfural yield of 84.8%. The final yield was much higher than that obtained with H_2SO_4, HCl, and H_3PO_4 at the same amount of $AlCl_3$ (0.25 mmol). According these authors, besides the salting-out effect which enhances the separation of furfural, chloride ions might increase reaction rate resulting in high yield. Moreover, the addition of $CrCl_3$ or $FeCl_3.6H_2O$ to [Bmim]Cl/$AlCl_3$ improved the yield of furfural compared with single $AlCl_3$ use.

In the study of Wang et al. (2014), the effects of the anions in salt catalysts on the conversion of xylose to furfural were carried out by using chlorides, sulfates, and nitrates of different metals. The results showed that chlorides had the highest catalytic performance and $SnCl_4$ was the most effective chloride, giving a furfural yield of 63% in a homogenous dimethyl sulfoxide (DMSO)-water system. It was suggested that Cl^- ions engender the transformation of the aldose to 1,2-enediol, which can be easily dehydrated to form furfural (Marcotullio and De Jong, 2010). Moreover, the hydrolysis of Sn^{4+} behaving Lewis acid in the aqueous solution lowers the pH of the reactive system, promoting xylan hydrolysis to xylose. Thus, the combined effect of Sn^{4+} and Cl^- ions explained the high furfural yield in this study (Wang et al., 2015).

Sodium molybdate Mo(VI) was also used as a catalyst for transforming xylan to furfural under microwave-assisted heating (Hricovíniová, 2013). Under identical conditions, higher amounts of furfural (53%) were obtained than in the reaction without Mo(VI) ions (42%). The results reveal that Mo(VI) plays a double role: it catalyzes xylose conversion and improves the dielectric properties of solution, facilitating the energy transfer from microwave source to solution.

In addition, the simultaneous use of metal salt with other acid catalysts improves the catalytic performance, promoting further high yield of furfural. The HCl-$CrCl_3$ mixture was found to increase the furfural yield from 29% to 39%, and the reaction time was shortened by a factor

of 5 when compared to using HCl alone (Choudhary et al., 2012). According to the authors, the combination between Lewis acid of $CrCl_3$ and Brønsted acid of HCl changed the reaction pathway of xylose in such a way that the activation energy required for dehydration was reduced (Figure I-11).

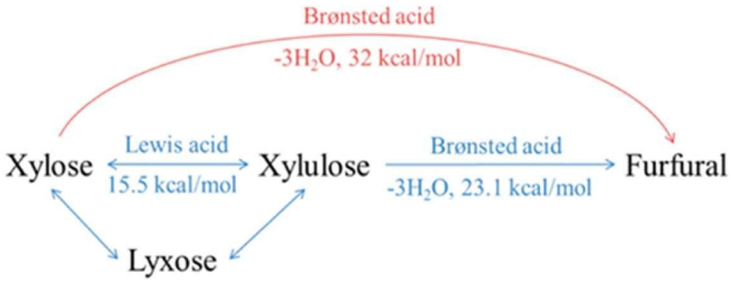

Figure I-11: Overall paths to produce furfural from xylose in the presence of a single Brønsted acid catalyst and of both Lewis and Brønsted acid catalysts (Choudhary et al., 2012).

Table I-8: Comparison of some advantages and drawbacks of homogeneous catalysts.

Homogeneous catalyst	Advantages	Drawbacks
Mineral acids	Higher catalytic activity	-Catalytic deactivation (side reactions) -Environmental impact (toxic, corrosive) -Higher cost
Organic acids	-Cheaper -Environmental friendliness -More stable	Lower catalytic activity (need higher quantity)
Metal salts	-Environmental friendliness	-Lower catalytic activity (need higher quantity) -Lower stability (problem of leaching)

By comparing the advantages and disadvantages of different homogeneous catalysts shown in Table I-8, organic acids emerge as a promising option for the production of furfural, given their catalytic activity, environmental friendliness, and cost-effectiveness. Among these, formic acid, which has already been used in several research studies, is chosen for this work. Although much research has been conducted on producing furfural using formic acid as a catalyst, these studies typically use synthetic solutions of C_5 sugars (i.e., xylose and arabinose). Therefore, this work will investigate the feasibility of using formic acid as a catalyst for the production of furfural from raw biomass to address this gap in the literature.

Heterogeneous catalysts

Because of their ease of post-separation via a simple filtration step or their ability to operate as fixed-beds, heterogeneous catalysts have emerged as promising candidates for overcoming the reusability issues associated with homogeneous catalysts (Karinen et al., 2011). Furthermore, solid catalysts provide high catalytic activity and are less corrosive compared to some homogeneous catalysts, attracting current attention in the field of catalyzed conversion (Agirrezabal-Telleria et al., 2014b).

The details of each heterogeneous catalyst will not be presented in this chapter, as this project focuses primarily on homogeneous catalysts, as previously mentioned. The different heterogeneous catalysts and the corresponding furfural yield obtained from each catalyst are summarized in Table I-9.

Table I-9: Overviews of different heterogeneous catalysts for furfural production.

***T* (°C)**	**Substrate**	**Solvent**	**Catalyst**	**Fur yield (%)**	**Ref.**
			Metal oxide-based		
170	Xylose	Water/toluene	Nb_2O_5	50	García-Sancho et al. (2014)
170	Xylose	water/n-butanol	SO_4^{2-}/ZrO_2-TiO_2	54.3	Zhang et al. (2012)
160	Xylan	Water	Cr-$LaCo_{0.8}Cu_{0.2}O_3$	21.2	Li et al. (2013)
			Solid phosphates		
170	Xylose	Water	ZrP-HT via the hydrothermal method	52	Cheng et al. (2013)
160	Xylose	Water	$Nb_3O_{20}P_5$	43	Bernal et al. (2015)
150	sugarcane bagasse (SCB)	Water	$Nb_2O_2 \cdot nH_2O$ ($NbOPO_4 \cdot nH_2O$	52.1 g/kg of SCB 59.3 g/kg of SCB	Catrinck et al. (2020)
150	Wheat straw	Water	$FePO_4$ + NaH_2PO_4	92	Xia et al. (2017)
160	Xylose wheat straw	water/tetrahydrofuran (THF)	$CrPO_4$	88 67	Xu et al. (2018b)
170	Xylose	Water	$CrPO_4$	52	Cheng et al. (2013)
			Heteropolyacids		
140	Xylose	DMSO	cesium salts of 12-tungstophosphoric acid (CsPW)	45	A. S. Dias et al. (2006)
200	Xylose	Water/DMSO	($SnxCs_{3-4x}PW$)	63	Guo et al. (2018)

140	Xylose	DMSO	$H_{14}[NaP_5W_{30}O_{110}]$	73	Pardo Cuervo et al. (2020)
			Zeolites and other mesoporous silica-alumina		
170	Xylose	Water	H-mordenite (Si/Al=10)	21	Metkar et al. (2015)
200	Xylose	Water	H-ZSM-5	46	O'Neill et al. (2009)
170	Xylose	Water	H-MCM-22	71	Jae et al., 2011
170	Xylose	Water/ GVL	H-mordenite	80	Gürbüz et al. (2013a)
170	Xylose	Water/toluene	Delaminated H-Nu (Si/Al=29)	47	Lima et al. (2008)
260	Xylose	Water/toluene	H_3PO_4-Mordenite 13	98	Lessard et al. (2010)
170	HemiCel	Water/N_2	HUSY (Si/Al=15)	12	Dhepe and Sahu (2010)
170	Xylose	Water/toluene	SAPO-11	34-38	Lima et al. (2010c)
140	Xylose	Water/toluene	H-Beta	25	Kim et al.
	Xylose	DMSO	H-mordenite	24	(2011)
170	Bagasse	Water/p-xylene	HUSY (Si/Al=15)	18	Sahu and Dhepe (2012)
160	Bagasse	Water/toluene	SAPO-44	93	Bhaumik and Dhepe (2014)
180	Xylose	SBP/NaCl-DMSO	Sn-MMT	82	H. Li et al.
	Corncob			54	(2015)
190	Xylose	Water/GVL	SAPO-34	40	Bruce et al.
	Switchgrass			31	(2016)
			Carbon-based catalysts		
200	Xylose	Water	sulfonated graphene oxide	61	Lam et al. (2012)
200	Corn stover	GVL	sulfonated mesoporous carbon material (SC-CaC_t-700)	93	Li et al. (2017)
	Xylose		resorcinol-	80	
170	corn stover	Water	formaldehyde resin carbon	68.6	Zhu et al. (2017)
175	Xylose	Water/CPME	Starbon®450-SO_3H	64.6	Gómez Millán et al., 2019b
			Supported catalysts		
170	Xylose	Water	propylsulfonic SBA-15	85	Agirrezabal-Telleria et al. (2012)
170	Xylose	Water	Al-TUD-1 (Si/Al = 21)	60	Lima et al., 2010a
170	Xylose	Water	zeolite Beta (BEA) (Si/Al = 12) TUD	74	Lima et al., 2010b
180	Xylan	Water (NaCl)/THF	silica supported hafnium phosphide (HfP/SiO_2)	85	(Xu et al., 2020).

Polymeric solid catalysts/Sulfonated biopolymer					
150	Xylose	DMSO	Nafion 117	60	Lam et al., 2011b
190	Xylose Xylan	Water (NaCl)/CPME	sulfonated sporopollenin (SSP)	69 37	Wang et al. (2017b)
175	Xylose	Water/toluene	Amberlyst 70	70	Agirrezabal-Telleria et al. (2011)
120	Arabinose, rhamnose, lactone	DMF	Amberlyst 15, hydrotalcite	21.1-26.5	Tuteja et al. (2012)
140	Xylose	Water/toluene Water/DMSO	SBA-15, Amberlyst 70	55 59	Agirrezabal-Telleria et al. (2012)
140	Xylose	[Bmim]Cl	Amberlyst-5	80	Zhang et al. (2013a)
170	Xylose Arabinose Xylan	Water/CPME	Nafion NR-50, NaCl	80 42 55	Le Guenic et al. (2016)
175	Corncob	GVL	SPTPA	74	Zhang et al. (2017)
170	Corn stover	MIBK	Purolite CT275	80	Mittal et al. (2017)
190	Corn stover	Water/GVL	MSPFR	43.4	T. Zhang et al. (2018)
170	*Camellia oleifera* shell	Water/γ-butyrolactone	PDVB-SO_3	61.3	Zhang et al. (2018a)

Regarding the type of acid, it was found that some heterogeneous catalysts can function as both Lewis and Brønsted acids. This contrasts with homogeneous catalysts, which are predominantly Brønsted acids, except for metal salts, which act as Lewis acids. The identified Lewis acid heterogeneous catalysts include metal oxide-based compounds, solid phosphates, zeolites, and other mesoporous silica-alumina. The Lewis acid properties of these heterogeneous catalysts arise from the presence of metal ions serving as Lewis acidic sites, such as Al, Nb, Fe, Sn, etc.

Consequently, the reaction mechanism for converting C_5 sugars into furfural differs when using Lewis acid heterogeneous catalysts compared to homogeneous catalysts or purely Brønsted acid heterogeneous catalysts as previously explained. This difference explains the variation in furfural yield and selectivity between different types of catalysts. Furthermore, it was discovered that the ratio between Brønsted (B) and Lewis (L) acidic sites can impact furfural production. A higher B/L ratio results in high furfural selectivity with a low consumption rate of xylose (Xing et al., 2016). Table I-10 presents the benefits and disadvantages of homogeneous and heterogeneous catalysts.

Table I-10: Benefits and disadvantages of homogeneous and heterogeneous catalysts.

Catalyst type	Advantages	Drawbacks
Homogeneous	-High catalytic activity	-Separation challenges
	-Selective catalysis	-Catalyst Deactivation (side reactions)
	-Ease of control	-Environmental Impact (toxic)
	-Higher solubility (easily interact)	-Higher cost
Heterogeneous	-Easy separation	-Lower Activity
	-Higher stability (longer catalyst lifetimes)	-Mass Transfer Limitations
	-Reusability	-Selectivity Challenges
	-Environmental Friendliness	-Complex Catalyst Synthesis

Ultimately, the choice between homogeneous and heterogeneous catalysis depends on the specific needs of the reaction, including cost, environmental impact, selectivity, catalytic activity, and ease of separation. The selection of the most appropriate catalytic process will rely on the specific requirements of the reaction under investigation, as each type of catalysis has its own advantages and disadvantages. As previously discussed, despite the drawbacks of homogeneous catalysts, particularly the challenges in separation, **formic acid** was chosen as the catalyst for furfural production in this study.

I.3.2.2 Solvent systems

Besides the development of catalysts, which greatly affects the conversion of biomass into furfural, the reaction environment is considered another critical factor playing a vital role in furfural production. Due to the different properties and different functional groups of solvents, they are not just a physical medium but can also be another reactant involved in dispersion and conversion of xylose as well as distribution, degradation, and separation of furfural (Zhao et al., 2021). Thus, gaining insight into various solvents will be necessary in order to optimize the furfural synthesis. The solvent systems can be divided into two categories: single-phase systems and biphasic systems. This section will detail each individual system.

Monophasic system

Water

Since water is an ecologically safe, cheapest, and most abundant solvent that is widely spread throughout nature, it is revealed as an interesting solvent choice for industrial applications. Depending on the conditions of temperature and pressure, the properties of water will be changed, having consequences for chemical reactions. When the temperature and the

pressure of water are under the related values defining the critical point (T_c = 374 °C, P_c = 22.1 MPa, ρ_c = 320 kg/m^3) (Kruse and Dinjus, 2007), subcritical water, also called hot compressed water, is obtained which has two unique characteristics (Zhao et al., 2021). First, it has a low relative dielectric constant, similar to that of ambient methanol and acetone (Eckert et al., 2000), and can thus be used to extract hydrophobic substances from various resources (Rodríguez-Meizoso et al., 2006). The another is a high ion product, meaning that the concentrations of hydrogen and hydroxyl ions are high compared to ambient water. Therefore, water can act as an acid or base catalyst for the hydrolysis and dehydration of biomass without the use of an additional catalyst (Krammer and Vogel, 2000).

Antal et al. (1991) studied the dehydration of xylose in high temperature liquid water (HTLW) at 250 °C. Approximately 30% of furfural yield was attained for 100 s without any acid catalyst addition. The dehydration of xylose into furfural is possibly carried out by an autocatalytic involving an acidic product of xylose composition like formic acid. Later, the kinetics of non-catalyzed decompositions of xylose and its decomposition product furfural in HTLW were studied (Jing and Lü, 2007b). Under HTLW conditions, furfural and formic acid were the main products of xylose decomposition. In addition, furfural can degrade to formic acid, leading to the autocatalytic reaction as mentioned in the previous study (Antal et al., 1991).

García et al. (2019) used a central composite experimental design to optimize furfural production from southern cattail (*Typha domingensis*) plants by hydrolysis with water (autohydrolysis). Based on the response surfaces, the highest furfural concentration of 3.14 g/L was achieved at 189 °C for 45 min, corresponding to 24% of xylan in the raw material. In spite of the intriguing properties of subcritical water, the furfural yield achieved is moderate, indicating that its simple use as an acidic catalyst for the dehydration of xylose cannot ensure a high furfural yield.

Ionic liquids

Ionic liquids (ILs) are salts (e.g., salts which are liquids below 100 °C) composed of large organic cations and inorganic or organic anions (Stark, 2011). The unique properties of ILs, including very low volatility, good dissolving capacity, as well as chemical and thermal stability, make them attractive as a reaction medium for furfural production (Zhang et al., 2011). Moreover, some studies shown that IL can stabilize the platform molecules and the continuous removal could increase their yield (Sievers et al., 2009). Z. Zhang et al., 2014 also prove that some IL could be reused several times without a significant decrease in furfural yield

(68% after 8th runs against 75% for the first run). Although ILs show potential as solvents with their unique properties for furfural production, challenges are encountered for their utilization in the industry (Peleteiro et al., 2016a). The high cost of ILs is frequently highlighted in literature as a principle economic drawback (Tadesse and Luque, 2011). Moreover, some of them are found toxic, corrosive, and very hygroscopic, especially chloride based ILs. Anyway, because of "tunable" or "designable" character of ILs, they can be factionalized to form acidic ILs, either Brønsted (BAILs) or Lewis (LAILs), behaving as catalyst for xylose dehydration into furfural (Peleteiro et al., 2016b). Thus, the limitation of ILs' use dealing with their drawbacks associated with high used quantity was suppressed (Matsagar et al., 2017). SO_3H-functionalized ionic liquid namely 1-propylsulfonic-3 methylimidazolium chloride was investigated by Lin et al. (2017) and proved that due to the SO_3H group behaving as a Brønsted acid, the enolization of xylose and the subsequent dehydration of the intermediate to form furfural were effectively catalyzed. Additionally, chloride anion stabilizes the intermediates, leading to the selective formation of furfural.

In recent years, not only Brønsted acidic ionic liquids (BAILs), but also Lewis acidic ionic liquids (LAILs) have received extensive research. S. Wang et al. (2017) developed Lewis acidic ionic liquid 1-butyl-3-methylimidazolium chloroaluminate ([Bmim]Cl-$AlCl_3$, IL) for the furfural production from xylose and arabinose in GVL-water mixture. A maximum furfural yield of 79.76% was gained from xylose at 140 °C which was similar to what obtained in study of Serrano-Ruiz et al. (2012) where selected Brønsted acidic ionic liquid afforded 74% of furfural yield from xylose in aqueous solvent. Table I-11 summarizes the reported furfural yield values testing different ionic liquids for furfural production.

Table I-11: Overviews of different ionic liquids for furfural production

T (°C)	Substrate	Solvent	Catalyst	Fur yield (%)	Ref.
-	Pine wood	[Bmim]Cl	$CrCl_3$	31	Zhang and Zhao (2010)
120	Miscanthus Giganteus	[Bmim]HSO_4	[Bmim]HSO_4	33	Brandt et al. (2011)
160	Corncob	[Bmim]Cl	$AlCl_3$	19.1	Zhang et al. (2013b)
160	Corncob	[Bmim]Cl	$H_3PW_{12}O_{40}$	15.3	(L. Zhang et al., 2013a)
160	Xylose	[Bmim]Cl	$CrCl_3$	50	Peleteiro et al. (2014)
161	Wheat straw	[Bmim]HSO_4	[Bmim]HSO_4	32.2	Carvalho et al. (2015)
160	Eucalyptus wood	[Bmim]HSO_4	[Bmim]HSO_4	59.1	Peleteiro et al. (2016b)

T (°C)	Substrate	Solvent	Catalyst	Fur yield (%)	Ref.
130	Xylose Corn stalk	[Emim]Br	$SnCl_4$	71 55	Nie et al. (2019)
120	Rice husk Soy peel	Water, H_2SO_4	[Bmim]Br	34 59	Scapin et al. (2020)
100	Xylose	[Emim]HSO_4/toluene	[Emim]HSO_4	84	Lima et al. (2009)
150	Xylose	Water/MIBK	$[C_4SO_3Hmim]HSO_4$	91	Tao et al. (2011)
170	Xylose	Water/toluene	$[C_3SO_3Hmim]HSO_4$	73	Matsagar et al. (2015)
140	Xylose	Water/toluene	[Bmim] HSO_4	73.8	Peleteiro et al. (2015)
170	Beechwood	Water/toluene	[Bmim]HSO_4	85	Matsagar et al. (2017)
140	Xylose	Water/butanone	[Bmim]Cl/$FeCl_3$	75	Zhao et al. (2019)
140	Arabinose	Water/butanone	[Bmim]HSO_4	60	Zhao et al. (2019b)

Deep eutectic solvents

Owing to poor biodegradability, biocompatibility, sustainability and deep property understanding of ionic liquids, a special sort of IL named deep eutectic solvents (DESs) was developed (Loow et al., 2017). The extra advantages of DESs, which are low price, low toxicity, bio-degradability, environmental friendliness, and ease of preparation, making DESs receive recently a great attention and tend to be use alternatively to ILs as green media (L.-X. Zhang et al., 2014). DESs are made up by mixing two or more compounds, of which one is a hydrogen bond acceptor (HBA) and the other is a hydrogen bond donor (HBD). A high fraction of H-bonds which formed between HBD and the anion of HBA led to a high depression in the melting point of DESs (Paiva et al., 2014). It was been shown that differences in effectiveness of acid based DESs could be attributed to carbon chain lengths. Increasing the latter reduced the strength of H-bonds formed between HBA and HBD. This leads to a decrease in H^+ concentration in the system for hydrolysis and dehydration reactions (Lee et al., 2019). Table I-12 summarizes some of the studies of deep eutectic solvent system in furfural production.

Table I-12: Deep eutectic solvent system in furfural production

T (°C)	Substrate	Solvent	Catalyst	Fur yield (%)	Ref.
140	Xylan	ChCl-citric acid	ChCl-citric acid, $AlCl_3.6H_2O$ ChCl-citric acid, $FeCl_3.6H_2O$	51.3 50.1	Zhang and Yu (2013)
100	Xylan	ChCl-oxalic acid	ChCl-oxalic acid, $AlCl_3.6H_2O$ ChCl-oxalic acid, $FeCl_3.6H_2O$	39.8 38.4	L.-X. Zhang et al. (2014)
140	Macauba pulp	ChCl-oxalic acid	ChCl-oxalic acid, TiO_2	14.99	da Silva Lacerda et al. (2015)

T (°C)	Substrate	Solvent	Catalyst	Fur yield (%)	Ref.
160	Sunflower stalk	ChCl-oxalic acid	ChCl-oxalic acid	3.37	Sert et al. (2018)
160	Switchgrass	ChCl	ChCl-$AlCl_3$	48.22	Chen et al. (2018)
120	Rice straw	ChCl-lactic acid	ChCl-lactic acid	11.51	A.-L. Li et al. (2018)
140	Herbal residues	ChCl-FA	ChCl-FA, $SnCl_4$	49.6	Yu et al. (2019)
100	Oil palm fronds	ChCl-oxalic acid	ChCl-oxalic acid	9.74	Lee et al., 2019
150	Xylan	ChCl-malic acid/ GVL	ChCl-malic acid	75	Morais et al. (2020)

Use of supercritical CO_2

Since carbon dioxide (CO_2) is readily available, nontoxic, nonflammable, highly soluble in various organic solvent, and has a low critical temperature (31.1 °C) and pressure (73.9 bar), the use of supercritical CO_2 (Sc-CO_2) for biomass processing is gaining interest (Relvas et al., 2015). According to Sako et al. (1992), supercritical CO_2 is often used as an extraction medium. In this study, a maximum furfural yield of 69.9% was reached in the presence of 0.05 M H_2SO_4 with simultaneous Sc-CO_2 extraction, while the furfural yield without extraction did not exceed 40%. More than 80% of furfural selectivity was also obtained due to the fact that Sc-CO_2 extraction could suppress the side reaction of produced furfural. Later, (Sangarunlert et al., 2007) applied a two-level fractional factorial design method to optimize the production of furfural from rice husks over acid hydrolysis accompanied by Sc-CO_2 extraction. After optimization of parameters, the highest furfural yield of 90% was achieved by using a two-stage process with Sc-CO_2.

In the presence of water, carbonic acid can be produced in situ by the dissolution of CO_2 (Magalhães da Silva et al., 2014). The last acid dissociates due to its unstable nature, resulting in an increase in hydronium ion concentration, which can effectively promote the hydrolysis of biomass and further dehydration of sugars into furans (Morais et al., 2015). Since CO_2 is removed during the depressurization step, this acidification does not consequently cause corrosion problems, as encountered in industrial processes with mineral acids (Toscan et al., 2017).

Gairola and Smirnova (2012) explored the use of Sc-CO_2 for furfural extraction in the hydrothermal conversion of xylose and hemicellulose. It was observed that xylose conversion was, in all cases, 97%, which was higher than the predicted value (95%). This phenomenon might be attributed to a rate enhancement due to the catalytic effect of carbonic acid formed by

dissolved CO_2 in water. Simultaneous Sc-CO_2 extraction led to high furfural yields of 68% from xylose at 230 °C and 12 MPa, while a lower value was obtained when biomass hydrolysates were used under the optimum conditions. Later, Morais et al. (2016) proposed a novel method where xylose and hemicellulose from wheat straw were converted into furfural by a CO_2-catalyst in a water/THF system with MIBK as the extracting solvent. A high furfural yield of 56.6% and selectivity of 62.3% were obtained from xylose at 180 °C and 5 MPa of CO_2 pressure for 60 min. Under the same conditions, hemicellulose sugar yielded 43% of furfural with a selectivity of 44%. Recently, Sato et al. (2019) investigated the influence of Sc-CO_2 extraction on the furfural production using solid acid-catalyzed batch and semi-batch processes. Compared to the biphasic water/toluene system, the water/CO_2 batch system produced a lower furfural yield for all employed catalysts. This is explained by the fact that furfural is less soluble in Sc-CO_2 than in toluene. Utilizing a semi-batch reactor with continuous CO_2 flow enhanced the furfural production, reaching the highest furfural yield of 52.3% with Amberlyst-70 and a CO_2 flow rate of 3.77 g/min at 150 °C.

Green solvents

Since water is an inexpensive, green, and abundant solvent, it has been extensively used in large-scale furfural production as a reaction medium (Kim et al., 2020). However, numerous studies showed that water, due to its strong polarity, promotes several furfural degradation reactions (e.g., fragmentation, resinification and condensation) resulting in low furfural yield and selectivity (Gürbüz et al., 2013; Hu et al., 2014). This is why other green solvents have recently been investigated in order to overcome these obstacles and meet the development of green reaction process.

Hu et al. (2014) investigated the acid-catalyzed conversion of xylose to furfural by Amberlyst 70 in 20 solvents including water, alcohol, ketones, furans, ethers, esters, hydrocarbons, and aromatics. Among them, DMSO afforded the highest furfural yield because it can preserve furfural in an acidic medium by providing a shielding effect. However, the separation of produced furfural from DMSO is problematic because their boiling points are relatively closed: 162 °C and 189 °C for furfural and DMSO, respectively. 2-Butanol was another promising solvent in this study since it could stabilize the reactive intermediates and promote the formation of furfural with a maximum furfural yield higher than 55%. This finding was in agreement with that reported one (Iglesias et al., 2016) where 2-propanol was the most appropriate solvent compared to other alcohols for furfural production by using H-ZSM-5 as a catalyst. It was also found that the formation of furfural in acetone was rapid. Nevertheless, the

acetone can react with furfural, forming an undesired product via condensation, leading to a low yield with prolonged reaction time.

Recently, a novel green solvent, namely γ-valerolactone (GVL), has increasingly attracted attention because of its advantages in furfural production. Alonso et al. (2013) found that the GVL increases the stability of the furfural and the reaction rate of cellulose conversion in the simultaneous conversion of hemicellulose to furfural and cellulose to levulinic acid (LA). Moreover, GVL can solubilize lignin and other degradation products (i.e., humines), eliminating plugging problems in flow reactors and solids accumulation issues in batch reactors. Because of the higher boiling point of GVL (208 °C), desired furfural can be continuously removed from reaction medium by distillation under elevated temperatures (137 °C) without any product degradation. Later, the reaction kinetic study on the acid-catalyzed conversion of xylose into furfural was done by Mellmer et al. (2014). The activity energy for furfural formation was found to be lower in GVL (114 kJ/mol) than in water (145 kJ/mol), and the use of GVL increased the barrier for furfural degradation, leading to high selectivity. Furthermore, the stability of acidic protons was affected by GVL, resulting in an acceleration of the reaction rate. Indeed, a maximum furfural yield of 71.68% was obtained from corn cob using H-ZSM-5 and GVL as the catalyst and the solvent, respectively, at 190 °C for 60 min (X. Li et al., 2018). Table I-13 summarizes some of the studies of organic solvent system in furfural productions.

Table I-13: Organic solvents for furfural production

***T* (°C)**	**Substrate**	**Solvent**	**Catalyst**	**Fur yield (%)**	**Ref.**
170	Corn stover	GVL	H_2SO_4	63	Alonso et al. (2013)
160	Corn fiber	GVL	H-Beta zeolite	62	Gallo et al. (2013)
175	Poplar wood chips	GVL	H-mordenite zeolite	75	Gürbüz et al. (2013)
185	Corncob	GVL	$FeCl_3$	79.6	L. Zhang et al. (2014)
175	Wheat straw	Methanol	H_2SO_4	40.6	Grisel et al. (2014)
170 190	Xylan Corn stalk	GVL	PTSA-POM	69.2 83.5	Xu et al. (2015)
280	Oil Palm Fronds	Ethanol	Formic acid	35.8	Yong et al. (2016)
175	Corncob	GVL γ-butyrolactone γ-undecalactone	Sulfonated polytriphenylamine	66 59.9 53	Zhang et al. (2017)
200	Corn stover	GVL γ-butyrolactone	Sc-CaC_t-700	93 89	Li et al. (2017)
200	Xylose	GVL	OMC-SO_3H	58.6	Wang et al. (2021)

As detailed in this section, there are many types of solvents used in single-phase systems where xylose dehydration into furfural occurs. Among them, water is the most commonly used in the industry due to its low cost and wide availability. Green solvents such as DMSO, CPME, GVL, and CO_2 have also attracted attention to support the development of environmentally friendly reaction processes. New solvents, like ionic liquids (ILs) and deep eutectic solvents (DESs), have been the subject of extensive research to increase process efficiency and achieve the goals of green chemistry. In addition to their ability to dissolve biomass, ILs and DESs have strong acidic properties, enabling them to act as both catalysts and solvents without the need for additional catalysts, thereby fulfilling the principles of sustainable development. Despite the advantages of these solvents, side reactions that reduce furfural yield still pose a challenge. In this context, using a biphasic system appears to be an appealing approach to increase process productivity by preventing secondary degradation reactions through the continuous removal of furfural from the reaction medium. The details of this system are provided below.

Biphasic systems

The use of a biphasic system including an aqueous phase and an organic phase is a promising way to go for improving furfural production. In this system, desirable furfural is extracted once it is produced from the aqueous phase into the organic phase. This leads to suppression of furfural degradation reactions, which are carried out in the aqueous phase (L. Zhang et al., 2018). In order to avoid the latter reactions, a suitable solvent for extracting furfural must exhibit some properties like good chemical stability, no azeotrope formation with furfural, a high furfural partition coefficient, and minimal mutual solubility in water (Lin et al., 2015). The different solvents used as organic phases in biphasic systems for furfural production are: MIBK, toluene, cyclohexanol, 2-MeTHF and THF (Xu et al., 2018).

In a two-phase system at a 1: 1 mass ratio of MIBK to aqueous xylose solution, it was found favorable for the dehydration of xylose to furfural in acidic media (0.1 M HCl) (Weingarten et al., 2010). Under given optimum conditions, over 80% of furfural yield was achieved, which was two-fold more than that obtained in the single aqueous phase system. Based on kinetic study, the addition of extracting solvent to form a biphasic system did not alter the fundamental kinetics of its monophase analogue. Gómez Millán et al. (2019a) evaluated the furfural production from xylose in auto-catalyzed conditions using a biphasic system including water-immiscible solvents, namely isophorone, 2-MTHF and cyclopentyl

methyl ether (CPME). Among them, CPME afforded the highest furfural yield of 78% for 93% of selectivity at organic solvent to aqueous solution volume ratio of 1:1. A relative high furfural yield (71%) was also given by using 2-MTHF under similar conditions while water-isophorone system accomplished the lowest furfural yield (48%).

Another advantage of the biphasic systems' use is the reusability of the homogeneous catalyst existing in the aqueous phase, leading to an effective and environmentally friendly furfural production process. The results indicated that the activity of $FeCl_3$ contained in the aqueous phase after removing the organic CPME phase was maintained during four consecutive tests (Guenic et al., 2015). The corresponding furfural yield ranged from 76 to 80%. However, the furfural yield had to decrease slightly to 70% after the four consecutive runs.

Moreover, the use of biphasic system with heterogeneous catalysis could improve the process of furfural production by enhancing product yield, separation and recovery. Xu et al. (2018a) used chromium phosphate ($CrPO_4$) as a catalyst in a water/THF biphasic system for furfural production. Under given optimum conditions, 88% and 67% of furfural yields were afforded from xylose and wheat straw, respectively. Furthermore, it was found that the $CrPO_4$ was easily recovered and that great catalytic activity was available where a moderate 47% furfural yield was achieved after four cycles. Table I-14 summarizes some furfural productions using biphasic system.

Table I-14: Biphasic solvent system for furfural production

***T* (°C)**	**Substrate**	**Solvent**	**Catalyst**	**Fur yield (%)**	**Ref.**
160	Poplar	Water/THF	$AlCl_3.6H_2O$, NaCl	64	Y. Yang et al. (2012)
170	Cardoon	Water/CPME	H_2SO_4, NaCl	> 80	Campos Molina et al. (2012)
-	Xylose	Water/toluene	H_2SO_4, NaCl	83	Rong et al. (2012)
170	Maple wood	Water/MIBK	H_2SO_4	85.3	T. Zhang et al. (2013)
160	Corn stover	Water/THF	γ-Al_2O_3/SO_4^{2-}	35.9	Yi et al. (2013)
140	Corncob	Water/toluene	$CrCl_3.6H_2O$, NaCl	23.9	Y. Zhang et al. (2014)
170	Bagasse	Water/toluene	SAPA-44	< 30	Bhaumik and Dhepe (2014)
150	Xylan	Water/2-MTHF	$SnCl_4$	78.1	Wang et al. (2015)
160	Pine	Water/toluene	H_2SO_4, $ZnSO_4$	64.4	Li et al. (2016)
170	Concentrated pre-hydrolysis liquor-NaCl	CPHL-NaCl/DCM	Sulfonated carbon based	81.1	Deng et al. (2016)

T (°C)	Substrate	Solvent	Catalyst	Fur yield (%)	Ref.
170	Corn stover	Water/MIBK Water/toluene	H_2SO_4	80.1 76.3	Mittal et al. (2017)
200	Pubescens	Water/THF	NaCl	76.9	Luo et al. (2017)
190	Corncob	Water/toluene	SO_4^{2-}/SnO_2-MMT	66.1	Qing et al. (2017)
150	Sugarcane bagasse	Water/acetone	H_3PO_4	45.8	Wang et al. (2018)
190	Xylose	Water/2-sec-butylpnol	-	59	Gómez Millán et al. (2021)
170	Liquid *Quercus mongolica* hydrolysate	Water/DMSO	H_2SO_4	68.2	Kim et al. (2020)

Regarding the solvent system, water was chosen for the batch system in this study due to its advantages such as low cost, abundance, and ecological safety. Additionally, green organic solvents, including cyclopentyl methyl ether (CPME) and ethyl butyrate (EB), were used in a biphasic system to simultaneously extract the formed furfural. This approach avoids the side reactions that occur in the aqueous phase, enhancing furfural yield and selectivity.

I.3.2.3 Reaction conditions

Reaction temperature, reaction duration, catalyst and sugar loading, as well as a catalyst/xylose and solid/liquid ratio, are all frequent operational parameters examined in the literature for catalyzed furfural production (W. Yang et al., 2012; Papaioannou et al., 2019; Wang et al., 2021).

Reaction temperature

The reaction temperature is the most important factor in all thermochemical conversion processes, and influential in the distribution of formed products (O'Neill et al., 2009; W. Yang et al., 2012). In general, for industrial batch or continuous furfural production processes, the reaction temperature ranging from 153 °C to 184 °C is investigated (Dias et al., 2010).

According to many publications, increasing the reaction temperature accelerates the depolymerization of pentosan and the dehydration of xylose to furfural, resulting in a high furfural yield. At 200 °C for 45 min, a 77% furfural yield and complete xylose conversion were accomplished, while at 160 °C for 90 min, a lower furfural yield of 30% with a 60% xylose conversion was reached (Wang et al., 2021). W. Yang et al. (2012) also reported that a high furfural yield was obtained at elevated temperatures when optimizing furfural production from

xylose catalyzed by formic acid. Specifically, the highest yield of 74% was achieved at 180°C, while a lower yield of 50% was observed at 160 °C under the same reaction conditions.

A high reaction temperature, on the other hand, can enhance another competing mechanism, namely the formation of liquid and/or solid products via repolymerization, condensation, and cyclization of the intermediates that consume the liquid products, including furfural. O'Neill et al. (2009) investigated the dehydration of xylose to furfural catalyzed by ZSM-5 zeolite. They observed that furfural had degraded to half of its highest value after 10 min at 220 °C, whereas the best furfural yield was obtained at 200 °C. Furthermore, Gao et al. (2014) found that when the temperature reached over 190 °C, which was the optimum temperature in this investigation, not only the yield but also the selectivity of furfural declined drastically. Yemiş and Mazza (2011) also discovered that at 190 °C, the drop in furfural yield from xylan was accompanied by an increase in solid char yield. W. Yang et al. (2012) reported a similar observation, stating that at 160 °C, minimal resin adhered to the autoclave's internal wall. However, as the reaction temperature increased from 190 °C, its quantity increased dramatically. Based on the kinetic analysis, the ratio of the rate constant of dehydration of xylose into furfural to the rate constant of the accompanying side reactions rose with increasing reaction temperature (W. Yang et al., 2012). As a result, a suitable temperature must be determined to achieve a balance between the rates of creation and degradation of furfural, leading to high yield and selectivity of furfural.

According to the literature review of furfural production in different systems catalyzed by various types of catalysts, the temperatures investigated ranged from 120 °C to 280 °C. Most studies found that effective furfural production occurs at temperatures between 140 °C and 200 °C. Therefore, this study focused on investigating furfural production within this temperature range of 140-200 °C.

Reaction time

Reaction time is another important factor with great influence on the dehydration of xylose (Guenic et al., 2015). Doiseau et al. (2014) discovered that the furfural yield increased with reaction time when employing different solid acid catalysts in pure water. Longer reaction periods have increased the generation of by-products for a category of catalysts, such as strong acids. Prolonged reaction durations at 150 °C for weaker solid acids have little effect on furfural selectivity. Later, Jaafari et al. (2019) found that regardless of catalyst type, the furfural yield declined as reaction time rose. Agirrezabal-Telleria et al. (2011) investigated the evolution of the furfural yield in a biphasic water/toluene system at 175 °C for non-catalyzed reaction

systems or reaction systems catalyzed by sulfonic ion-exchange resins (Amberlyst 70). Their results demonstrated that the furfural yield reached its maximum value at 150 min and subsequently gradually declined. They also mentioned that the yield-loss reaction was promoted by an extended residence time. This result was similar to one previously described in which ethanol was utilized as an extractive phase. The furfural yield increased significantly for the first 20 min before declining when the reaction time was increased to 30 min (Yong et al., 2016). Based on liquid–liquid equilibrium, the furfural in the extractive phase would return to the aqueous phase when the furfural in the aqueous phase degraded. As a result, the furfural yield declined as the residence time increased (Yang et al., 2013).

In addition, reaction temperature and time have a significant impact on furfural production (Riansa-ngawong and Prasertsan, 2011). According to (Lamminpää and Tanskanen, 2009), maximal selectivity and yield would be reached with shorter reaction times at higher temperatures. Furfural resinification was increased by longer reaction periods (> 20 min) at high temperatures (200 °C), resulting in low furfural selectivity and yield. Riansa-ngawong and Prasertsan (2011) optimized the conditions for furfural production for furfural synthesis from hemicellulose derived from delignified palm pressed fiber (dPPF) by using sulfuric acid as a catalyst. It was shown that higher furfural yields (4.92-8.52 g/L) can be obtained at a higher temperature with a shorter reaction time (140 °C/90 min) than at a lower temperature with a longer reaction time (120 °C/150 min). Delbecq et al. (2016) studied betaine-formic acid combination catalysts for the conversion of xylose to furfural in a cyclopentylmethyl ether (CPME)-water biphasic system. After 20 min of stirring at 180 °C, 63% of the yield was produced, which was higher than that obtained at 170 °C for the same period. Unfortunately, the furfural selectivity was significantly lower, at 87% against 92% at 170 °C.

As previously discussed, in a batch system, high temperature with a short reaction time seems preferable to low temperature with a longer reaction time, as the latter increases contact between the formed furfural and other molecules, enhancing side reactions that lower furfural yield. However, in semi-batch and continuous systems where furfural is extracted from the reaction medium, a longer reaction time at moderate temperature could be beneficial. This depends on the extraction rate, reaction rate, and the capacity of the extracting agent to efficiently remove furfural from the reaction medium.

Initial xylose concentration

In acid catalytic dehydration of xylose, the initial xylose concentration has a significant impact on furfural yield and selectivity (Xing et al., 2011). Tao et al. (2011) used the acidic

ionic liquid 1-(4-sulfonic acid) butyl-3-methylimidazolium hydrogen sulfate as a catalyst in a methyl isobutyl ketone (MIBK)-water biphasic system to design a catalytic process for the conversion of xylose to furfural. With varied beginning concentrations of xylose, the rate of xylose conversion had minimal effect, but the furfural yield decreased gradually as the initial xylose concentration increased. When the amount of xylose was doubled (from 1 g/L to 2 g/L), the furfural production dropped from 91.4% to 78%. The decrease in furfural yield was caused by a higher xylose concentration, which increased the secondary loss reactions (self- or cross-polymerization) (Dunlop, 1951). This effect is more important when employing a complex starting material, such as oil palm biomass, as described by Yong et al. (2016). Furfural loss processes occur not only between furfural but also with other intermediates and fragments in the biomass, lowering furfural yield in this case.

More recently, Delbecq et al. (2016) investigated the conversion of xylose to furfural in a biphasic system including CPME and water. They discovered that when the amount of xylose in the mixture increased, the yield of furfural became inversely proportional to the amount of xylose. Because of the increased viscosity of the aqueous layer, the yield began to decline after the content reached 600 g/L. As a result, efficient furfural extraction by CPME was prevented, resulting in a significant rate of cross-polymerization between produced furfural and xylose. Similar findings were reported by xylose According to the authors, the viscosity of the reaction fluid increased as the substrate concentration increased, resulting in non-uniform heating in the microwave reactor and difficulty for the extracting solvent in accessing furfural (Weingarten et al., 2010; Saggadi et al., 2014).

Low initial xylose concentrations, on the other hand, necessitate a larger reactor and greater heat to produce the same amount of furfural in a commercial process. Thus, the initial xylose concentration should not be too low for economic reasons (W. Yang et al., 2012a), as suggested by previous studies (Yang et al., 2012; Baktash et al., 2015; Kangle et al., 2023), with a recommended range between 50 g/L to 100 g/L. Nevertheless, the amount of xylose obtained from untreated biomass using any method appeared to be below 50 g/L. For example, the highest concentration of xylose achieved from raw biomass using the LEEBio^{TM} process was 30 g/L. This concentration will be used as the maximum concentration examined in this study.

Catalyst dosage

In the context of catalytic conversion, catalyst dosage is a critical factor that has a significant impact on the formation of furfural (Zhang et al., 2016). Yang et al. (2013)

conducted a study to investigate the impact of formic acid concentration (ranging from 5 to 25 g/L) on furfural production from xylose in a water-o-nitrotoluene system. The results showed that the furfural yield initially increased and then decreased as the formic acid concentration increased. Additionally, there was a slight decrease in selectivity with increasing formic acid concentration. This finding corroborated the report by Lamminpää and Tanskanen (2009).

Under atmospheric pressure, Rong et al. (2012) examined the dehydration of xylose to furfural in a biphasic mixture of toluene and an aqueous solution of xylose with H_2SO_4 as a catalyst. They found that the yield of furfural was higher in high-concentration H_2SO_4 systems than in low-concentration H_2SO_4 systems. The highest furfural yield, 75%, was achieved using a 10% (w/w) acid concentration. However, increasing the H2SO4 concentration further to 12.5% (w/w) resulted in a decreased yield of 51%. Mittal et al. (2017) discovered that as the acid concentration increased, xylose conversion increased as well, approaching total conversion at 0.05 and 0.1 M H2SO4. With increasing acid concentration, the furfural yield also increased, reaching a maximum yield of 76% at 0.05 M H2SO4. However, increasing the acid content (to 0.1 M) resulted in a reduction in furfural yield to 71%. Furthermore, according to Xing et al. (2011), a high acid concentration is required to achieve good furfural selectivity. As the HCl concentration raised from 0.22 M to 0.44 M, the furfural selectivity increased from 79.4% to 92.0%. However, when the HCl concentration was increased to 0.57 M, the furfural selectivity dropped to 84%. This was probably due to the fact that excessive catalyst use resulted in side reactions including xylose dehydration to various aldehydes, furfural degradation, or furfural polymerization (Xu et al., 2018a). Furthermore, xylose generates oligosaccharides with reactive hydroxyl groups, resulting in increased cross polymerization rates with reactive intermediates and furfural (Rong et al., 2012). All of the findings suggest that acidity levels higher than the optimum have a negative impact on the conversion of xylose to furfural. To produce a high furfural yield and selectivity, the optimal acid concentration will be necessary.

Solid/liquid ratio

When raw biomass is employed as a starting material, the solid/liquid ratio becomes one of the most critical elements to optimize in order to achieve the highest yield (H.-L. Li et al., 2013). The impact of the solid/liquid ratio on furfural yield was only mentioned in one paper. Li et al. (2013) investigated the conversion of xylan to furfural in ultrapure water using chromium-loaded perovskite-type oxides as a solid catalyst. The furfural production rose with the weight ratio of xylan to water, reaching the highest furfural yield of 13.7% at 160 °C for 8

h in a 1:600 weight ratio. When the weight ratio was adjusted to 1:800, however, the yield fell to 10.5%. It is possible that this is due to the water molecule competes for available protons with the hydroxyl groups on xylose, reducing catalytic activity.

Ratio of aqueous phase to organic phase

Aside from the nature of the organic solvent, as previously mentioned, the ratio of aqueous and organic phases has a significant impact on extraction performance and thus furfural selectivity when exploring biphasic system (Aellig et al., 2015; Papaioannou et al., 2019).

According to Yang et al. (2013), the volume percentage of the extracting solvent (o-nitrotoluene) had a substantial impact on the furfural yield and selectivity. The furfural yield and selectivity increased from 30% to 70% and 70% to 99%, respectively, as the o-nitrotoluene volume percentage grew from 0 to 80%. By vigorous stirring at high speed, the reactive solution was dispersed in o-nitrotoluene. Each aqueous drop can be thought of as a mini-reactor. Furfural was produced in aqueous droplets and then extracted into the organic phase right away. This maintained a low concentration of furfural in aqueous solution, resulting in good selectivity due to the elimination of several side reactions (Rong et al., 2012). At high o-nitrotoluene volume percentage, the aqueous drop became significantly smaller which had a distinct character and resulted in a high yield of furfural.

Gómez Millán et al. (2021) found that furfural yield builds up as the aqueous-to-organic volume ratio rises from 1:5 to 1:1, reaching the maximum furfural production (17%) in 0.5h at 190 °C with a 1:1 aqueous-to-2-sec-Butylphenol (SBP) phase ratio. At high aqueous-to-organic volume ratios, however, the formation of increased degradation products prevented a high furfural yield. The furfural selectivity rose as the aqueous-to-SBP phase ratio was increased from 1:5 to 1:2 (by volume), but decreased as the ratio was increased to 5:1. A similar observation was made by Gómez Millán et al. (2019a), when isophorone, 2-MTHF, and CPME were used as extraction agents. They believe this is due to the saturation of the SBP's ability to extract furfural; as a result, the latter remains in the aqueous phase, where degradation reactions may occur. Even though increasing the organic to aqueous phase ratio in a biphasic solvent system improves furfural production performance, it is not practical for industrial applications because it increases reactor volumes, downstream separation costs, and overall energy demand (Papaioannou et al., 2019; Gómez Millán et al., 2019c).

As discussed above, an appropriate volume ratio between the aqueous and organic phases is crucial for achieving high furfural yield and selectivity. A high aqueous-to-organic

phase volume ratio is unfavorable for furfural production due to the saturation of furfural in the organic phase. Conversely, a lower aqueous-to-organic phase volume ratio is advantageous for furfural production. However, this ratio should not be too low due to the associated process cost. In this study, a wide range of volume ratios between aqueous and organic phases, including 1:1, 1:3, 1:6, and 1:13, was explored. The purpose of using a very low ratio (i.e., 1:13) was to gain further insights into this effect, as no previous studies have investigated this ratio.

All these operating parameters must therefore be selected carefully, as they have a major influence on the performance of the process. Table I-15 groups together the fields of study that seem interesting according to the state of the art and should be covered in this manuscript.

Table I-15: value ranges of operating parameters investigated for furfural production.

Parameter	Unit	Value range
Reaction Temperature	°C	0 – 200
Residence time	h	0 – 5
Initial xylose concentration	g/L	10 – 30
Catalyst dosage (Formic acid)	wt%	0 – 30
Ratio of aqueous to organic phases	v/v	1:1 – 1:13

The domains have been deliberately chosen to be fairly broad to allow for more comprehensive modeling. This approach aims to subsequently develop a robust optimization model with a wider range of optimization options.

I.3.3 Possible separation methods of furfural

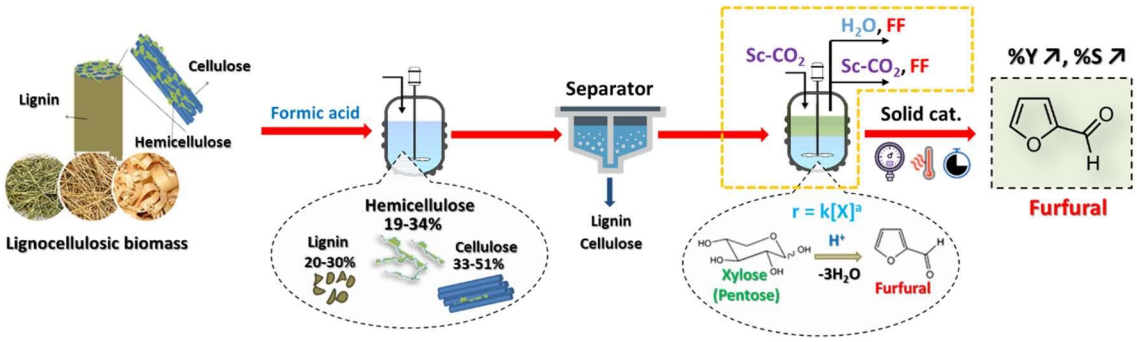

As formed furfural can undergo the secondary loss reactions (i.e., polymerization and condensation) due to its active aldehyde and furan groups. Separating produced furfural from catalytic system is thus required which is very significant for its subsequent transformation and application (Hu et al., 2020). Conventional processes for furfural separation are distillation,

solid adsorption and liquid-liquid extraction (LLE) (Pei et al., 2008; Mao et al., 2021). The characters and some examples of each technique are detailed below.

I.3.3.1 Distillation

The vapor-liquid equilibrium for the furfural-water system reveals an azeotrope with an atmospheric boiling point of 97.85 °C at 36% furfural (Zeitsch, 2000). Condensation of vapors with this composition results in two phases, allowing furfural recovery (Vila et al., 2003). As shown in Figure I-13, a typical simple distillation plant comprises of two distillation columns. Because the heterogeneous azeotrope of furfural-water is separated at the top of the column, while other heavy components (such as extractives, levulinic acid, and sulfuric acid) are discovered at the bottom, the first column is referred to as an azeotropic column. The furfural-water azeotrope is subsequently separated into two liquid phases using a decanter. The light aqueous phase is returned by reflux to the first column, while the heavy furfural-rich phase is introduced to the second distillation column. Finally, high-purity furfural is collected from the bottom of the column, while azeotrope is fed to a decanter before being recycled back to the first column (Zeitsch, 2000; Nhien et al., 2021).

Mandalika and Runge (2012) investigated batch reactive distillation to produce furfural with a high yield from pentosans extracted from biomass. By continually removing vapors from the reactor headspace and condensing them to obtain a dilute furfural solution, this technique was able to produce more than 85% of the furfural yield. Metkar et al. (2015) developed a reactive distillation process to produce furfural from synthetic and industrial pre-hydrolysate liquor (PHL) feeds using solid acid catalysts. Furfural was immediately removed from the reaction zone in this procedure by steam-stripping of the furfural, yielding a maximum furfural yield of 75% at 175 °C. In addition, by using sulfolane as an extraction solvent, an *in situ* catalyst regeneration was possible, resulting in a longer catalytic life. By using a simplified feed consisting only pentose and water, Jong and Marcotullio (2012) showed that a furfural yield of 87.5% was achieved by a continuous reactive distillation column-assisted heat pump. Moreover, this process reduced energy consumption by 84% compared to the conventional process. To improve the purification process for furfural manufacturing, Nhien et al. (2021) presented a hybrid extraction and distillation process as shown on Figure I-12. The difference between reactive distillation and this hybrid process is that the dilute furfural stream goes through a liquid-liquid extraction in the extractor before being sent to the distillation columns with solvent-rich furfural. The findings of the simulation analysis showed that high furfural

purity of 99% was reached while saving 51.7% and 62% of the reboiler energy compared to the conventional process by using toluene and butyl chloride as extracting solvents, respectively.

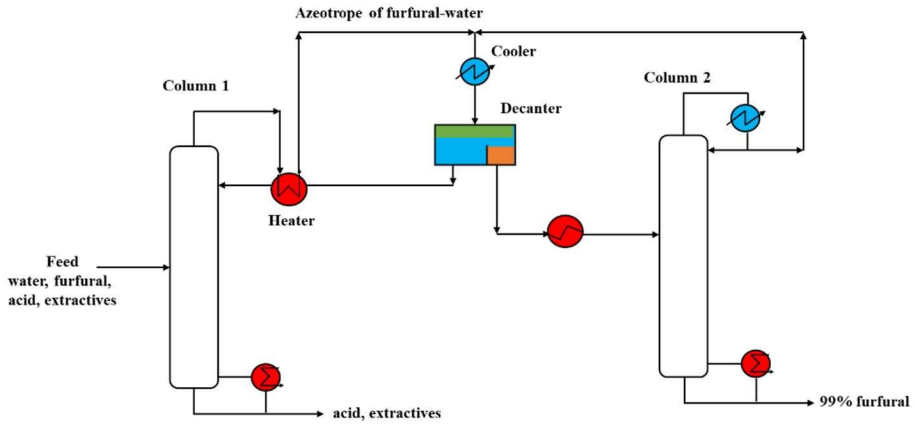

Figure I-12: Simple distillation plant for furfural recovery (Nhien et al., 2021).

I.3.3.2 Adsorption

Adsorption is a useful and energy-efficient process for purifying or bulk-separating a wide range of materials, including biomass products, fine chemicals, and industrial wastes (Jia et al., 2015). Furfural can easily reach adsorbent pores because it is a hydrophobic small molecule. Activated carbon (Sahu et al., 2008); (Cuevas et al., 2014); (Manz et al., 2016), biochar (Y. Li et al., 2013; Li et al., 2014), nanoporous materials (Anbia and Mohammadi, 2009a; Anbia and Mohammadi, 2009b), and polymeric resins (Carter et al., 2011; Sandhya et al., 2013) have all been demonstrated to be capable of adsorbing furfural in previous adsorption investigations (Fang and Yang, 2021).

Cuevas et al. (2014) investigated the use of commercial activated carbon to remove furfural from liquid effluents with levels of furfural ranging from 0.1 to 2 g/L. The results revealed that 90% of furfural removal was obtained in a batch heterogeneous reactor. In another study, soluble cationic polyelectrolyte polyethyleneimene (PEI) was used to separate inhibitory chemicals such as furfural, 5-HMF, and acetic acid from simple aqueous solutions (Carter et al., 2011). Up to 89.1, 58.6, and 81.5% of acetic acid, 5-HMF, and furfural were eliminated from simple solutions when PEI was added at a ratio of 1 mol of functional group to 1 mol inhibitor. After removing the polyelectrolyte/inhibitor complex, furfural and 5-HMF were recovered using a weak sulfuric acid solution to wash the polyelectrolyte/inhibitor complex. Furfural and 5-HMF recovery rates of up to 81.0 and 97.0% were achieved, respectively.

The polymeric sorbent and activated carbon, on the other hand, are costly. Furthermore, it is difficult to regenerate, and the process can result in mass loss (Y. Li et al., 2013). Y. Li et al. (2013) investigated the feasibility of removing furfural from bio-oil using bamboo charcoal as an adsorbent. They discovered that 200 g/L of adsorbent provided over 95% removal effectiveness in just 24 h at room temperature. For the adsorption of furfural from aqueous solution, Anbia and Mohammadi (2009b) produced MCM-48 with cetyltrimethylammonium bromide (CTAB) as the cationic surfactant. Batch adsorption tests showed a maximum adsorption capacity of 196.1 mg/g (2.04 mmol/g) for the systems. Aside from the high adsorption capacity, the equilibrium period for furfural adsorption is short (1 h), indicating a good approach for furfural removal from aqueous solutions.

Despite the various research on furfural adsorption reported in the literature, the focus was mostly on the recovery of low-level furfural from wastewater (Nanoti et al., 2008; Jia et al., 2015). Only one research that we are aware of, studied the separation of furfural with a greater concentration using an adsorption approach (Jia et al., 2015). The use of D141 macroporous resin to separate and enrich furfural from a hydrolysate containing 1 % furfural was studied in this work. 96.97% of the ultimate recovery yield of furfural was attained under optimal conditions. Furfural was dissolved with ethanol, resulting in an elute that was then streamed to recover furfural using ethanol that was recycled. D141 was also reused three times with little change in adsorption capacity, indicating that it is highly reusable.

I.3.3.3 Liquid-liquid extraction (LLE)

Extraction, along with adsorption, is a former alternative method of distillation that has found extensive use commercially for the recovery of furfural from aqueous solutions (Dunlop, 1951). The extraction is based on the fact that furfural has different solubilities in two kinds of immiscible solvents (Hu et al., 2020). Various organic solvents are commonly used as extracting agents in the traditional furfural extraction procedure. Since the partition coefficient and extraction efficiency of furfural are affected by the types of extracting agents, the effectiveness of the furfural extraction process is heavily reliant on them (Hu et al., 2020).

Ethyl acetate was first used for extracting furfural from aqueous solutions using an extraction column packed with porcelain Raschig rings (Dunlop, 1951). In this study, a 7% aqueous solution of furfural was extracted with an equivalent weight of ethyl acetate. The results indicated that 99.9% of the furfural had been extracted (Dunlop, 1951). In another study, Pei et al. (2008) investigated imidazolium-based ionic liquids ([C_4mim][PF_6], [C_6mim][PF_6],

and [C_8mim][PF_6]) to recover furfural from aqueous solution. The best extraction ability was discovered in [C_6mim] [PF_6], which can extract 76% of furfural from aqueous solution at room temperature. The ILs could be reused for the next extraction stage after recovering furfural from them by reduced pressure distillation. However, due to the high cost of ILs, this is not cost-effective technique of recovering furfural in the industry process.

Games et al. (1997) demonstrated that carbon dioxide is an excellent alternative to organic solvents with comparable extraction results. Indeed, continuous furfural extraction in a counter-currently driven high-pressure extraction column (130 bar) revealed that 90.77% of furfural can be extracted from an aqueous feed containing 1% furfural and 5% acetic acid in 3h. Recently, hydrophobic deep eutectic solvents (HDES) were used as an effective extractant to recover furfural from aqueous condensate (Sai, 2021). The highest extraction efficiency of 97.5% was obtained with the 1-tetradecanol and thymol based HDES. Furthermore, at room temperature and a 0.5 extractant to feed ratio, the latter may be recycled five times with identical effectivity.

In-situ extraction is a sort of liquid-liquid extraction that has received a lot of attention in recent years (T. Zhang et al., 2013). In contrast to the traditional extraction method, the *in-situ* extraction method is frequently used in combination with biphasic systems, as previously explained, in which furfural is first produced in various reaction solvents (such as water, ILs, and DESs), and then transferred immediately into the appropriate extracting agents (such as MIBK, THF, ILs, etc.) (Gürbüz et al., 2012). This method not only minimizes furfural degradation, but it also enhances furfural selectivity and yield (H. Li et al., 2014).

T. Zhang et al. (2013) investigated the effectiveness of the organic solvent methyl isobutyl ketone (MIBK) in improving furfural yields from maple wood. Under identical reaction conditions of 170 °C in 0.1 M H_2SO_4 at a 1:1 organic to aqueous phase weight ratio, furfural yield improved from 64% without extraction to 85%. Similarly, tetrahydrofuran (THF) was used to extract furfural from the dilute acid hydrolysate of *Quercus mongolica* (Kim et al., 2020). After 120 min at 170 °C, a furfural yield of 68.20% was obtained based on pentose in the hydrolysate. With the addition of NaCl, the furfural extraction was found to be improved, with 86.03% of the furfural produced being in the organic phase. In addition, two further extractions with fresh THF increased the furfural extraction rate to 94.63%. Using the ionic liquid tributyltetradecylphosphonium chloride ([$P_{444(14)}$]Cl as an extracting solvent, Morais et al. (2021) developed a new technique for integrated furfural synthesis (from xylans) and separation. In 1 min, a maximum furfural yield of 78.8% and an extraction efficiency to the IL-

rich phase of 85.5% were attained in the microwave reactor at 140 °C. Furthermore, while the efficacy of furfural extraction was maintained after three reaction cycles, there was a slight decrease in furfural yield from 78.8 to 69.9%, demonstrating the ILs' strong reusability.

In this study, two extraction methods were investigated to simultaneously extract furfural from the reaction medium, thereby enhancing its production. The first method is reactive distillation or steam stripping, where the produced furfural is extracted by steam during the reaction and recovered by condensation. The advantage of this method is that it requires no additional chemicals, allowing the furfural solution to be directly recovered after condensation. The second method is liquid-liquid extraction using different extracting agents, including supercritical CO_2 (Sc-CO_2) and organic solvents. This method is advantageous due to the higher partition coefficient compared to water, enabling more efficient furfural extraction.

I.4 Project CATALFUR

I.4.1 Presentation of project

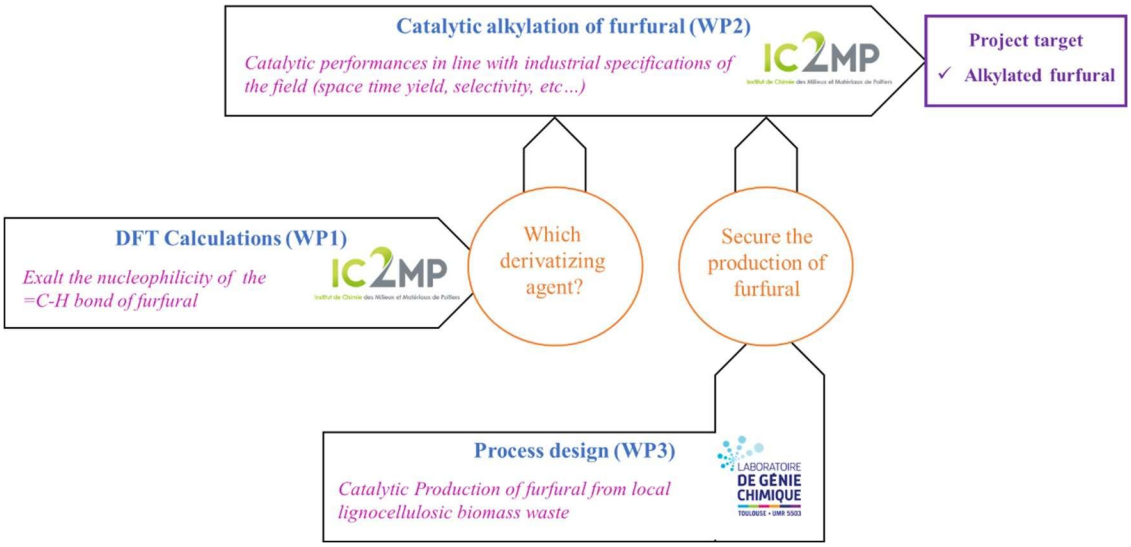

Figure I-13: Methodology of CATALFUR.

The thesis project is part of the CATALFUR project. The CATALFUR project, an acronym for CATalytic ALkylation of FURfural with alkyl alcohols, is a research project supported by ANR under the CNRS research federation INCREASE with a duration of 48 months. The project CATALFUR is also connected to the international scene through the International Symposium on Green Chemistry and involved in actions towards scientific mediation. The background of the project lies in addressing the challenge posed by the limited

reactivity of functional groups within furfural, particularly the =C-H bonds. Thus, the potential for furfural to generate molecular complexity and variety is significantly restricted. *The objective of this project is, therefore, to investigate the catalytic alkylation of the =C-H bond of furfural.* To reach this objective, three work packages have been established, as shown in Figure I-13:

- WP 1: DFT Calculations, will be devoted to computational evaluation of the reaction paths characteristics, and first-principles determination of promising furfural derivatizing agents.

- WP 2: Catalytic alkylation of furfural, will be devoted to catalytic experiments involving homogeneous catalyst use at first sight and further heterogeneous catalyst employment.

- WP 3: Process design, in which this thesis is part, will be devoted to securitization of the furfural supply for CATALFUR.

I.4.2 WP 3: furfural production from lignocellulosic biomass waste

The group BIOSSENT, a local wine and spirits manufacturer, produces 12 tons of lignocellulosic biomass waste each day. Thus, we will investigate the furfural production from this local lignocellulosic biomass waste focusing on the technology LEEBio^{TM} patented by BioEB. The benefit of this approach is that it produces a lignin-free hemicellulose fraction while the purity of co-produced cellulose and lignin meets industrial criteria for use in papermaking (or textiles) and energy production, respectively. In the LEEBio^{TM} technology, formic acid is used as a solvent for the fractionation of the lignocellulosic biomass (Delmas, 2019). We consider in WP3 that formic acid could be also advantageously used as an acid catalyst to further convert hemicellulose to furfural. Various fundamental studies have confirmed this possibility, albeit with xylose chosen as a model molecule (Lamminpää et al., 2012; Qiao et al., 2022; Tongtummachat et al., 2022).

I.4.2.1 Extracting hemicellulose from lignocelluloic raw material (Delmas, 2021)

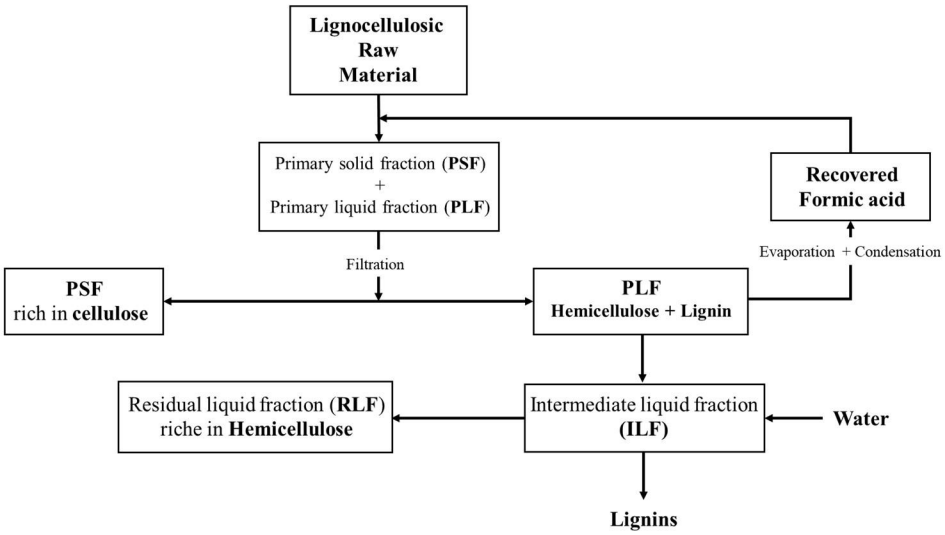

Figure I-14: Main step of hemicellulose extraction from lignocellulosic raw biomass (Delmas, 2021).

The solid lignocellulosic raw material is put into a liquid mixture composed of water and formic acid at an 85:15 weight ratio, with a ratio of solid/liquid mixture comprised of between 1 and 15. This mixture is heated in a glass reactor at atmospheric pressure for a predetermined period of time (4 h-6 h) under controlled temperature between 80 °C and 110 °C. At the end of the preceding extraction step, the primary solid fraction (PSF) rich in cellulose is separated from the primary liquid fraction (PLF) containing lignin and hemicellulose by filtration. Formic acid is recovered by evaporation-condensation at 100 mbar with a heating range of 40 °C to 50 °C, giving an intermediate liquid fraction (ILF). To separate the lignin from the ILF, the precipitation by adding water will be carried out, and the residual liquid fraction (RLF) will be obtained. The whole process is schematically illustrated in Figure I-14.

I.4.2.2 Production of furfural from hemicellulose

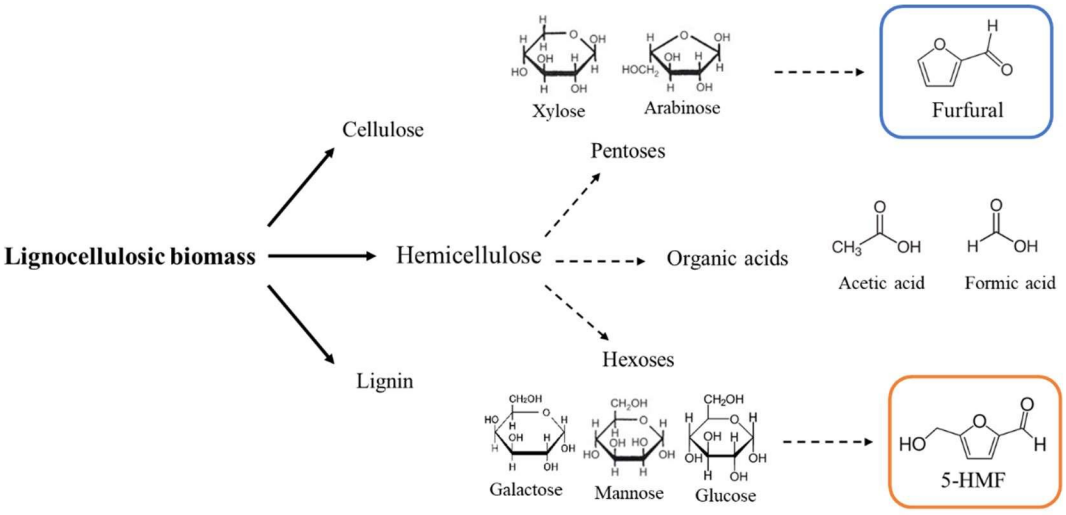

Figure I-15: Furfural production from hemicellulose.

In acidic conditions, hemicellulose can be degraded to monosaccharides, primarily xylose. arabinose, glucose, mannose, and galactose are some of the other hydrolysis products. xylose and other pentoses can be dehydrated further to produce furfural, while hexose sugars (i.e., glucose, mannose, and galactose) are converted into 5-HMF, as illustrated in Figure I-15 (Istasse and Richel, 2020). Remarkably, formic acid is one of the by-products during furfural production, obtained from the cleavage of the formyl group or the hydrolytic fission of the aldehyde group of furfural. So, it can realize the catalyst system's self-production and reduce the production costs (Yong et al., 2016).

I.5 Conclusion of the state of the art

The current state of research emphasizes several key points. Firstly, biomass recovery is increasingly recognized as crucial from both societal and environmental perspectives. Within the biomass fractions, hemicellulose, primarily composed of xylose or xylan, has emerged as a promising feedstock for producing valuable compounds. While xylose and xylan molecules themselves have limited utility, they can serve as precursors for synthesizing high-value molecules. In this context, furfural has been selected as the focus of this study.

Furfural synthesis processes, as revealed by the state-of-the-art, remain complex and are not yet fully industrialized. Most studies are conducted in batch mode, with few attempts to extend findings to continuous processes. Despite the apparent simplicity of the chemical reaction involved, the reactor environment significantly influences performance. The primary

objective of this thesis is to build upon existing batch studies by optimizing the process. This will involve systematically studying the impact of each operational parameter on furfural production. The chosen synthesis route involves homogeneous catalysis using formic acid, alongside a simultaneous extraction process that includes steam stripping and organic solvent extraction, aimed at preventing furfural degradation within the reactor.

Current furfural production methods still rely on strong acids and toxic solvents, making them environmentally unfriendly. To align with green chemistry principles and sustainable development goals, this thesis aims to enhance environmental sustainability. This will be achieved firstly by employing heterogeneous catalysts to improve the catalytic efficiency of formic acid in dehydrating xylose to furfural. Secondly, toxic solvents will be replaced with greener alternatives such as supercritical CO_2 for extracting furfural from the reaction medium, thereby enhancing both furfural yield and selectivity.

Furthermore, the synthesis of furfural is recognized as challenging, with multiple potential reaction mechanisms under consideration. Among these, three mechanisms are particularly prominent, with one pathway suggesting the presence of xylose intermediates. Therefore, another aim of this thesis is to validate or refute this favored pathway and propose refinements to these mechanistic insights. Additionally, kinetic modeling focusing on the preferred mechanism will be developed and utilized to optimize processes across various reactor configurations.

I.6 References

Abraham, A., Mathew, A.K., Park, H., Choi, O., Sindhu, R., Parameswaran, B., Pandey, A., Park, J.H., Sang, B.-I., 2020. Pretreatment strategies for enhanced biogas production from lignocellulosic biomass. Bioresour. Technol. 301, 1–13. https://doi.org/10.1016/j.biortech.2019.122725

Aellig, C., Scholz, D., Dapsens, P.Y., Mondelli, C., Pérez-Ramírez, J., 2015. When catalyst meets reactor: continuous biphasic processing of xylan to furfural over GaUSY/Amberlyst-36. Catal. Sci. Technol. 5, 142–149. https://doi.org/10.1039/C4CY00973H

Agirrezabal-Telleria, I., Gandarias, I., Arias, P.L., 2014a. Heterogeneous acid-catalysts for the production of furan-derived compounds (furfural and hydroxymethylfurfural) from renewable carbohydrates: A review. Catal. Today 234, 42–58. https://doi.org/10.1016/j.cattod.2013.11.027

Agirrezabal-Telleria, I., Gandarias, I., Arias, P.L., 2014b. Heterogeneous acid-catalysts for the production of furan-derived compounds (furfural and hydroxymethylfurfural) from renewable carbohydrates: A review. Catal. Today 234, 42–58. https://doi.org/10.1016/j.cattod.2013.11.027

Agirrezabal-Telleria, I., Larreategui, A., Requies, J., Güemez, M.B., Arias, P.L., 2011. Furfural production from xylose using sulfonic ion-exchange resins (Amberlyst) and simultaneous stripping with nitrogen. Bioresour. Technol. 102, 7478–7485. https://doi.org/10.1016/j.biortech.2011.05.015

Agirrezabal-Telleria, I., Requies, J., Güemez, M.B., Arias, P.L., 2012. Pore size tuning of functionalized SBA-15 catalysts for the selective production of furfural from xylose. Appl. Catal. B Environ. 115–116, 169–178. https://doi.org/10.1016/j.apcatb.2011.12.025

Aida, T.M., Shiraishi, N., Kubo, M., Watanabe, M., Smith, R.L., 2010. Reaction kinetics of d-xylose in sub- and supercritical water. J. Supercrit. Fluids 55, 208–216. https://doi.org/10.1016/j.supflu.2010.08.013

Alonso, D.M., Wettstein, S.G., Mellmer, M.A., Gurbuz, E.I., Dumesic, J.A., 2013. Integrated conversion of hemicellulose and cellulose from lignocellulosic biomass. Energy Env. Sci 6, 76–80. https://doi.org/10.1039/C2EE23617F

Anbia, M., Mohammadi, K., 2009a. An Effective Method For Removal of Dichromate Ion and Furfural From Aqueous Solutions Using A Nanoporous Adsorbent. Asian J Chem 21.

Anbia, M., Mohammadi, N., 2009b. A nanoporous adsorbent for removal of furfural from aqueous solutions. Desalination 249, 150–153. https://doi.org/10.1016/j.desal.2008.06.027

Antal, M.J., Leesomboon, T., Mok, W.S., Richards, G.N., 1991. Mechanism of formation of 2-furaldehyde from d-xylose. Carbohydr. Res. 217, 71–85. https://doi.org/10.1016/0008-6215(91)84118-X

Baktash, M.M., Ahsan, L., Ni, Y., 2015. Production of furfural from an industrial pre-hydrolysis liquor. Sep. Purif. Technol. 149, 407–412. https://doi.org/10.1016/j.seppur.2015.06.003

Beckman, E.J., 2004. Supercritical and near-critical CO2 in green chemical synthesis and processing. J. Supercrit. Fluids 28, 121–191. https://doi.org/10.1016/S0896-8446(03)00029-9

Bernal, H.G., Galletti, A.M.R., Garbarino, G., Busca, G., Finocchio, E., 2015. NbP catalyst for furfural production: FT IR studies of surface properties. Appl. Catal. Gen. 502, 388–398. https://doi.org/10.1016/j.apcata.2015.06.031

Berntsson, T., Sandén, B., Olsson, L., Åsblad, A., 2012. What is a biorefinery?, in: Systems Perspectives on Biorefineries 2012, 2.1. Chalmers University of Technology, Göteborg, pp. 16–25.

Bhaumik, P., Dhepe, P.L., 2014. Exceptionally high yields of furfural from assorted raw biomass over solid acids. RSC Adv. 4, 26215–26221. https://doi.org/10.1039/c4ra04119d

Bohre, A., Dutta, S., Saha, B., Abu-Omar, M.M., 2015. Upgrading Furfurals to Drop-in Biofuels: An Overview. ACS Sustain. Chem. Eng. 3, 1263–1277. https://doi.org/10.1021/acssuschemeng.5b00271

Bozell, J.J., Petersen, G.R., 2010. Technology development for the production of biobased products from biorefinery carbohydrates—the US Department of Energy's "Top 10" revisited. Green Chem. 12, 539–554. https://doi.org/10.1039/b922014c

Brandt, A., Ray, M.J., To, T.Q., Leak, D.J., Murphy, R.J., Welton, T., 2011. Ionic liquid pretreatment of lignocellulosic biomass with ionic liquid–water mixtures. Green Chem. 13, 2489–2499. https://doi.org/10.1039/c1gc15374a

Brownlee, H.J., Miner, C.S., 1948. Industrial Development of Furfural. Ind. Eng. Chem. 40, 201–204. https://doi.org/10.1021/ie50458a005

Bruce, S.M., Zong, Z., Chatzidimitriou, A., Avci, L.E., Bond, J.Q., Carreon, M.A., Wettstein, S.G., 2016. Small pore zeolite catalysts for furfural synthesis from xylose and switchgrass in a γ-valerolactone/water solvent. J. Mol. Catal. Chem. 422, 18–22. https://doi.org/10.1016/j.molcata.2016.02.025

Burket, C., Sabesan, S., 2013. Process for furfural production from biomass. US8524924B2.

Campos Molina, M.J., Mariscal, R., Ojeda, M., López Granados, M., 2012. Cyclopentyl methyl ether: A green co-solvent for the selective dehydration of lignocellulosic pentoses to furfural. Bioresour. Technol. 126, 321–327. https://doi.org/10.1016/j.biortech.2012.09.049

Carà, P.D., Pagliaro, M., Elmekawy, A., Brown, David.R., Verschuren, P., Shiju, N.R., Rothenberg, G., 2013. Hemicellulose hydrolysis catalysed by solid acids. Catal. Sci. Technol. 3, 2057–2061. https://doi.org/10.1039/c3cy20838a

Carrasco, F., 1993. Production of furfural by dilute-acid hydrolysis of wood: methods for calculating furfural yield. WOOD FIBER Sci. 25, 91–102.

Carter, B., Gilcrease, P.C., Menkhaus, T.J., 2011. Removal and recovery of furfural, 5-hydroxymethylfurfural, and acetic acid from aqueous solutions using a soluble polyelectrolyte. Biotechnol. Bioeng. 108, 2046–2052. https://doi.org/10.1002/bit.23153

Carvalheiro, F., Garrote, G., Parajó, J.C., Pereira, H., Gírio, F.M., 2008. Kinetic Modeling of Breweryapos;s Spent Grain Autohydrolysis. Biotechnol. Prog. 21, 233–243. https://doi.org/10.1021/bp049764z

Carvalho, A.V., da Costa Lopes, A.M., Bogel-Łukasik, R., 2015. Relevance of the acidic 1-butyl-3-methylimidazolium hydrogen sulphate ionic liquid in the selective catalysis of the biomass hemicellulose fraction. RSC Adv. 5, 47153–47164. https://doi.org/10.1039/C5RA07159C

Catrinck, M.N., Barbosa, P.S., Filho, H.R.O., Monteiro, R.S., Barbosa, M.H.P., Ribas, R.M., Teófilo, R.F., 2020. One-step process to produce furfural from sugarcane bagasse over niobium-based solid acid catalysts in a water medium. Fuel Process. Technol. 207, 106482. https://doi.org/10.1016/j.fuproc.2020.106482

Chen, H., Qin, L., Yu, B., 2015. Furfural production from steam explosion liquor of rice straw by solid acid catalysts (HZSM-5). Biomass Bioenergy 73, 77–83. https://doi.org/10.1016/j.biombioe.2014.12.013

Chen, H., Wang, L., 2017. Chapter 6 - Sugar Strategies for Biomass Biochemical Conversion, in: Chen, H., Wang, L. (Eds.), Technologies for Biochemical Conversion of Biomass. Academic Press, Oxford, pp. 137–164. https://doi.org/10.1016/B978-0-12-802417-1.00006-5

Chen, Z., Reznicek, W.D., Wan, C., 2018. Aqueous Choline Chloride: A Novel Solvent for Switchgrass Fractionation and Subsequent Hemicellulose Conversion into Furfural. ACS Sustain. Chem. Eng. 6, 6910–6919. https://doi.org/10.1021/acssuschemeng.8b00728

Chen, Z., Zhang, W., Xu, J., Li, P., 2015. Kinetics of xylose dehydration into furfural in acetic acid. Chin. J. Chem. Eng. 23, 659–666. https://doi.org/10.1016/j.cjche.2013.08.003

Cheng, L., Guo, Xiangke, Song, C., Yu, G., Cui, Y., Xue, N., Peng, L., Guo, Xuefeng, Ding, W., 2013. High performance mesoporous zirconium phosphate for dehydration of xylose to furfural in aqueous-phase. RSC Adv. 3, 23228. https://doi.org/10.1039/c3ra43413c

Cherubini, F., 2010. The biorefinery concept: Using biomass instead of oil for producing energy and chemicals. Energy Convers. Manag. 51, 1412–1421. https://doi.org/10.1016/j.enconman.2010.01.015

Cherubini, F., Jungmeier, G., 2010. LCA of a biorefinery concept producing bioethanol, bioenergy, and chemicals from switchgrass. Int. J. Life Cycle Assess. 15, 53–66. https://doi.org/10.1007/s11367-009-0124-2

Chheda, J.N., Román-Leshkov, Y., Dumesic, J.A., 2007. Production of 5-hydroxymethylfurfural and furfural by dehydration of biomass-derived mono- and poly-saccharides. Green Chem 9, 342–350. https://doi.org/10.1039/B611568C

Choudhary, V., Pinar, A.B., Sandler, S.I., Vlachos, D.G., Lobo, R.F., 2011. Xylose Isomerization to Xylulose and its Dehydration to Furfural in Aqueous Media. ACS Catal. 1, 1724–1728. https://doi.org/10.1021/cs200461t

Choudhary, V., Sandler, S.I., Vlachos, D.G., 2012. Conversion of Xylose to Furfural Using Lewis and Brønsted Acid Catalysts in Aqueous Media. ACS Catal. 2, 2022–2028. https://doi.org/10.1021/cs300265d

Cuevas, M., García, J.F., Sánchez, S., 2014. Enhanced enzymatic hydrolysis of pretreated almond-tree prunings for sugar production. Carbohydr. Polym. 99, 791–799. https://doi.org/10.1016/j.carbpol.2013.08.089

da Silva Lacerda, V., López-Sotelo, J.B., Correa-Guimarães, A., Hernández-Navarro, S., Sánchez-Bascones, M., Navas-Gracia, L.M., Martín-Ramos, P., Pérez-Lebeña, E., Martín-Gil, J., 2015. A kinetic study on microwave-assisted conversion of cellulose and lignocellulosic waste into hydroxymethylfurfural/furfural. Bioresour. Technol. 180, 88–96. https://doi.org/10.1016/j.biortech.2014.12.089

Dahmen, N., Lewandowski, I., Zibek, S., Weidtmann, A., 2019. Integrated lignocellulosic value chains in a growing bioeconomy: Status quo and perspectives. GCB Bioenergy 11, 107–117. https://doi.org/10.1111/gcbb.12586

Danon, B., Hongsiri, W., Van Der Aa, L., De Jong, W., 2014. Kinetic study on homogeneously catalyzed xylose dehydration to furfural in the presence of arabinose and glucose. Biomass Bioenergy 66, 364–370. https://doi.org/10.1016/j.biombioe.2014.04.007

Dashtban, M., 2012. Production of furfural: overview and challenges. J--J. Sci. Technol. For. Prod. Process. 2, 44–53.

Delbecq, F., Wang, Y., Len, C., 2016. Conversion of xylose, xylan and rice husk into furfural via betaine and formic acid mixture as novel homogeneous catalyst in biphasic system by microwave-assisted dehydration. J. Mol. Catal. Chem. 423, 520–525. https://doi.org/10.1016/j.molcata.2016.07.003

Delbecq, F., Wang, Y., Muralidhara, A., El Ouardi, K., Marlair, G., Len, C., 2018. Hydrolysis of Hemicellulose and Derivatives—A Review of Recent Advances in the Production of Furfural. Front. Chem. 6, 146. https://doi.org/10.3389/fchem.2018.00146

Delmas, M., 2021. A lignocellulosic biomass based process for production of lignins and syngas, and electricity production efficient syngas. US20210009908A1.

Delmas, M., 2019. A lignocellulosic biomass based process for production of lignins and syngas, and electricity production efficient syngas. EP3527531A1.

Deng, A., Lin, Q., Yan, Y., Li, H., Ren, J., Liu, C., Sun, R., 2016. A feasible process for furfural production from the pre-hydrolysis liquor of corncob via biochar catalysts in a new biphasic system. Bioresour. Technol. 216, 754–760. https://doi.org/10.1016/j.biortech.2016.06.002

Dey, P.M., Brownleader, M.D., Harborne, J.B., 1997. 1 - The Plant, the Cell and its Molecular Components, in: Dey, P.M., Harborne, J.B. (Eds.), Plant Biochemistry. Academic Press, London, pp. 1–47. https://doi.org/10.1016/B978-012214674-9/50002-3

Dhepe, P.L., Sahu, R., 2010. A solid-acid-based process for the conversion of hemicellulose. Green Chem. 12, 2153. https://doi.org/10.1039/c004128a

Dias, A.S., Lima, S., Pillinger, M., Valente, A.A., 2010. Furfural and Furfural-Based Industrial Chemicals, in: Ideas in Chemistry and Molecular Sciences. John Wiley & Sons, Ltd, pp. 165–186. https://doi.org/10.1002/9783527630554.ch8

Dias, A.S., Lima, S., Pillinger, M., Valente, A.A., 2006. Acidic cesium salts of 12-tungstophosphoric acid as catalysts for the dehydration of xylose into furfural. Carbohydr. Res. 341, 2946–2953. https://doi.org/10.1016/j.carres.2006.10.013

Dodds, D.R., Gross, R.A., 2007. Chemicals from Biomass. Science 318, 1250–1251. https://doi.org/10.1126/science.1146356

Doiseau, A.-C., Rataboul, F., Burel, L., Essayem, N., 2014. Synergy effect between solid acid catalysts and concentrated carboxylic acids solutions for efficient furfural production from xylose. Catal. Today 226, 176–184. https://doi.org/10.1016/j.cattod.2013.10.034

Drew, K.N., Zajicek, J., Bondo, G., Bose, B., Serianni, A.S., 1998. 13C-labeled aldopentoses: detection and quantitation of cyclic and acyclic forms by heteronuclear 1D and 2D NMR spectroscopy. Carbohydr. Res. 307, 199–209. https://doi.org/10.1016/S0008-6215(98)00040-8

Dunlop, A.P., 1951. Production of furfural. US2536732A.

Dussan, K., Girisuta, B., Lopes, M., Leahy, J.J., Hayes, M.H.B., 2015. Conversion of Hemicellulose Sugars Catalyzed by Formic Acid: Kinetics of the Dehydration of D -Xylose, L -Arabinose, and D -Glucose. ChemSusChem 8, 1411–1428. https://doi.org/10.1002/cssc.201403328

Eckert, C.A., Bush, D., Brown, J.S., Liotta, C.L., 2000. Tuning Solvents for Sustainable Technology. Ind. Eng. Chem. Res. 39, 4615–4621. https://doi.org/10.1021/ie000396n

Eisenbies, M.H., Volk, T.A., Posselius, J., Shi, S., Patel, A., 2015. Quality and Variability of Commercial-Scale Short Rotation Willow Biomass Harvested Using a Single-Pass Cut-and-Chip Forage Harvester. BioEnergy Res. 8, 546–559. https://doi.org/10.1007/s12155-014-9540-7

Emerson, R., Hoover, A., Ray, A., Lacey, J., Cortez, M., Payne, C., Karlen, D., Birrell, S., Laird, D., Kallenbach, R., Egenolf, J., Sousek, M., Voigt, T., 2014. Drought effects on composition and yield for corn stover, mixed grasses, and *Miscanthus* as bioenergy feedstocks. Biofuels 5, 275–291. https://doi.org/10.1080/17597269.2014.913904

Enslow, K.R., Bell, A.T., 2015. $SnCl_4$ -catalyzed isomerization/dehydration of xylose and glucose to furanics in water. Catal. Sci. Technol. 5, 2839–2847. https://doi.org/10.1039/C5CY00077G

Eseyin, A., E., Steele, P., H., 2015. An overview of the applications of furfural and its derivatives. Int. J. Adv. Chem. 3, 42–47. https://doi.org/10.14419/ijac.v3i2.5048

Fang, K., Yang, R., 2021. Modified activated carbon by air oxidation as a potential adsorbent for furfural removal. Alex. Eng. J. 60, 2325–2333. https://doi.org/10.1016/j.aej.2020.12.032

Fang, Z., Jr, R.L.S., Qi, X., 2017. Production of Platform Chemicals from Sustainable Resources, 1st ed, Biofuels and Biorefineries. Springer.

Feather, M.S., Harris, D.W., Nichols, S.B., 1972. Routes of conversion of D-xylose, hexuronic acids, and L-ascorbic acid to 2-furaldehyde. J. Org. Chem. 37, 1606–1608. https://doi.org/10.1021/jo00975a032

Finore, I., Poli, A., Di Donato, P., Lama, L., Trincone, A., Fagnano, M., Mori, M., Nicolaus, B., Tramice, A., 2016. The hemicellulose extract from Cynara cardunculus: a source of value-added biomolecules produced by xylanolytic thermozymes. Green Chem. 18, 2460–2472. https://doi.org/10.1039/C5GC02774H

Fitzpatrick, S.W., 1990. Lignocellulose degradation to furfural and levulinic acid. US4897497A.

Furfural Market Size, Share, Growth & Trends Report, 2030 [WWW Document], n.d. URL https://www.grandviewresearch.com/industry-analysis/furfural-market (accessed 5.23.24).

Gairola, K., Smirnova, I., 2012. Hydrothermal pentose to furfural conversion and simultaneous extraction with SC-CO2 – Kinetics and application to biomass hydrolysates. Bioresour. Technol. 123, 592–598. https://doi.org/10.1016/j.biortech.2012.07.031

Gallo, J.M.R., Alonso, D.M., Mellmer, M.A., Yeap, J.H., Wong, H.C., Dumesic, J.A., 2013. Production of Furfural from Lignocellulosic Biomass Using Beta Zeolite and Biomass-Derived Solvent. Top. Catal. 56, 1775–1781. https://doi.org/10.1007/s11244-013-0113-3

Games, T., Marr, R., Fröschl, F., Siebenhofer, M., 1997. Extraction of Furfural with Carbon Dioxide. Sep. Sci. Technol. 32, 355–371. https://doi.org/10.1080/01496399708003203

Gao, H., Liu, H., Pang, B., Yu, G., Du, J., Zhang, Y., Wang, H., Mu, X., 2014. Production of furfural from waste aqueous hemicellulose solution of hardwood over ZSM-5 zeolite. Bioresour. Technol. 172, 453–456. https://doi.org/10.1016/j.biortech.2014.09.026

García, M.T., Zamudio, M.A.M., Loaiza, J.M., Morales, A.B., Alfaro, A., Lopez, F., García, J.C., 2019. Characterization and use of southern cattail for biorefining-based production of furfural. Biomass Convers. Biorefinery 9, 333–339. https://doi.org/10.1007/s13399-018-0355-1

García-Sancho, C., Rubio-Caballero, J.M., Mérida-Robles, J.M., Moreno-Tost, R., Santamaría-González, J., Maireles-Torres, P., 2014. Mesoporous Nb2O5 as solid acid catalyst for dehydration of d-xylose into furfural. Catal. Today 234, 119–124. https://doi.org/10.1016/j.cattod.2014.02.012

Garrett, E.R., Dvorchik, B.H., 1969. Kinetics and Mechanisms of the Acid Degradation of the Aldopentoses to Furfural. J. Pharm. Sci. 58, 813–820. https://doi.org/10.1002/jps.2600580703

Gómez Millán, G., Bangalore Ashok, R.P., Oinas, P., Llorca, J., Sixta, H., 2021. Furfural production from xylose and birch hydrolysate liquor in a biphasic system and techno-economic analysis. Biomass Convers. Biorefinery 11, 2095–2106. https://doi.org/10.1007/s13399-020-00702-4

Gómez Millán, G., Hellsten, S., King, A.W.T., Pokki, J.-P., Llorca, J., Sixta, H., 2019a. A comparative study of water-immiscible organic solvents in the production of furfural from xylose and birch hydrolysate. J. Ind. Eng. Chem. 72, 354–363. https://doi.org/10.1016/j.jiec.2018.12.037

Gómez Millán, G., Phiri, J., Mäkelä, M., Maloney, T., Balu, A.M., Pineda, A., Llorca, J., Sixta, H., 2019b. Furfural production in a biphasic system using a carbonaceous solid acid catalyst. Appl. Catal. Gen. 585, 1–8. https://doi.org/10.1016/j.apcata.2019.117180

Gravitis, J., Vedernikov, N., Zandersons, J., Kokorevics, A., 2001. Furfural and Levoglucosan Production from Deciduous Wood and Agricultural Wastes, in: Chemicals and Materials from Renewable Resources, ACS Symposium Series. American Chemical Society, pp. 110–122. https://doi.org/10.1021/bk-2001-0784.ch009

Grisel, R.J.H., van der Waal, J.C., de Jong, E., Huijgen, W.J.J., 2014. Acid catalysed alcoholysis of wheat straw: Towards second generation furan-derivatives. Catal. Today 223, 3–10. https://doi.org/10.1016/j.cattod.2013.07.008

Guenic, S.L., Delbecq, F., Ceballos, C., Len, C., 2015. Microwave-assisted dehydration of D-xylose into furfural by diluted inexpensive inorganic salts solution in a biphasic system. J. Mol. Catal. Chem. 410, 1–7. https://doi.org/10.1016/j.molcata.2015.08.019

Guo, X., Guo, F., Li, Y., Zheng, Z., Xing, Z., Zhu, Z., Liu, T., Zhang, X., Jin, Y., 2018. Dehydration of D-xylose into furfural over bimetallic salts of heteropolyacid in DMSO/H2O mixture. Appl. Catal. Gen. 558, 18–25. https://doi.org/10.1016/j.apcata.2018.03.027

Gürbüz, E.I., Gallo, J.M.R., Alonso, D.M., Wettstein, S.G., Lim, W.Y., Dumesic, J.A., 2013. Conversion of Hemicellulose into Furfural Using Solid Acid Catalysts in γ-Valerolactone. Angew. Chem. Int. Ed. 52, 1270–1274. https://doi.org/10.1002/anie.201207334

Gürbüz, E.I., Wettstein, S.G., Dumesic, J.A., 2012. Conversion of Hemicellulose to Furfural and Levulinic Acid using Biphasic Reactors with Alkylphenol Solvents. ChemSusChem 5, 383–387. https://doi.org/10.1002/cssc.201100608

Gurgenova, K., Bogeł-Łukasik, R., Wawrzyniak, P., 2013. High Pressure Vapour-Liquid Equilibrium of Volatiles in Supercritical Carbon Dioxide. Chem. Process Eng. 34, 387–392. https://doi.org/10.2478/cpe-2013-0031

Han, J., Murat Sen, S., Luterbacher, J.S., Alonso, D.M., Dumesic, J.A., Maravelias, C.T., 2015. Process systems engineering studies for the synthesis of catalytic biomass-to-fuels strategies. Comput. Chem. Eng. 81, 57–69. https://doi.org/10.1016/j.compchemeng.2015.04.007

Haq, I., Qaisar, K., Nawaz, A., Akram, F., Mukhtar, H., Zohu, X., Xu, Y., Mumtaz, M., Rashid, U., Ghani, W., Choong, T., 2021. Advances in Valorization of Lignocellulosic Biomass towards Energy Generation. Catalysts 11, 1–25. https://doi.org/10.3390/catal11030309

Hernández-Beltrán, J.U., Hernández-De Lira, I.O., Cruz-Santos, M.M., Saucedo-Luevanos, A., Hernández-Terán, F., Balagurusamy, N., 2019. Insight into Pretreatment Methods of Lignocellulosic Biomass to Increase Biogas Yield: Current State, Challenges, and Opportunities. Appl. Sci. 9, 1–29. https://doi.org/10.3390/app9183721

Hricovíniová, Z., 2013. Xylans are a valuable alternative resource: Production of d-xylose, d-lyxose and furfural under microwave irradiation. Carbohydr. Polym. 98, 1416–1421. https://doi.org/10.1016/j.carbpol.2013.07.066

Hu, L., Jiang, Y., Wu, Z., Wang, X., He, A., Xu, Jiaxing, Xu, Jiming, 2020. State-of-the-art advances and perspectives in the separation of biomass-derived 5-hydroxymethylfurfural. J. Clean. Prod. 276, 1–22. https://doi.org/10.1016/j.jclepro.2020.124219

Hu, X., Westerhof, R.J.M., Dong, D., Wu, L., Li, C.-Z., 2014. Acid-Catalyzed Conversion of Xylose in 20 Solvents: Insight into Interactions of the Solvents with Xylose, Furfural, and the Acid Catalyst. ACS Sustain. Chem. Eng. 2, 2562–2575. https://doi.org/10.1021/sc5004659

Iglesias, J., Melero, J.A., Morales, G., Paniagua, M., Hernández, B., 2016. Dehydration of Xylose to Furfural in Alcohol Media in the Presence of Solid Acid Catalysts. ChemCatChem 8, 2089–2099. https://doi.org/10.1002/cctc.201600292

Istasse, T., Richel, A., 2020. Mechanistic aspects of saccharide dehydration to furan derivatives for reaction media design. RSC Adv. 10, 23720–23742. https://doi.org/10.1039/D0RA03892J

Jaafari, L., Ibrahim, H., Jaffary, B., Idem, R., 2019. Catalytic production of furfural by pressurized liquid water liquefaction of flax straw. Renew. Energy 130, 1176–1184. https://doi.org/10.1016/j.renene.2018.08.065

Jia, C., Li, X., Liu, Z., Xu, B., Yao, S., Song, H., 2015. Adsorption process and mechanism for furfural separation with macroporous resin. Desalination Water Treat. 56, 2214–2224. https://doi.org/10.1080/19443994.2014.960455

Jing, Q., Lü, X., 2007a. Kinetics of Non-catalyzed Decomposition of D-xylose in High Temperature Liquid Water. Chin. J. Chem. Eng. 15, 666–669. https://doi.org/10.1016/S1004-9541(07)60143-8

Jing, Q., Lü, X., 2007b. Kinetics of Non-catalyzed Decomposition of D-xylose in High Temperature Liquid Water. Chin. J. Chem. Eng. 15, 666–669. https://doi.org/10.1016/S1004-9541(07)60143-8

Jones, B.W., Venditti, R., Park, S., Jameel, H., Koo, B., 2013. Enhancement in enzymatic hydrolysis by mechanical refining for pretreated hardwood lignocellulosics. Bioresour. Technol. 147, 353–360. https://doi.org/10.1016/j.biortech.2013.08.030

Jong, W. de, Marcotullio, G., 2012. Process for the production of furfural from pentoses. US20120108829A1.

Julio, R., Albet, J., Vialle, C., Vaca-Garcia, C., Sablayrolles, C., 2017. Sustainable design of biorefinery processes: existing practices and new methodology. Biofuels Bioprod. Biorefining 11, 373–395. https://doi.org/10.1002/bbb.1749

Kamm, B., Gerhardt, M., Dautzenberg, G., 2013. Catalytic Processes of Lignocellulosic Feedstock Conversion for Production of Furfural, Levulinic Acid, and Formic Acid-Based Fuel Components, in: New and Future Developments in Catalysis. Elsevier, pp. 91–113. https://doi.org/10.1016/B978-0-444-53878-9.00005-9

Kangle, N., Gaikwad, K., Angal, S., 2023. Manufacture of Furfural from Sugarcane Bagasse. Int. J. Eng. Res. Appl. 13, 96–102. https://doi.org/DOI: 10.9790/9622-130196102

Kanzler, W., Schedler, J., 1983. Method for the recovery of furfural, acetic acid and formic acid. US4401514A.

Karinen, R., Vilonen, K., Niemelä, M., 2011. Biorefining: Heterogeneously Catalyzed Reactions of Carbohydrates for the Production of Furfural and Hydroxymethylfurfural. ChemSusChem 4, 1002–1016. https://doi.org/10.1002/cssc.201000375

Kenney, K.L., Smith, W.A., Gresham, G.L., Westover, T.L., 2013. Understanding biomass feedstock variability. Biofuels 4, 111–127. https://doi.org/10.4155/bfs.12.83

Keskin, T., Nalakath Abubackar, H., Arslan, K., Azbar, N., 2019. Biohydrogen Production From Solid Wastes, in: Biohydrogen. Elsevier, pp. 321–346. https://doi.org/10.1016/B978-0-444-64203-5.00012-5

Kim, E.S., Liu, S., Abu-Omar, M.M., Mosier, N.S., 2012. Selective Conversion of Biomass Hemicellulose to Furfural Using Maleic Acid with Microwave Heating. Energy Fuels 26, 1298–1304. https://doi.org/10.1021/ef2014106

Kim, J.-H., Cho, S.-M., Choi, J.-H., Jeong, H., Lee, S.M., Koo, B., Choi, I.-G., 2020. A Simultaneous Conversion and Extraction of Furfural from Pentose in Dilute Acid Hydrolysate of Quercus mongolica Using an Aqueous Biphasic System. Appl. Sci. 11, 1–12. https://doi.org/10.3390/app11010163

Kim, M., Day, D.F., 2011. Composition of sugar cane, energy cane, and sweet sorghum suitable for ethanol production at Louisiana sugar mills. J. Ind. Microbiol. Biotechnol. 38, 803–807. https://doi.org/10.1007/s10295-010-0812-8

Kim, S.B., You, S.J., Kim, Y.T., Lee, S., Lee, H., Park, K., Park, E.D., 2011. Dehydration of D-xylose into furfural over H-zeolites. Korean J. Chem. Eng. 28, 710–716. https://doi.org/10.1007/s11814-010-0417-y

Kiminki, K., Kulmala, R., Sipila, S., 1977. Acid hydrolysis of polysaccharide-containing raw material. US4029515A.

Köchermann, J., Mühlenberg, J., Klemm, M., 2018. Kinetics of Hydrothermal Furfural Production from Organosolv Hemicellulose and D -Xylose. Ind. Eng. Chem. Res. 57, 14417–14427. https://doi.org/10.1021/acs.iecr.8b03402

Krammer, P., Vogel, H., 2000. Hydrolysis of esters in subcritical and supercritical water. J. Supercrit. Fluids 16, 189–206. https://doi.org/10.1016/S0896-8446(99)00032-7

Kruse, A., Dinjus, E., 2007. Hot compressed water as reaction medium and reactant: Properties and synthesis reactions. J. Supercrit. Fluids 39, 362–380. https://doi.org/10.1016/j.supflu.2006.03.016

Lam, E., Chong, J.H., Majid, E., Liu, Y., Hrapovic, S., Leung, A.C.W., Luong, J.H.T., 2012. Carbocatalytic dehydration of xylose to furfural in water. Carbon 50, 1033–1043. https://doi.org/10.1016/j.carbon.2011.10.007

Lamminpää, K., Ahola, J., Tanskanen, J., 2014. Kinetics of furfural destruction in a formic acid medium. RSC Adv 4, 60243–60248. https://doi.org/10.1039/C4RA09276G

Lamminpää, K., Ahola, J., Tanskanen, J., 2012. Kinetics of Xylose Dehydration into Furfural in Formic Acid. Ind. Eng. Chem. Res. 51, 6297–6303. https://doi.org/10.1021/ie2018367

Lamminpää, K., Tanskanen, J., 2009. STUDY OF FURFURAL FORMATION USING FORMIC ACID. Proc. Eighth World Congr. Chem. Eng. 1–7.

Le Guenic, S., Gergela, D., Ceballos, C., Delbecq, F., Len, C., 2016. Furfural Production from d-Xylose and Xylan by Using Stable Nafion NR50 and NaCl in a Microwave-Assisted Biphasic Reaction. Molecules 21, 1–11. https://doi.org/10.3390/molecules21081102

Lee, C.B.T.L., Wu, T.Y., Ting, C.H., Tan, J.K., Siow, L.F., Cheng, C.K., Md. Jahim, J., Mohammad, A.W., 2019. One-pot furfural production using choline chloride-dicarboxylic acid based deep eutectic solvents under mild conditions. Bioresour. Technol. 278, 486–489. https://doi.org/10.1016/j.biortech.2018.12.034

Lemus, R., Brummer, E.C., Moore, K.J., Molstad, N.E., Burras, C.L., Barker, M.F., 2002. Biomass yield and quality of 20 switchgrass populations in southern Iowa, USA. Biomass Bioenergy 23, 433–442.

Lessard, J., Morin, J.-F., Wehrung, J.-F., Magnin, D., Chornet, E., 2010. High Yield Conversion of Residual Pentoses into Furfural via Zeolite Catalysis and Catalytic Hydrogenation of Furfural to 2-Methylfuran. Top. Catal. 53, 1231–1234. https://doi.org/10.1007/s11244-010-9568-7

Li, A.-L., Hou, X.-D., Lin, K.-P., Zhang, X., Fu, M.-H., 2018. Rice straw pretreatment using deep eutectic solvents with different constituents molar ratios: Biomass fractionation, polysaccharides enzymatic digestion and solvent reuse. J. Biosci. Bioeng. 126, 346–354. https://doi.org/10.1016/j.jbiosc.2018.03.011

Li, C., Ding, D., Xia, Q., Liu, X., Wang, Y., 2016. Conversion of raw lignocellulosic biomass into branched long-chain alkanes through three tandem steps. ChemSusChem 9, 1712–1718. https://doi.org/10.1002/cssc.201600386

Li, H., Deng, A., Ren, J., Liu, C., Wang, W., Peng, F., Sun, R., 2014. A modified biphasic system for the dehydration of d-xylose into furfural using SO42−/TiO2-ZrO2/La3+ as a solid catalyst. Catal. Today 234, 251–256. https://doi.org/10.1016/j.cattod.2013.12.043

Li, H., Ren, J., Zhong, L., Sun, R., Liang, L., 2015. Production of furfural from xylose, water-insoluble hemicelluloses and water-soluble fraction of corncob via a tin-loaded montmorillonite solid acid catalyst. Bioresour. Technol. 176, 242–248. https://doi.org/10.1016/j.biortech.2014.11.044

Li, H.-L., Wang, S.-Y., Wang, W.-J., Ren, J.-L., Peng, F., Sun, R.-C., Liang, L., 2013. One-Step Heterogeneous Catalytic Process for the Dehydration of Xylan into Furfural. BioResources 8, 3200–3211. https://doi.org/10.15376/biores.8.3.3200-3211

Li, W., Zhu, Y., Lu, Y., Liu, Q., Guan, S., Chang, H., Jameel, H., Ma, L., 2017. Enhanced furfural production from raw corn stover employing a novel heterogeneous acid catalyst. Bioresour. Technol. 245, 258–265. https://doi.org/10.1016/j.biortech.2017.08.077

Li, X., Liu, Q., Si, C., Lu, L., Luo, C., Gu, X., Liu, W., Lu, X., 2018. Green and efficient production of furfural from corn cob over H-ZSM-5 using γ-valerolactone as solvent. Ind. Crops Prod. 120, 343–350. https://doi.org/10.1016/j.indcrop.2018.04.065

Li, X.-L., Pan, T., Deng, J., Fu, Y., Xu, H.-J., 2015. Catalytic dehydration of D -xylose to furfural over a tantalum-based catalyst in batch and continuous process. RSC Adv. 5, 70139–70146. https://doi.org/10.1039/C5RA11411J

Li, Y., Shao, J., Wang, X., Deng, Y., Yang, H., Chen, H., 2014. Characterization of Modified Biochars Derived from Bamboo Pyrolysis and Their Utilization for Target Component (Furfural) Adsorption. Energy Fuels 28, 5119–5127. https://doi.org/10.1021/ef500725c

Li, Y., Shao, J., Wang, X., Yang, H., Chen, Y., Deng, Y., Zhang, S., Chen, H., 2013. Upgrading of Bio-oil: Removal of the Fermentation Inhibitor (Furfural) from the Model Compounds of Bio-oil Using Pyrolytic Char. Energy Fuels 27, 5975–5981. https://doi.org/10.1021/ef401375q

Lima, S., Fernandes, A., Antunes, M.M., Pillinger, M., Ribeiro, F., Valente, A.A., 2010. Dehydration of Xylose into Furfural in the Presence of Crystalline Microporous Silicoaluminophosphates. Catal. Lett. 135, 41–47. https://doi.org/10.1007/s10562-010-0259-6

Lima, S., Neves, P., Antunes, M.M., Pillinger, M., Ignatyev, N., Valente, A.A., 2009. Conversion of mono/di/polysaccharides into furan compounds using 1-alkyl-3-methylimidazolium ionic liquids. Appl. Catal. Gen. 363, 93–99. https://doi.org/10.1016/j.apcata.2009.04.049

Lima, S., Pillinger, M., Valente, A.A., 2008. Dehydration of d-xylose into furfural catalysed by solid acids derived from the layered zeolite Nu-6(1). Catal. Commun. 9, 2144–2148. https://doi.org/10.1016/j.catcom.2008.04.016

Lin, H., Chen, J., Zhao, Y., Wang, S., 2017. Conversion of C5 Carbohydrates into Furfural Catalyzed by SO 3 H-Functionalized Ionic Liquid in Renewable γ-Valerolactone. Energy Fuels 31, 3929–3934. https://doi.org/10.1021/acs.energyfuels.6b01975

Lin, L., Ma, S., Li, P., Zhu, T., Chang, H., 2015. Mutual Solubilities for the Water–2-*sec* -Butylphenol System and Partition Coefficients for Furfural and Formic Acid in the Water–2- *sec* -Butylphenol System. J. Chem. Eng. Data 60, 1926–1933. https://doi.org/10.1021/acs.jced.5b00170

Liu, S., 2017. Batch Reactor, in: Bioprocess Engineering. Elsevier, pp. 139–178. https://doi.org/10.1016/B978-0-444-63783-3.00004-6

Loow, Y.-L., New, E.K., Yang, G.H., Ang, L.Y., Foo, L.Y.W., Wu, T.Y., 2017. Potential use of deep eutectic solvents to facilitate lignocellulosic biomass utilization and conversion. Cellulose 24, 3591–3618. https://doi.org/10.1007/s10570-017-1358-y

Lu, Y., He, Q., Fan, G., Cheng, Q., Song, G., 2021. Extraction and modification of hemicellulose from lignocellulosic biomass: A review. Green Process. Synth. 10, 779–804. https://doi.org/10.1515/gps-2021-0065

Luo, Y., Li, Z., Li, X., Liu, X., Fan, J., Clark, J.H., Hu, C., 2019. The production of furfural directly from hemicellulose in lignocellulosic biomass: A review. Catal. Today 319, 14–24. https://doi.org/10.1016/j.cattod.2018.06.042

Luo, Y., Li, Z., Zuo, Y., Su, Z., Hu, C., 2017. A Simple Two-Step Method for the Selective Conversion of Hemicellulose in *Pubescens* to Furfural. ACS Sustain. Chem. Eng. 5, 8137–8147. https://doi.org/10.1021/acssuschemeng.7b01766

Lynd, L.R., Wyman, C.E., Gerngross, T.U., 1999. Biocommodity Engineering. Biotechnol. Prog. 15, 777–793. https://doi.org/10.1021/bp990109e

Machado, G., Leon, S., Santos, F., Lourega, R., Dullius, J., Mollmann, M.E., Eichler, P., 2016. Literature Review on Furfural Production from Lignocellulosic Biomass. Nat. Resour. 07, 115–129. https://doi.org/10.4236/nr.2016.73012

Magalhães da Silva, S.P., Morais, A.R.C., Bogel-Łukasik, R., 2014. The CO_2 -assisted autohydrolysis of wheat straw. Green Chem 16, 238–246. https://doi.org/10.1039/C3GC41870G

Mamman, A.S., Lee, J.-M., Kim, Y.-C., Hwang, I.T., Park, N.-J., Hwang, Y.K., Chang, J.-S., Hwang, J.-S., 2008. Furfural: Hemicellulose/xylosederived biochemical. Biofuels Bioprod. Biorefining 2, 438–454. https://doi.org/10.1002/bbb.95

Mandalika, A., Runge, T., 2012. Enabling integrated biorefineries through high-yield conversion of fractionated pentosans into furfural. Green Chem. 14, 3175–3184. https://doi.org/10.1039/c2gc35759c

Mansilla, H.D., Baeza, J., Urzúa, S., Maturana, G., Villaseñor, J., Durán, N., 1998. Acid-catalysed hydrolysis of rice hull: Evaluation of furfural production. Bioresour. Technol. 66, 189–193. https://doi.org/10.1016/S0960-8524(98)00088-1

Manz, K.E., Haerr, G., Lucchesi, J., Carter, K.E., 2016. Adsorption of hydraulic fracturing fluid components 2-butoxyethanol and furfural onto granular activated carbon and shale rock. Chemosphere 164, 585–592. https://doi.org/10.1016/j.chemosphere.2016.09.010

Mao, H., Li, S.-H., Zhang, A.-S., Xu, L.-H., Lu, H.-X., Lv, J., Zhao, Z.-P., 2021. Furfural separation from aqueous solution by pervaporation membrane mixed with metal organic framework MIL-53(Al) synthesized via high efficiency solvent-controlled microwave. Sep. Purif. Technol. 272, 1–12. https://doi.org/10.1016/j.seppur.2021.118813

Marcotullio, G., De Jong, W., 2010. Chloride ions enhance furfural formation from d-xylose in dilute aqueous acidic solutions. Green Chem. 12, 1739. https://doi.org/10.1039/b927424c

Mardani, A., Jusoh, A., Zavadskas, E., Cavallaro, F., Khalifah, Z., 2015. Sustainable and Renewable Energy: An Overview of the Application of Multiple Criteria Decision Making

Techniques and Approaches. Sustainability 7, 13947–13984. https://doi.org/10.3390/su71013947

Mariscal, R., Maireles-Torres, P., Ojeda, M., Sádaba, I., López Granados, M., 2016. Furfural: a renewable and versatile platform molecule for the synthesis of chemicals and fuels. Energy Environ. Sci. 9, 1144–1189. https://doi.org/10.1039/C5EE02666K

Matsagar, B.M., Hossain, S.A., Islam, T., Alamri, H.R., Alothman, Z.A., Yamauchi, Y., Dhepe, P.L., Wu, K.C.-W., 2017. Direct Production of Furfural in One-pot Fashion from Raw Biomass Using Brønsted Acidic Ionic Liquids. Sci. Rep. 7, 1–7. https://doi.org/10.1038/s41598-017-13946-4

Matsagar, B.M., Munshi, M.K., Kelkar, A.A., Dhepe, P.L., 2015. Conversion of concentrated sugar solutions into 5-hydroxymethyl furfural and furfural using Brönsted acidic ionic liquids. Catal. Sci. Technol. 5, 5086–5090. https://doi.org/10.1039/C5CY00858A

Mazar, A., Jemaa, N., Wafa Al Dajani, W., Marinova, M., Perrier, M., 2017. Furfural production from a pre-hydrolysate generated using aspen and maple chips. Biomass Bioenergy 104, 8–16. https://doi.org/10.1016/j.biombioe.2017.05.016

McKendry, P., 2002. Energy production from biomass (part 1): overview of biomass. Bioresour. Technol., Reviews Issue 83, 37–46. https://doi.org/10.1016/S0960-8524(01)00118-3

Medeiros, D.J., Burnett, M.B., 1985. Furfural process. US4533743A.

Mellmer, M.A., Sener, C., Gallo, J.M.R., Luterbacher, J.S., Alonso, D.M., Dumesic, J.A., 2014. Solvent Effects in Acid-Catalyzed Biomass Conversion Reactions. Angew. Chem. Int. Ed. 53, 11872–11875. https://doi.org/10.1002/anie.201408359

Metkar, P.S., Till, E.J., Corbin, D.R., Pereira, C.J., Hutchenson, K.W., Sengupta, S.K., 2015. Reactive distillation process for the production of furfural using solid acid catalysts. Green Chem. 17, 1453–1466. https://doi.org/10.1039/C4GC01912A

Mittal, A., Black, S.K., Vinzant, T.B., O'Brien, M., Tucker, M.P., Johnson, D.K., 2017. Production of Furfural from Process-Relevant Biomass-Derived Pentoses in a Biphasic Reaction System. ACS Sustain. Chem. Eng. 5, 5694–5701. https://doi.org/10.1021/acssuschemeng.7b00215

Morais, A.R.C., da Costa Lopes, A.M., Bogel-Łukasik, R., 2015. Carbon Dioxide in Biomass Processing: Contributions to the Green Biorefinery Concept. Chem. Rev. 115, 3–27. https://doi.org/10.1021/cr500330z

Morais, A.R.C., Matuchaki, M.D.D.J., Andreaus, J., Bogel-Lukasik, R., 2016. A green and efficient approach to selective conversion of xylose and biomass hemicellulose into furfural in aqueous media using high-pressure CO_2 as a sustainable catalyst. Green Chem. 18, 2985–2994. https://doi.org/10.1039/C6GC00043F

Morais, E.S., Freire, M.G., Freire, C.S.R., Coutinho, J.A.P., Silvestre, A.J.D., 2020. Enhanced Conversion of Xylan into Furfural using Acidic Deep Eutectic Solvents with Dual Solvent and Catalyst Behavior. ChemSusChem 13, 784–790. https://doi.org/10.1002/cssc.201902848

Morais, E.S., Schaeffer, N., Freire, M.G., Freire, C.S.R., Coutinho, J.A.P., Silvestre, A.J.D., 2021. Integrated Production and Separation of Furfural Using an Acidic-Based Aqueous Biphasic System. ACS Sustain. Chem. Eng. 9, 12205–12212. https://doi.org/10.1021/acssuschemeng.1c03733

Nanoti, A., Gupta, P., Dasgupta, S., Garg, M.O., Goswami, A.N., 2008. Process studies for development of adsorption technology for furfural recovery from waste water. Environ. Prog. 27, 308–312. https://doi.org/10.1002/ep.10279

Nhien, L.C., Long, N.V.D., Lee, M., 2021. Novel Hybrid Reactive Distillation with Extraction and Distillation Processes for Furfural Production from an Actual Xylose Solution. Energies 14, 1–16. https://doi.org/10.3390/en14041152

Nie, Y., Hou, Q., Li, W., Bai, C., Bai, X., Ju, M., 2019. Efficient Synthesis of Furfural from Biomass Using SnCl4 as Catalyst in Ionic Liquid. Molecules 24, 1–18. https://doi.org/10.3390/molecules24030594

Oefner, P.J., Lanziner, A.H., Bonn, G., Bobleter, O., 1992. Quantitative studies on furfural and organic acid formation during hydrothermal, acidic and alkaline degradation ofD-xylose. Monatshefte Für Chem. Chem. Mon. 123, 547–556. https://doi.org/10.1007/BF00816848

O'Neill, R., Ahmad, M.N., Vanoye, L., Aiouache, F., 2009. Kinetics of Aqueous Phase Dehydration of Xylose into Furfural Catalyzed by ZSM-5 Zeolite. Ind. Eng. Chem. Res. 48, 4300–4306. https://doi.org/10.1021/ie801599k

Oriez, V., Labauze, H., Benjelloun-Mlayah, B., Deleau, T., Hiraga, Y., Watanabe, M., Condoret, J.-S., Camy, S., 2023. Catalyst-free synthesis of 5-hydroxymethylfurfural from fructose by extractive reaction in supercritical CO2 – subcritical H2O two-phase system. J. Supercrit. Fluids 198, 1–10. https://doi.org/10.1016/j.supflu.2023.105904

Paiva, A., Craveiro, R., Aroso, I., Martins, M., Reis, R.L., Duarte, A.R.C., 2014. Natural Deep Eutectic Solvents – Solvents for the 21st Century. ACS Sustain. Chem. Eng. 2, 1063–1071. https://doi.org/10.1021/sc500096j

Papaioannou, M., Kleijwegt, R.J.T., van der Schaaf, J., Neira d'Angelo, M.F., 2019. Furfural Production by Continuous Reactive Extraction in a Millireactor under the Taylor Flow Regime. Ind. Eng. Chem. Res. 58, 16106–16115. https://doi.org/10.1021/acs.iecr.9b00604

Pardo Cuervo, O.H., Romanelli, G.P., Cubillos, J.A., Rojas, H.A., Martínez, J.J., 2020. Selective Catalytic Dehydration of Xylose to Furfural and Fructose and Glucose to 5-Hydroximethylfurfural (HMF) Using Preyssler Heteropolyacid. ChemistrySelect 5, 4186–4193. https://doi.org/10.1002/slct.202000657

Pei, Y., Wu, K., Wang, J., Fan, J., 2008. Recovery of Furfural from Aqueous Solution by Ionic Liquid Based Liquid–Liquid Extraction. Sep. Sci. Technol. 43, 2090–2102. https://doi.org/10.1080/01496390802064018

Peleteiro, S., da Costa Lopes, A.M., Garrote, G., Parajó, J.C., Bogel-Łukasik, R., 2015. Simple and Efficient Furfural Production from Xylose in Media Containing 1-Butyl-3-Methylimidazolium Hydrogen Sulfate. Ind. Eng. Chem. Res. 54, 8368–8373. https://doi.org/10.1021/acs.iecr.5b01771

Peleteiro, S., Garrote, G., Santos, V., Parajó, J.C., 2014. Conversion of hexoses and pentoses into furans in an ionic liquid 202–206.

Peleteiro, S., Rivas, S., Alonso, J.L., Santos, V., Parajó, J.C., 2016a. Furfural production using ionic liquids: A review. Bioresour. Technol. 202, 181–191. https://doi.org/10.1016/j.biortech.2015.12.017

Peleteiro, S., Santos, V., Garrote, G., Parajó, J.C., 2016b. Furfural production from Eucalyptus wood using an Acidic Ionic Liquid. Carbohydr. Polym. 146, 20–25. https://doi.org/10.1016/j.carbpol.2016.03.049

Pinelo, M., Jonsson, G., Meyer, A.S., 2009. Membrane technology for purification of enzymatically produced oligosaccharides: Molecular and operational features affecting performance. Sep. Purif. Technol. 70, 1–11. https://doi.org/10.1016/j.seppur.2009.08.010

Prasad, A., Sotenko, M., Blenkinsopp, T., Coles, S.R., 2016. Life cycle assessment of lignocellulosic biomass pretreatment methods in biofuel production. Int. J. Life Cycle Assess. 21, 44–50. https://doi.org/10.1007/s11367-015-0985-5

Qiao, H., Han, M., Ouyang, S., Zheng, Z., Ouyang, J., 2022. An integrated lignocellulose biorefinery process: Two-step sequential treatment with formic acid for efficiently producing ethanol and furfural from corn cobs. Renew. Energy 191, 775–784. https://doi.org/10.1016/j.renene.2022.04.027

Qing, Q., Guo, Q., Zhou, L., Wan, Y., Xu, Y., Ji, H., Gao, X., Zhang, Y., 2017. Catalytic conversion of corncob and corncob pretreatment hydrolysate to furfural in a biphasic system with addition of sodium chloride. Bioresour. Technol. 226, 247–254. https://doi.org/10.1016/j.biortech.2016.11.118

Qu, T., Guo, W., Shen, L., Xiao, J., Zhao, K., 2011. Experimental Study of Biomass Pyrolysis Based on Three Major Components: Hemicellulose, Cellulose, and Lignin. Ind. Eng. Chem. Res. 50, 10424–10433. https://doi.org/10.1021/ie1025453

Rabemanolontsoa, H., Saka, S., 2016. Various pretreatments of lignocellulosics. Bioresour. Technol. 199, 83–91. https://doi.org/10.1016/j.biortech.2015.08.029

Rabemanolontsoa, H., Saka, S., 2013. Comparative study on chemical composition of various biomass species. RSC Adv. 3, 3946–3956. https://doi.org/10.1039/C3RA22958K

Rackemann, D.W., Bartley, J.P., Doherty, W.O.S., 2014. Methanesulfonic acid-catalyzed conversion of glucose and xylose mixtures to levulinic acid and furfural. Ind. Crops Prod. 52, 46–57. https://doi.org/10.1016/j.indcrop.2013.10.026

Relvas, F.M., Morais, A.R.C., Bogel-Lukasik, R., 2015. Kinetic modeling of hemicellulose-derived biomass hydrolysis under high pressure CO2–H2O mixture technology. J. Supercrit. Fluids 99, 95–102. https://doi.org/10.1016/j.supflu.2015.01.022

Riansa-ngawong, W., Prasertsan, P., 2011. Optimization of furfural production from hemicellulose extracted from delignified palm pressed fiber using a two-stage process. Carbohydr. Res. 346, 103–110. https://doi.org/10.1016/j.carres.2010.10.009

Rodrigues, P.D.O., Corrêa, A.G., Baffi, M.A., Pasquini, D., 2023. Potential Applications of Hemicellulose, in: Thomas, S., Hosur, M., Pasquini, D., Jose Chirayil, C. (Eds.), Handbook of Biomass. Springer Nature Singapore, Singapore, pp. 1–31. https://doi.org/10.1007/978-981-19-6772-6_27-1

Rodríguez-Meizoso, I., Marin, F.R., Herrero, M., Señorans, F.J., Reglero, G., Cifuentes, A., Ibáñez, E., 2006. Subcritical water extraction of nutraceuticals with antioxidant activity from oregano. Chemical and functional characterization. J. Pharm. Biomed. Anal. 41, 1560–1565. https://doi.org/10.1016/j.jpba.2006.01.018

Rong, C., Ding, X., Zhu, Y., Li, Y., Wang, L., Qu, Y., Ma, X., Wang, Z., 2012. Production of furfural from xylose at atmospheric pressure by dilute sulfuric acid and inorganic salts. Carbohydr. Res. 350, 77–80. https://doi.org/10.1016/j.carres.2011.11.023

Root, D.F., 1956. KINETICS OF THE ACID CATALYZED CONVERSION OF XYLOSE TO FU RFURAL 9, 158–165.

Rose, I.C., Epstein, N., Watkinson, A.P., 2000. Acid-Catalyzed 2-Furaldehyde (Furfural) Decomposition Kinetics. Ind. Eng. Chem. Res. 39, 843–845. https://doi.org/10.1021/ie990550+

Rubin, E.M., 2008. Genomics of cellulosic biofuels. Nature 454, 841–845. https://doi.org/10.1038/nature07190

Saggadi, H., Luart, D., Thiebault, N., Polaert, I., Estel, L., Len, C., 2014. Toward the synthesis of 6-hydroxyquinoline starting from glycerol via improved microwave-assisted modified Skraup reaction. Catal. Commun. 44, 15–18. https://doi.org/10.1016/j.catcom.2013.07.029

Sahu, A.K., Srivastava, V.C., Mall, I.D., Lataye, D.H., 2008. Adsorption of Furfural from Aqueous Solution onto Activated Carbon: Kinetic, Equilibrium and Thermodynamic Study. Sep. Sci. Technol. 43, 1239–1259. https://doi.org/10.1080/01496390701885711

Sahu, R., Dhepe, P.L., 2012. A One-Pot Method for the Selective Conversion of Hemicellulose from Crop Waste into C5 Sugars and Furfural by Using Solid Acid Catalysts. ChemSusChem 5, 751–761. https://doi.org/10.1002/cssc.201100448

Sai, M.S.N., 2021. Sustainable production and purification of furfural from waste agricultural residue: An insight into integrated biorefinery. J. Clean. Prod. 327, 1–17. https://doi.org/10.1016/j.jclepro.2021.129467

Saini, J.K., Saini, R., Tewari, L., 2015. Lignocellulosic agriculture wastes as biomass feedstocks for second-generation bioethanol production: concepts and recent developments. 3 Biotech 5, 337–353. https://doi.org/10.1007/s13205-014-0246-5

Sako, T., Taguchi, T., Sugeta, T., Nakazawa, N., Okubo, T., Hiaki, T., Sato, M., 1992. Kinetic Study of Furfural Formation Accompanying Supercritical Carbon Dioxide Extraction. J. Chem. Eng. Jpn. 25, 372–377. https://doi.org/10.1252/jcej.25.372

Sandhya, S.V., Kiran, K., Kuttiraja, M., Preeti, V.E., Sindhu, R., Vani, S., Kumar, S.R., Pandey, A., Binod, P., 2013. Evaluation of polymeric adsorbent resins for efficient detoxification of liquor generated during acid pretreatment of lignocellulosic biomass. INDIAN J EXP BIOL 51, 1012–1017.

Sangarunlert, W., Piumsomboon, P., Ngamprasertsith, S., 2007. Furfural production by acid hydrolysis and supercritical carbon dioxide extraction from rice husk. Korean J. Chem. Eng. 24, 936–941. https://doi.org/10.1007/s11814-007-0101-z

Sato, O., Mimura, N., Masuda, Y., Shirai, M., Yamaguchi, A., 2019. Effect of extraction on furfural production by solid acid-catalyzed xylose dehydration in water. J. Supercrit. Fluids 144, 14–18. https://doi.org/10.1016/j.supflu.2018.10.004

Scapin, E., Rambo, M.K.D., Viana, G.C.C., Marasca, N., Lacerda, G.E., Rambo, M.C.D., Fernandes, R. de M.N., 2020. Sustainable production of furfural and 5-hidroximetilfurfural from rice husks and soybean peel by using ionic liquid. Food Sci. Technol. 40, 83–87. https://doi.org/10.1590/fst.04419

Seemala, B., Haritos, V., Tanksale, A., 2016. Levulinic Acid as a Catalyst for the Production of 5-Hydroxymethylfurfural and Furfural from Lignocellulose Biomass. ChemCatChem 8, 640–647. https://doi.org/10.1002/cctc.201501105

Seidl, P.R., Goulart, A.K., 2016. Pretreatment processes for lignocellulosic biomass conversion to biofuels and bioproducts. Curr. Opin. Green Sustain. Chem. 2, 48–53. https://doi.org/10.1016/j.cogsc.2016.09.003

Serrano-Ruiz, J.C., Campelo, J.M., Francavilla, M., Romero, A.A., Luque, R., Menéndez-Vázquez, C., García, A.B., García-Suárez, E.J., 2012. Efficient microwave-assisted production of furfural from C5 sugars in aqueous media catalysed by Brönsted acidic ionic liquids. Catal. Sci. Technol. 2, 1828–1832. https://doi.org/10.1039/c2cy20217d

Sert, M., Arslanoğlu, A., Ballice, L., 2018. Conversion of sunflower stalk based cellulose to the valuable products using choline chloride based deep eutectic solvents. Renew. Energy 118, 993–1000. https://doi.org/10.1016/j.renene.2017.10.083

Shen, F., Xiong, X., Fu, J., Yang, J., Qiu, M., Qi, X., Tsang, D.C.W., 2020. Recent advances in mechanochemical production of chemicals and carbon materials from sustainable biomass resources. Renew. Sustain. Energy Rev. 130, 1–20. https://doi.org/10.1016/j.rser.2020.109944

Shi, J., Kang, X., Mao, L., Jiang, Y., Zhao, S., Liu, Y., Zhai, B., Jin, H., Guo, L., 2023. Supercritical CO2-applied equipment for chemical synthesis and transformation: Current status and perspectives. Chem. Eng. J. 459, 1–19. https://doi.org/10.1016/j.cej.2023.141608

Sievers, C., Musin, I., Marzialetti, T., Valenzuela Olarte, M.B., Agrawal, P.K., Jones, C.W., 2009. Acid-Catalyzed Conversion of Sugars and Furfurals in an Ionic-Liquid Phase. ChemSusChem 2, 665–671. https://doi.org/10.1002/cssc.200900092

Stark, A., 2011. Ionic liquids in the biorefinery: a critical assessment of their potential. Energy Env. Sci 4, 19–32. https://doi.org/10.1039/C0EE00246A

Sun, Shaoni, Sun, Shaolong, Cao, X., Sun, R., 2016. The role of pretreatment in improving the enzymatic hydrolysis of lignocellulosic materials. Bioresour. Technol. 199, 49–58. https://doi.org/10.1016/j.biortech.2015.08.061

Suxia, R., Haiyan, X., Jinling, Z., Shunqing, L., Xiaofeng, H., Tingzhou, L., 2012. Furfural production from rice husk using sulfuric acid and a solid acid catalyst through a two-stage process. Carbohydr. Res. 359, 1–6. https://doi.org/10.1016/j.carres.2012.07.006

Tadesse, H., Luque, R., 2011. Advances on biomass pretreatment using ionic liquids: An overview. Energy Environ. Sci. 4, 3913–3929. https://doi.org/10.1039/c0ee00667j

Taha, M., Foda, M., Shahsavari, E., Aburto-Medina, A., Adetutu, E., Ball, A., 2016. Commercial feasibility of lignocellulose biodegradation: possibilities and challenges. Curr. Opin. Biotechnol. 38, 190–197. https://doi.org/10.1016/j.copbio.2016.02.012

Taherzadeh, M., Karimi, K., 2008. Pretreatment of Lignocellulosic Wastes to Improve Ethanol and Biogas Production: A Review. Int. J. Mol. Sci. 9, 1621–1651. https://doi.org/10.3390/ijms9091621

Tao, F., Song, H., Chou, L., 2011. Efficient process for the conversion of xylose to furfural with acidic ionic liquid. Can. J. Chem. 89, 83–87. https://doi.org/10.1139/V10-153

Tayyab, M., 2018. BIOETHANOL PRODUCTION FROM LIGNOCELLULOSIC BIOMASS BY ENVIRONMENT-FRIENDLY PRETREATMENT METHODS: A REVIEW. Appl. Ecol. Environ. Res. 16, 225–249. https://doi.org/10.15666/aeer/1601_225249

Templeton, D.W., Sluiter, A.D., Hayward, T.K., Hames, B.R., Thomas, S.R., 2009. Assessing corn stover composition and sources of variability via NIRS. Cellulose 16, 621–639. https://doi.org/10.1007/s10570-009-9325-x

Tongtummachat, T., Jaree, A., Akkarawatkhoosith, N., 2022. Continuous hydrothermal furfural production from xylose in a microreactor with dual-acid catalysts. RSC Adv. 12, 23366–23378. https://doi.org/10.1039/D2RA03609F

Toscan, A., Morais, A.R.C., Paixão, S.M., Alves, L., Andreaus, J., Camassola, M., Dillon, A.J.P., Lukasik, R.M., 2017. High-pressure carbon dioxide/water pre-treatment of sugarcane bagasse and elephant grass: Assessment of the effect of biomass composition on process efficiency. Bioresour. Technol. 224, 639–647. https://doi.org/10.1016/j.biortech.2016.11.101

Tuteja, J., Nishimura, S., Ebitani, K., 2012. One-Pot Synthesis of Furans from Various Saccharides Using a Combination of Solid Acid and Base Catalysts. Bull. Chem. Soc. Jpn. 85, 275–281. https://doi.org/10.1246/bcsj.20110287

Ulber, R., Sell, D. (Eds.), 2007. White Biotechnology, Advances in Biochemical Engineering/Biotechnology. Springer Berlin Heidelberg, Berlin, Heidelberg. https://doi.org/10.1007/978-3-540-45696-4

Vanholme, R., Demedts, B., Morreel, K., Ralph, J., Boerjan, W., 2010. Lignin Biosynthesis and Structure. Plant Physiol. 153, 895–905. https://doi.org/10.1104/pp.110.155119

Vaz Jr., S., Donate, P.M., 2015. Microwave-Assisted Green Production of Furfural from D-xylose of Sugarcane Bagasse. BioResources 10, 8168–8180. https://doi.org/10.15376/biores.10.4.8168-8180

Vila, C., Santos, V., Parajó, J.C., 2003. Recovery of lignin and furfural from acetic acid–water–HCl pulping liquors. Bioresour. Technol. 90, 339–344. https://doi.org/10.1016/S0960-8524(03)00030-0

Vispute, T.P., Zhang, H., Sanna, A., Xiao, R., Huber, G.W., 2010. Renewable Chemical Commodity Feedstocks from Integrated Catalytic Processing of Pyrolysis Oils. Science 330, 1222–1227. https://doi.org/10.1126/science.1194218

Wang, Q., Zhuang, X., Wang, W., Tan, X., Yu, Q., Qi, W., Yuan, Z., 2018. Rapid and simultaneous production of furfural and cellulose-rich residue from sugarcane bagasse using a pressurized phosphoric acid-acetone-water system. Chem. Eng. J. 334, 698–706. https://doi.org/10.1016/j.cej.2017.10.089

Wang, S., Zhao, Y., Lin, H., Chen, J., Zhu, L., Luo, Z., 2017. Conversion of C5 carbohydrates into furfural catalyzed by a Lewis acidic ionic liquid in renewable γ-valerolactone. Green Chem. 19, 3869–3879. https://doi.org/10.1039/C7GC01298E

Wang, W., Li, H., Ren, J., Sun, R., Zheng, J., Sun, G., Liu, S., 2014. An efficient process for dehydration of xylose to furfural catalyzed by inorganic salts in water/dimethyl sulfoxide system. Chin. J. Catal. 35, 741–747. https://doi.org/10.1016/S1872-2067(14)60031-0

Wang, W., Ren, J., Li, H., Deng, A., Sun, R., 2015. Direct transformation of xylan-type hemicelluloses to furfural via SnCl4 catalysts in aqueous and biphasic systems. Bioresour. Technol. 183, 188–194. https://doi.org/10.1016/j.biortech.2015.02.068

Wang, X., Qiu, M., Tang, Y., Yang, J., Shen, F., Qi, X., Yu, Y., 2021. Synthesis of sulfonated lignin-derived ordered mesoporous carbon for catalytic production of furfural from xylose. Int. J. Biol. Macromol. 187, 232–239. https://doi.org/10.1016/j.ijbiomac.2021.07.155

Wang, Y., 2010. Integration of conventional electrodialysis and electrodialysis with bipolar membranes for production of organic acids. J. Membr. Sci. 365, 294–301. https://doi.org/10.1016/j.memsci.2010.09.018

Wang, Y., Len, T., Huang, Y., Diego Taboada, A., Boa, A.N., Ceballos, C., Delbecq, F., Mackenzie, G., Len, C., 2017. Sulfonated Sporopollenin as an Efficient and Recyclable Heterogeneous Catalyst for Dehydration of D -Xylose and Xylan into Furfural. ACS Sustain. Chem. Eng. 5, 392–398. https://doi.org/10.1021/acssuschemeng.6b01780

Weingarten, R., Cho, J., Conner, Jr., Wm.C., Huber, G.W., 2010. Kinetics of furfural production by dehydration of xylose in a biphasic reactor with microwave heating. Green Chem. 12, 1423–1429. https://doi.org/10.1039/c003459b

Weng, Y.-H., Wei, H.-J., Tsai, T.-Y., Lin, T.-H., Wei, T.-Y., Guo, G.-L., Huang, C.-P., 2010. Separation of furans and carboxylic acids from sugars in dilute acid rice straw hydrolyzates by nanofiltration. Bioresour. Technol. 101, 4889–4894. https://doi.org/10.1016/j.biortech.2009.11.090

Wertz, J.-L., Bédué, O., 2013. Lignocellulosic Biorefineries, First. ed. PPUR Presses polytechniques, EPFL Press, Spain.

Wood, L., 2019. Global Furfural Market 2019-2024 - Emerging Demand for Furfural Derivatives (Apart From Furfuryl Alcohol) in Various Applications [WWW Document]. GlobeNewswire Notif. URL https://www.marketsandmarkets.com/Market-Reports/furfural-market-101056456.html (accessed 10.5.21).

Xia, H., Xu, S., Yang, L., 2017. Efficient conversion of wheat straw into furan compounds, bio-oils, and phosphate fertilizers by a combination of hydrolysis and catalytic pyrolysis. RSC Adv. 7, 1200–1205. https://doi.org/10.1039/C6RA27072G

Xing, R., Qi, W., Huber, G.W., 2011. Production of furfural and carboxylic acids from waste aqueous hemicellulose solutions from the pulp and paper and cellulosic ethanol industries. Energy Environ. Sci. 4, 2193–2205. https://doi.org/10.1039/c1ee01022k

Xu, S., Pan, D., Wu, Y., Song, X., Gao, L., Li, W., Das, L., Xiao, G., 2018a. Efficient production of furfural from xylose and wheat straw by bifunctional chromium phosphate catalyst in biphasic systems. Fuel Process. Technol. 175, 90–96. https://doi.org/10.1016/j.fuproc.2018.04.005

Xu, S., Pan, D., Wu, Y., Song, X., Gao, L., Li, W., Das, L., Xiao, G., 2018b. Efficient production of furfural from xylose and wheat straw by bifunctional chromium phosphate catalyst in biphasic systems. Fuel Process. Technol. 175, 90–96. https://doi.org/10.1016/j.fuproc.2018.04.005

Xu, S., Pan, D., Wu, Y., Song, X., Gao, L., Li, W., Das, L., Xiao, G., 2018c. chromium phosphate catalyst in biphasic systems. Fuel Process. Technol. 175, 90–96.

Xu, S., Wu, N., Yuan, H., Chen, Y., Pan, D., Wu, Y., Fan, J., Gao, L., Xiao, G., 2020. An Effective and Stable HfP/SiO2 Catalyst for the Production of Furfural from Xylan. Catal. Lett. 150, 1121–1127. https://doi.org/10.1007/s10562-019-02994-2

Xu, Z., Li, W., Du, Z., Wu, H., Jameel, H., Chang, H., Ma, L., 2015. Conversion of corn stalk into furfural using a novel heterogeneous strong acid catalyst in γ-valerolactone. Bioresour. Technol. 198, 764–771. https://doi.org/10.1016/j.biortech.2015.09.104

Yan, K., Wu, G., Lafleur, T., Jarvis, C., 2014. Production, properties and catalytic hydrogenation of furfural to fuel additives and value-added chemicals. Renew. Sustain. Energy Rev. 38, 663–676. https://doi.org/10.1016/j.rser.2014.07.003

Yang, W., Li, P., Bo, D., Chang, H., 2012a. The optimization of formic acid hydrolysis of xylose in furfural production. Carbohydr. Res. 357, 53–61. https://doi.org/10.1016/j.carres.2012.05.020

Yang, W., Li, P., Bo, D., Chang, H., 2012b. The optimization of formic acid hydrolysis of xylose in furfural production. Carbohydr. Res. 357, 53–61. https://doi.org/10.1016/j.carres.2012.05.020

Yang, W., Li, P., Bo, D., Chang, H., Wang, X., Zhu, T., 2013. Optimization of furfural production from d-xylose with formic acid as catalyst in a reactive extraction system. Bioresour. Technol. 133, 361–369. https://doi.org/10.1016/j.biortech.2013.01.127

Yang, Y., Hu, C., Abu-Omar, M.M., 2012. Conversion of carbohydrates and lignocellulosic biomass into 5-hydroxymethylfurfural using $AlCl_3 \cdot 6H_2O$ catalyst in a biphasic solvent system. Green Chem 14, 509–513. https://doi.org/10.1039/C1GC15972K

Yemiş, O., Mazza, G., 2011. Acid-catalyzed conversion of xylose, xylan and straw into furfural by microwave-assisted reaction. Bioresour. Technol. 102, 7371–7378. https://doi.org/10.1016/j.biortech.2011.04.050

Yi, J., He, T., Jiang, Z., Li, J., Hu, C., 2013. AlCl3 catalyzed conversion of hemicellulose in corn stover. Chin. J. Catal. 34, 2146–2152. https://doi.org/10.1016/S1872-2067(12)60718-9

Yong, T.L.-K., Mohamad, N., Yusof, N.N.M., 2016. Furfural Production from Oil Palm Biomass Using a Biomass-derived Supercritical Ethanol Solvent and Formic Acid Catalyst. Procedia Eng. 148, 392–400. https://doi.org/10.1016/j.proeng.2016.06.495

Yu, Q., Song, Z., Zhuang, X., Liu, L., Qiu, W., Shi, J., Wang, W., Li, Y., Wang, Z., Yuan, Z., 2019. Catalytic conversion of herbal residue carbohydrates to furanic derivatives in a deep eutectic solvent accompanied by dissolution and recrystallisation of choline chloride. Cellulose 26, 8263–8277. https://doi.org/10.1007/s10570-019-02372-6

Zeitsch, K.J., 2008. Verfahren zur herstellung von furfural. DE60035029T2.

Zeitsch, K.J., 2004. Process for the manufacture of furfural. US6743928B1.

Zeitsch, K.J., 2000. The Chemistry and Technology of Furfural and its Many By-Products. Elsevier.

Zhang, J., Lin, L., Liu, S., 2012. Efficient Production of Furan Derivatives from a Sugar Mixture by Catalytic Process. Energy Fuels 26, 4560–4567. https://doi.org/10.1021/ef300606v

Zhang, L., He, Y., Zhu, Y., Liu, Y., Wang, X., 2018. Camellia oleifera shell as an alternative feedstock for furfural production using a high surface acidity solid acid catalyst. Bioresour. Technol. 249, 536–541. https://doi.org/10.1016/j.biortech.2017.10.061

Zhang, L., Xi, G., Chen, Z., Jiang, D., Yu, H., Wang, X., 2017a. Highly selective conversion of glucose into furfural over modified zeolites. Chem. Eng. J. 307, 868–876. https://doi.org/10.1016/j.cej.2016.09.001

Zhang, L., Xi, G., Zhang, J., Yu, H., Wang, X., 2017b. Efficient catalytic system for the direct transformation of lignocellulosic biomass to furfural and 5-hydroxymethylfurfural. Bioresour. Technol. 224, 656–661. https://doi.org/10.1016/j.biortech.2016.11.097

Zhang, L., Yu, H., 2013. Conversion of Xylan and Xylose into Furfural in Biorenewable Deep Eutectic Solvent with Trivalent Metal Chloride Added. BioResources 8, 6014–6025. https://doi.org/10.15376/biores.8.4.6014-6025

Zhang, L., Yu, H., Wang, P., 2013a. Solid acids as catalysts for the conversion of d-xylose, xylan and lignocellulosics into furfural in ionic liquid. Bioresour. Technol. 136, 515–521. https://doi.org/10.1016/j.biortech.2013.03.054

Zhang, L., Yu, H., Wang, P., Dong, H., Peng, X., 2013b. Conversion of xylan, d-xylose and lignocellulosic biomass into furfural using AlCl3 as catalyst in ionic liquid. Bioresour. Technol. 130, 110–116. https://doi.org/10.1016/j.biortech.2012.12.018

Zhang, L., Yu, H., Wang, P., Li, Y., 2014. Production of furfural from xylose, xylan and corncob in gamma-valerolactone using FeCl3·6H2O as catalyst. Bioresour. Technol. 151, 355–360. https://doi.org/10.1016/j.biortech.2013.10.099

Zhang, L.-X., Yu, H., Yu, H.-B., Chen, Z., Yang, L., 2014. Conversion of xylose and xylan into furfural in biorenewable choline chloride–oxalic acid deep eutectic solvent with the addition of metal chloride. Chin. Chem. Lett. 25, 1132–1136. https://doi.org/10.1016/j.cclet.2014.03.029

Zhang, Q., Zhang, S., Deng, Y., 2011. Recent advances in ionic liquid catalysis. Green Chem. 13, 2619–2637. https://doi.org/10.1039/c1gc15334j

Zhang, T., Kumar, R., Wyman, C.E., 2013. Enhanced yields of furfural and other products by simultaneous solvent extraction during thermochemical treatment of cellulosic biomass. RSC Adv. 3, 9809–9819. https://doi.org/10.1039/c3ra41857j

Zhang, T., Li, W., An, S., Huang, F., Li, X., Liu, J., Pei, G., Liu, Q., 2018. Efficient transformation of corn stover to furfural using p-hydroxybenzenesulfonic acid-formaldehyde resin solid acid. Bioresour. Technol. 264, 261–267. https://doi.org/10.1016/j.biortech.2018.05.081

Zhang, T., Li, W., Xu, Z., Liu, Q., Ma, Q., Jameel, H., Chang, H., Ma, L., 2016. Catalytic conversion of xylose and corn stalk into furfural over carbon solid acid catalyst in γ-valerolactone. Bioresour. Technol. 209, 108–114. https://doi.org/10.1016/j.biortech.2016.02.108

Zhang, Y., Chen, M., Wang, J., Hu, Q., 2014. Synthesis of Furfural from D-Xylose and Corncob with Chromium Chloride as Catalyst in Biphasic System. Asian J. Chem. 26, 1717–1720. https://doi.org/10.14233/ajchem.2014.17333

Zhang, Z., Du, B., Quan, Z.-J., Da, Y.-X., Wang, X.-C., 2014. Dehydration of biomass to furfural catalyzed by reusable polymer bound sulfonic acid (PEG-OSO3H) in ionic liquid. Catal. Sci. Technol. 4, 633–638. https://doi.org/10.1039/c3cy00888f

Zhang, Z., Zhao, Z.K., 2010. Microwave-assisted conversion of lignocellulosic biomass into furans in ionic liquid. Bioresour. Technol. 101, 1111–1114. https://doi.org/10.1016/j.biortech.2009.09.010

Zhao, Y., Lu, K., Xu, H., Zhu, L., Wang, S., 2021. A critical review of recent advances in the production of furfural and 5-hydroxymethylfurfural from lignocellulosic biomass through homogeneous catalytic hydrothermal conversion. Renew. Sustain. Energy Rev. 139, 1–27. https://doi.org/10.1016/j.rser.2021.110706

Zhao, Y., Xu, H., Lu, K., Qu, Y., Zhu, L., Wang, S., 2019a. Dehydration of xylose to furfural in butanone catalyzed by Brønsted-Lewis acidic ionic liquids. Energy Sci. Eng. 7, 2237–2246. https://doi.org/10.1002/ese3.444

Zhao, Y., Xu, H., Lu, K., Qu, Y., Zhu, L., Wang, S., 2019b. Experimental and Kinetic Study of Arabinose Conversion to Furfural in Renewable Butanone–Water Solvent Mixture Catalyzed by Lewis Acidic Ionic Liquid Catalyst. Ind. Eng. Chem. Res. 58, 17088–17097. https://doi.org/10.1021/acs.iecr.9b03420

Zhou, F., Wang, C., Wei, J., 2013. Separation of acetic acid from monosaccharides by NF and RO membranes: Performance comparison. J. Membr. Sci. 429, 243–251. https://doi.org/10.1016/j.memsci.2012.11.043

Zhu, T., Li, P., Wang, X., Yang, W., Chang, H., Ma, S., 2014. Optimization of formic acid hydrolysis of corn cob in xylose production. Korean J. Chem. Eng. 31, 1624–1631. https://doi.org/10.1007/s11814-014-0073-8

Zhu, Y., Li, W., Lu, Y., Zhang, T., Jameel, H., Chang, H., Ma, L., 2017. Production of furfural from xylose and corn stover catalyzed by a novel porous carbon solid acid in γ-valerolactone. RSC Adv. 7, 29916–29924. https://doi.org/10.1039/C7RA03995F

II. Chapter 2

Materials and methods

This chapter lists all the chemicals and experimental setups used throughout the project. The methods used to collect the experimental data and quantify each substance are also provided. Additionally, the compositions of the solutions used in various investigations are listed by categorizing them within each segment of the experiment. Finally, the extraction of hemicellulose from raw biomass through the LEEBio^{TM} process is detailed.

II.1 Chemicals

Standard reagents of furfural (>99.0 wt%), formic acid (>98.0 wt%) and toluene (99.9 wt%) were purchased from Acros Organic (FR). Mannose (99 wt%), xylose (>99.0 wt%) and glucose (99 wt%) were purchased from Thermoscientific (FR). Fructose (99 wt%), galactose (99 wt%), arabinose (99 wt%), cyclopentyl methyl ether (CPME, 100 wt%), 5-hydroxymethylfurfural (5-HMF, >99.0 wt%), ethyl butyrate (EB, 99 wt%), Aquivion-PW98 and Amberlyst-15 were purchased from Sigma Aldrich (FR). Xylulose (>95 wt%) was purchased from VWR (US). The characteristics of the monosaccharides and desired products as well as organic solvents were listed in Table II-1 and Table II-2, respectively. Carbon dioxide (99.98 vol%) was supplied by Air Liquide. The solid catalyst zeolite, including H-ZSM-5 (SiO_2/Al_2O_3 = 23) and H-Mordenite (SiO_2/Al_2O_3 = 18), was purchased from TOSOH. All of the chemicals were analytical grade and used without further purification. All solutions were prepared in deionized water (resistivity: 18.2 MΩ.cm). The hydrolysate derived from fir wood was provided by BioEB Company (Auzeville-Tolosane, France) and the Oil Palm Empty Fruit Bunch (OPEFB) was kindly supplied by Universitas Indonesia (Depok, Indonesia). After harvesting raw OPEFB, the first step involved drying them under the sun (35-38 °C) for 2 days (moisture content ~ 15%). Following this, the dried OPEFB underwent milling to reduce particle size to below 2 mm before being stored at room temperature until further use. The OPEFB was treated using the LEEBio^{TM} procedure to produce the hydrolysate rich in hemicellulose, followed by acid hydrolysis to determine the content of sugars, lignin, acetyl groups, and ash.

Table II-1: Physico−chemical properties of mono-sugars

Compound	Xylose	Xylulose	Glucose	Mannose	Arabinose	Galactose
Chemical formula	$C_5H_{10}O_5$	$C_5H_{10}O_5$	$C_6H_{12}O_6$	$C_6H_{12}O_6$	$C_5H_{10}O_5$	$C_6H_{12}O_6$
Structure	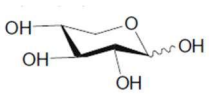	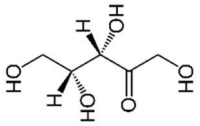	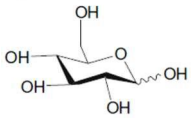	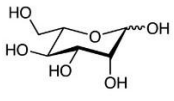	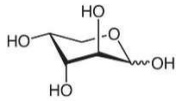	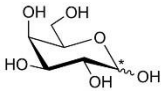
Molecular weight (g/mol)	150.13	150.13	180.16	180.16	150.13	180.16
Hydrosolubility at 25 °C (g/L)	100	-	900	713	834	180
Dissociation constant (pK_a, 25 °C)	12.14	-	12.46	12.92	12.33	11.3

Table II-2: Physico−chemical properties of organic acid, solvents and desired products

Compound	Furfural	5-HMF	Formic acid	Toluene	CPME	EB
Chemical formula	$C_5H_4O_2$	$C_6H_6O_3$	HCOOH	C_7H_8	$C_6H_{12}O$	$C_6H_{12}O_2$
Structure	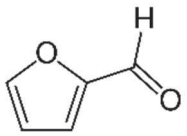	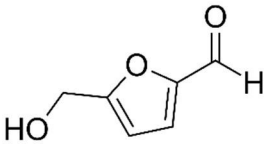	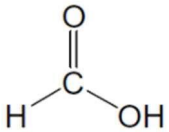	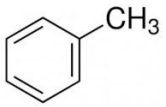	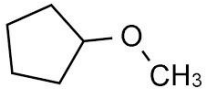	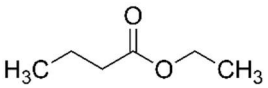
Molecular weight (g/mol)	96.08	126.11	46.03	92.14	100.16	116.16
Hydrosolubility à 20 °C (g/L)	83	364	1000	0.53	0.011	6.2
Boiling point (°C, 1 atm)	162	114	101	110.58	106	121
Density (20 °C)	1.16	1.29	1.22	0.87	0.86	0.879
Dissociation constant (pK_a, 25 °C)	-	-	3.75	-	-	-

II.2 Production of furfural from xylose in batch system

II.2.1 Furfural production at atmospheric pressure

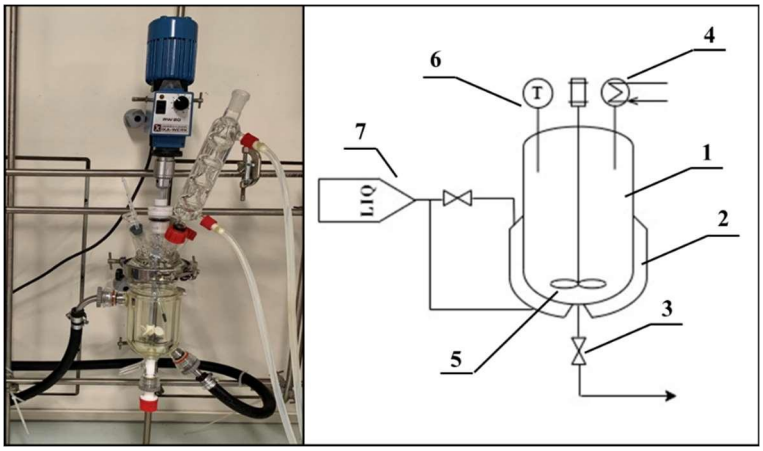

Figure II-1: The experimental setup for synthesis at atmospheric pressure. (1) glass reactor vessel; (2) double jacket; (3) Emptying valve; (4) glass condenser; (5) mechanical stirrer; (6) thermometer; (7) circulation water bath

The components of the experimental system include a double jacketed glass reactor (440 mL, 630 mm inner diameter x 150 mm height) with a thermometer, a mechanical stirrer, and a condenser as shown in Figure II-1. A series of experiments were conducted using xylose as a reference reagent. The choice of xylose as a representative compound was based on the fact that hemicellulose in lignocellulosic materials is predominantly composed of xylose units. The synthetic solutions contained only xylose (10 g/L) and formic acid (10-30 wt%). Their concentration was representative of the hemicellulose hydrolysate resulting from biomass hydrolysis by formic acid in the LEEBio^{TM} process. The experimental conditions are shown in Tables II-3 and II-4 for synthesis in monophasic and biphasic solvent systems, respectively.

A typical procedure for the experiment is listed as follows: first the condenser was turned by activated the water circulation through it, then the thermofluidic oil is circulated in the double envelope. Once the temperature inside the reactor was 5-10 °C below the boiling point (~100 °C), 200 mL of solution composed of xylose (10 g/L) and formic acid (10-30 wt%) (or organic solvent and prepared xylose solution contained formic acid for biphasic solvent systems trials) was poured into the reactor and the speed of the stirrer was fixed to 400 rpm. The reaction time was recorded when the boiling point was reached. After the desired reaction time, the solution was drained through the discharge valve into a container placed in an ice batch to instantly cool the solution to room temperature. The total volume of liquid was

measured, and a sample was taken for composition analysis with the specific analysis described in Section II.6.

Concerning biphasic solvent systems, reaction solutions were separated by separating funnels after cooling to room temperature. The extractive phase and the aqueous phase were used for the analysis of furfural and xylose quantities, respectively.

Table II-3: Experimental conditions from dehydration of xylose in monophasic system at atmospheric pressure

Entry	*t* (min)	Compounds/Concentration	
		Xyl (g/L)	FA (wt%)
1	40	10	10
2	60		
3	300		
4	300		30
5	540		
6[a]	300		
7[b]	300		
8[c]	300		

[a] The pure xylose solution is fed continuously for 120 min, similar to the semi-continuous system.

[b] 2.0 g of Aquivion PW98 was added.

[c] 1.2 g of Amberlyst-15 was added.

Op. Cond.: volume of the mixture = 200 mL; stirring = 400 rpm; temperature (boiling point) and atmospheric pressure.

Table II-4: Experimental conditions from dehydration of xylose in biphasic solvent system at atmospheric pressure

Entry	Organic solvent	Phase aqueous to phase organic ratio (v/v)
1[a]	Toluene	1:3
2[a]	CPME	
3[a*]	Toluene	
4[a**]	Toluene	
5[b]	Toluene	1:15

Op Cond.: volume of the mixture = 200 mL; stirring = 400 rpm; temperature (boiling point); atmospheric pressure. a: xylose concentration (10 g/L) and formic acid concentration (30 wt%), b: xylose concentration (100 g/L); formic acid concentration (30 wt%) and 2.4 g of NaCl.

** The pure xylose solution is fed continuously for 60 min, similar to the semi-continuous system.*

** 0.3 g of Amberlyst-15 was added.*

II.2.2 Furfural production under pressure

II.2.2.1 Experimental set-up

Two high-pressure reactors are used for furfural production under pressure, being determined by the maximum capacity of the reactors (90 mL and 250 mL). The compact reactor (90 mL) was acquired from Top Industrie (FR), as depicted in Figure II-2, and its specifications are outlined in Table II-5. The larger one (250 mL) was acquired from Equilabo (FR) as depicted in Figure II-3, and its characteristics are outlined in Table II-6.

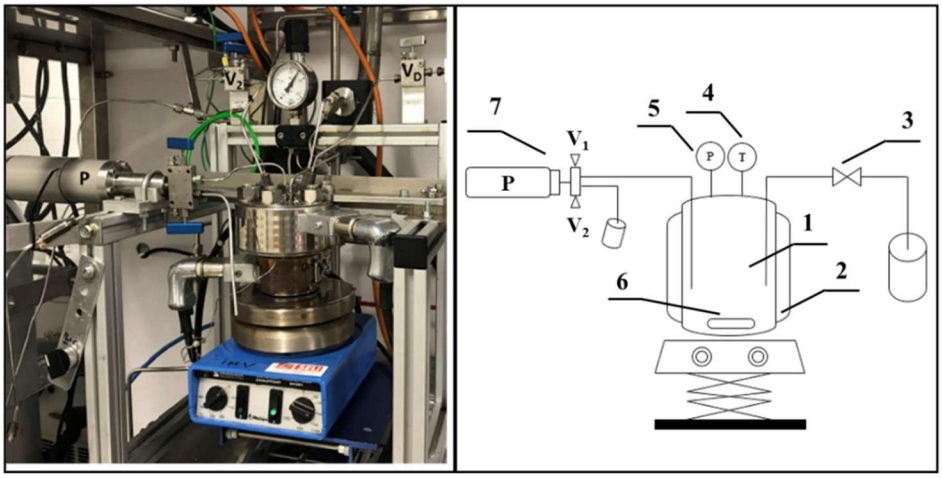

Figure II-2: The schematic diagram of the experimental setup of high-pressure reactor (1) stainless-steel autoclave; (2) electric jacket; (3) expansion valve; (4) thermocouple; (5) pressure gauge; (6) magnetic stirrer; (7) sampling device

Table II-5: Characteristic of high-pressure reactor (Top industrie)

High-pressure reactor (Top Industrie, FR)	
Cylindrical tank	d_{ex} = 5.8 cm, d_{in} = 4.5 cm, H = 6.0 cm
Maximum volume	90 mL
Maximum temperature	250 °C
Maximum pressure	38 MPa
Material	Inox

The “Top Industrie” reactor consists of a cylindrical tank installed on its base and surrounded by two electric heaters (Figure II-2). The cover on the outside is made up of a tube dipping into the reactor, a type K thermocouple and a pressure gauge coupled with a sensor (Keller). The dip tube is connected to a sampling device with a maximum capacity of 2.5 mL. It allows to take under pressure a sample of aqueous phase or gaseous phase in the biphasic mixture studied. This system also allows the injection of reagents if necessary. The maximum operating absolute pressure for this sampler is 35 MPa and the maximum operating temperature is 250 °C. The thermocouple inserted in a glove finger is used to measure the temperature and the pressure inside the reactor. The pressure gauge displays the pressure in the reactor with the pressure range between 0 and 40 MPa. Stirring can be done magnetically using a bar magnet which is driven in rotation by a magnetic stirring block placed under the reactor.

Table II-6: Characteristics of the high-pressure reactor "Equilabo"

High-pressure reactor (Equilabo, FR)	
Cylindrical tank	d_{ex} = 7.50 cm, d_{in} = 6.35 cm, H = 10.16 cm
Volume	V_{max} = 234 mL, V_{min} = 126 mL
Maximum temperature	350 °C
Maximum pressure	20 MPa
Material	Inox 316 SS

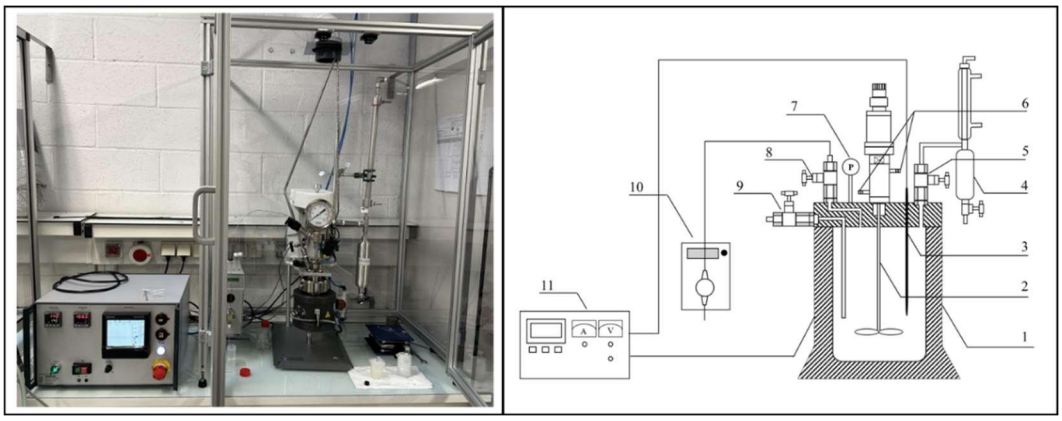

Figure II-3: The schematic diagram of the experimental setup of high-pressure reactor "Equilabo". (1) Stainless steel autoclave; (2) magnetic stirrer; (3) thermocouple; (4 and 6) condenser; (5) Vapor bleed valve; (7) pressure gauge; (8) liquid feed valve; (9) liquid bleed valve; (10) pump; (11) intelligent temperature controller

The "Equilabo" reactor consists of a cylindrical vessel mounted on a fixed-head frame and surrounded by two half-shells (Figure II-3). The outer cover consists of a dip tube in the reactor, a J-type thermocouple and a Bourdon tube pressure gauge with 3% accuracy. The dip tube is connected to an HPLC pump (Eldex 5976 Optos 2SM 1/8'' Head SS) for reagent introduction. The reactor is also equipped with a sample outlet. A thermocouple inserted in a glove finger measures temperature and pressure inside the reactor. The pressure gauge displays the pressure in the reactor, with a range from 0 to 20 MPa. Mechanical agitation is provided by a 316 SS hollow propeller driven by an electric motor. Speed can vary from 0 to 1700 rpm. A statistical basket for the catalyst can be installed above this hollow propeller, to prevent deterioration of solid catalysts. The reactor is heated by an electric furnace fitted with a thermocouple and insulated by a stainless-steel jacket. This furnace slides along one of the frame's axes and can therefore be lowered quickly in the event of an exothermic reaction. This reactor (Figure II-3, No. 4) enables both semi-continuous and continuous syntheses due to the presence of a condenser with a liquid capacity of 150 mL.

II.2.2.2 Xylose dehydration catalyzed by formic acid and heterogeneous catalysts

For this section, the reactions were carried out using "Top Industrie" reactor. In a typical experiment, 65 mL of pure formic acid solution was introduced into a high-pressure reactor under the magnetic stirring of 400 rpm. Then, 5 mL of pure xylose solution was injected into the reactor using the sampling device when the temperature inside of reactor was 3 °C lesser than the desired reaction temperature. The concentration of formic acid and xylose were prepared in such a way that their final concentrations in the reactor reached the desired value. The reaction time was calculated after the desired temperature was reached. At the end of the reaction, the reactor was quenched in an ice bath to instantly cool the solution to room temperature. A sample was taken for composition analysis by HPLC.

When using heterogeneous catalysts, the solid catalyst was added to the reactor at the beginning of the reaction along with 65 mL of formic acid solution. The amount of solid catalyst used for xylose was fixed at a 1:1 weight ratio. After the reaction, the reactor was cooled down and the solid catalyst was separated from the solution by vacuum filtration using a Buchner funnel. The filtrate was collected for composition analysis by HPLC. The solid catalyst was then rinsed with water at least twice and dried by exposure to air. The experimental conditions are shown in Table II-7.

Table II-7: Experimental conditions from dehydration of xylose in monophasic system under pressure

No.	Catalyst	*T* (°C)	*t* (min)	Compounds/Concentration	
				Xylose (g/L)	Formic acid (wt%)
1	-	140	180	100	-
2		140	40 & 80	10	5
3		140	40	10	10 & 30
4		140	210	10	10
5		170	40	10	5 & 10 & 20
6		170	0-60	10	10
7		170	40	20 & 30	10
8		200	40	10	10
9	Aquivion PW-98	140	40	10	-
10		140	40	10	10
11	Al_2O_3	140	40	10	-

No.	Catalyst	T (°C)	t (min)	Compounds/Concentration	
				Xylose (g/L)	Formic acid (wt%)
12	Al_2O_3	140	40	10	10
13		170	40	10	10
14	ZSM-5	140	210	10	-
15		140	40 & 210	10	10
16		170	40	10	10
17	ZSM-5*	140	40 & 80	10	5
18		170	40	10	5
19	Mordenite	140	210	10	-
20		140	210	10	10

Op Cond.: volume of the mixture = 70 mL; stirring = 400 rpm; mass ratio catalyst/xylose = 1 : 1.
**The mass ratio catalyst/xylose = 10 : 1.*

II.3 Production of furfural from xylose with simultaneous extraction

II.3.1 Furfural production with extraction by steam stripping in semi-batch system

In In this section, the “Equilabo” reactor was used. The utilization of the larger volume reactor, the “Equilabo”, facilitated the examination of the impact of flow rate on furfural extraction. This was achievable due to the increased capacity for distillate collection over the same duration compared to the smaller reactor “Top Industrie”. The characteristics of the high-pressure reactor “Equilabo” are presented in Table II-6.

A typical experiment, 140 mL of pure formic acid solution was introduced into a reactor under the mechanical stirring of 400 rpm (Figure II-3). Then, 10 mL of pure xylose solution was injected into the reactor using the pump when the temperature inside of reactor was 3 °C lesser than the desired reaction temperature (170 °C). Once the desired temperature was attained, the vapor sampling valve (N° 5 in Figure II-3) was gradually opened to facilitate the continuous liberation of the vapor phase. This gradual opening ensured the reaction system boiled at the studied temperature. Subsequently, the vapor phase was passed through the condenser, which was cooled using refrigerating fluid at -2 °C, and the distillate was collected in a measuring receiver. The deionized water was pumped continuously at the same flow rate as the vapor phase (1.5–3.5 mL/min) to maintain a constant volume in the reactor (150 mL).

The vapor flow rate is defined by the volume of distillate recovered during a specified time, while the valve N°5 in Figure II-3 is fixed at a specific level. The vapor phase flow rates studied were 1.5 mL/min and 3.5 mL/min, representing the lowest and highest flow rates available from the vapor sampling valve. The reaction time was determined subsequent to the observation of the first droplet of vapor phase in a measuring receiver. At the end of the reaction, the reactor was quenched in an ice bath to instantly cool the solution to room temperature. A sample of each phase was taken to determine the composition by HPLC. The experimental conditions are shown in Table II-8.

Table II-8: Experimental conditions from dehydration of xylose with steam stripping in semi-batch system

No.	*T* (°C)	*t* (min)	Vapor flow rate (mL/min)	Compounds/Concentration	
				Xyl (g/L)	FA (wt%)
1	170	40	1.5	10 & 20 & 30	10
2			3.5	10 & 20 & 30	10

Op Cond.: volume of the mixture = 150 mL; stirring = 400 rpm.

II.3.2 Furfural production with extraction by organic solvent in biphasic system

The experiments of furfural production in biphasic system were carried out by using reactor “Top Industrie” with a maximum volume of 90 mL. The experiment was carried out in the same way as that of the batch system. Instead of introducing only formic acid solution into the reactor, a certain volume of organic solvent was added in such a way that the studied volume ratios between the aqueous phase and the organic phase were obtained. After cooling down the reactor, the aqueous phase was separated from the organic phase by the separating funnel. The composition of each phase was quantified by HPLC.

The application of organic solvent extraction in a biphasic system was also extended to the xylose conversion catalyzed by heterogeneous catalysts. The experimental procedures remained consistent with those without solid catalysts. In this case, the solid catalyst was added to the reactor at the beginning of the reaction with the formic acid solution. The quantity of solid catalyst employed for xylose conversion was maintained at a consistent 1:1 weight ratio. Additionally, the volume ratio between the aqueous and organic phases was held at 1:3, utilizing CPME as the organic solvent. Subsequent to the separation of the organic phase from the aqueous phase, the catalyst was isolated from the latter through vacuum filtration using a Buchner funnel. The resultant filtrate and organic phase were collected for composition quantification in the aqueous and organic phases, respectively, via HPLC analysis. The solid

catalyst was subsequently rinsed with water at least two times and then dried by exposure to air. The experimental conditions are detailed in Table II-9.

Table II-9: Experimental conditions from dehydration of xylose in biphasic system.

No.	Organic solvent	Aq/Org (v/v)	Solid catalyst	*T* (°C)	*t* (min)	Compounds/Concentration	
						Xylose (g/L)	Formic acid (wt%)
1	Toluene	1 : 1	-	170	40	10	10
2		1 : 3		170	40	10	
3		1 : 6		170	40	10	
4		1 : 13		170	40	10	
5	CPME	1 : 3	-	140	40 & 210	10	
6				170	40	10 & 20 & 30	
7			Al_2O_3	140	40	10	
8				170	40	10	
9			ZSM-5	140	40 & 210	10	
10				170	40	10	
11			Mordenite	140	210	10	
12	EB		-	170	40	10	

Op Cond.: volume of the mixture = 70 mL; stirring = 400 rpm.

II.3.3 Furfural synthesis with simultaneous extraction by Sc-CO_2

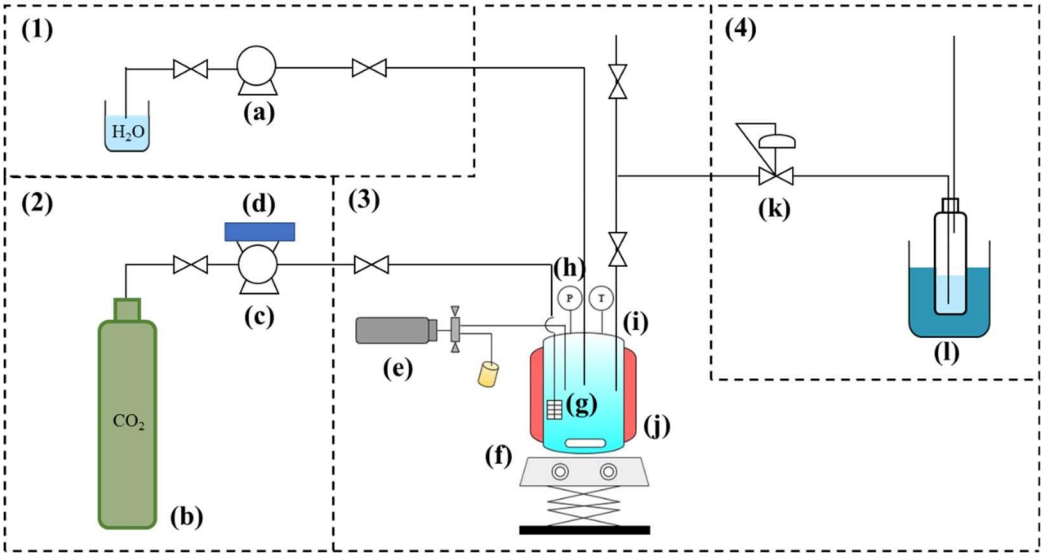

Figure II-4: The schematic diagram of the experimental setup for Sc-CO_2 extraction. (a) water pump, (b) CO_2 cylinder, (c) CO_2 pump, (d) cooling device, (e) sampling device, (f) magnetic stirring bar and plate, (g) porous diffuser, (h) pressure gauge and thermocouple, (i) reactor, (j) heating collars, (k) heated back-pressure regulator, (l) ice bath

The effect of Sc-CO_2 extraction on furfural production from xylose was carried out using an apparatus shown in Figure II-4. The apparatus was a semi-flow type and consisted of four main sections: (1) a device to supply water; (2) a device to supply continuous Sc-CO_2; (3) a reactor with an inlet for Sc-CO_2; and (4) a cooling trap for extract. The experiments were divided into two parts: xylose conversion in batch and semi-batch systems with Sc-CO_2 extractions.

II.3.3.1 Xylose conversion in batch system with Sc-CO_2

In a typical experiment, a high-pressure reactor (Top Industrie, inner volume 90 mL) was charged with 33.5 mL of pure formic acid solution under magnetic stirring at 400 rpm. Subsequently, 4 mL of pure xylose solution was injected into the reactor, followed by 2.5 mL of water, using a sampling device once inside of reactor was 3 °C lesser than the desired reaction temperature. Introducing water after injecting the xylose solution serves the purpose of ensuring the complete injection of all xylose into the reactor. Formic acid and xylose concentrations were adjusted so that their concentrations in the reactor reached the desired values after the mixing step at high temperature. Once the temperature inside the reactor reached the desired value, the reactor was immediately charged with CO_2 to the desired

pressure (5, 10 and 20 MPa) using a piston pump with three heads (Dose HPP400-C, SFE Process). The system was cooled with a refrigerating fluid at 2 °C, and the reaction time was recorded. At the end of the 5-hour reaction time, the reactor was cooled to 50 °C, and the high-pressure CO_2 was released by gently opening the outlet valve to return to atmospheric pressure. The released CO_2 was then passed through ice-cooled water to recover the product solubilized in the CO_2 phase. Samples from both phases (the liquid in the reactor and that in the cooling trap) were taken for composition analysis by HPLC. Table II-10 shows the experimental conditions of xylose conversion in batch system with Sc-CO_2.

Table II-10: Experimental conditions of xylose conversion in batch system with Sc-CO_2.

No.	P_{CO2} (MPa)	T (°C)	t (min)	Compounds/Concentration	
				Xyl (g/L)	FA (wt%)
1	-	140	300	10	-
2	-			10 & 20 & 30	10
3	50			10	10
4	100			10 & 20 & 30	10
5	200			10	-
6	200			10	10

Op Cond.: volume of the mixture = 40 mL; stirring = 400 rpm.

II.3.3.2 Xylose conversion with Sc-CO_2 extraction in semi-batch systems

The experiment was conducted similarly to the batch system described in Section 4.3.1 but was modified to incorporate a constant flow of CO_2, making it a semi-batch process. After the desired reaction temperature was reached, CO_2 was pumped continuously through the reactor using a piston pump with three heads (Dose HPP400-C, SFE Process). The pump, actively cooled by a refrigerating fluid maintained at 2 °C, facilitated the investigation of different flow rates for the study. The system pressure was regulated at 5, 10 and 20 MPa using a heated back-pressure regulator (TESCOM, S/N 87122M). During the reaction, the effluent CO_2 gas from the back pressure valve was passed through ice-cooled water. Simultaneously, water was consistently pumped into the reactor (at rates ranging from 0.11 to 0.21 g/min) using a syringe pump (Model 302, GILSON) to maintain a constant water volume in the reactor (40 mL). The water flow rate was initially determined theoretically based on the value of the water solubility in Sc-CO_2, calculated using the Chrastil model as mentioned Eq. 1 (Chrastil, 1982). Subsequently, it was adjusted experimentally by weighing the extract collected at the outlet over a given time period. At the end of the 5-hour reaction time, the CO_2 flow was stopped,

and the reactor was then cooled to 50 °C. The high-pressure CO_2 in the reactor was gradually released into ice-cooled water using the back pressure valve. Samples from both phases (the liquid in the reactor and that in the cooling trap) were collected for composition analysis by HPLC. The experimental conditions of xylose conversion in semi batch system with extraction of Sc-CO_2 are presented in Table II-11.

$$c = \rho^{k} \exp\left(\frac{a}{T} + b\right) \quad (1)$$

Where c is a solubility of compound (g/L of a gaz), ρ is density of CO_2 (g/L), T is a temperature (K) and the calculated parameters k (-1.549), a (-2826.4) and b (-0.807) for water.

Table II-11: Experimental conditions of xylose conversion in semi batch system with extraction of Sc-CO_2.

No.	CO_2 flow rate (g/min)	P_{CO2} (MPa)	T (°C)	t (min)	Compounds/Concentration	
					Xyl (g/L)	FA (wt%)
1	5	100	140	300	10	10
2		200			10 & 20 & 30	10
3	10	100			10	10
4		200			10	10

Op Cond.: volume of the mixture = 40 mL; stirring = 400 rpm.

II.4 Production of furfural from raw biomass by LEEBio™ process

II.4.1 Production of hydrolysate rich in hemicellulose

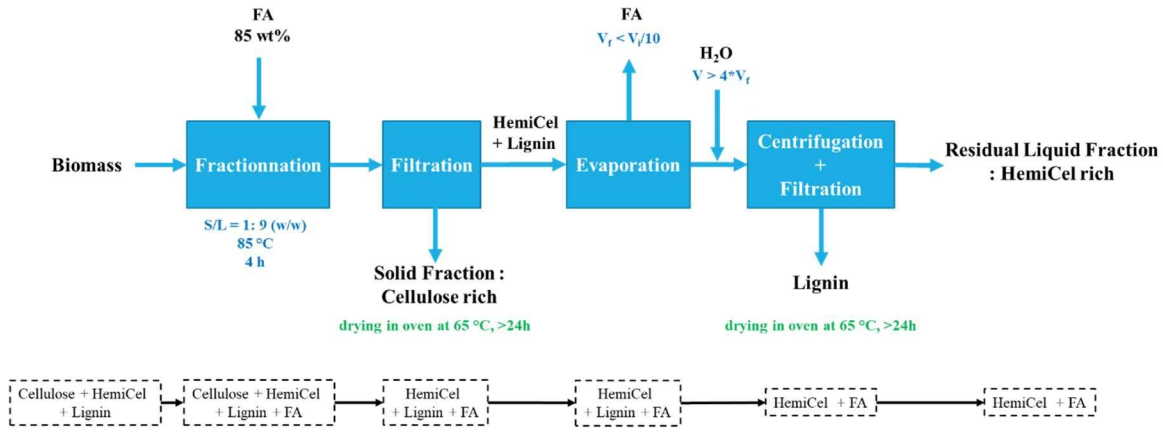

Figure II-5: Experimental process for hemicellulose extraction from biomass.

The extraction of hemicellulose from raw biomass was carried out using the LEEBio^{TM} process, which involves two distinct steps as depicted in Figure II-5. The initial stage entailed the fractionation of biomass into solid cellulose and a mixture of soluble lignin and hemicellulose referred as hydrolysate. This step was exclusively performed when OPEFB was utilized as the initial substrate, as the BioEB company conducted this step when fir wood was used. The second step was the separation of lignin from the hydrolysate to obtain a hydrolysate rich in hemicellulose. Ultimately, three fractions, consisting of solid cellulose, lignin, and a hemicellulose-rich hydrolysate, were successfully recovered without any degradation (Figure II-6).

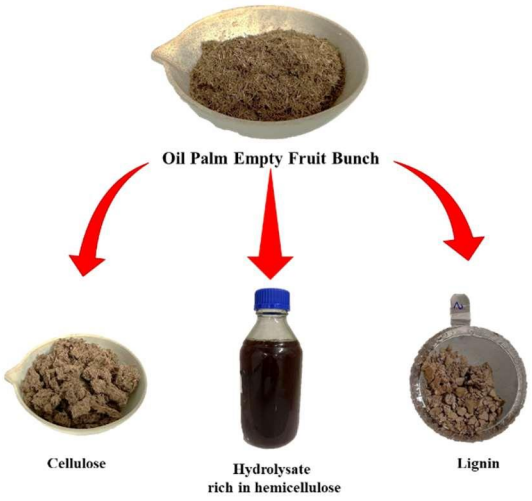

Figure II-6:Three fractions obtained from biomass using LEEBio^{TM} process.

II.4.1.1 Hemicellulose extraction from biomass by LEEBio^{TM} process

Figure II-7: Experimental set-up for hemicellulose extraction from biomass.

The raw biomass was mixed with an 85 wt% formic acid solution at a ratio between the solid and liquid fractions of 1: 9 (w/w) in the glass reactor (inner volume 1.5 L) as shown in Figure II-7. The mixture was heated at 85 °C while being mechanically stirred at 700 rpm for 4h before cooling to room temperature. The cellulose-rich solid fractions were separated from the hydrolysate by filtration using a Buchner funnel with filter paper (with a pore size of 11 µm) and was washed with water at least three times before being dried in a vented oven at 65 °C. The hydrolysate rich in hemicellulose, lignin and formic acid was obtained and was stored at 4 °C for the second step involving the separation of lignin.

II.4.1.2 Separation of lignin from hydrolysate obtained from biomass extraction by the LEEBio™ process

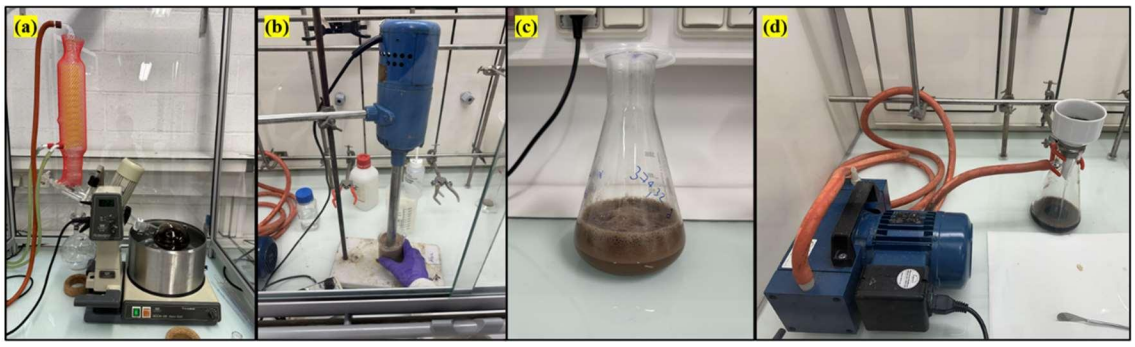

Figure II-8: Separation of lignin from hydrolysate.
(a) Elimination of formic acid by rotative evaporator; (b) precipitation of lignin by Ultra-Turrax type "rotor/stator" disperser; (c) settling of lignin in the hydrolysate; (d) separation of lignin from hydrolysate.

500 mL of the black extraction liquor (hemicellulose + Lignin + formic acid) was thereafter transferred into the rotavapor receptacle after determining the dry matter content (Figure II-8a). The whole volume of liquor containing formic acid (> 80%) and water (20%) was evaporated by heating to approximately 40 °C, lowering the internal pressure to less than 200 mbar, and stirring moderately until a residual dry mass rate of greater than 60% was attained in the liquor. At least two portions of hot water (50−60°C) were added to the concentrated liquor while stirring at 60−70°C in order to precipitate the lignin particles (brown solid) and separate them from the hydrolysate (brown liquid). To facilitate the separation of lignin from the hydrolysate, the diluted liquor was rapidly suspended for 2-5 min using an Ultra-Turrax type "rotor/stator" disperser, and the solid was allowed to settle for at least 1 h (Figure II-8b). The lignin (a brown solid) was separated from the hydrolysate (a brown liquid) using centrifugation. The hemicellulose-rich supernatants were then filtered using a Buchner-

type vacuum filtration equipment with filter paper (with a pore size of 11 µm) (Figure II-8d). The recovered pellet (lignin) was washed with water and dried in a vented oven at 65 °C for at least 24 h. Lignin was weighed and stored in an airtight container at room temperature. After determining the hemicellulose juice's dry matter content ($\chi_{hydrolysate}$), it was divided into two parts: one is utilized immediately for furfural synthesis without additional chemicals and the other is used to determine the percentage of hemicellulose in biomass. To do that, the hydrolysate rich in hemicellulose was deposited into the rotavapor container and was evaporated by heating to approximately 60 °C. The internal pressure was reduced to less than 200 mbar, and stirring moderately until the remaining dry mass rate in the hydrolysate exceeded 50%. After the dry matter content was determined (χ_{syrup}), a very viscous black syrup was stored in a cold (20 °C) and well-ventilated chamber.

The proportion of cellulose, lignin and hemicellulose was calculated using the following formulas:

$$\text{Percentage of cellulose (\%)} = \frac{\text{weighed mass after 65 °C over night in the oven}}{\text{mass}_{\text{biomass}}} \quad (2)$$

$$\text{Percentage of lignin (\%)} = \frac{\text{weighed mass after 65 °C over night in the oven}}{\text{mass}_{\text{biomass}}} \quad (3)$$

$$\text{Percentage of hemicellulose (\%)} = \frac{\text{mass}_{\text{hydrolysate}} \times \chi_{\text{hydrolysate}} \times \chi_{\text{syrup}}}{\text{mass}_{\text{biomass}}} \quad (4)$$

$$\text{Percentage of ash (\%)} = \frac{\text{mass}_{\text{biomass}} - \left(\text{mass}_{\text{cellulose}} + \text{mass}_{\text{lignin}} + \text{mass}_{\text{hemicel}}\right)}{\text{mass}_{\text{biomass}}} \quad (5)$$

In order to achieve economic efficiency and meet the environmentally-friendly concepts, it is crucial to maximize the recovery of formic acid from hydrolysate. However, it is important to note that the residual formic acid in the hydrolysate should be at a level that can potentially convert xylose into furfural. In order to accomplish this, the hydrolysate rich in hemicellulose underwent evaporation using a rotavapor receptacle. This involved heating the solution to approximately 60 °C while gradually reducing the internal pressure to below 200 mbar, while stirring moderately until the final volume reached either four or nine times less than the initial volume. The resulting concentrated hydrolysate was then diluted with deionized water in equal quantity to the condensate. This addition of deionized water served to reduce the viscosity of the hydrolysate. Consequently, the hydrolysate subjected to evaporation resulting in final volumes four and nine times less than the initial volume were labeled as hydrolysate 4/4 and 9/9, respectively.

II.4.1.3 Quantification of monosaccharides in hydrolysates

The hydrolysis of dissolved polysaccharides in hemicellulose hydrolysate was carried out in a high-pressure reactor (Equi Labo) without additional chemicals. 150 mL of hydrolysate was poured in the reactor and was heated at 120 °C for 7h, with mechanical agitation at 400 rpm. Throughout the procedure, samples were taken every 30 min for subsequent composition analysis via HPLC. The concentration of mono-sugars in hydrolysate was recorded prior to their conversion to furanic aldehyde molecules, at which point they decreased (after 240 min at 120 °C).

II.4.2 Furfural production from raw biomass hydrolysates

All experiments involving hydrolysates derived from unprocessed biomass were carried out in the “Equilabo” high-pressure reactor (Figure II-3).

II.4.2.1 Furfural production in batch system

Before conducting the furfural synthesis with biomass hydrolysate, xylans, which are polysaccharides made up of xylose, were utilized as the initial material for furfural production using “Equilabo” reactor.

In a typical experiment, 1.5 g of xylan was introduced into the reactor with 150 mL formic acid solution (10 wt%) at the beginning of reaction. Concerning the use of hemicellulose hydrolysate obtained from raw biomass as starting material, 150 mL of the hydrolysate was added directly in the reactor at the beginning of reaction, while subjecting it to mechanical agitation at a speed of 400 rpm. The reaction time was calculated after the desired temperature was reached. At the end of the reaction, the reactor was quenched in an ice bath to instantly cool the solution to room temperature. A sample was taken for composition analysis by HPLC. The experimental conditions of furfural production in batch system using xylans and biomass hydrolysates as starting material are presented in Table II-12 and Table II-13 (No.1-4), respectively.

Table II-12: Experimental conditions of furfural production using biomass xylans in batch system.

No.	Xylan	*T* (°C)	*t* (min)	FA (%wt)
1	Birchwood	170	40 & 60	10
2	Oat Spelts		40 & 60	10

Op Cond.: volume of the mixture = 150 mL; stirring = 400 rpm.

Table II-13: Experimental conditions of furfural production using biomass hydrolysate in different systems.

No.	System	Biomass	*T* (°C)	*t* (min)
1	Batch	Fir wood	170	40 & 60
2		OPEFB		40 & 60
3		Fir wood[a]		40
4		Fir wood[b]		40
5	Semi-batch*	Fir wood		40
6		OPEFB		40
7	Biphasic**	Fir wood		40
8		OPEFB		40

Op Cond.: volume of the mixture = 150 mL; stirring = 400 rpm.
[a]Hydrolysate used was a hydrolysate 4/4
[b]Hydrolysate used was a hydrolysate 9/9
**Vapor flow rate = 3.5 mL/min*
***Aq/Org = 1 : 3 (v/v), Org phase = CPME*

II.4.2.2 Furfural production with extraction by steam stripping

The experiment followed the same procedure as the batch system described in Section II.2.2.3. When the desired temperature was reached, the vapor sampling valve (N° 5 in Figure II-3) was opened to continuously liberate the vapor phase, and the water was pumped continuously (3.5 mL/min) to maintain a constant volume in the reactor (150 mL). The vapor phase was passed through the condenser, which was cooled using refrigerating fluid at -2 °C, and the distillate was collected in a measuring receiver. The reaction system was kept boiling by gradually lowering the pressure to keep it below the vapor pressure. A sample of each phase (liquid phase and vapor phase or distillate) was taken to determine the composition by HPLC. The experimental conditions of furfural production using biomass hydrolysates in semi-batch system with steam stripping are presented in Table II-13 No. 5-6.

II.4.2.3 Furfural production with extraction by organic solvents

The experiment was conducted similarly to the batch system described in Section II.4.2.1. A certain volume of organic solvent (CPME) was added at the beginning of reaction in such a way that the studied volume ratio between the aqueous phase and the organic phase was 1:3. After cooling down the reactor, the aqueous phase was separated from the organic phase by the separating funnel. The composition of each phase was quantified by HPLC. The experimental conditions of furfural production using biomass hydrolysates in biphasic solvent system are presented in Table II-13 No. 7-8.

II.5 Kinetic modeling of furfural production from xylose and application to raw biomass hydrolysates

In this study, three distinct xylose dehydration schemes into furfural were examined as shown in Figure II-9.

They are differing mostly in terms of their side reactions. Mechanism 1 has a first-order reaction kinetic, in which furfural is only degraded by self-polymerization and xylose is directly decomposed. Furfural degradation is also regulated by cross-polymerization between xylose and furfural in Mechanism 2. Furfural dehydration via an intermediate specie which is xylulose and its cross-polymerization with furfural is considered in Mechanism 3. Mechanisms 2 and 3 have a second-order reaction kinetic for cross-polymerization.

The kinetic modeling of the conversion of xylose into furfural was divided into two sections. The first section specifically examines the kinetics of furfural degradation, as this reaction was represented by the three reaction mechanisms studied in this research. The second stage involved the modeling of the breakdown of xylose and the production of furfural. The kinetic parameters of the furfural degradation reaction remained constant and were identical to those determined in the initial section.

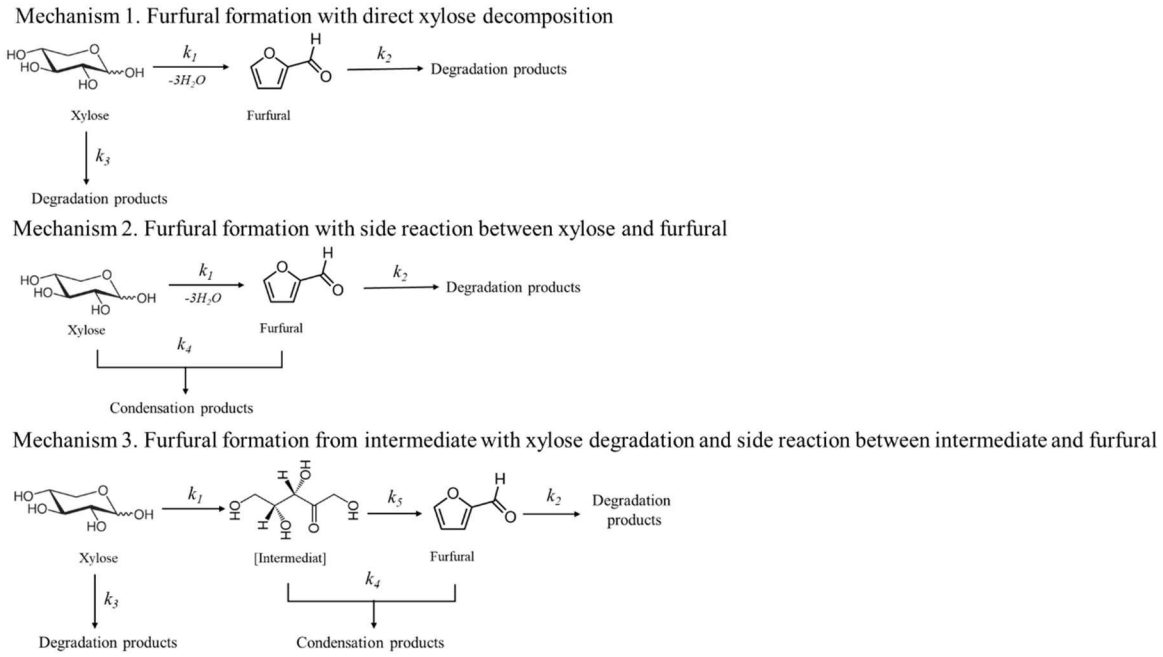

Figure II-9: Reaction mechanisms for kinetic study of acid-catalyzed dehydration of xylose into furfural.

All experiments aimed at kinetic modeling of furfural production from xylose were conducted using the "Equilabo" high-pressure reactor (Figure II-3).

II.5.1 Furfural degradation reaction

In a typical experiment, 130 mL of the formic acid solution was added into the reactor under the mechanical stirring of 400 rpm. Then, 10 mL of furfural solution was injected into the reactor, followed by 10 mL of ultrapure water using the pump when the temperature inside the reactor was 3 °C lesser than the desired reaction temperature. The concentrations of formic acid and furfural were prepared in such a way that their final concentrations in the reactor reached the desired value. The reaction time was calculated after the desired temperature was reached. Throughout the procedure, samples were periodically taken during the reaction. The first 0.7 mL of sample was discarded to avoid contamination with the previous sample. Subsequently, 0.5-1.0 mL of sample was taken for composition analysis using HPLC. At the end of the reaction, the reactor was quenched in an ice bath to instantly cool the solution to room temperature. The experimental conditions of furfural degradation reaction are presented in Table II-14.

Table II-14: Experimental conditions of furfural degradation reaction

No.	*T* (°C)	*t* (min)	Compounds/Concentration	
			Fur (g/L)	FA (wt%)
1	140	360	5	5 & 10 & 20
2			15	10
3	170	60	5	5 & 10 & 20
4			15	10
5	200	60	5	5 & 10 & 20
6			15	10

Op Cond.: volume of the mixture = 150 mL; stirring = 400 rpm.

II.5.2 Xylose decomposition and furfural formation

In a typical experiment, 125 mL of the formic acid solution was added into the reactor under the mechanical stirring of 400 rpm. Then, 15 mL of either xylose solution or a xylose-furfural mixture was injected into the reactor, succeeded by the addition of 10 mL of ultrapure water using the pump when the temperature inside the reactor was 3 °C lesser than the desired reaction temperature. The concentrations of xylose and formic acid, as well as xylose-furfural mixture, were prepared in such a way that their final concentrations in the reactor reached the desired value. The reaction time was calculated after the desired temperature was reached. Throughout the procedure, samples were periodically collected during the reaction for subsequent composition analysis using HPLC. At the end of the reaction, the reactor was quenched in an ice bath to instantly cool the solution to room temperature. The experimental conditions of xylose decomposition furfural formation reactions are presented in Table II-15.

Table II-15: Experimental conditions of xylose decomposition and furfural formation reactions

No.	*T* (°C)	*t* (min)	Compounds/Concentration		
			Xyl (g/L)	Fur (g/L)	FA (wt%)
1	140	360	10 & 30	-	-
2			10 & 30	-	5 & 10 & 20
3			10 & 30	5	5 & 10 & 20
4			10 & 30	15	10
5	170	60	10 & 30	-	-
6			10 & 30	-	5 & 10 & 20
7			10 & 30	5	5 & 10 & 20
8			10 & 30	15	10
9	200	60	10 & 30	-	-
10			10 & 30	-	5 & 10 & 20
11			10 & 30	5	5 & 10 & 20
12			10 & 30	15	10

Op Cond.: volume of the mixture = 150 mL; stirring = 400 rpm.

II.5.3 Kinetic modeling

The reaction rate constant expression of different reactions in this study was derived from previous research by Lamminpää et al. (2012). In the specific acid−base catalysis the rate constant can be expressed as given in Eq. 6 (Laidler, 1979). Each term has its own activation energy.

$$k = k_0 + k_{\mathrm{H}} C_{\mathrm{H}} + k_{\mathrm{OH}} C_{\mathrm{OH}} \tag{6}$$

where k_0 is the rate constant for the uncatalyzed reaction; k_{H} and k_{OH} are the rate constants for catalysis by hydrogen ions (H^+) and hydroxide ions (OH^-), respectively; C_{H} is the hydrogen ion concentration; and C_{OH} is the hydroxide ion concentration. Because $C_{\mathrm{H}} \gg C_{\mathrm{OH}}$, the base term has no influence on the reaction. Also, it was assumed that the activation energies for k_0 and k_{H} are the same. In addition, the common reparametrization, which used the reaction rate constant in the reference temperature instead of the pre-exponential factor, was utilized to reduce the correlation between the estimated parameters. Thus, the rate constant is represented as Eq. 7.

$$k_{\mathrm{i}} = \left(k_{0,\mathrm{i}} + k_{\mathrm{H,i}} C_{\mathrm{H}}\right) \mathrm{e}^{-\frac{E_{\mathrm{i}}}{R}\left(\frac{1}{T} - \frac{1}{T_{\mathrm{mean}}}\right)} \tag{7}$$

where $k_{0,\mathrm{i}}$ is the rate constant of uncatalyzed reaction in water solvent and $k_{\mathrm{H,i}}$ is the rate constant of acid catalyst (H^+) in the reference temperature T_{mean} (443 K), C_{H} is the hydrogen ion concentration in reaction temperature (mol/L), T is reaction temperature (K), E_{i} is activation energy (J/mol) and R is the universal gas constant (8.314 J/(mol.K)).

Concerning the furfural degradation reaction, it was found that as the temperature increased, the acid concentration had a more significant impact on the reaction rate. Consequently, separate activation energies were necessary for the uncatalyzed and acid-catalyzed parts in the rate constant equation which was rewritten as shown in Eq. 8.

$$k_{\mathrm{i}} = k_{0,\mathrm{i}} \mathrm{e}^{-\frac{E_{0,\mathrm{i}}}{R}\left(\frac{1}{T} - \frac{1}{T_{\mathrm{mean}}}\right)} + k_{\mathrm{H,i}} C_{\mathrm{H}} \mathrm{e}^{-\frac{E_{\mathrm{H,i}}}{R}\left(\frac{1}{T} - \frac{1}{T_{\mathrm{mean}}}\right)} \tag{8}$$

where $E_{0,\mathrm{i}}$ and $E_{\mathrm{H,i}}$ are the activation energy of uncatalyzed and the acid-catalyzed terms, respectively.

In this study, the hydrogen ion concentration of formic acid was used in kinetic modeling referred as C_{H}. The temperature dependence was taken into account by Eq. 9 obtained by Kim et al. (1996) which shows the temperature dependence of dissociation constant (pK_a) for formic acid.

$$\mathrm{p}K_\mathrm{a} = -57{,}528 + \frac{2773{,}9}{T} + 9{,}1232\ln T \tag{9}$$

Where T is temperature in K.

The H^+-concentrations (mol/L) are calculated using a system of nonlinear equations based on restrictions for the system from equilibrium state and ion balances as mentioned in Eq. 10. The initial formic acid concentration, $C_{H,0}$, at room temperature (23−25 °C) was measured using HPLC from initial reactant solutions presented in Table II-14 and II-15. H^+-concentrations in reaction temperature were calculated using the temperature data of each experiment, Eq. 9-10, and the initial formic acid concentration at room temperature.

$$C_H = \frac{-K_a + \sqrt{K_a^2 + 4C_{H,0}K_a}}{2} \tag{10}$$

Where C_H is the hydrogen ion concentration in reaction temperature, $C_{H,0}$ is the initial formic acid concentration at room temperature and K_a is acidity constant of formic acid.

The reaction rate equations used for the modelling of the kinetics that follow the mechanisms described in Figure II-9 for xylose are presented as follows:

Mechanism 1

$$\frac{\mathrm{d}C_\mathrm{x}}{\mathrm{d}t} = -k_1 C_\mathrm{x} - k_2 C_\mathrm{x} \tag{11}$$

$$\frac{\mathrm{d}C_\mathrm{F}}{\mathrm{d}t} = k_1 C_\mathrm{x} - k_\mathrm{F} C_\mathrm{F} \tag{12}$$

Mechanism 2

$$\frac{\mathrm{d}C_\mathrm{x}}{\mathrm{d}t} = -k_1 C_\mathrm{x} - k_4 C_\mathrm{x} C_\mathrm{F} \tag{13}$$

$$\frac{\mathrm{d}C_\mathrm{F}}{\mathrm{d}t} = k_1 C_\mathrm{x} - k_4 C_\mathrm{x} C_\mathrm{F} - k_2 C_\mathrm{F} \tag{14}$$

Mechanism 3

$$\frac{\mathrm{d}C_\mathrm{x}}{\mathrm{d}t} = -k_1 C_\mathrm{x} - k_2 C_\mathrm{x} \tag{11}$$

$$\frac{\mathrm{d}C_\mathrm{F}}{\mathrm{d}t} = k_5 C_\mathrm{I} - k_2 C_\mathrm{F} - k_4 C_\mathrm{I} C_\mathrm{F} \tag{15}$$

$$\frac{\mathrm{d}C_\mathrm{I}}{\mathrm{d}t} = k_1 C_\mathrm{x} - k_5 C_\mathrm{I} - k_4 C_\mathrm{I} C_\mathrm{F} \tag{16}$$

where k_1, k_2, k_3, k_4 and k_5 are rate constants and C_X, C_F, and C_I are concentrations (in mol/L) for xylose, furfural, and intermediate, respectively.

The model equations were implemented in a Python environment, and the Python codes of kinetic modeling were provided in an appendix. The system of ordinary differential equations (ODEs) was solved numerically by ODEINT, a solver for stiff systems that is based on the numerical differentiation formulas. The kinetic parameters were estimated using nonlinear regression analysis. The estimation was done by the Nelder-Mead algorithm available within Python's optimization function. The "fit_report" function in the Python package "lmfit" was used to generate the best-fit values for the parameters, with their uncertainties (±) estimated using the statistical approach "Confidence Intervals" at 95%.

The coefficient of determination (R^2) for each model, which evaluates the models' goodness of fit was calculated according to Eq. 17 as follows:

$$R^2 = 1 - \frac{\sum_{i=1}^{n}\left(C_i - \hat{C}_i\right)^2}{\sum_{i=1}^{n}(C_i - C_m)^2} \quad (17)$$

Where C_i is the experimental concentration of xylose or furfural, $\hat{C}_i$ is the predicted concentration determined by the kinetic model, C_m is the mean of xylose or furfural concentration, and n denotes the number of experimental data points.

II.5.4 Optimization of operating parameters

Table II-16: Range and step for each operating parameter used for the optimization in Matlab.

Parameter	Setting value		Step
	Min	Max	
Temperature (K)	413	473	1
Formic acid concentration (mol/L)	0.1	5.3	0.5
Reaction time (s)	0	∞	10

The objective of this phase is to optimize the operational parameters, such as reaction temperature, residence time, and formic acid concentration, while maintaining a constant concentration of xylose. When utilizing xylose and xylan as initial materials, the concentration of xylose remained fixed at 10 g/L, whereas both the xylose and formic acid concentrations were fixed when employing biomass hydrolysates. In this case, the concentration of xylose was the concentration of all pentose sugars present in the hydrolysates. The optimization process involved implementing the kinetic equations in the MATLAB software. The numerical optimization was performed using the *fminsearch* function. Table II-16 provides the specific

range and step values for each operating parameter that were altered during the optimization process. The resultant optimal conditions were validated through experimental trials. The experimental conditions derived from optimization for xylose and xylan are detailed in Table II-17, while those for hydrolysates are presented in Table II-18.

Table II-17: Experimental conditions derived from optimization for xylose and xylans.

No.	Substance	*T* (°C)	*t* (min)	FA (%wt)	Model
1	Xylose & Xylan from Birchwood & Xylan from Oat Spelts	153	77	20	1
2	Xylose	143	212	20	3

Op Cond.: initial concentration = 10 wt% of formic acid; volume of the mixture = 150 mL; stirring = 400 rpm.

Table II-18: Experimental conditions derived from optimization for biomass hydrolysates

No.	Biomass	*T* (°C)	*t* (min)	Model
1	Fir wood	144	224	3
2	OPEFB	142	284	3

Op Cond.: initial concentration = 10 wt% of formic acid; volume of the mixture = 150 mL; stirring = 400 rpm.

II.6 Analytical methods

Formic acid, furfural, 5-HMF and xylulose in the aqueous phase were determined by using high-performance liquid chromatography, HPLC, (Thermo Accela, United States) equipped with a Bio-Rad Aminex HPX-87H ion exclusion column (300 mm x 7.8 mm, 9 µm), refractive index (RI), and UV detectors. Formic acid (retention time, t_R = 10.4 min) was detected in UV detector at 210 nm while furfural (t_R = 36.4 min) and 5-HMF (t_R = 23.2 min) were detected in UV detector at 280 nm. Xylulose was detected in RI detector and was quantified using a deconvolution method. The column and detector temperatures were kept constant at 50 °C. The separation was conducted using the isocratic technique, with 10 mM sulfuric acid serving as the mobile phase at a flow rate of 0.8 mL/min. The injection volume is 20 µL, and the duration of the analysis is 45 min. Monosaccharides, including xylose (t_R = 13.3 min), arabinose (t_R = 15.7 min), mannose (t_R = 16.5 min), glucose (t_R = 12.2 min) and galactose (t_R = 14.3 min), and fructose (t_R = 17.3 min), were measured in RI detector by HPLC (Thermo Accela, United States) equipped with a Bio-Rad Aminex HPX-87P (300 × 7.8 mm, 9 µm) column. Deionized water was used as the mobile phase with a 0.6 mL/min flow rate at 75 °C

under the isocratic method. The injection volume is 20 µL and the duration of the analysis is 50 min. All standards and samples are filtered through a 0.22 µm syringe filter before being analyzed.

Furfural (t_R = 2.1 min) and 5-HMF (t_R = 1.5 min) in the organic phase were analyzed by ultra-high-performance liquid chromatography (UHPLC) with a UV detector at 280 nm. The column used was Thermo Fisher Scientific Accucore^{TM} C18 (150 mm x 3 mm, 2.6 µm), maintained at a temperature of 30 °C. The mobile phase used in the isocratic technique was a mixture of water and acetonitrile at 90:10 (v/v) with a 1 mL/min flow rate. The injection volume is 20 µL.

The quantification of inorganic elements in the biomass hydrolysate was performed using an inductively coupled plasma (ICP). ICP measurements were carried out using Horiba's Ultima2 ICP-AES by Marie-Line DeSolan (SAP-LGC technician). Hence, further detail on this analytical procedure is not provided within this report.

The concentration of the components is determined through a calibration curve where the peak area is plotted against the corresponding quantities of each component (standard). Regular calibration checks were performed in order to avoid any experimental errors in all measurements presented in this work.

Conversion, yield and selectivity were calculated according to the following expressions:

$$\text{Xylose conversion}: X_{xyl}\,(\%) = \frac{n_{Xyl,i} - n_{Xyl,f}}{n_{Xyl,i}} \times 100 \quad (18)$$

$$\text{Furfural yield}: Y_{Fur}\,(\%) = \frac{n_{Fur}}{n_{Xyl,i}} \times 100 \quad (19)$$

$$\text{Furfural selectivity}: S_{Fur}\,(\%) = \frac{n_{Fur}}{n_{Xyl,i} - n_{Xyl,f}} \times 100 \quad (20)$$

With $n_{Xyl,i}$ and $n_{Xyl,f}$ the mole amount of xylose at initial time and at the end of reaction, respectively. n_{Fur} is the mole amount of furfural produced.

The separation efficiency was defined as the ratio of the molar quantity of furfural extracted ($n_{Fur,extract}$) and the total amount of furfural produced (n_{Fur}) as expressed below:

$$\text{Separation efficiency}: \tau_{Fur}\,(\%) = \frac{n_{Fur,extract}}{n_{Fur}} \times 100 \quad (21)$$

In the case where raw biomass was used as starting material, the furfural yield and 5-HMF were calculated according to the following expressions:

$$\text{Furfural yield}: \ Y_{Fur}\ (\%) = \frac{n_{Fur}}{\left(n_{Xyl,i} + n_{Ara,i}\right)} \times 100 \quad (22)$$

$$5 - \text{HMF yield}: \ Y_{5-HMF}\ (\%) = \frac{n_{5-HMF}}{\left(n_{Glu,i} + n_{Man,i} + n_{Gal,i}\right)} \times 100 \quad (23)$$

With $n_{Ara,i}$, $n_{Glu,i}$, $n_{Man,i}$, and $n_{Gal,i}$ the mole amount of arabinose, glucose, mannose and galactose at initial time, respectively. $n_{5\text{-}HMF}$ is the mole amount of 5-HMF produced.

II.7 References

Chrastil, J., 1982. Solubility of solids and liquids in supercritical gases. J. Phys. Chem. 86, 3016–3021.

Kim, M.H., Kim, C.S., Lee, H.W., Kim, K., 1996. Temperature dependence of dissociation constants for formic acid and 2,6-dinitrophenol in aqueous solutions up to 175 °C. J Chem Soc Faraday Trans 92, 4951–4956. https://doi.org/10.1039/FT9969204951

Laidler, K.J., 1979. Theories of Chemical Reaction Rates. R. E. Krieger Publishing Company.

Lamminpää, K., Ahola, J., Tanskanen, J., 2012. Kinetics of Xylose Dehydration into Furfural in Formic Acid. Ind. Eng. Chem. Res. 51, 6297–6303. https://doi.org/10.1021/ie2018367

III. Chapter 3

Development of a homogeneously catalyzed process for furfural production with classical extraction system.

This chapter details the investigation of furfural production using formic acid as a catalyst, exploring both atmospheric and pressurized conditions. It also examines simultaneous extraction processes through steam stripping and aqueous-organic-biphasic systems.

The methods for conducting these manipulations, both analytically and experimentally, have been previously outlined in Chapter 2. The experimental setup utilized for this part is detailed in Section II.2.2.1. Furthermore, specific techniques such as extraction via steam stripping in a semi-batch system and extraction using organic solvents in a biphasic system are elaborated upon in Sections II.3.1 and II.3.2, respectively. Lastly, the fractionation of raw biomass through the LEEBio^{TM} process, resulting in the separate recovery of solid cellulose, lignin, and a hemicellulose-rich hydrolysate is presented in Section II.4.

The subsequent section of this chapter outlines experimental results on furfural production from xylose catalyzed by formic acid under pressure, followed by extraction processes and their application to raw biomass hydrolysates. Firstly, the results of furfural production in a batch system are introduced, highlighting the determination of optimal conditions for maximizing furfural yield through parameter variations. Subsequently, these optimal conditions are explored in the context of furfural production coupled with extraction methods: steam stripping in a semi-batch system and extraction using organic solvents in a biphasic system. The paragraph then discusses the application of the identified optimum conditions from both extraction systems to furfural production from raw biomass hydrolysates. The study's findings are compared with those of other research to assess the catalytic efficacy of formic acid and the efficiency of the investigated extraction methods. The final section of this chapter presents complementary experimental results and a discussion on furfural production from xylose catalyzed by formic acid at atmospheric pressure. Additionally, furfural extraction using organic solvents in a biphasic system was explored under these conditions.

The experimental results and discussion on furfural production from xylose catalyzed by formic acid under pressure, along with the extraction processes presented in this chapter, are extracted

from the article entitled “Formic Acid as a Catalyst in Furfural Production by Simultaneous Extraction Processes via Steam Stripping and Biphasic Systems”, which has been submitted to the *Journal of Biomass and Bioenergy* [July 11, 2024].

III.1 The furfural production catalyzed by formic acid with simultaneous extraction processes via steam stripping and biphasic systems

The following results are presented as part of the scientific article entitled "Formic Acid as a Catalyst in Furfural Production by Simultaneous Extraction Processes via Steam Stripping and Biphasic Systems", which has been submitted to the *Journal of Biomass and Bioenergy* [July 11, 2024]

This work examines the second role of formic acid as an efficient catalyst for pentose sugar dehydration into furfural and as a solvent for lignocellulosic biomass depolymerization. The effect of the reaction temperature, residence time, and initial xylose concentration on the conversion of xylose into furfural was evaluated in batch conditions. In addition, furfural extraction throughout the reaction medium, including the steam stripping in the semi-batch system and the use of organic solvents in the biphasic solvent system, was investigated to enhance the yield and selectivity of furfural. The extraction efficiency of these methods was also evaluated. Besides conducting experiments with synthetic mixtures containing xylose and formic acid, the furfural production using hydrolysate produced from raw biomass through the LEEBio^{TM} process was optimized in all investigated systems. The results achieved were then compared with findings from other studies.

III.1.1 Xylose dehydration in a batch system

Before using the hemicellulose hydrolysate for furfural production via dehydration, a series of initial experiments were conducted using xylose as a model chemical. The choice of xylose as a representative compound was based on the fact that hemicellulose in lignocellulosic materials is predominantly composed of xylose units. The synthetic solutions contained only xylose (10–30 g/L) and formic acid (10 wt%). Their concentration was representative of the hemicellulose hydrolysate resulting from biomass hydrolysis by formic acid in the LEEBio^{TM} process (Delmas, 2021). This section aims to study the effect of operating parameters on xylose conversion to furfural: reaction temperature, residence time, and initial concentration of xylose. The obtained optimum conditions are investigated for the steam stripping and the biphasic solvent systems, respectively.

III.1.1.1 Influence of reaction temperature

Table III-1: Effect of reaction temperature on xylose conversion, furfural yield, and furfural selectivity.

Entry	*T* (°C)	Xyl conv (%)	Fur yield (%)	Fur selectivity (%)
1*	100	2	/	/
2	140	18	10	55
3**	170	93	58	62
4	200	98	49	50

Op. Cond.: initial concentration = 10 g/L of xylose and 10 wt% of formic acid; residence time = 40 min, volume of the mixture = 150 mL.
**The experiment was carried out at atmospheric pressure.*
***Repeated three times: the standard deviation of xylose conversion, furfural yield and furfural selectivity are 3%, 2% and 4 %, respectively.*

The reaction temperature is critical in all thermochemical conversion processes, including xylose dehydration into furfural. This study investigated the effect of different temperatures (100, 140, 170, and 200 °C) on furfural formation from xylose using formic acid as a catalyst (Table III-1). The experimental results showed that the maximum furfural yield of 58% and selectivity of 62% were obtained at 170 °C. However, lower (100, 140 °C) and higher (200 °C) temperatures gave less satisfactory results. Therefore, 170 °C was selected as the optimal reaction temperature in the subsequent experiments.

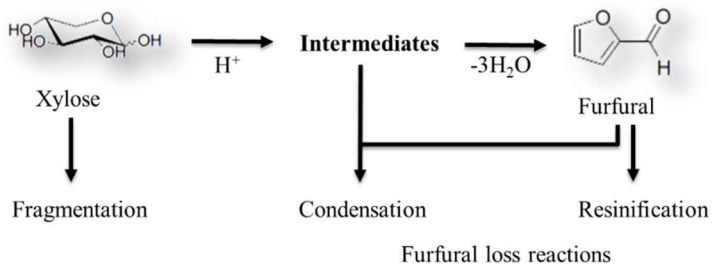

Figure III-1: Simplified scheme of possible reactions in xylose-to-furfural conversion.

Regarding the scheme of the furfural formation (Figure III-1), the conversion of xylose into furfural depends on the different reaction rates. At lower temperatures, the dehydration rate of xylose into furfural is low; hence, the furfural yield is low. Increasing the reaction temperature accelerates not only the rate of xylose dehydration into furfural but also that of accompanying side reactions. This means that beyond a certain temperature, the rate of furfural

production is lower than side reactions. Raman and Gnansounou (2015) observed that the conversion of xylose into furfural exhibited an initial increase with rising temperature, reaching a peak and declining at extremely high temperatures. Under extreme conditions of high temperature and prolonged reaction time, nearly all of the xylose and a notable portion of furfural converted into humines due to furan and sugar condensation reactions. This phenomenon ultimately resulted in a decreased furfural yield.

Moreover, the black solid particles, or humines, were observed at 200 °C. This confirmed that high temperatures promote side-loss reactions, resulting in low yield and selectivity of furfural. A similar observation was made in Yang et al. (2012)'s study, where the dehydration of xylose to furfural catalyzed by formic acid in a semi-batch system was optimized using response surface methodology. It was revealed that the drop in furfural yield was accompanied by an increase in the quantity of resin adhered to the internal wall of the autoclave. At 160 °C, negligible resin adhered to the internal wall of the autoclave. Nonetheless, its quantity increased significantly once the reaction temperature rose above 190 °C. As a result, the best temperature for converting xylose to furfural is a compromise between a high enough temperature to achieve good reaction kinetics due to the high activation energy and a low enough temperature to minimize product degradation reactions and reduce process costs.

III.1.1.2 Influence of reaction time

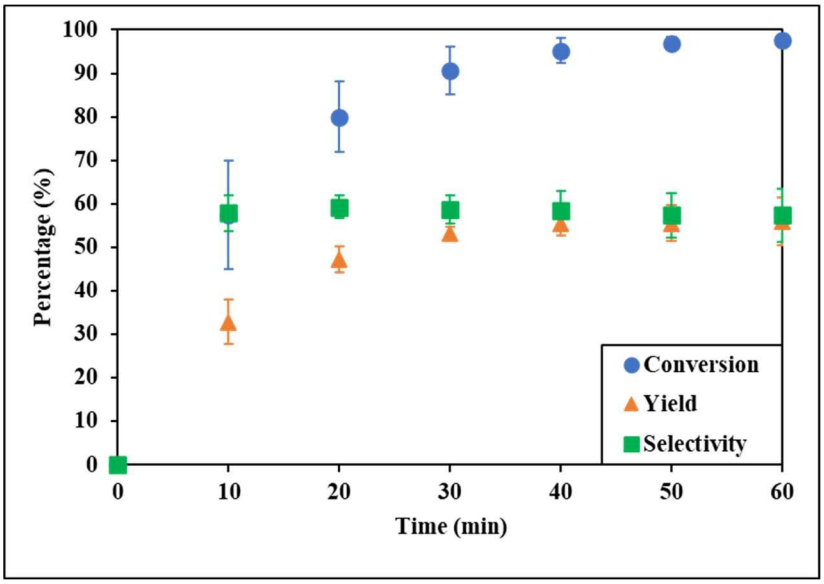

Figure III-2: Reaction profile for the xylose dehydration catalyzed by formic acid. Op. Cond.: initial concentration = 10 g/L of xylose and 10 wt% of formic acid; residence time = 60 min; volume of the mixture = 150 mL; reaction temperature = 170 °C.
The experiments were conducted in triplicate.

Next, keeping the best temperature condition, the effect of reaction time was examined. It can be seen from Figure III-2 that after 40 min of stirring, both furfural yield and selectivity increased progressively until they reached their maximum values of 59% and 66%, respectively. The xylose conversion continued to increase beyond this point and was complete after 60 min, whereas the yield and selectivity of furfural dropped. The decrease in yield and selectivity after the optimum time can be explained by the fact that the produced furfural undergoes secondary reactions. Indeed, the color of the mixture became darker after 40 min, which evidenced the formation of humines. This was consistent with previous reports that longer reaction times promote the generation of by-products such as levulinic acid and humines for a category of catalysts, including strong Lewis or Brønsted acids (Doiseau et al., 2014).

Note also that reaction temperature and residence time synergistically influence furfural synthesis. Yield and selectivity are maximized at higher temperatures with shorter reaction time, and vice versa. However, the optimal yield and selectivity of furfural achieved at 140 °C (45%, 58% after 5 h) and 200 °C (51%, 53% after 10 min) were lower than those produced at 170 °C, which was in agreement with the reported one (Lamminpää and Tanskanen, 2009). This confirmed that the optimal reaction temperature in this study was 170 °C for a residence time of 40 min.

III.1.1.3 Influence of initial xylose concentration

Table III-2: Effect of initial xylose concentration on xylose conversion into furfural.

Entry	Xyl Conc (g/L)	Xyl Conv (%)	Fur yield (%)	Fur selectivity (%)
1	2	88	63	71
2*	10	93 ± 4	54 ± 3	59 ± 5
3	10	93 ± 3	58 ± 2	62 ± 4
4	20	95 ± 3	57 ± 1	60 ± 2
5	30	95 ± 4	54 ± 1	57 ± 4

Op. Cond.: initial concentration = 10 wt% of formic acid; residence time = 40 min; volume of the mixture = 150 mL; reaction temperature = 170 °C.
The experiments were conducted in triplicate.
**The experiment was carried out with 5 wt% of formic acid*

The influence of an initial xylose concentration ranging from 2 g/L to 30 g/L was investigated at optimal reaction temperature and residence time, and the experimental results

are reported in Table III-2. The xylose conversion was unaffected by varying xylose concentrations; nevertheless, the furfural yield and selectivity decreased steadily as the starting xylose concentration increased. Consequently, our study selected an initial xylose concentration of 10 g/L for further investigation. However, the reduction of furfural yield is not particularly obvious because the xylose concentrations in our study were not too high compared to those of other authors. For instance, Yang et al. (2012) discovered that as xylose concentration rose from 40 g/L to 120 g/L, furfural yield and selectivity declined from 70% to 60% and 78% to 65%, respectively, using steam stripping in a semi-batch system. Delbecq et al. (2016) found that the furfural yield decreased from 81% to 65% as the xylose concentration increased from 100 g/L to 600 g/L in a microwave-assisted biphasic system using CPME as the extracting solvent. The decrease in yield and selectivity may be due to excess xylose, which promotes side reactions. This effect is more important when employing a complex starting material, such as oil palm biomass, as Yong et al. (2016) described. Furfural loss processes occur between furfural and other intermediates and fragments in the biomass, lowering furfural yield. On the other hand, low initial xylose concentrations necessitate a larger reactor and greater heat to produce the same amount of furfural in a commercial process. The initial xylose concentration should not be too low for economic reasons, as suggested by previous studies (Yang et al., 2012; Baktash et al., 2015; Kangle et al., 2023), with a recommended range between 50 g/L to 100 g/L. However, this study investigated xylose concentrations ranging from 10–30 g/L, as this range is representative of C_5 sugars in the real biomass hydrolysates used.

III.1.2 Xylose dehydration with steam stripping in a semi-batch system

The decrease in furfural yield and selectivity, resulting from increased undesirable products in the reaction media, is primarily caused by secondary loss reactions, as shown in the previous section. This section aims to improve the process efficiency regarding furfural yield and selectivity by continuously removing the produced furfural from the reaction medium as a vapor mixed with steam in the semi-batch system. The dehydration of xylose into furfural was carried out under optimal conditions identified in the batch system.

III.1.2.1 Influence of vapor flow rate

Table III-3: Furfural production from xylose with steam stripping in a semi-batch system.

Entry	Flow rate (mL/min)	Xyl Conc (g/L)	Xyl Conv (%)	Fur yield (%)	Fur selectivity (%)	τ_{Fur} (%)
1*	1.5	10	95	66 (63)	70 (66)	95
2	1.5	10	95	59 (45)	61 (47)	77
3	3.5	10	95	62 (54)	66 (57)	86
4	3.5	20	92	64 (60)	67 (63)	95
5**	3.5	30	95	80 (71)	87 (78)	89

The number in the bracket is the value in the vapor phase.
Op. Cond.: initial concentration = 10 wt% of formic acid; residence time = 40 min; volume of the mixture = 150 mL; reaction temperature = 170 °C.
**The experiment was carried out without adding water.*
***Repeated three times: the standard deviation of xylose conversion, furfural yield and furfural selectivity are 2%, 2% and 1%, respectively.*

The results of the influence of the vapor flow rate on xylose conversion into furfural and furfural extraction are presented in Table III-3 (Entries1-3). As expected, one can see that the yield and selectivity of furfural in the vapor phase were higher than those in the liquid phase, with their correlation relationship determined by vapor-liquid equilibrium. In addition, the yield and selectivity of furfural and the efficiency of separating furfural in the vapor phase increased when the vapor flow rate was increased. Specifically, the furfural yield in the vapor phase increased from 45% to 54% while maintaining the same total furfural yield of 60% when the flow rate was increased from 1.5 mL/min to 3.5 mL/min. A similar trend in the furfural production from rice husk by hydrolysis accompanying supercritical CO_2 extraction was reported by Sangarunlert et al. (2007). Increasing the flow rate of CO_2 resulted in a higher yield, as a greater amount of CO_2 facilitated the dissolution of more furfural from the reaction mixture. When comparing it to the experiment conducted without extraction (Table III-2, Entry 3), it was observed that the steam extraction did not substantially enhance furfural production regarding the overall furfural yield. This phenomenon could be attributed to the formic acid dilution process by adding water and its subsequent extraction through steam. This could be explained by the fact that the concentration of formic acid in the reactor at the end of the reaction was less than half its initial concentration. Consequently, the conversion rate of xylose to furfural declined during extraction, leading to a similar furfural yield in both systems.

A supplementary experiment was conducted without continuous water injection into the reactor, and the results are presented in Table III-3, Entry 1. The formic acid and xylose concentrations in this system were not diluted throughout the extraction process due to the water addition. The experiment was performed in a high-pressure reactor with an initial volume of 70 mL. Within 40 min, 60 mL of the extract was recovered, resulting in an average flow rate of 1.5 mL/min. When no water was added, the extraction process showed nearly equal results regarding xylose conversion, furfural yield, and furfural selectivity, even when the vapor flow rates were the same.

Nevertheless, the system with no water added achieved a higher separation efficiency since the extraction procedure allowed for the complete recovery of the mixture in the reactor. These findings indicated that the formic acid concentration in the system with water addition was high enough to sustain the reaction rate of xylose conversion into furfural. This was supported by similar results regarding xylose conversion, furfural yield, and furfural selectivity obtained from the experiment using 5 wt% of formic acid, as shown in Table III-2, Entry 2. The low initial xylose concentration could, in this case, be a cause for the indifferent results between the xylose dehydration in batch and semi-batch extraction systems. The following section will examine the impact of the initial xylose concentration on furfural extraction by steam in a semi-batch system to confirm this hypothesis.

III.1.2.2 Influence of initial xylose concentration

The experiments with varying initial xylose concentrations were carried out to show the efficiency of furfural simultaneous extraction by steam. A high initial reactant concentration should provide a correspondingly high product concentration during extraction. Therefore, a high furfural can be derived from a high xylose concentration. Table III-3 (Enties 3-5) shows that the furfural yield achieved through simultaneous extraction rose as the initial xylose concentration increased. The highest furfural yield in the vapor phase, reaching 71%, was obtained with 30 g/L of xylose.

Nevertheless, the results of Telleria's study contradicted these findings where nitrogen was used to stripe furfural produced from xylose dehydration catalyzed by sulfonic ion-exchange resins (Agirrezabal-Telleria et al., 2011). The study revealed a significant decrease in furfural yield, from 70% to 25%, when the xylose concentration was increased from 1% to 10%. Despite the continual removal of furfural from the reaction media, the by-product formation was inevitable and even more enhanced at high initial xylose concentrations. The high initial

xylose concentration investigated could explain the difference, as mentioned in Section III.1.1.3. The catalyst type may be another reason for these dissimilar results since the surface of solid catalysts can serve as a place for secondary reactions.

Compared to the batch system, the semi-batch method provided better furfural yield with optimal purity due to formic acid co-extraction. This effect was particularly pronounced when using high initial xylose concentrations, with a yield of 54% in the batch system compared to 80% in the semi-batch system using 30 g/L of xylose. This phenomenon can be explained by the rapid extraction of furfural by steam, preventing furfural from accumulating in the reaction media, where side reactions occur. This discovery highlighted that steam extraction in a semi-batch system can avoid unwanted loss reactions and improve furfural production. Additionally, this approach allows high xylose concentrations, resulting in a larger furfural concentration in the extract, lowering post-extraction processing requirements.

III.1.3 Xylose dehydration in biphasic solvent system

This section investigated the utilization of a biphasic solvent system, which operates on a similar concept to steam stripping in a semi-batch process where the furfural produced is simultaneously extracted throughout the reaction. This prevents its degradation caused by side reactions in an aqueous phase. The objective was to enhance the efficiency of the process in terms of furfural yield and selectivity by implementing more selective green solvents.

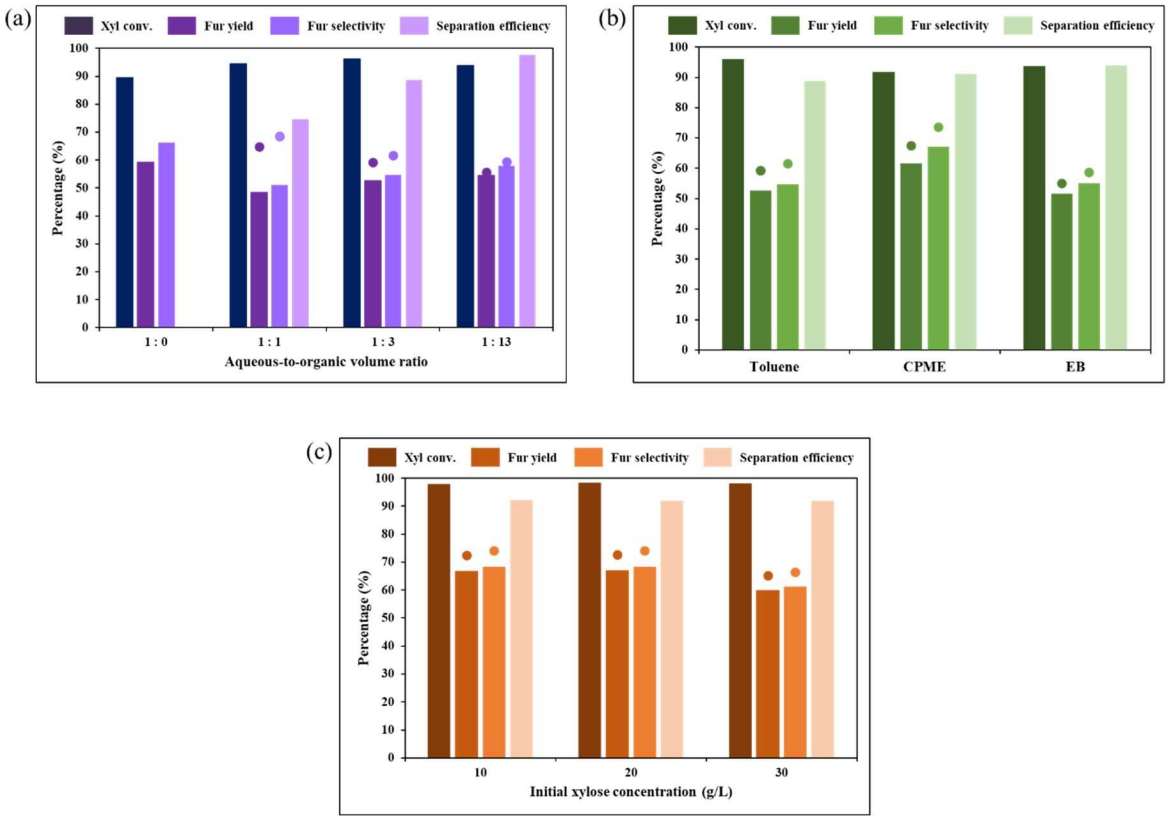

Figure III-3: Furfural production from xylose in a biphasic system.
Xylose conversion, furfural yield and selectivity in the organic phase (columns), furfural yield and furfural selectivity in both phases (circles).
(a) Effect of the aqueous-to-organic volume ratio. Op. Cond.: initial concentration = 10 g/L of xylose and 10 wt% of formic acid; residence time = 40 min; volume of the mixture = 150 mL; reaction temperature = 170 °C; organic solvent = toluene.
(b) Effect of the organic solvent type. Op. Cond.: initial concentration = 10 g/L of xylose and 10 wt% of formic acid; residence time = 40 min; volume of the mixture = 150 mL; reaction temperature = 170 °C; aqueous-to-organic volume ratio = 1 : 3.
(c) Effect of initial xylose concentration. Op. Cond.: initial concentration = 10 wt% of formic acid; residence time = 40 min; volume of the mixture = 150 mL; reaction temperature = 170 °C; aqueous-to-organic volume ratio = 1 : 3; organic solvent = CPME.

III.1.3.1 Influence of aqueous-to-organic volume ratio

Under the optimum conditions obtained in the previous section, the effect of three-volume ratios of aqueous to organic (1:1, 1:3, and 1:13) was investigated using toluene as an organic solvent. Toluene was used in this part as it exhibited a high furfural partition coefficient and low hydrosolubility (Agirrezabal-Telleria et al., 2012a; Hua et al., 2016; Mittal et al., 2017). Figure III-3a demonstrated that, as expected, the yield and selectivity of furfural in the organic phase increased with toluene volume and reached a maximum of 54% and 58%, respectively, at aqueous to organic volume ratio of 1:13. A recent paper using 2-sec-butylphenol (SBP) to extract furfural produced under autocatalytic conditions confirmed comparable findings (Gómez Millán et al., 2021). The decrease in furfural production at a high-volume ratio of water

to organic solvent (i.e., aqueous to organic = 1:1 (v/v)) can be explained by the saturation of toluene and its capacity to extract furfural. As a result, furfural remains in the water phase, susceptible to degradation processes.

Despite the high recovery of furfural in the organic phase, increasing the volume of organic solvent or decreasing the aqueous-to-organic volume ratio, particularly at 1:13 (v/v), resulted in a low xylose-to-furfural conversion. Moreover, the overall yield and selectivity of furfural decreased as the volume ratio of aqueous-to-organic decreased. According to Qing et al. (2017), an excess organic solvent hindered the contact between reactants and catalyst in the aqueous phase, resulting in a low conversion of xylose into furfural and a consequently low furfural yield. In addition, increasing the volume of organic solvent is impractical for industrial applications since it increases the reactor volumes, the downstream separation costs, and overall energy requirement (Gómez Millán et al., 2019; Papaioannou et al., 2019). Subsequent investigations were conducted utilizing a volumetric ratio of 1:3 (v/v) between organic and aqueous solvents, which produced comparable furfural yield, selectivity, and separation efficiency.

III.1.3.2 Influence of organic solvent types

Even though toluene has a good affinity for furfural and a low solubility in water, it is very toxic (Rong et al., 2012). Two eco-friendly solvents, CPME and EB, were then investigated under optimal conditions; the results are shown in Figure III-3b. Interestingly, CPME was the best-extracting solvent, giving the highest yield of 67% with a selectivity of 74% for the aqueous-to-organic volume ratio of 1:3. The results were consistent with the reported one (Molina et al., 2015; Gómez Millán et al., 2019). It was also noticed that the final concentration of formic acid in the aqueous phase was reduced more than twofold when CPME and EB were used as organic solvents compared to toluene. Similar observations have been reported regarding the rise in pH of the aqueous phase after each reuse cycle in the water-CPME biphasic system (Delbecq et al., 2016). This indicates that formic acid was transported at elevated temperatures in CPME and EB, whereas xylose was not found in these active extraction solvents (Guenic et al., 2015). The decreased formic acid concentration in the aqueous phase seems to be the reason for the greater furfural yield observed when using CPME and EB instead of toluene. At the examined water-to-organic volume ratio, a fraction of the extracted furfural migrated back from the organic phase to the aqueous phase due to the saturation of the organic solvent, as previously mentioned. A significant amount of formic acid

during toluene extraction facilitated its degradation, resulting in a diminished yield and selectivity of furfural. Furthermore, the aqueous phase exhibited a deeper color when toluene was employed as the extraction solvent, owing to the presence of humines, compared to the combination of CPME or EB.

The degradation of furfural in CPME and EB containing formic acid was examined by heating the organic phase obtained from the previous experiment at 170 °C for 40 min. It was discovered that the concentration of furfural in the organic phase remained nearly unchanged (the relative gap was less than 5%), confirming that furfural in CPME and EB was stable despite the presence of formic acid.

III.1.3.3 Influence of initial xylose concentration

As stated previously, the furfural yield and selectivity decreased as the initial xylose concentration increased in batch processing; the effect of the starting xylose concentration on the performance of a biphasic system was then investigated. In this section, CPME was used as the extracting solvent at an aqueous-to-organic volume ratio of 1:3. Figure III-3c showed that, given similar xylose conversion (95%), the overall furfural yield decreased when increasing the initial xylose concentration: the furfural yield dropped from 73% to 65% when the xylose concentration rose from 10 g/L to 30 g/L. The unexpected results may arise from the inadequate volume of CPME utilized at the aqueous-to-organic volume ratio of 1:3. As stated in Section III.1.3.1, increasing the volume of organic solvent, which prevents furfural saturation in the organic phase, could potentially increase the furfural yield. Similarly, Guenic et al. (2015) discovered that furfural yield was inversely proportional to the xylose loading when investigating the microwave-assisted dehydration of xylose into furfural by sodium chloride in water-CPME. This was due to the increased viscosity of the aqueous layer, which caused nonuniform heating in the microwave reactor and difficulty in extracting solvent to gain access to furfural. Compared to the batch condition (Table III-2, Entries 3-5), the biphasic system afforded a higher yield and selectivity of furfural at all xylose concentrations. These findings showed that the biphasic system can inhibit secondary degradation reactions, leading to a high yield and selectivity of furfural.

III.1.4 Furfural production from hemicellulose hydrolysate produced from biomasses via LEEBio™ process

Table III-4: Biomass hydrolysate composition after hydrolysis at 120 °C for 240 min

Component	Unit	Fir wood	OPEFB
Ara	g/L	3.6 ± 0.8	2.8 ± 0.4
Galac	g/L	4.4 ± 0.8	1.6 ± 0.3
Glu	g/L	8.7 ± 0.5	0.8 ± 0.2
Mann	g/L	30.1 ± 1.2	1.5 ± 0.3
Xyl	g/L	10.8 ± 0.3	26.2 ± 3.3
FA	g/L	166.2 ± 17.4	141.1 ± 10.7
Fur	g/L	0.5 ± 0.2	2.1 ± 0.6
5-HMF	g/L	0.4 ± 0.1	n.d

n.d : non-detected
The experiments were conducted in triplicate.

After optimizing the operating parameters in the batch system and validating the beneficial effect of simultaneous extraction by steam and organic solvents using synthetic solutions, the approach was extended to convert raw biomass hydrolysate to furfural. This study used the hemicellulose hydrolysate without additional reactants under optimum conditions. It is worth noting that the hydrolysate of hemicellulose obtained from raw biomass comprises both C_5 sugars (xylose and arabinose) and C_6 sugars (glucose, mannose, and galactose). The concentration of these sugars varies depending on the type of biomass, as indicated in Table III-4. The study utilized two categories of biomass: hardwood, represented by fir wood, and residual biomass, exemplified by OPEFB. The purpose was to demonstrate the versatility of this procedure with different types of biomasses. In the presence of formic acid at high temperatures, C_5 sugars underwent dehydration to produce furfural, whereas C_6 sugars were transformed into 5-HMF.

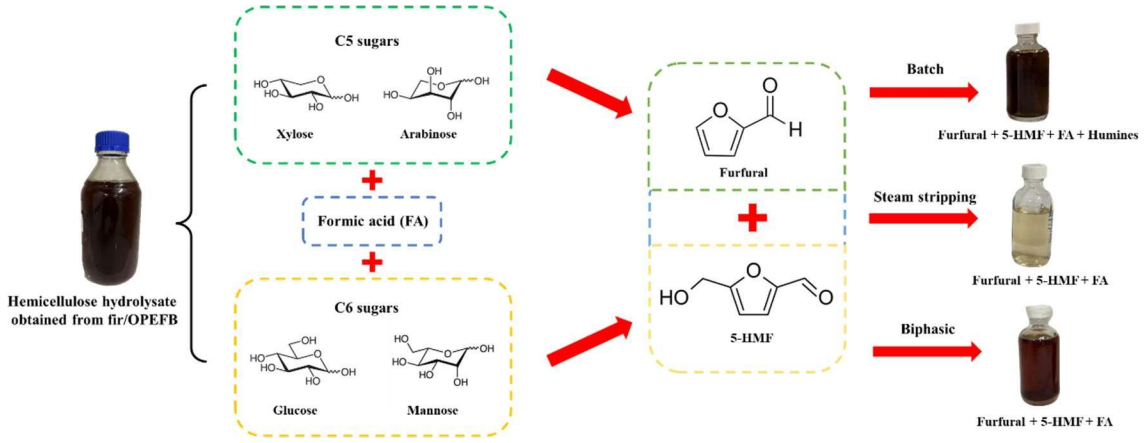

Figure III-4: Scheme of the conversion of hemicellulose hydrolysate from raw biomass to furfural and 5-HMF.

Consequently, the utilization of raw biomass hydrolysate led to the production of furfural and 5-HMF, both important platform chemicals for producing value-added fuels and chemicals, as illustrated in Figure III-4. The results of furfural and 5-HMF production from raw biomass hydrolysate in different systems are presented in Table III-5. The study revealed that the furfural yield derived from OPEFB hydrolysate (70%) surpassed that of fir wood hydrolysate (55%), mostly due to the significantly higher concentration of C_5 sugars in OPEFB hydrolysate, which was almost three times greater than that of fir wood hydrolysate.

Table III-5: Furfural and 5-HMF production from hemicellulose hydrolysate produced from raw biomass in different systems.

System	Biomass	Yield (%)		Separation efficiency: τ (%)	
		Fur	5-HMF	Fur	5-HMF
Batch	Fir wood	55	38	/	/
	OPEFB	70	46	/	/
Semi-batch*	Fir wood	72 (68)	39 (1)	93	1
	OPEFB	79 (74)	48 (0)	94	0
Biphasic**	Fir wood	76 (70)	58 (34)	92	58
	OPEFB	83 (77)	62 (37)	92	60

The number in the bracket is the value in the vapor and organic phases for steam stripping in semi-batch and biphasic systems, respectively.
Op. Cond.: residence time = 40 min, volume of the mixture = 150 mL; reaction temperature = 170 °C. The experiments were conducted without replication.
** vapor flow rate = 3.5 mL/min, adding continuously water in the reactor*
***aqueous-to-organic volume ratio = 1 : 3; organic solvent = CPME.*

When compared to the synthetic solution at an equivalent xylose concentration, it was observed that the furfural yield derived from fir wood (55%) was inferior to that generated from the synthetic solution (Table III-2, Entry 3, 58%). Agirrezabal-Telleria et al. (2012b) also observed a comparable result, examining the impact of additional glucose on the conversion of xylose to furfural. The experiment showed that combining xylose and glucose reduced furfural production compared to utilizing only xylose solution from 66% to 42% at 175 °C despite having the same xylose conversion (60%). The primary cause of this phenomenon is the increased secondary reactions resulting from the interaction between the furfural generated and the high glucose concentration. By studying the kinetics of homogeneously catalyzed xylose dehydration to furfural in the presence of arabinose and glucose, Danon et al. (2014) found the conversion rate of pentoses in complex saccharide solutions was comparable to that of individual pentose solutions. Furfural, however, undergoes faster degradation in more complex saccharide solutions, particularly at higher reaction temperatures (> 200 °C). According to these authors, the reduced yield can be attributed to the breakdown of organic acids (i.e., levulinic acid and formic acid) derived from glucose, which enhanced the degradation of furfural. In contrast, the furfural yield (70%) derived from OPEFB was significantly greater than that of synthetic solutions (Table III-2, Entry 4, 57%). The unexpected results may be attributed to (1) the significant disparity in the concentration of C_6 sugars compared to C_5 sugars, which deviated from the composition observed in fir wood hydrolysate, Agirrezabal-Telleria et al. (2012b)'s study (mass concentration ratio of xylose/glucose = 0.66), and Danon et al. (2014)'s investigation (concentration of xylose = glucose = arabinose = 0.05 mol/L). In this case, the existence of C_6 sugars and their by-products may facilitate the transformation of C_5 sugars into furfural; (2) the presence of different metal ions (i.e., K^+, Ca^{2+}, Al^{3+}, etc.) in the raw biomass hydrolysate, which act as Lewis acid, improving the catalytic performance of formic acid toward the C_5 sugar conversion into furfural (Lopes et al., 2015; Qiao et al., 2022). In their study investigating the impact of chloride salts as co-catalysts for converting xylose into furfural catalyzed by formic acid, Lopes et al. (2017) observed a substantial increase in furfural yield. Specifically, when $AlCl_3$ was introduced, the yield reached to 68%, compared to 55% obtained solely with formic acid as the catalyst. Moreover, the results showed a significant increase in furfural yield from 57% to 70% with the increase in Al^{3+} concentration from 0.2 mol/L to 0.8 mol/L in the presence of formic acid. Additionally, Lee et al. (2020) documented that OPEFB exhibited notably elevated concentrations of metal ions, even higher than Fir wood (Cutter and McGinnes, 1979). Comparatively, OPEFB exhibited a 135-fold increase in Al^{3+} content and a 7-fold increase in Ca^{2+} content compared to fir wood. The results strongly support

the notion that the combination of metal ions and formic acid enhances furfural production. This elucidates why the furfural yield from OPEFB surpassed that from fir wood and pure xylose.

The simultaneous extraction by steam stripping in a semi-batch system and using an organic solvent in a biphasic system significantly improved furfural yield and 5-HMF yield, as presented in Table III-5. These approaches offered an even higher yield compared to the experiment using synthetic solutions. For instance, the furfural yield rose from 70% in the batch system to 79% in the semi-batch system and further to 83% in the biphasic system when OPEFB was employed as the starting material. Similarly, the yield of 5-HMF increased from 46% in batch systems to 48% and 62% in semi-batch and biphasic systems, respectively. Besides the overall yield, the furfural yield in the extract was also higher than that in the residue phase (liquid phase in the semi-batch system and aqueous phase in the biphasic system) and in the batch system using both synthetic solutions and raw biomass hydrolysate, indicating a high level of separation efficiency. For example, when OPEFB was utilized, the furfural yield in the batch system was 70%. In contrast, steam stripping in the semi-batch system and the biphasic solvent system afforded furfural yields in the extract of 74% and 77%, respectively.

However, the conclusion was distinct for 5-HMF, as it predominantly remained in the residual phases for both extraction methods. For example, the separation efficiency achieved in the semi-batch extraction and biphasic solvent systems was only 1% and approximately 60%, respectively, for both biomass hydrolysates. 5-HMF possesses an additional alcohol group in its chemical structure, resulting in a higher level of polarity than furfural. The increased hydrosolubility of 5-HMF (364 g/L at 25°C) compared to furfural (83 g/L at 20 °C) supports this statement. This elucidated why using a nonpolar organic solvent to extract 5-HMF was insufficient compared to the furfural extraction, ultimately leading to a diminished separation efficiency in a biphasic system. During the steam stripping process, the extraction of 5-HMF should be more efficient than furfural due to its stronger polarity and lower boiling point (T_b =115 °C) in contrast to furfural (T_b =160 °C). Nevertheless, our observations did not align with that. Agirrezabal-Telleria et al. (2012b) also reported a comparable finding in which furfural and 5-HMF were extracted using N_2. The liquid phase exhibited a higher concentration of 5-HMF than the vapor phase, with a concentration ratio 0.1 between the two phases. In contrast, the concentration ratio of furfural was about 6-8. The understanding of the water-HMF and water-furfural equilibrium was insufficient, necessitating further investigation to explain the reported results.

The furfural was obtained alongside 5-HMF in the extract, leading to a low purity level and requiring separation in subsequent steps to recover them individually. The use of membrane methods in the pretreatment step to separate C_5 sugars from C_6 sugars holds potential for the individual production of furfural and 5-HMF, enhancing the efficient utilization of biomass and serving practical applications. Furthermore, these membrane techniques can concentrate each variety of sugar, enhancing the production of furfural and 5-HMF while simultaneously employing extraction methods.

III.1.5 Comparison of furfural production in various system

This section compares our furfural production results and similar methods that utilize formic acid as a catalyst in different systems, as detailed in Table III-6. We compared various process and system types, operating conditions, biomass types, and production performance regarding xylose conversion, furfural yield, and selectivity to demonstrate our production performance.

Within the batch system, it was noted that using synthetic solutions resulted in a lower furfural yield and a lengthier reaction time. However, our method was conducted at a reduced temperature and lower formic acid concentration. This could substantially decrease operational expenses and the danger associated with the high formic acid concentration utilized in previous investigations (Lamminpää and Tanskanen, 2009; Lopes et al., 2017). Compared to the Lopes et al. (2017) process, the separation or recovery of mineral salt is not required in our study since only formic acid was used without additional reactants. As a result, the expenses associated with post-treatment in the downstream processing of the salt-saturated aqueous phase are reduced. However, it was evident that our approach yielded a higher amount of furfural when using raw biomass compared to other studies that utilized high temperatures for faster reaction times (Yong et al., 2016) and mineral salt (Qiao et al., 2022). As mentioned earlier, this rendered the procedure uneconomical.

Table III-6: Comparison of furfural production using formic acid as a catalyst with literature.

Starting material	Process	System	Solvent	Catalyst	Optimal operating conditions			Results			Ref.
					T (°C)	*t* (min)	Xyl Conc (g/L)	Xyl Conv (%)	Fur yield (%)	Fur selectivity (%)	
Xyl	Batch	Monophasic	Water	FA (10 wt%)	170	40	10	93	58	62	This work
Xyl	Batch	Monophasic	Water	FA (30 wt%)	200	20	10	96.7	65.4	67.6	Lamminpää and Tanskanen (2009)
Xyl	Batch	Monophasic	Water	FA (55 wt%) + $AlCl_3$ (0.4 M)	130	30	45	90	68	75	Lopes et al. (2017)
Xyl	Batch	Biphasic	Water/CPME (1:3, v/v)	FA (10 wt%)	170	40	10	98	73	74	This work
Xyl	Batch	Biphasic	Water/o-nitrotoluene (1:3, v/v)	FA (20 g/L)	190	75	80	86	74	86	Yang et al. (2013)
Xyl	Batch	Biphasic	Water/CPME (1:3, v/v)	FA (125 g/L) +betaine (0.07 g)	170	60	150 mg	n.p	80	n.p	Delbecq et al. (2016)
Xyl	Semi-batch	Monophasic	Water	FA (10 wt%)	170	40	30	92	71	78	This work
Xyl	Semi-batch	Monophasic	Water	FA (10 g/L)	180	120	40	95	74	78	Yang et al. (2012)
Fir wood	Batch	Monophasic	Water	FA (150 g/L)	170	40	10	n.p	55	n.p	This work
OPEFB	Batch	Monophasic	Water	FA (150 g/L)	170	40	25	n.p	70	n.p	This work

Starting material	Process	System	Solvent	Catalyst	Optimal operating conditions			Results			Ref.
					T (°C)	*t* (min)	Xyl Conc (g/L)	Xyl Conv (%)	Fur yield (%)	Fur selectivity (%)	
Oil palm fronds (OPF)	Batch	Monophasic	Water+Ethanol	FA	240	1	n.p	n.p	35.8	n.p	Yong et al. (2016)
Corn cobs	Batch	Monophasic	Water	FA (31.3 g/L) + $AlCl_3$ (100 mM)	160	60	n.p	n.p	49.3	n.p	Qiao et al. (2022)
Fir wood	Batch	Biphasic	Water/CPME (1:3, v/v)	FA (150 g/L)	170	40	10	n.p	76	n.p	This work
OPEFB	Batch	Biphasic	Water/CPME (1:3, v/v)	FA (150 g/L)	170	40	25	n.p	83	n.p	This work
Rice husk	Batch	Biphasic	Water/CPME (1:3, v/v)	FA (50 kg/L) +betaine (0.08 g)	190	60	n.p	n.p	6	n.p	Delbecq et al. (2016)

n.p =non provided

Regarding the production in a biphasic solvent system, our reaction was conducted using an environmentally friendly solvent without additional catalysts, fulfilling the requirement of green chemistry and the principle of sustainable development. Furthermore, it is noteworthy that our outcomes in the biphasic batch system utilizing raw biomass were superior to all other comparable procedures. The highest furfural yields of 76% and 83% were obtained from fir wood and OPEFB, respectively. Additionally, the furfural yield achieved by this system surpassed that obtained with steam stripping across all investigated conditions and starting materials. This superiority can be attributed to the organic solvents' (apolar) heightened affinity for furfural compared to water steam, as previously discussed. Despite the elevated formic acid concentration, our research yielded results comparable to those of Yang et al. (2012) in a semi-batch system by utilizing a reduced temperature and a shorter reaction time. As stated previously, the membrane process could reduce the concentration of formic acid while keeping the concentration of sugars constant. Our study demonstrates that manufacturing furfural utilizing synthetic solutions and hydrolysate obtained from raw biomass is promising. These findings indicate that biomass residue can be effectively recycled to provide valuable and practical products.

The above results showed that optimization of furfural production can be achieved by selecting the appropriate study system and operating conditions (i.e., temperature and time). However, all these studies were conducted under pressure (~15 bar at 200 °C). This raises the question of whether working at a lower pressure, such as atmospheric pressure, could be considered to reduce the energy and equipment costs of the process.

III.2 Complementary study: Furfural synthesis in biphasic system at atmospheric pressure

As far as we know, research on the dehydration of xylose to furfural at atmospheric pressure remains limited. Early investigations centered on the use of hydrochloric acid, notably examined by Fulmer et al. (1936). In their pioneering work, they utilized hydrochloric acid-sodium chloride solutions within a toluene-water biphasic system, achieving a maximum furfural yield of 53%. Subsequent studies by Hockett et al. (1943) in 1943 explored furfural production from xylose and arabinose using 12% hydrochloric acid under atmospheric pressure conditions. Further advancements were made by Rong et al. (2012), who optimized furfural production from xylose in a toluene-water biphasic system employing sulfuric acid as a catalyst

and inorganic salt ($FeCl_3$) as a promoter. Remarkably, under these conditions, a best furfural yield of 83% was attained. Despite these advancements, there remains a notable gap in research concerning furfural synthesis from xylose using organic acids such as formic acid under atmospheric pressure conditions. Hence, our initial investigation focuses on exploring furfural production under mild experimental conditions, specifically using formic acid as a catalyst and operating at atmospheric pressure.

III.2.1 Furfural synthesis in monophasic system at atmospheric pressure

Initially, furfural production from xylose was conducted using formic acid as a catalyst in a monophasic system. The results from these experiments are detailed in Table III-7.

Table III-7: Experimental conditions and results obtained from dehydration of xylose in monophasic system at atmospheric pressure

Entry	*t* (min)	Concentration		Xyl conv (%)	Fur yield (%)	Fur selectivity (%)
		Xyl (g/L)	FA (wt%)			
1	40	10	10	1.7	-	-
2	60	10	10	1.5	-	-
3	300	10	10	3.7	-	-
4	300	10	30	8.9	0.8	9.5
5	540	10	30	12.7	1.6	12.2
6[a]	300	10	30	5.7	0.5	9.2
7[b]	300	10	30	10.3	1.1	10.5
8[c]	300	10	30	8.1	1.5	18.9

[a] *The pure xylose solution is fed continuously for 120 min, similar to the semi-continuous system.*
[b] *2.0 g of Aquivion PW98 was added.*
[c] *1.2 g of Amberlyst-15 was added.*
Op. Cond.: volume of the mixture = 200 mL; stirring = 400 rpm; temperature (boiling) and atmospheric pressure.

Furfural was only produced under specific conditions (i.e., 10 g/L xylose and 30 wt% formic acid for 300 min), as shown in Table III-7. Under the appropriate conditions, Furfural yield varied from 0.5% to 1.6% for a xylose conversion range of 5.7% to 12.7% and furfural selectivity of 9.2% to 18.9%.

When the reaction time was extended, the yield of furfural increased, just like the conversion of xylose and the selectivity of furfural. Despite these improvements, the yield attained in this study was considerably lower than that documented in existing literature. This disparity in furfural yield could plausibly be attributed to the relatively low catalytic efficiency

of formic acid, an organic acid, as opposed to the more potent mineral acids such as hydrochloric or sulfuric acid.

To avoid secondary loss reactions (i.e., condensation), pure xylose solution was added constantly for 2 h throughout the course of 3 h (Entry 6 in Table III-7), which was similar to a semi-continuous procedure. In the end, the yield of furfural was lower than that obtained in a batch process under the same conditions.

Furthermore, it was discovered that Brønsted heterogeneous catalysts improved formic acid catalytic performance during the dehydration of xylose to furfural (Entries 7 and 8 in Table III-7). Interestingly, there was no significant difference in terms of furfural yield systems employing Brønsted heterogeneous catalysts and those without. This observation could be explained by the relatively low reaction temperature utilized to enhance the catalytic performance of heterogeneous catalysts. Our findings align with previous research, indicating that the majority of heterogeneous catalysts utilized for xylose conversion into furfural operate at temperatures exceeding 120 °C (Tuteja et al., 2012).

To improve performance at atmospheric pressure, a two-phase system is proposed, as in the previous study, to remove produced furfural during the reaction. This approach aims to limit its degradation due to side reactions.

III.2.2 Furfural synthesis in biphasic system at atmospheric pressure

Table III-8: Experimental conditions and results obtained from dehydration of xylose in biphasic solvent system at atmospheric pressure

Entry	Organic solvent	Phase aqueous to phase organic ratio (v/v)	Xyl conv (%)	Fur yield (%)	Fur selectivity (%)
1[a]	Toluene	1:3	24.0	-	-
2[a]	CPME	1:3	11.6	-	-
3[a*]	Toluene	1:3	16.0	-	-
4[a**]	Toluene	1:3	22.7	-	-
5[b]	Toluene	1:15	64.2	3.2	5.0

Op. cond.: volume of the mixture = 200 mL; stirring = 400 rpm; temperature (boiling); atmospheric pressure; t = 300 min.
a: xylose concentration (10 g/L) and formic acid concentration (30 wt%), b: xylose concentration (100 g/L), formic acid concentration (30 wt%) and 2.4 g of NaCl.
[*] *The pure xylose solution is fed continuously for 60 min, similar to the semi-continuous system.*
[**] *0.3 g of Amberlyst-15 was added.*

Following furfural production in the aqueous monophasic system, experimentation extended to the biphasic solvent system. Here, furfural produced was extracted into the extracting phase to mitigate potential side reactions in the aqueous phase and preferentially drive the reaction towards furfural formation. The results of this part are presented in Table III-8.

As demonstrated in Table III-8, xylose conversion was higher in a biphasic solvent system than in a single aqueous system, however furfural formation was not ideal. Among the examined organic solvents, toluene proved to have the greatest performance for extracting produced furfural from the aqueous phase, which was consistent with previous results (Rong et al., 2012; Hua et al., 2016). The dehydration of xylose into furfural was not improved by feeding pure xylose solution into a biphasic system using toluene as an extracting solvent. Furthermore, adding Amberlyst-15, which boosts formic acid's catalytic activity in a single aqueous system, had no effect on furfural synthesis in the biphasic solvent system. Increasing the initial concentration of xylose, on the other hand, was found to increase the production of furfural. Using 100 g/L of xylose, 30 wt% of formic acid, and a toluene/aqueous ratio of 15:1 (v/v), the best furfural yield of 3.2% for 64.2% xylose conversion was obtained.

Since toluene is toxic and derived from petrochemical sources, cyclopentyl methyl ether (CPME), a green solvent that is less toxic than other ethers (Gómez Millán et al., 2019), was investigated. Under the assessed conditions described herein, no improvement in the conversion of xylose into furfural was observed. Moreover, a lower level of xylose conversion was achieved with CPME, and furfural formation was not enhanced compared to using toluene as the extracting solvent.

III.3 Conclusion chapter

Regarding the conversion of xylose into furfural under atmospheric pressure, it was found that furfural formation in both monophasic and biphasic solvent systems was suboptimal due to the low catalytic activity of formic acid in dehydrating xylose to furfural under these conditions. The addition of Brønsted heterogeneous catalysts improved the catalytic performance of formic acid in terms of xylose conversion, although furfural yield remained low (< 2%). However, a significant increase in furfural yield was observed at higher temperatures (> 140°C). Under optimal conditions (170°C for 40 minutes), successful furfural synthesis was achieved, with 58% and 70% furfural obtained from synthetic solutions containing 10 g/L of xylose and raw biomass hydrolysates derived from OPEFB, respectively.

Chapter 3: Development of a homogeneously catalyzed process for furfural production with classical extraction system.

Implementation of simultaneous furfural extraction methods, including steam stripping and the use of eco-friendly solvents within a biphasic system, resulted in notable enhancements in furfural production. Yields consistently exceeded 70%, with separation efficiencies surpassing 90% across all examined conditions and starting materials.

These findings underscored the versatility of formic acid, which serves both as a solvent for lignocellulosic biomass depolymerization and as an efficient catalyst for xylose dehydration to furfural. This integrated process facilitates the individual extraction of three biomass fractions, optimizing resource utilization. Moreover, this environmentally friendly approach promotes sustainability, requiring no additional chemicals for hydrolysate utilization. These results hold promise for diverse biomass applications and provide a crucial reference for scaling up to pilot and semi-industrial production levels.

Despite the fact that these initial results are very promising, the scalability of this process from a green and economic perspective remains questionable. Therefore, the next chapter is dedicated to exploring greener alternatives, such as using supercritical CO_2 or heterogeneous catalysts, to minimize the use of formic acid.

III.4 References

Agirrezabal-Telleria, I., Larreategui, A., Requies, J., Güemez, M.B., Arias, P.L., 2011. Furfural production from xylose using sulfonic ion-exchange resins (Amberlyst) and simultaneous stripping with nitrogen. Bioresour. Technol. 102, 7478–7485. https://doi.org/10.1016/j.biortech.2011.05.015

Agirrezabal-Telleria, I., Requies, J., Güemez, M.B., Arias, P.L., 2012a. Furfural production from xylose + glucose feedings and simultaneous N2-stripping. Green Chem. 14, 3132–3140. https://doi.org/10.1039/c2gc36092f

Agirrezabal-Telleria, I., Requies, J., Güemez, M.B., Arias, P.L., 2012b. Pore size tuning of functionalized SBA-15 catalysts for the selective production of furfural from xylose. Appl. Catal. B Environ. 115–116, 169–178. https://doi.org/10.1016/j.apcatb.2011.12.025

Baktash, M.M., Ahsan, L., Ni, Y., 2015. Production of furfural from an industrial pre-hydrolysis liquor. Sep. Purif. Technol. 149, 407–412. https://doi.org/10.1016/j.seppur.2015.06.003

Brownlee, H.J., Miner, C.S., 1948. Industrial Development of Furfural. Ind. Eng. Chem. 40, 201–204. https://doi.org/10.1021/ie50458a005

Cutter, B.E., McGinnes, E.A., 1979. Inorganic concentrations in selected woods and charcoals measured using naa. WOOD FIBER 12, 72–79.

Danon, B., Hongsiri, W., Van Der Aa, L., De Jong, W., 2014. Kinetic study on homogeneously catalyzed xylose dehydration to furfural in the presence of arabinose and glucose. Biomass Bioenergy 66, 364–370. https://doi.org/10.1016/j.biombioe.2014.04.007

Delbecq, F., Wang, Y., Len, C., 2016. Conversion of xylose, xylan and rice husk into furfural via betaine and formic acid mixture as novel homogeneous catalyst in biphasic system by microwave-assisted dehydration. J. Mol. Catal. Chem. 423, 520–525. https://doi.org/10.1016/j.molcata.2016.07.003

Delmas, M., 2021. A lignocellulosic biomass based process for production of lignins and syngas, and electricity production efficient syngas. US20210009908A1.

Doiseau, A.-C., Rataboul, F., Burel, L., Essayem, N., 2014. Synergy effect between solid acid catalysts and concentrated carboxylic acids solutions for efficient furfural production from xylose. Catal. Today 226, 176–184. https://doi.org/10.1016/j.cattod.2013.10.034

Dussan, K., Girisuta, B., Lopes, M., Leahy, J.J., Hayes, M.H.B., 2015. Conversion of Hemicellulose Sugars Catalyzed by Formic Acid: Kinetics of the Dehydration of D -Xylose, L -Arabinose, and D -Glucose. ChemSusChem 8, 1411–1428. https://doi.org/10.1002/cssc.201403328

Fulmer, E.I., Christensen, L.M., Hixon, R.M., Foster, R.L., 1936. The Production of Furfural from Xylose Solutions by Means of Hydrochloric Acid–Sodium Chloride Systems. J. Phys. Chem. 40, 133–141. https://doi.org/10.1021/j150370a017

Gómez Millán, G., Bangalore Ashok, R.P., Oinas, P., Llorca, J., Sixta, H., 2021. Furfural production from xylose and birch hydrolysate liquor in a biphasic system and techno-economic analysis. Biomass Convers. Biorefinery 11, 2095–2106. https://doi.org/10.1007/s13399-020-00702-4

Gómez Millán, G., Hellsten, S., King, A.W.T., Pokki, J.-P., Llorca, J., Sixta, H., 2019. A comparative study of water-immiscible organic solvents in the production of furfural from xylose and birch hydrolysate. J. Ind. Eng. Chem. 72, 354–363. https://doi.org/10.1016/j.jiec.2018.12.037

Guenic, S.L., Delbecq, F., Ceballos, C., Len, C., 2015. Microwave-assisted dehydration of D-xylose into furfural by diluted inexpensive inorganic salts solution in a biphasic system. J. Mol. Catal. Chem. 410, 1–7. https://doi.org/10.1016/j.molcata.2015.08.019

Hockett, R.C., Guttag, A., Smith, M.E., 1943. The Production of Furfural from D-Lyxose and D-Ribose. J. Am. Chem. Soc. 65, 1–3. https://doi.org/10.1021/ja01241a001

Hua, D.-R., Wu, Y.-L., Liu, Y.-F., Chen, Y., Yang, M.-D., Lu, X.-N., Li, J., 2016. Preparation of furfural and reaction kinetics of xylose dehydration to furfural in high-temperature water. Pet. Sci. 13, 167–172. https://doi.org/10.1007/s12182-015-0069-y

Kamm, B., Gerhardt, M., Dautzenberg, G., 2013. Catalytic Processes of Lignocellulosic Feedstock Conversion for Production of Furfural, Levulinic Acid, and Formic Acid-Based Fuel Components, in: New and Future Developments in Catalysis. Elsevier, pp. 91–113. https://doi.org/10.1016/B978-0-444-53878-9.00005-9

Kangle, N., Gaikwad, K., Angal, S., 2023. Manufacture of Furfural from Sugarcane Bagasse. Int. J. Eng. Res. Appl. 13, 96–102. https://doi.org/DOI: 10.9790/9622-130196102

Lamminpää, K., Tanskanen, J., 2009. Study of furfural formation using formic acid. 8th World Congr. Chem. Eng. 7.

Lee, J.H., Ahmed, M.A., Choi, I.-G., Choi, J.W., 2020. Fractionation of Cellulose-Rich Products from an Empty Fruit Bunch (EFB) by Means of Steam Explosion Followed by Organosolv Treatment. Appl. Sci. 10, 2–11. https://doi.org/10.3390/app10030835

Lopes, M., Dussan, K., Leahy, J., 2015. Chloride Salts as Co-Catalysts for the Conversion of D-Xylose to Furfural with Formic Acid. Presented at the 23rd European Biomass Conference and Exhibition, Vienna, Austria, pp. 1130–1133. https://doi.org/10.5071/23rdEUBCE2015-3AV.3.48

Lopes, M., Dussan, K., Leahy, J.J., 2017. Enhancing the conversion of D-xylose into furfural at low temperatures using chloride salts as co-catalysts: Catalytic combination of AlCl 3 and formic acid. Chem. Eng. J. 323, 278–286. https://doi.org/10.1016/j.cej.2017.04.114

Marcotullio, G., De Jong, W., 2010. Chloride ions enhance furfural formation from d-xylose in dilute aqueous acidic solutions. Green Chem. 12, 1739. https://doi.org/10.1039/b927424c

Mittal, A., Black, S.K., Vinzant, T.B., O'Brien, M., Tucker, M.P., Johnson, D.K., 2017. Production of Furfural from Process-Relevant Biomass-Derived Pentoses in a Biphasic Reaction System. ACS Sustain. Chem. Eng. 5, 5694–5701. https://doi.org/10.1021/acssuschemeng.7b00215

Molina, M.J.C., Granados, M.L., Gervasini, A., Carniti, P., 2015. Exploitment of niobium oxide effective acidity for xylose dehydration to furfural. Catal. Today 254, 90–98. https://doi.org/10.1016/j.cattod.2015.01.018

Papaioannou, M., Kleijwegt, R.J.T., Van Der Schaaf, J., Neira d'Angelo, M.F., 2019. Furfural Production by Continuous Reactive Extraction in a Millireactor under the Taylor Flow Regime. Ind. Eng. Chem. Res. 58, 16106–16115. https://doi.org/10.1021/acs.iecr.9b00604

Qiao, H., Han, M., Ouyang, S., Zheng, Z., Ouyang, J., 2022. An integrated lignocellulose biorefinery process: Two-step sequential treatment with formic acid for efficiently producing ethanol and furfural from corn cobs. Renew. Energy 191, 775–784. https://doi.org/10.1016/j.renene.2022.04.027

Qing, Q., Guo, Q., Zhou, L., Wan, Y., Xu, Y., Ji, H., Gao, X., Zhang, Y., 2017. Catalytic conversion of corncob and corncob pretreatment hydrolysate to furfural in a biphasic system with addition of sodium chloride. Bioresour. Technol. 226, 247–254. https://doi.org/10.1016/j.biortech.2016.11.118

Raman, J.K., Gnansounou, E., 2015. Furfural production from empty fruit bunch – A biorefinery approach. Ind. Crops Prod. 69, 371–377. https://doi.org/10.1016/j.indcrop.2015.02.063

Rong, C., Ding, X., Zhu, Y., Li, Y., Wang, L., Qu, Y., Ma, X., Wang, Z., 2012. Production of furfural from xylose at atmospheric pressure by dilute sulfuric acid and inorganic salts. Carbohydr. Res. 350, 77–80. https://doi.org/10.1016/j.carres.2011.11.023

Sangarunlert, W., Piumsomboon, P., Ngamprasertsith, S., 2007. Furfural production by acid hydrolysis and supercritical carbon dioxide extraction from rice husk. Korean J. Chem. Eng. 24, 936–941. https://doi.org/10.1007/s11814-007-0101-z

Tongtummachat, T., Jaree, A., Akkarawatkhoosith, N., 2022. Continuous hydrothermal furfural production from xylose in a microreactor with dual-acid catalysts. RSC Adv. 12, 23366–23378. https://doi.org/10.1039/D2RA03609F

Tuteja, J., Nishimura, S., Ebitani, K., 2012. One-Pot Synthesis of Furans from Various Saccharides Using a Combination of Solid Acid and Base Catalysts. Bull. Chem. Soc. Jpn. 85, 275–281. https://doi.org/10.1246/bcsj.20110287

Yan, K., Wu, G., Lafleur, T., Jarvis, C., 2014. Production, properties and catalytic hydrogenation of furfural to fuel additives and value-added chemicals. Renew. Sustain. Energy Rev. 38, 663–676. https://doi.org/10.1016/j.rser.2014.07.003

Yang, W., Li, P., Bo, D., Chang, H., 2012. The optimization of formic acid hydrolysis of xylose in furfural production. Carbohydr. Res. 357, 53–61. https://doi.org/10.1016/j.carres.2012.05.020

Yang, W., Li, P., Bo, D., Chang, H., Wang, X., Zhu, T., 2013. Optimization of furfural production from d-xylose with formic acid as catalyst in a reactive extraction system. Bioresour. Technol. 133, 361–369. https://doi.org/10.1016/j.biortech.2013.01.127

Yong, T.L.-K., Mohamad, N., Yusof, N.N.M., 2016. Furfural Production from Oil Palm Biomass Using a Biomass-derived Supercritical Ethanol Solvent and Formic Acid Catalyst. Procedia Eng. 148, 392–400. https://doi.org/10.1016/j.proeng.2016.06.495

Zeitsch, K.J., 2000. The Chemistry and Technology of Furfural and its Many By-Products. Elsevier.

Zhang, L., He, Y., Zhu, Y., Liu, Y., Wang, X., 2018. Camellia oleifera shell as an alternative feedstock for furfural production using a high surface acidity solid acid catalyst. Bioresour. Technol. 249, 536–541. https://doi.org/10.1016/j.biortech.2017.10.061

IV. Chapter 4

Towards more environmentally-friendly processes.

This chapter focuses on environmentally-friendly processes for furfural production from xylose. These processes include (1) using supercritical carbon dioxide (Sc-CO_2) as an extracting agent to prevent the degradation of produced furfural by removing it from the reaction medium, and (2) combining heterogeneous acid catalysts with formic acid to convert xylose into furfural. The chapter is divided into two sections: the first section presents a study on furfural production from xylose using formic acid as a catalyst with simultaneous extraction using Sc-CO_2. The second section addresses furfural production from xylose using a combination of heterogeneous catalysts and formic acid.

The methods for conducting these manipulations, encompassing both analytical and experimental approaches, have been previously delineated in Chapter 2. Specifically, the experimental setup employed for this study is described in Section II.2.1. Additionally, the extraction method utilizing Sc-CO_2 is stated upon in Section II.3.3.

The subsequent section of this chapter presents experimental results concerning furfural production utilizing Sc-CO_2 in both batch and semi-batch systems. Initially, the results of furfural production in a batch system using Sc-CO_2 are detailed, emphasizing the catalytic activity of Sc-CO_2 in facilitating xylose conversion to furfural. Subsequently, the investigation examines furfural production accompanied by simultaneous Sc-CO_2 extraction in a semi-batch system, focusing on the identification of optimal conditions to enhance furfural yield through parameter adjustments. Finally, the study's findings are compared with those of other investigations, aiming to evaluate the efficacy of Sc-CO_2 extraction for furfural production across various catalyst types. The experimental results presented in this section are extracted from the article entitled "Integrated supercritical carbon dioxide extraction for efficient furfural production from xylose using formic acid as a catalyst", The *Journal of Supercritical Fluids*, (2024) 106274.

The second section of this chapter presents experimental results concerning furfural production from xylose using a combination of heterogeneous catalysts and formic acid. First, the impact of adding Lewis heterogeneous catalysts on furfural production in monophasic and biphasic

systems is discussed. Then, the effect of temperature on xylose conversion into furfural through heterogeneous catalysis is detailed for both monophasic and biphasic systems.

IV.1 The production of furfural from xylose using formic acid as a catalyst and simultaneous extraction with supercritical carbon dioxide

The following results are presented as part of the scientific article entitled "Integrated supercritical carbon dioxide extraction for efficient furfural production from xylose using formic acid as a catalyst", The *Journal of Supercritical Fluids*, (2024) 106274.

In this study, an extensive investigation was carried out by combining formic acid as a catalyst and Sc-CO_2 as an extraction agent for the dehydration of xylose into furfural. Firstly, the catalytic properties of CO_2, as well as the synergistic effects of formic acid and CO_2 on xylose dehydration to furfural, were studied in batch mode. Secondly, the performance of Sc-CO_2 extraction to recover furfural from the reaction medium, while avoiding its degradation in semi-batch processes, was also examined. Synthetic solutions, containing mainly xylose (10–30 g/L) and formic acid (10 wt%) were used, with their concentrations representative of a juice resulting from the hydrolysis of biomass by formic acid in the LEEBio^{TM} process.

IV.1.1 Xylose conversion in batch system with Sc-CO_2

IV.1.1.1 Catalytic effect of CO_2

The objective of this section is to investigate the catalytic properties of CO_2 in the dehydration of xylose to furfural catalyzed by formic acid.

Table IV-1 (Entries 2, 3, and 6) presents the results of furfural synthesis in batch mode in a two-phase H_2O-CO_2 medium at different pressures. It was observed that the xylose conversion achieved in the CO_2 experiments was higher than that obtained by the process using only formic acid (Table IV-1, Entry 1) or only CO_2 without formic acid (9% and 5%, respectively, at 20 MPa for conversion rate and furfural yield).

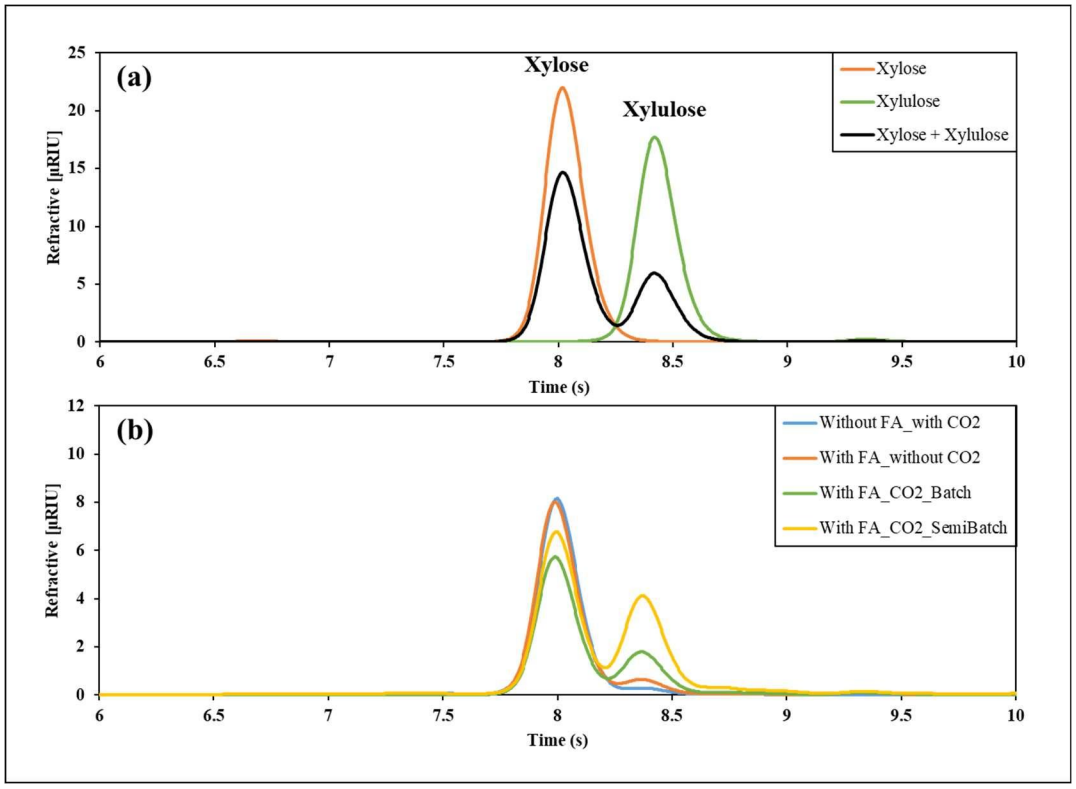

Figure IV-1: HPLC chromatograms on a Bio-Rad Aminex HPX-87H column with a refractive index detector: (a) standard of xylose, xylulose and their mixture; (b) the mixture remained in the reactor after 1h of dehydration in different cases.
Op. Cond.: initial concentration = 10 g/L of xylose and 10 wt% of formic acid; residence time = 5h; volume of the mixture = 55 mL; temperature = 140 °C; CO_2 pressure = 20 MPa.

Upon analyzing the reaction mixture sampled during the dehydration of xylose to furfural catalyzed by formic acid in the presence of CO_2, xylulose, an isomer of xylose, was detected. According to Liu et al. (2021), xylulose can be formed via the isomerization of xylose catalyzed by a Lewis acid, which in this case was likely CO_2, as this isomer was only found in the presence of CO_2 (Figure IV-1b). Xylulose then rapidly dehydrates to furfural via a Brønsted acid, which in this study was formic acid, as illustrated in Figure IV-2. Choudhary et al. (2012) proposed a similar reaction mechanism while investigating the conversion of xylose to furfural using $CrCl_3$ as a Lewis acid and HCl as a Brønsted acid catalyst. The initial phase involves the isomerization of xylose into xylulose via a Lewis acid, as the activation barrier for xylulose dehydration (23.1 kcal/mol) is lower than that of xylose (30–32 kcal/mol). The subsequent step includes the dehydration of xylulose catalyzed by a Brønsted acid to produce furfural. Under the investigated conditions, where the pH of the solution (1.86) is lower than the pK_a (≈ 6.2) of CO_2/H_2CO_3, the predominant form of CO_2 was the dissolved CO_2 molecule (CO_2 (aq)), which can act as a Lewis acid (Beckman, 2004).

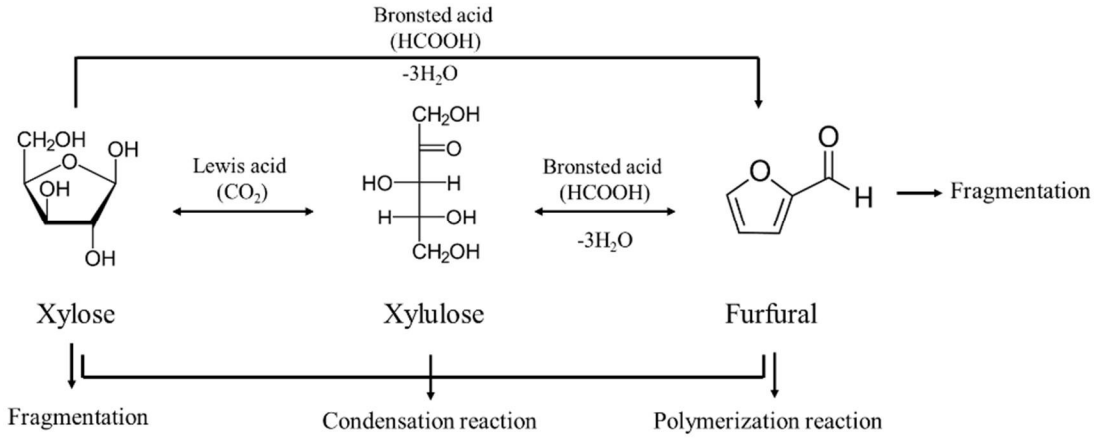

Figure IV-2: The reaction pathway of the formic acid-catalyzed dehydration of xylose into furfural in the presence of formic acid and of both formic acid and CO_2.

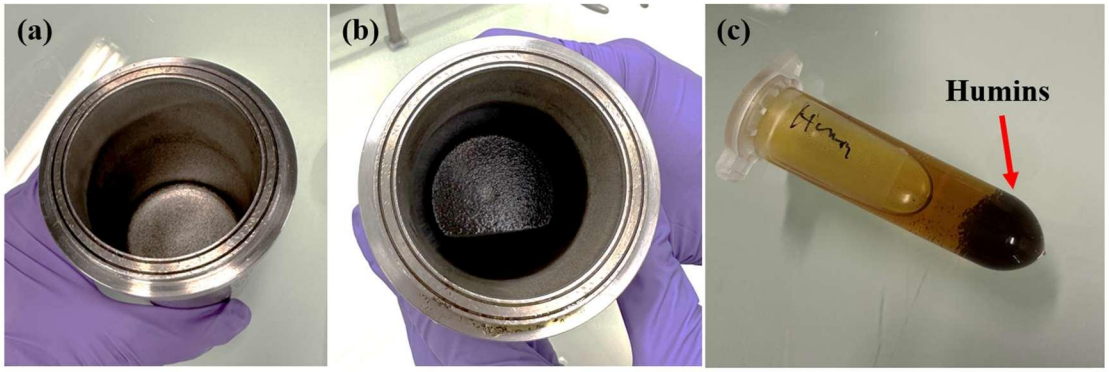

Figure IV-3: The black insoluble carbonaceous compound (Humines). (a): the reactor before the reaction, (b): the reactor after the reaction, (c): the black insoluble humines.

An additional trial was carried out to compare the Lewis acid performance of CO_2 to that of H-ZSM-5 (SiO_2/Al_2O_3 = 23, TOSOH) which possesses both Lewis and Brønsted acid sites. The results indicated that CO_2 (P = 5 MPa) was more effective than H-ZSM-5 (m = 0.4 g) as a Lewis acid for the conversion of xylose to furfural in the presence of formic acid. Under identical conditions (T = 140 °C, t = 5 h, C_{xyl} = 10 g/L, and C_{FA} = 10 wt%), the CO_2 experiment resulted in a greater furfural yield (61% vs. 33%) and selectivity (64% vs. 33%) for similar xylose conversion (95–100%). Moreover, xylulose was found in both CO_2 and H-ZSM-5 experiments, confirming that CO_2 can indeed act as a Lewis acid catalyst. The role of CO_2 as a Lewis acid could be the primary reason for the higher xylose conversion observed in the presence of CO_2 compared with its absence. This observation is consistent with the findings of Choudhary et al. (2011), who evaluated the possibility for single pot furfural synthesis from xylose via xylulose using hydrochloric acid (HCl) and the cation exchange resin Amberlyst-15

in an aqueous medium. They discovered that when xylulose was used as the reactant, the conversion reached 66%, and the furfural yield was 24%, whereas xylose did not react at low temperatures (< 120 °C) with Amberlyst-15 or HCl. This finding supports a reaction scheme in which xylulose dehydrates more quickly to furfural than xylose via Brønsted acid catalysis.

In addition to achieving a higher conversion of xylose, the experiments involving CO_2 demonstrated a higher furfural yield than those without CO_2. Comparable results were observed by Choudhary et al. (2012) using the combination of Lewis ($CrCl_3$) and Brønsted acids (HCl) in a single aqueous phase. The addition of HCl alone results in a furfural yield of 29%, while utilizing solely $CrCl_3$ led to a yield of 17%. By combining HCl and $CrCl_3$, a higher yield of 39% can be achieved under the same conditions. This can be explained by the formation of the reactive intermediate "xylulose," which dehydrates into furfural more rapidly and selectively than xylose. Nevertheless, similar furfural selectivity (~60%) was observed in both the presence and absence of CO_2. This phenomenon may be attributed to (i) the fact that the highly reactive intermediate xylulose undergoes subsequent loss reactions, and (ii) the rapidly produced furfural, which was not removed from the reaction medium, suffered from additional side reactions (i.e., condensation reactions) with xylose. This resulted in the formation of humins, a black insoluble carbonaceous compound observed in the reactor at the end of the reaction (Figure IV-3) (Lyu and Botte, 2021). Consequently, the furfural yield and selectivity were low.

Table IV-1: Effect of CO_2 pressure and flow rate on xylose conversion into furfural with the furfural extraction.

Entry	P_{CO2} (MPa)	Flow rate of CO_2 (g/min)	Amount of CO_2 used (g at 140 °C)	CO_2/Xyl ratio (g at 140 °C/g)	Xyl conv (%)	Fur yield (%)	Fur selectivity (%)	τ_{Fur} (%)
1*	-	-	-	-	83.5	47.6	57.1	-
2	5	-	4	8.8	95.0	61.0	64.2	1
3	10	-	8	19.3	94.3	63.5	67.3	2
4	10	5	1500	3750.0	97.0	59.4	61.2	99
5	10	10	3000	7500.0	96.7	53.9	55.7	100
6	20	-	18	44.7	94.9	62.5	65.9	8
7**	20	5	1500	3750.0	95.6	68.5	71.4	99
8	20	10	3000	7500.0	97.7	56.8	58.1	100

Operating conditions: initial concentration = 10 g/L of xylose and 10 wt% of formic acid; residence time = 5h; volume of the mixture = 40 mL; temperature = 140 °C.

**Repeated three times: the standard deviation of xylose conversion, furfural yield and furfural selectivity are 6.0%, 2.9% and 0.7 %, respectively.*

***Repeated three times: the standard deviation of xylose conversion, furfural yield and furfural selectivity are 0.3%, 2.9% and 3.0%, respectively.*

IV.1.1.2 Influence of CO_2 pressure

The effect of different pressures (5, 10, and 20 MPa) on the conversion of xylose to furfural in batch systems was initially investigated, considering pressure as one of the crucial parameters for furfural extraction by CO_2 (Sangarunlert et al., 2007). The results are summarized in Table IV-1 (Entries 2, 3, and 6). Under these experimental conditions, it was demonstrated that pressure had no effect on the conversion of xylose to furfural, resulting in an average furfural yield of 62% and a selectivity of 66%. Using Amberlyst-70 as a catalyst, Sato et al. (2019) observed an increase in furfural yield from 23.8% to 31.7% as CO_2 pressure increased from 5 MPa to 20 MPa. According to these authors, the enhanced furfural production was attributed to the solubility of high-pressure CO_2 into the water phase, generating carbonic acid. This in turn, accelerated the acid-catalyzed reaction in water. The disparity in results can be explained by the significantly greater catalytic activity of formic acid compared with that of Amberlyst-70 and the generated carbonic acid, thus hiding the effect of CO_2 pressure. Nonetheless, the separation efficiency increased with increasing pressure, reaching a maximum value of 8% at 20 MPa. As expected, this low value was obtained because of the low volume of the CO_2 phase in the reactor as detailed in Table IV-1. This result is consistent with a previous study (Gamse et al., 1996) where the solubilities of furfural in supercritical CO_2 at various temperatures (25–60 °C) and pressures (8–34 MPa) were measured. As stated by the authors, the solubility of furfural in CO_2 increases with pressure but decreases with temperature. It is worth noting that at the lowest studied pressure (5 MPa, Entry 2 in Table IV-1), CO_2 exists as a compressed gas; however, above the critical pressure (7.4 MPa, Entries 3 and 6, in Table IV-1), it exists as a supercritical fluid in which the solubility of organic molecules increases with pressure (Games et al., 1997).

IV.1.1.3 Influence of initial xylose concentration

The purpose of this section is to investigate the extraction capability of Sc-CO_2 in batch systems, inhibiting side reactions while providing high furfural yield and selectivity. In general, a high starting concentration of the reactant should result in a high concentration of the product. Hence, a high furfural concentration can be obtained from a high xylose concentration. The effect of the initial xylose concentration on xylose conversion into furfural was examined and the results are illustrated in Figure IV-4. Without Sc-CO_2 extraction, the furfural yield and selectivity increased from 47.6% to 53.3% and from 57.1% to 66.5%, respectively, for a similar xylose conversion as the initial xylose concentration increased from 10 g/L to 20 g/L. However,

as the xylose concentration was increased further to 30 g/L, the furfural yield and selectivity experienced a decline, reaching 44.7% and 55.2%, respectively.

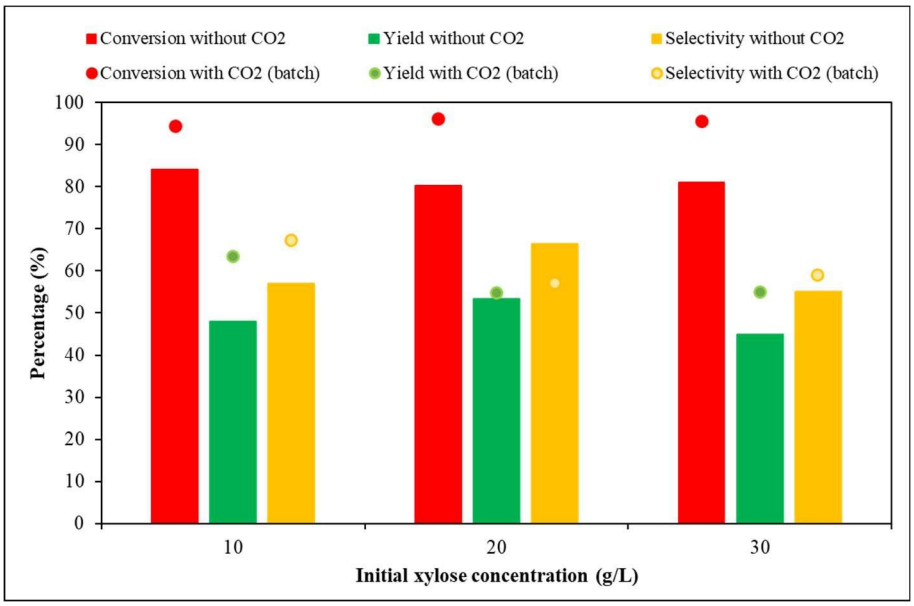

Figure IV-4: Effect of initial xylose concentration for xylose conversion into furfural and the extraction in batch system.
Op. Cond.: initial concentration = 10 wt% of formic acid; residence time = 5h; volume of the mixture = 40 mL; reaction temperature = 140 °C; CO_2 pressure = 10 MPa. The results of reaction without CO_2 extraction are presented in bars and those with CO_2 extraction are in dots. The xylose conversion (red), furfural yield (green) and furfural selectivity (yellow). The experiment realized with 30 g/L of xylose under 10 MPa of CO_2 was repeated three times: the standard deviation of xylose conversion, furfural yield and furfural selectivity are 1.3%, 1.9% and 2.5%, respectively.

This observation aligns with a reported study of Yang et al. (2012), where it was found that as the xylose concentration rose from 40 g/L to 120 g/L at 180 °C using 10 g/L of formic acid as a catalyst, furfural yield and selectivity declined from 70% to 60% and 78% to 65%, respectively. These results suggest that the high initial xylose concentration enhanced not only the dehydration of xylose to furfural but also the occurrence of side reactions, resulting in a lower furfural yield and selectivity. Indeed, the mixture at the end of the reaction became darker due to the formation of humines caused by the increase in xylose concentration. This observation confirms that, as previously stated, furfural was consumed through condensation reactions with xylose.

The experiments with Sc-CO_2 extraction demonstrate a similar tendency, with the maximum furfural yield of 63.5% and the highest selectivity of 67.3% occurring at the lowest xylose concentration (10 g/L). The system with Sc-CO_2 yielded superior results in terms of

xylose conversion, furfural yield, and selectivity compared with studies conducted without Sc-CO_2. By increasing the xylose concentration from 20 g/L to 30 g/L, the furfural yield (54%) and selectivity (57%) were maintained in the Sc-CO_2 extraction system, while these values decreased in the system without Sc-CO_2 extraction. These findings demonstrated that Sc-CO_2 extraction, even with a low amount of CO_2 present in the reactor in batch mode, can avoid secondary loss reactions in batch systems to a certain extent by extracting furfural from reaction aqueous medium.

IV.1.2 Xylose conversion with Sc-CO_2 extraction in semi-batch system

As demonstrated in the previous section, Sc-CO_2 exhibits limited influence in the batch mode of furfural synthesis. Consequently, this section aims to explore the potential of Sc-CO_2 in extracting furfural within a semi-batch system, where Sc-CO_2 is continuously supplied during the conversion of xylose to furfural.

IV.1.2.1 Influence of CO_2 flow rate

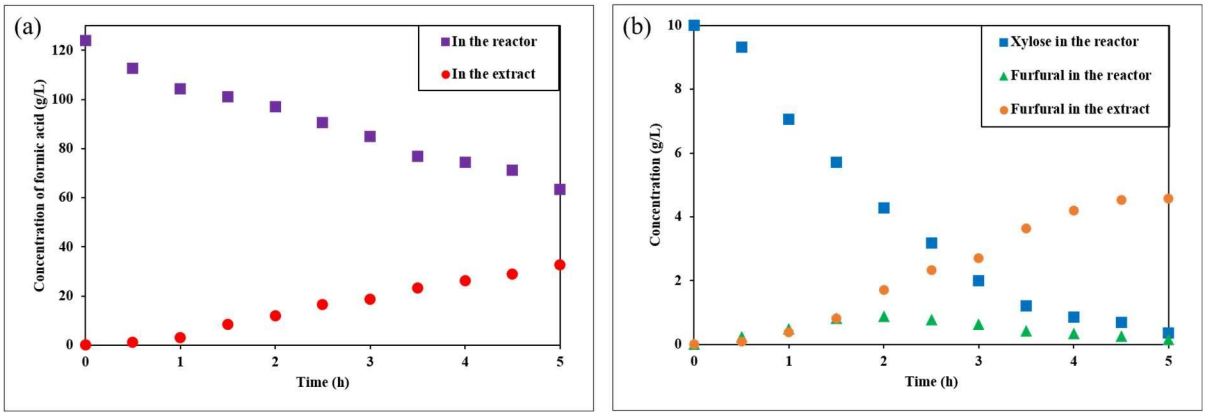

Figure IV-5: Evolution of different compound concentration during the Sc-CO_2 extraction.
(a): Formic acid concentration as a function of time.
(b): Xylose and furfural concentration as a function of time.
Op. Cond.: initial concentration = 10 g/L of xylose and 10 wt% of formic acid; residence time = 5h; volume of the mixture = 40 mL; reaction temperature = 140 °C; CO_2 pressure = 20 MPa; CO_2 flow rate = 5 g/min.

The results from the influence of CO_2 flow rate on xylose conversion into furfural and furfural extraction are presented in Table IV-1 (Entries 4-5). Surprisingly, upon increasing the CO_2 flow rate from 5 to 10 g/min, the yield and selectivity of furfural decreased and were even lower than those achieved in batch mode for similar xylose conversion when the extraction was

conducted under 10 MPa of CO_2 (Table IV-1, Entry 3). In theory, it would be expected for yield and selectivity to be enhanced by increasing the CO_2 flow rate, as more furfural from the reaction mixture could be dissolved as the amount of CO_2 increased (Sangarunlert et al., 2007). However, the unexpected outcome may be attributed to the co-extraction of formic acid by CO_2 steam, as shown in Figure IV-5a.

Additionally, we postulate that the presence of formic acid in CO_2 could reduce the solubility of furfural, thereby decreasing the capacity of CO_2 to extract furfural from the reaction medium. This explains why the influence of CO_2 flow rate observed in this work differed from other studies in which a solid catalyst was used and its quantity remained unaltered throughout the extraction (Kim and Lee, 2001; Gairola and Smirnova, 2012). Studying the phase equilibrium of the quaternary system furfural-water-acetic acid-CO_2, Games et al. (1997) has shown that the concentration of acetic acid affected the distribution behavior of furfural between water and CO_2. The distribution coefficient of furfural in the CO_2-water system increased with increasing acetic acid concentrations, reaching an optimum of 0.25 at a concentration of 5 wt% acetic acid, thereby enhancing furfural extraction. This property diminished as the acetic acid concentration continued to rise. An in-depth study of the interaction of formic acid with CO_2, water, and furfural is imperative to draw any further conclusions.

As the CO_2 flow rate increased, there was a notable rise in the loss of formic acid within the reactor. Consequently, the yield and selectivity of furfural during the semi-batch extraction at a high flow rate exhibited a decrease compared with those at a low flow rate. Surprisingly, the observed values were even lower than those attained in batch extraction, as observed in this study. A similar observation was reported by Gairola and Smirnova (2012) where they noted an increase in furfural production with an escalating CO_2 flow rate at 8 MPa without catalyst, which was technically limited to a maximum of 3.6 g/min. Higher flow rates caused the flooding of the reactor. This finding suggests that the CO_2 flow rates examined in our study might have been excessively high, potentially hindering the effective conversion of xylose to furfural and subsequent extraction. Unfortunately, the equipment used in this investigation does not allow the introduction of CO_2 at a lower flow rate than 5 g/min. In contrast to a batch system, this approach enables the recovery of all produced furfural with a portion of the formic acid as an extract, maintaining low xylose and furfural concentrations in the reactor (Figure IV-5b). Moreover, it facilitates the purification of furfural in the downstream step, enhancing the overall efficiency of the process.

IV.1.2.2 Influence of CO_2 pressure

The effect of CO_2 pressure in semi-batch mode was investigated by increasing the pressure from 10 MPa to 20 MPa while maintaining constant CO_2 flow rates (5 and 10 g/min), and the results are shown in Table IV-1 (Entries 7-8). At the same CO_2 flow rate, the furfural yield and selectivity increased when the CO_2 pressure was increased for a similar xylose conversion. The optimum conditions were observed at 20 MPa with a CO_2 flow rate of 5 g/min, yielding the highest furfural yield of 68.5%, the highest selectivity of 71.4%, and a separation efficiency of 99%. Therefore, the combination of 20 MPa with a flow rate of 5 g/min was selected as the most suitable conditions for the subsequent experiments. These values are comparable to the results of Sako et al. (1992), where the conversion of 2 wt.% xylose at 150 °C under 20 MPa, in the presence of 0.05 mol/L sulfuric acid, and simultaneous Sc-CO_2 extraction of furfural was conducted. Under these conditions, the maximum furfural yield reached 69.9%, with 85.6% of furfural being successfully recovered as an extract. It's noteworthy that without extraction, the furfural yield did not reach 40%. In another study, Gairola and Smirnova (2012) revealed that increasing the pressure from 8 to 12 MPa with a CO_2 flow rate of 3.6 g/min led to an increased furfural yield from 51% to 68%. This phenomenon can be attributed to the heightened solubility of furfural with an increase in CO_2 pressure, as discussed previously. Using the characteristic parameters of the Chrastil model (Chrastil, 1982) determined by Gamse et al. (1996), it was estimated, omitting the presence of formic acid, that the solubility of furfural in CO_2 increases from 0.07 mg of furfural/L of Sc-CO_2 to 38.18 mg of furfural/L of Sc-CO_2 when the pressure was increased from 10 MPa to 20 MPa at 140 °C.

IV.1.2.3 Influence of initial xylose concentration

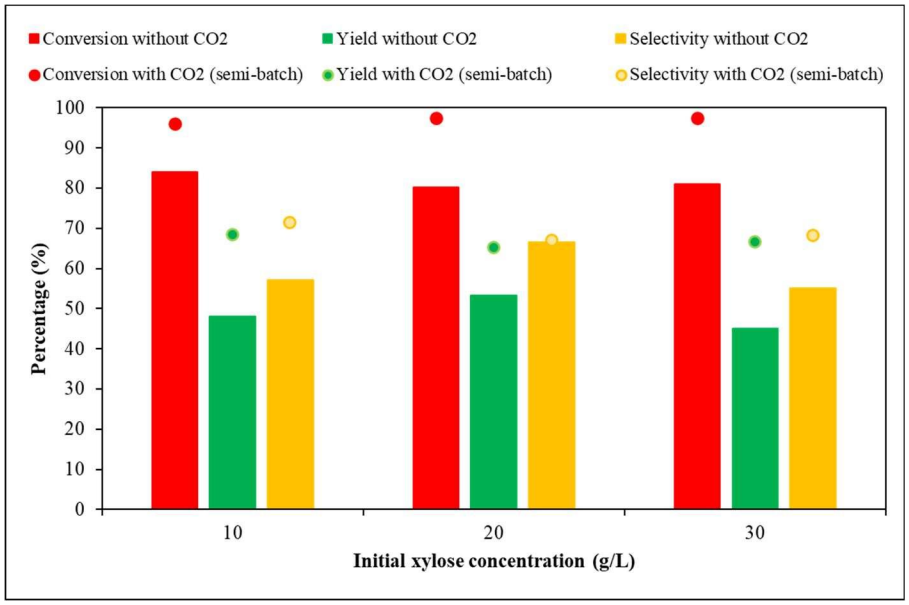

Figure IV-6: Effect of initial xylose concentration for xylose conversion into furfural and the extraction in semi-batch system in comparison with reaction without CO_2.
Op. Cond.: initial concentration = 10 wt% of formic acid; residence time = 5h; volume of the mixture = 40 mL; reaction temperature = 140 °C; CO_2 pressure = 20 MPa; CO_2 flow rate = 5 g/min. The results of reaction without CO_2 extraction are presented in bars and those with CO_2 extraction are in dots. The xylose conversion (red), furfural yield (green) and furfural selectivity (yellow).

The experiments with varying initial xylose concentrations were carried out to demonstrate the efficiency of simultaneous furfural extraction by Sc-CO_2. As depicted in Figure IV-6, it is evident that the xylose conversion, furfural yield, and selectivity achieved through simultaneous extraction (represented by dots in Figure IV-6) remained relatively stable across the three investigated concentrations. In contrast, results obtained without CO_2, especially regarding furfural yield and selectivity, declined as the xylose concentration increased. This parallels the observations made during batch extraction. In comparison with batch extraction, the utilization of CO_2 in semi-batch extraction resulted in enhanced selectivity and furfural yield, as along with improved separation efficiency and optimal purity due to the presence of formic acid. These findings demonstrate the solvent-extracting properties of Sc-CO_2, effectively inhibiting secondary degradation reactions and consequently ensuring a high yield and selectivity of furfural.

IV.1.3 Comparison of the extraction of furfural with Sc-CO_2 using various catalytic systems

This section discusses the advantages and drawbacks of combining an organic acid homogeneous catalyst (i.e., formic acid) with Sc-CO_2 extraction for furfural production. The analysis includes a comparative assessment against various catalyst types, encompassing reactions without catalysts, homogeneous catalysts, and heterogeneous catalysts. Table IV-2 summarizes furfural production reported with various catalyst types, alongside simultaneous Sc-CO_2 extraction. It is noteworthy that the separation efficiency achieved in this study (99%) surpassed that of Gairola and Smirnova (2012)'s experiment, despite a comparable furfural yield (68%). Moreover, elevated temperatures were found to catalyze secondary reactions, resulting in an overall decrease in both furfural yield and selectivity. In contrast to our findings, the need for higher temperatures to achieve a quicker reaction time in the referenced instance raises concerns about the economic viability of the process due to excessive energy consumption. To evaluate these findings within the context of sustainable development, a comprehensive energy balance must be performed. As a catalyst, formic acid emerges as a potentially preferable choice over inorganic acid catalysts, such as H_2SO_4, aligning with the objectives of green chemistry that are increasingly embraced by governments, industries, and numerous organizations worldwide. Notably, formic acid possesses lower volatility, thereby facilitating more straightforward recovery and separation processes. This characteristic, in turn, leads to a reduction in operating costs. It is important to highlight that the lower catalytic activity of formic acid necessitated a substantial quantity to attain a comparable furfural yield and separation efficiency (Kim and Lee, 2001; Gairola and Smirnova, 2012). However, this choice avoided many drawbacks of inorganic acid catalysts, such as acid corrosion and high pollution emissions. In light of these findings, the use of formic acid as a catalyst in combination with Sc-CO_2 extraction for the practical production and recovery of furfural within the homogeneous catalysts category appears highly promising. Considering the use of heterogeneous catalysts that are simple to separate and reusable, such as in Kim and Lee (2001) and Sato et al. (2019) investigations, it was observed that these catalysts gave lower furfural yields (~40%) and selectivity (~60%) despite achieving a similar xylose conversion (80–100%). This may be a result of their low catalytic activity. Additionally, drawbacks such as catalyst deactivation and reduced catalytic activity post-regeneration due to the loss of active sites were identified in the context of heterogeneous catalysts. The utilization of formic acid as a catalyst not only enhances furfural yield and selectivity but also significantly reduces reaction

time by threefold and the amount of CO_2 by more than twofold when compared with solid catalysts. This dual benefit makes the processes more cost-effective and environmentally friendly. However, as previously mentioned, the furfural recovered in CO_2 steam is impure due to the solubilization of formic acid in CO_2. The azeotropic nature of the water, formic acid, and furfural mixture poses a challenge for further purification and separation of furfural in this case. Nonetheless, a practicable method for recovering furfural from the azeotrope mixture has been disclosed (Nhien et al., 2021), specifically involving the use of two distillation columns. It was also discovered that the use of formic acid with Sc-CO_2 as an extracting agent is a prospective method for the production of furfural, as this method provides greater process productivity than biphasic solvent systems. These findings affirm the viability of utilizing Sc-CO_2 together with formic acid to optimize furfural production, representing a significant step toward a greener and more sustainable process by substituting traditional solvents and procedures.

Table IV-2: Overviews of furfural production and extraction by Sc-CO_2.

Catalyst type	Optimal operating conditions						Results				Ref
	Catalyst	*T* (°C)	*P* (MPa)	*t* (min)	Flow rate (/min)	Xyl conc (g/L)	Xyl conv (%)	Fur yield (%)	Fur selectivity (%)	τ_{Fur} (%)	
No catalyst	-	230	12	25	3.6 g	40	n.p	68	n.p	90.0	Gairola and Smirnova (2012)
Homogeneous	H_2SO_4	150	20	300	5 L	20	83.2	69.9	84.0	85.6	Sako et al. (1992)
	H_2SO_4	180	20.3	180	5 g	rice husks	n.p	90	n.p	n.p	Sangarunlert et al. (2007)
	FA	140	20	300	5 g	10	95.6	68.5	71.4	99.4	This work
	FA[a]		-		-		93.6	57.7	61.7	78.5	
Heterogeneous	Sulfated titania	180	20	-	2 NL	20	70.6	60.0	85.0	n.p	Kim and Lee (2001)
	sulfated zirconia						69.4	50.0	72.0	n.p	
	Amberlyst 70	150	20	960	3.77 g	10	87.8	52.3	59.6	n.p	Sato et al. (2019)
	MOR-type zeolites M-20						78.6	42.1	53.6	n.p	
	Amberlyst 70[b]		-		-		65.7	40.9	62.3	n.p	
	MOR-type zeolites M-20[b]		-		-		75.8	42.6	56.2	n.p	

[a]*Biphasic system; water: cyclopentyl methyl ether = 1 : 1 (v/v); V_{tot} = 70 mL.*

[b]*Biphasic system; water:toluene = 2 : 1 (v/v); V_{tot} = 60 mL*

n.p : not provided

IV.2 Furfural production from xylose using the combination of heterogeneous catalysts and formic acid.

Previously mentioned, heterogeneous catalysts present a promising solution to address the reusability challenges associated with homogeneous catalysts (Karinen et al., 2011). Additionally, they exhibit heightened catalytic activity and lower corrosiveness compared to certain homogeneous catalysts (Agirrezabal-Telleria et al., 2014). Heterogeneous catalysts can be categorized into three groups based on their acidity: pure Bronsted acid (BA) catalysts, such as polymeric solid catalysts and sulfonated biopolymer (Amberlyst-15 and Nafion); pure Lewis acid (LA) catalysts, exemplified by halide metals; and mixed BA/LA catalysts, including acid-catalysts supported on ordered mesoporous silica materials like zeolite and modernite. Furthermore, research indicates that both the mechanism and furfural production can be modified depending on the acid type employed.

Takagaki et al. (2010) conducted experiments demonstrating that using Amberlyst-15 alone resulted in a negligible furfural yield (0.5%) and poor selectivity for furfural (below 1%). When hydrotalcite was introduced, furfural production was completely absent. However, an efficient furfural production process emerged with the concurrent use of Amberlyst-15 and hydrotalcite, affording a furfural yield of 24% with a selectivity of 42%. Analytical investigations revealed that, xylulose formation occurred through xylose isomerization catalyzed by a base, hydrotalcite. This ketose was subsequently converted into furfural by the addition of a solid acid, Amberlyst-15. This reaction pathway differed significantly from that observed with an individual acid catalyst, where furfural formation involved a direct intramolecular rearrangement of the protonated pyranose as proposed by quantum mechanical calculations. This distinction in reaction pathways elucidates the variance in furfural yield between using a singular acid catalyst and employing a combination of acid and base catalysts.

In the same year, Binder et al. (2010) proposed a similar reaction pathway utilizing chromium halide as a catalyst along with bromide additives in N, N-dimethylacetamide (DMA). Their findings revealed that the addition of bromide additives, such as LiBr, significantly enhanced furfural yields up to 56%, compared to 30–40% yields achieved using solely $CrCl_2$ or $CrCl_3$ in DMA. Through deuterium-labeling experiments, Binder et al. (2010) demonstrated that chromium facilitates xylose isomerization via a 1,2-hydride shift. Functioning as a Lewis acid, chromium then converts the resulting xylulose into an oxocarbenium ion. Subsequent deprotonation of this species yields an enol, which

subsequently loses two molecules of water to yield furfural. This mechanistic pathway aligns with the findings of Choudhary et al. (2011), who explored the synergistic effect of Sn-beta (Lewis acid) with HCl (Brønsted acid) for furfural production from xylose in a single step at temperatures below 120 °C in an aqueous medium.

Subsequently, these researchers (Choudhary et al., 2012) explored the cascade of reactions for xylose conversion within a single-pot reactor, employing $CrCl_3$ as a Lewis acid to isomerize xylose into xylulose, and HCl as a Brønsted acid to dehydrate xylulose into furfural. This combined approach yielded a furfural yield of approximately 39%, compared to approximately 29% when using HCl alone, within a single aqueous phase. Moreover, employing these dual catalyst functionalities in a biphasic system (toluene/water = 1:1) at low temperatures (140 °C) and short durations (120 min), yielded a significantly higher furfural yield of 76%. By applying a first-order reaction rate expression to the initial xylulose dehydration kinetics, the apparent activation barrier of xylulose was estimated to be 23.1 kcal/mol, notably lower than that reported in the literature for xylose dehydration (~30−32 kcal/mol) (Weingarten et al., 2010). These findings suggest that in the combined presence of Lewis and Brønsted acids, furfural production predominantly follows a cascade mechanism. Initially, xylose undergoes isomerization to xylulose facilitated by the Lewis acid, followed by dehydration to furfural catalyzed by the Brønsted acid.

Lastly, this approach was further applied to furfural production from xylan. Yang et al. (2017) documented a remarkable yield of up to 87.8% utilizing $Al_2(SO_4)_3$ in a γ-valerolactone/water biphasic solvent under microwave conditions. The exceptional catalytic efficiency of $Al_2(SO_4)_3$, attributed to its combined Lewis and Brønsted acidity, along with its capability to facilitate effective phase separation, contributed significantly to achieving such a high yield.

In light of the synergistic benefits derived from the combination of Lewis and Brønsted acid catalysts in furfural production, our focus is to implement this strategy within our system, which already includes the Brønsted acid, formic acid. Consequently, various heterogeneous Lewis acid catalysts were examined for their potential in furfural production from xylose in conjunction with formic acid. The experimental results and discussions regarding these investigations are elaborated upon in this section.

IV.3.1 Impact of heterogenous catalyst on furfural production

Initially, we conducted the experiments under optimal conditions determined in a batch system, utilizing two distinct solid catalysts: Al_2O_3, renowned as a pure LA catalyst (Kim et al., 2011), and H-ZSM-5 (SiO_2/Al_2O_3 = 23), which exhibited both LA and BA acid sites. The experimental findings regarding furfural production from xylose using a combination of heterogeneous catalysts and formic acid as a catalyst, are outlined in Table IV-3. These experiments encompassed both aqueous and biphasic solvent systems, offering insights into the efficacy of the catalysts across varied conditions.

Table IV-3: Effect of heterogeneous catalyst on xylose conversion into furfural.

Entry	System	Catalyst	Xyl conc (g/L)	FA conc (wt%)	Xyl conv (%)	Fur yield (%)	Fur selectivity (%)
1	Monophasic	-	10	10	93	58	62
2		-	10	5	90	56	62
3		Al_2O_3	10	10	94	58	62
4		ZSM-5	10	10	99	43	43
5		ZSM*	10	5	96	53	55
6	Biphasic	-	10	10	92	59	65
7		Al_2O_3	10	10	93	62	67
8		ZSM-5	10	10	96	50	52

Op. Cond.: xylose/solid catalyst = 1 : 1 (w/w); residence time = 40 min; volume of the mixture = 70 mL; temperature = 170 °C.
Biphasic system: water/CPME = 1 : 3 (v/v)
** xylose/solid catalyst = 10 : 1 (w/w)*

In the aqueous monophasic system, we observed no discernible difference in furfural production between using the Al_2O_3-formic acid combination and solely employing formic acid. However, when comparing the combination of ZSM-5-formic acid to the sole use of formic acid for identical xylose conversion, we noted a decrease in furfural yield. This could be attributed to the excess acid, which potentially intensified side-loss reactions, consequently leading to diminished furfural yield. Furthermore, the active acid sites present in ZSM-5 may have a propensity to facilitate the self-polymerization reaction of furfural by providing a site for this side reaction. Evidence of this was observed in the color change of the catalyst from white to black at the end of the reaction. The black solid deposited on the surface could also obscure the active acidic sites of the catalyst, further contributing to reduced production. Additionally, we observed degradation of the solid catalyst, likely attributable to the combination of high temperature and formic acid concentration (Figure IV-7).

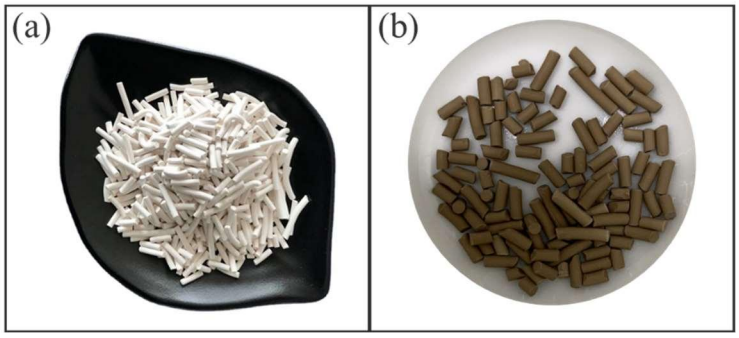

Figure IV-7: Zeolite H-ZSM-5 catalyst. (a) before and (b) after the reaction in an aqueous monophasic system at 170 °C.

Complementary experiments were conducted using a low concentration of formic acid and a reduced quantity of solid catalyst (Entries 4 and 5, Table IV-3). Interestingly, it was observed that the furfural yield (53%) obtained from the ZSM-5-formic acid system (Entry 5, Table IV-3) exceeded that (43%) obtained from the same combination with a higher catalyst quantity (Entry 4, Table IV-3). However, no significant difference was noted when compared with the experiment using solely formic acid. This observation may be attributed to the elevated concentration of formic acid, potentially masking the catalytic effect of LA in ZSM-5. Additionally, it is worth noting that this catalyst exhibited both BA and LA sites, suggesting a possible deficiency in LA sites within the combination system. Consequently, xylose was converted into furfural without undergoing isomerization into xylulose. However, further reductions in formic acid concentration or increases in ZSM-5 quantity were not performed in this study and should be explored. This decision was based on the understanding that a more substantial decrease in formic acid would not reflect conditions found in raw biomass hydrolysate, and an excessive quantity of solid catalyst would deviate from both catalyst principles and sustainable process considerations.

Following this, a biphasic solvent system utilizing CPME as the extracting solvent was implemented. This approach aimed to mitigate side reactions occurring between the produced furfural and other substances in the aqueous medium, as well as prevent catalyst deactivation by black solid particles, known as humines. The findings from this aspect of the study are detailed in Table IV-3, Entries 6-8. Compared with aqueous monophasic system, the biphasic solvent system achieved higher furfural yield especially in the combination of ZSM-5 with formic acid where the yield increased from 43 % to 50%. Moreover, the color of solid catalyst remained unchanged at the end of reaction, indicating that the biphasic solvent system can efficiently prohibit the deactivation of catalyst from humines (Figure IV-8). However, the

obtained furfural yield in biphasic solvent system was still lower than that obtained in monophasic batch system using solely formic acid.

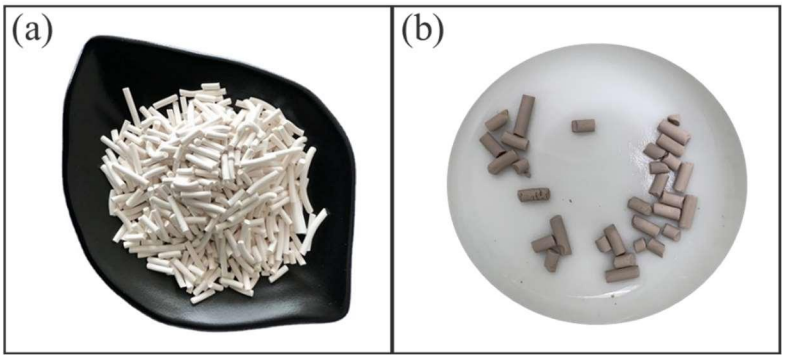

Figure IV-8: Zeolite H-ZSM-5 catalyst. (a) before and (b) after the reaction in CPME/water biphasic system at 170 °C.

Overall, it was noted that the utilization of Lewis acid heterogeneous catalysts in conjunction with formic acid did not enhance the production of furfural. Despite the introduction of simultaneous furfural extraction using organic solvents in a biphasic system, the furfural yield remained inferior when compared to the monophasic batch system utilizing only formic acid. As mentioned earlier, this can be ascribed to the interaction between high temperature and excessive acid, which may have increased side-loss reactions, resulting in a reduced furfural yield. Given the fixed amount of formic acid, future experiments will be conducted at lower temperatures in order to enhance furfural synthesis.

IV.3.2 Impact of temperature in heterogenous catalysis on furfural production

Subsequent experiments were conducted at a lower temperature to prevent degradation of the solid catalyst and moderate the rate of xylose dehydration into furfural using the combination of formic acid and solid catalysts. In this part, Al_2O_3 was excluded from the study as no enhancement in furfural production was observed. Instead, another type of zeolite, H-mordenite (with a SiO_2/Al_2O_3 ratio of 18), was employed. It is noteworthy that this catalyst exhibited a higher proportion of LA sites compared to ZSM-5, attributed to its higher percentage of Al_2O_3. The reaction temperature was set at 140 °C and the optimum reaction time was determined using the combination of ZSM-5 and formic acid as a catalyst in aqueous monophasic system. The profile of xylose conversion, furfural yield and furfural selectivity was illustrated in Figure IV-9.

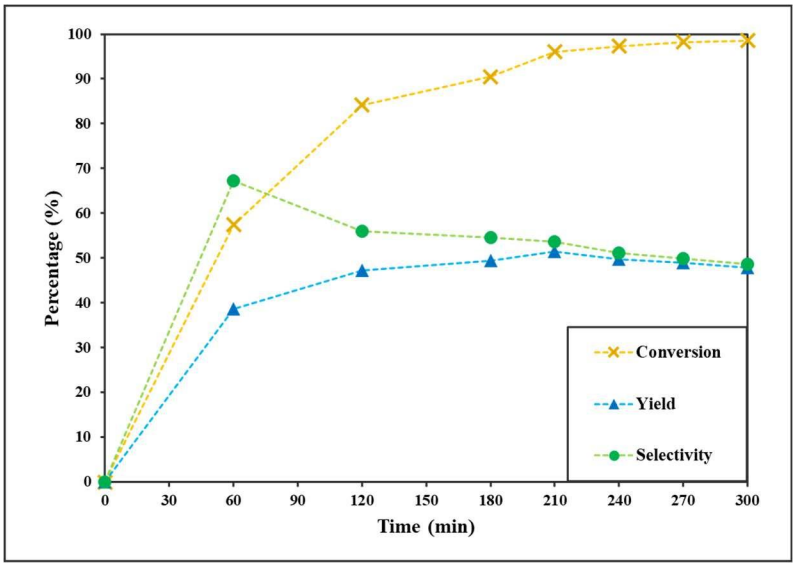

Figure IV-9: Profile of xylose conversion, furfural yield and furfural selectivity. Op. Cond.: initial concentration = 10 g/L of xylose and 10 wt% of formic acid; xylose/solid catalyst = 1 : 1 (w/w); solid catalyst = ZSM-5; residence time = 300 min; volume of the mixture = 70 mL; temperature = 140 °C.

Figure IV-9 illustrates the typical profile of xylose conversion, furfural yield, and selectivity. It depicts an increase in xylose conversion over time, accompanied by a rise in furfural yield and selectivity until reaching their peak values before gradually declining. Based on this profile, the optimum residence time was determined to be 210 min, which was consequently selected for the experiments conducted at 140°C. For further insights, detailed experimental results can be found in Table IV-4.

Table IV-4: Effect of heterogeneous catalyst on xylose conversion into furfural.

Entry	System	Catalyst	Xyl conc (g/L)	FA conc (wt%)	Xyl conv (%)	Fur yield (%)	Fur selectivity (%)
1		-	10	10	96	51	54
2		ZSM-5	10	-	33	9	28
3	Monophasic	ZSM-5	10	10	98	43	44
4		Mordenite	10	-	22	6	27
5		Mordenite	10	10	98	49	50
6		-	10	10	85	59	70
7	Biphasic	ZSM-5	10	10	98	57	58
8		Mordenite	10	10	98	61	62

Op. Cond.: xylose/solid catalyst = 1 : 1 (w/w); residence time = 210 min; volume of the mixture = 70 mL; temperature = 140 °C.
Biphasic system: water/CPME = 1 : 3 (v/v)

Table IV-4 reveals a consistent trend in the experimental results obtained at 170 °C. In the monophasic system, the combination of catalysts yielded a furfural output lower than when solely utilizing formic acid. Conversely, in the biphasic solvent system, comparable furfural yields were observed for both the combination of catalyst and sole formic acid. Furthermore, the furfural yield obtained from the biphasic solvent system slightly exceeded that obtained in the aqueous monophasic system.

Regarding catalyst types, Mordenite appeared to be more efficient than ZSM-5 in terms of catalytic activity. As previously stated, Mordenite exhibits more Lewis acid (LA) sites than ZSM-5, which likely enhances the conversion of xylose into furfural via the isomerization of xylose to xylulose. However, the furfural yield obtained using Mordenite with formic acid remained comparable to that obtained using only formic acid in both monophasic and biphasic systems. These results suggest that the proportion of LA to Brønsted acid (BA) sites could affect furfural production. An appropriate ratio between Lewis acid (LA) and Brønsted acid (BA) needs to be defined to optimize furfural production. The use of pure LA catalysts with formic acid needs further investigation to draw a definitive conclusion. As mentioned earlier, pure LA catalysts are typically halide metals, which require significantly more downstream processing for recovery compared to heterogeneous catalysts. Considering this, the use of pure LA catalysts was not investigated in our study.

Table IV-5: Comparison of furfural production using a combination of heterogeneous catalyst with formic acid at different temperatures.

Entry	System	*T* (°C)	*t* (min)	Hetero Catalyst	C_{xyl} (%)	Y_{Fur} (%)	S_{Fur} (%)
1	Monophasic	140	210	-	96	51	54
2				ZSM-5	98	43	44
3		170	40	-	93	58	62
4				ZSM-5	99	43	43
5	Biphasic	140	210	-	85	59	70
6				ZSM-5	98	57	58
7		170	40	-	92	59	65
8				ZSM-5	96	50	52

Op. Cond.: xylose concentration (10 g/L) and formic acid concentration (10 wt%), xylose/solid catalyst = 1 : 1 (w/w); volume of the mixture = 70 mL.
Biphasic system: water/CPME = 1 : 3 (v/v)

The comparison of xylose conversion into furfural catalyzed by a combination of a heterogeneous catalyst with formic acid at different temperatures is presented in Table IV-5. In the monophasic system, no improvement in furfural yield was observed when the reaction temperature was decreased from 170 °C to 140 °C using ZSM-5 with formic acid. However, in the biphasic system, the furfural yield at 140 °C was slightly higher than at 170 °C. Overall, even with a reduction in reaction temperature from 170 °C to 140 °C, the furfural yield using a combination of LA heterogeneous catalysts and formic acid in both monophasic and biphasic systems was lower compared to using only formic acid.

Despite the documented success of collaboration between BA and LA in previous literature for converting xylose into furfural, our study did not demonstrate the anticipated synergy from combining these two catalysts to enhance furfural yield. This discrepancy could be attributed to the high concentration of formic acid, which potentially conceals the LA activity of solid catalysts by directly converting xylose into furfural. The synergistic effect of LA and BA might become evident if the formic acid concentration in this study were lower. Moreover, the heterogeneous catalysts used in this study are not pure LA, so the quantity of LA sites is insufficient to optimize furfural production. However, as mentioned earlier, the study refrained from examining decreases in formic acid concentration since it falls beyond the concentration range typical of raw biomass hydrolysate. Additionally, the use of pure LA catalysts was excluded from this study due to their complex recovery process.

IV.3 Conclusion chapter

The present study reveals that Sc-CO_2, in addition to functioning as an extracting solvent, can act as a Lewis acid to enhance the dehydration of xylose to furfural. This occurs by transforming xylose into the reactive intermediate “xylulose”, which is subsequently converted into furfural by formic acid. The mechanistic process involves the dehydration of xylose by combining CO_2 addition with the presence of and formic acid, primarily following the reaction pathway illustrated in Figure 3. In contrast, the dehydration of xylose in the presence of formic acid follows a direct path, as shown at the top of Figure 3. The efficiency of Sc-CO_2 extraction was affected by the CO_2 flow rate, leading to a competition between furfural production and extraction rate. Additionally, the solubility of formic acid may reduce furfural solubility in CO_2 steam. Despite the presence of formic acid, simultaneous Sc-CO_2 extraction enables the recovery of all produced furfural in the extract and minimizes furfural degradation, maintaining a high furfural productivity even with a high initial xylose

concentration. A maximum furfural yield of 68.5% (71.4% selectivity and 99% separation efficiency) was achieved after 5 h at 140 °C and 20 MPa with a constant flow rate of 5 g/min of CO_2 and initial concentrations of 10 g/L of xylose and 10 wt% of formic acid.

Regarding the addition of both Brønsted and Lewis acid heterogeneous catalysts, it was observed that their combination with formic acid did not improve furfural production. In fact, using these heterogeneous catalysts alongside formic acid resulted in lower furfural yields compared to using formic acid alone. Additionally, decreasing the reaction temperature from 170 °C to 140 °C did not significantly impact the xylose conversion into furfural when using the combination of heterogeneous catalysts with formic acid. Specifically, in a monophasic system, the furfural yield decreased from 51% to 43% at 140 °C and from 58% to 43% at 170 °C. Furthermore, integrating a biphasic system did not lead to an improvement in furfural yield either. This outcome is likely due to the excess formic acid potentially masking the catalytic activity of the heterogeneous catalysts.

The following conditions should be chosen to produce furfural: (i) a homogeneous catalyst of the formic acid type, and (ii) a process with simultaneous extraction to prevent the degradation of furfural due to side reactions in the reaction medium. It is therefore essential to understand the reaction mechanisms in order to predict the performance of the process and subsequently propose a practical matrix process, which will be developed in the next chapter.

IV.4 References

Agirrezabal-Telleria, I., Gandarias, I., Arias, P.L., 2014. Heterogeneous acid-catalysts for the production of furan-derived compounds (furfural and hydroxymethylfurfural) from renewable carbohydrates: A review. Catal. Today 234, 42–58. https://doi.org/10.1016/j.cattod.2013.11.027

Beckman, E.J., 2004. Supercritical and near-critical CO2 in green chemical synthesis and processing. J. Supercrit. Fluids 28, 121–191. https://doi.org/10.1016/S0896-8446(03)00029-9

Binder, J.B., Blank, J.J., Cefali, A.V., Raines, R.T., 2010. Synthesis of Furfural from Xylose and Xylan. ChemSusChem 3, 1268–1272. https://doi.org/10.1002/cssc.201000181

Brunner, G., 1994. Gas extraction: an introduction to fundamentals of supercritical fluids and the application to separation processes, Topics in physical chemistry. Steinkopff Verlag ; Springer-Verlag, Darmstadt : New York.

Choudhary, V., Pinar, A.B., Sandler, S.I., Vlachos, D.G., Lobo, R.F., 2011. Xylose Isomerization to Xylulose and its Dehydration to Furfural in Aqueous Media. ACS Catal. 1, 1724–1728. https://doi.org/10.1021/cs200461t

Choudhary, V., Sandler, S.I., Vlachos, D.G., 2012. Conversion of Xylose to Furfural Using Lewis and Brønsted Acid Catalysts in Aqueous Media. ACS Catal. 2, 2022–2028. https://doi.org/10.1021/cs300265d

Chrastil, J., 1982. Solubility of solids and liquids in supercritical gases. J. Phys. Chem. 86, 3016–3021.

Curtis, R.G., Hatt, H.H., 1948. Equilibria in furfural-water systems under increased pressure and the influence of added salts upon the mutual solubilities of furfural and water. Aust. J. Sci. Res. Ser. A 213–235.

Gairola, K., Smirnova, I., 2012. Hydrothermal pentose to furfural conversion and simultaneous extraction with SC-CO2 – Kinetics and application to biomass hydrolysates. Bioresour. Technol. 123, 592–598. https://doi.org/10.1016/j.biortech.2012.07.031

Games, T., Marr, R., Fröschl, F., Siebenhofer, M., 1997. Extraction of Furfural with Carbon Dioxide. Sep. Sci. Technol. 32, 355–371. https://doi.org/10.1080/01496399708003203

Gamse, T., Marr, R., Fröschl, F., Siebenhofer, M., 1996. Solubilities and phase equilibria for the system furfural — CH3COOH — H2O and supercritical CO2, in: von Rohr, Ph.R., Trepp, Ch. (Eds.), Process Technology Proceedings, High Pressure Chemical Engineering. Elsevier, pp. 339–344. https://doi.org/10.1016/S0921-8610(96)80058-6

Karinen, R., Vilonen, K., Niemelä, M., 2011. Biorefining: Heterogeneously Catalyzed Reactions of Carbohydrates for the Production of Furfural and Hydroxymethylfurfural. ChemSusChem 4, 1002–1016. https://doi.org/10.1002/cssc.201000375

Kim, S.B., You, S.J., Kim, Y.T., Lee, S., Lee, H., Park, K., Park, E.D., 2011. Dehydration of D-xylose into furfural over H-zeolites. Korean J. Chem. Eng. 28, 710–716. https://doi.org/10.1007/s11814-010-0417-y

Kim, Y.C., Lee, H.S., 2001. Selective Synthesis of Furfural from Xylose with Supercritical Carbon Dioxide and Solid Acid Catalyst. J. Korean Soc. Atmospheric Environ. 7, 424–429.

Liu, C., Wei, L., Yin, X., Pan, X., Hu, J., Li, N., Xu, J., Jiang, J., Wang, K., 2021. Synthesis of furfural from xylan in γ-valerolactone/molten salt hydrate biphasic system. Chem. Eng. J. 425, 130608. https://doi.org/10.1016/j.cej.2021.130608

Lyu, X., Botte, G.G., 2021. Investigation of factors that inhibit furfural production using metal chloride catalysts. Chem. Eng. J. 403, 126271. https://doi.org/10.1016/j.cej.2020.126271

Magalhães da Silva, S.P., Morais, A.R.C., Bogel-Łukasik, R., 2014. The CO_2 -assisted autohydrolysis of wheat straw. Green Chem 16, 238–246. https://doi.org/10.1039/C3GC41870G

Nhien, L.C., Long, N.V.D., Lee, M., 2021. Novel Hybrid Reactive Distillation with Extraction and Distillation Processes for Furfural Production from an Actual Xylose Solution. Energies 14, 1152. https://doi.org/10.3390/en14041152

Oriez, V., Labauze, H., Benjelloun-Mlayah, B., Deleau, T., Hiraga, Y., Watanabe, M., Condoret, J.-S., Camy, S., 2023. Catalyst-free synthesis of 5-hydroxymethylfurfural from fructose by extractive reaction in supercritical CO2 – subcritical H2O two-phase system. J. Supercrit. Fluids 198, 1–10. https://doi.org/10.1016/j.supflu.2023.105904

Romo, J.E., Bollar, N.V., Zimmermann, C.J., Wettstein, S.G., 2018. Conversion of Sugars and Biomass to Furans Using Heterogeneous Catalysts in Biphasic Solvent Systems. ChemCatChem 10, 4805–4816. https://doi.org/10.1002/cctc.201800926

Sako, T., Taguchi, T., Sugeta, T., Nakazawa, N., Okubo, T., Hiaki, T., Sato, M., 1992. Kinetic Study of Furfural Formation Accompanying Supercritical Carbon Dioxide Extraction. J. Chem. Eng. Jpn. 25, 372–377. https://doi.org/10.1252/jcej.25.372

Sangarunlert, W., Piumsomboon, P., Ngamprasertsith, S., 2007. Furfural production by acid hydrolysis and supercritical carbon dioxide extraction from rice husk. Korean J. Chem. Eng. 24, 936–941. https://doi.org/10.1007/s11814-007-0101-z

Sato, O., Mimura, N., Masuda, Y., Shirai, M., Yamaguchi, A., 2019. Effect of extraction on furfural production by solid acid-catalyzed xylose dehydration in water. J. Supercrit. Fluids 144, 14–18. https://doi.org/10.1016/j.supflu.2018.10.004

Slak, J., Pomeroy, B., Kostyniuk, A., Grilc, M., Likozar, B., 2022. A review of bio-refining process intensification in catalytic conversion reactions, separations and purifications of hydroxymethylfurfural (HMF) and furfural. Chem. Eng. J. 429, 132325. https://doi.org/10.1016/j.cej.2021.132325

Takagaki, A., Ohara, M., Nishimura, S., Ebitani, K., 2010. One-pot Formation of Furfural from Xylose via Isomerization and Successive Dehydration Reactions over Heterogeneous Acid and Base Catalysts. Chem. Lett. 39, 838–840. https://doi.org/10.1246/cl.2010.838

Weingarten, R., Cho, J., Conner, Jr., Wm.C., Huber, G.W., 2010. Kinetics of furfural production by dehydration of xylose in a biphasic reactor with microwave heating. Green Chem. 12, 1423–1429. https://doi.org/10.1039/c003459b

Yang, T., Zhou, Y.-H., Zhu, S.-Z., Pan, H., Huang, Y.-B., 2017. Insight into Aluminum Sulfate-Catalyzed Xylan Conversion into Furfural in a γ-Valerolactone/Water Biphasic Solvent under Microwave Conditions. ChemSusChem 10, 4066–4079. https://doi.org/10.1002/cssc.201701290

Yang, W., Li, P., Bo, D., Chang, H., 2012. The optimization of formic acid hydrolysis of xylose in furfural production. Carbohydr. Res. 357, 53–61. https://doi.org/10.1016/j.carres.2012.05.020

Zeitsch, K.J., 2008. Verfahren zur herstellung von furfural. DE60035029T2.

Zeitsch, K.J., 2004. Process for the manufacture of furfural. US6743928B1.

V. Chapter 5

Advance process development with operational conditions optimization.

This chapter focuses on the development of the process for furfural production from raw biomass, consisting of three parts. The first part deals with preliminary studies, focusing on biomass characterization and the production of furfural from xylans. The second section examines the kinetics of furfural production from pentose using formic acid as a catalyst, and explores the practical application of this process to real biomass hydrolysates. The final section addresses complementary studies on furfural production from raw biomass hydrolysates with low formic acid concentration.

In the following part of this chapter, the experimental data on the chemical composition, the monosaccharides determined via acid hydrolysis and the inorganic elements present in the raw biomass utilized in this study are detailed. Subsequently, the experimental results concerning furfural production from xylans catalyzed by formic acid are presented. First, the different monosaccharides in xylose were quantified via acid hydrolysis. Following this, the dehydration of xylans into furfural was conducted. In the next section, the experimental findings on the kinetics of furfural production from pentose and raw biomass hydrolysates, catalyzed by formic acid, are detailed. Initially, a thorough examination of furfural degradation, a common reaction within the three investigated mechanisms in a batch system, is provided. Following this, the investigation on the kinetics of xylose decomposition and furfural formation across these three mechanisms. Notably, constant and kinetic parameters of various reactions were determined and juxtaposed with findings from other studies. Ultimately, the kinetic equations derived from the most suitable kinetic model were applied to optimize furfural yield, employing xylose, xylans, and real biomass hydrolysates as starting materials. The results presented in this section are extracted from the article entitled “Dehydration of Pentose to Furfural Catalyzed by Formic Acid – Kinetics and Application to Industrial Biomass Hydrolysates,” The *Journal of Environmental Chemical Engineering*, (2024) 113431. In the final section, the experimental results of furfural production from raw biomass hydrolysate with different formic acid concentrations are presented. The supplementary recovery of formic acid from raw biomass hydrolysate was first investigated, yielding hydrolysates with varied formic acid

concentrations. These resulting hydrolysates were then used to produce furfural via a dehydration reaction.

V.1 Preliminary studies

The preliminary studies consist of two parts: first, the characterization of raw biomass and xylans, and second, the focus on furfural production from xylans using formic acid as a catalyst.

V.1.1 Composition of raw biomass hydrolysates

This section aims to identify the chemical composition and inorganic elements present in the raw biomass utilized in this study. However, it's important to note that the characterization process was specifically undertaken for OPEFB. Due to the internal treatment of fir wood at the BioEB company, the identification of its chemical compositions was not feasible and thus is omitted from this section.

V.1.1.1 Chemical compositions

The chemical compositions of OPEFB quantified in this study are detailed in Table V-1 and are compared with values reported in the literature for comparison.

Table V-1: Chemical compositions of OPEFB

Component	Unit	Isroi et al. (2012)*	Chang (2014)*	Putri et al. (2021)*	This work**
Ash	%	-	3.5 ± 0.2	-	2.7 ± 0.5
Lignin	%	34.4 ± 0.2	22.3 ± 8.2	20.43	12.2 ± 0.3
Cellulose	%	39.1 ± 2.3	44.4 ± 20.7	49.29	57.8 ± 0.7
HemiCel	%	23.0 ± 2.8	27.1 ± 6.5	30.28	29.1 ± 1.5

**The OPEFB is untreated.*
*** The OPEFB is treated by LEEBio™ process*

The value obtained from this study aligns closely with those reported in the literature, reflecting consistency in the findings. Furthermore, it was observed that OPEFB possesses significant cellulose and hemicellulose content, which, upon hydrolysis, can be transformed into diverse chemical products through various processes like chemical processing or fermentation. For example, in this investigation, the hemicellulosic fraction underwent an acid-catalyzed dehydration reaction, yielding furanic compounds including furfural and 5-HMF.

V.1.1.2 Quantification of monosaccharides in raw biomass hydrolysates via acid hydrolysis.

To quantify the monosaccharides in hydrolysates derived from both raw biomass via the LEEBio^{TM} process, acid hydrolysis was conducted as outlined in Section II.4.1.3. Notably, the hydrolysates were utilized without additional chemicals, and the hydrolysis reaction occurred through the formic acid present in these hydrolysates. The variation in different monosaccharides in hydrolysates is illustrated in Figure V-1, while the concentrations recorded after 240 min at 120 °C, are detailed in Table V-2.

Table V-2: Biomass hydrolysate composition after hydrolysis at 120 °C for 240 min

Component	Unit	Fir wood	OPEFB
Ara	g/L	3.6 ± 0.8	2.8 ± 0.4
Galac	g/L	4.4 ± 0.8	1.6 ± 0.3
Glu	g/L	8.7 ± 0.5	0.8 ± 0.2
Mann	g/L	30.1 ± 1.2	1.5 ± 0.3
Xyl	g/L	10.8 ± 0.3	26.2 ± 3.3
FA	g/L	166.2 ± 17.4	141.1 ± 10.7
Fur	g/L	0.5 ± 0.2	2.1 ± 0.6
5-HMF	g/L	0.4 ± 0.1	n.d

n.d : non detected
Op. Cond.: volume of the mixture = 150 mL; reaction temperature = 120 °C; hydrolysis time = 360 min.

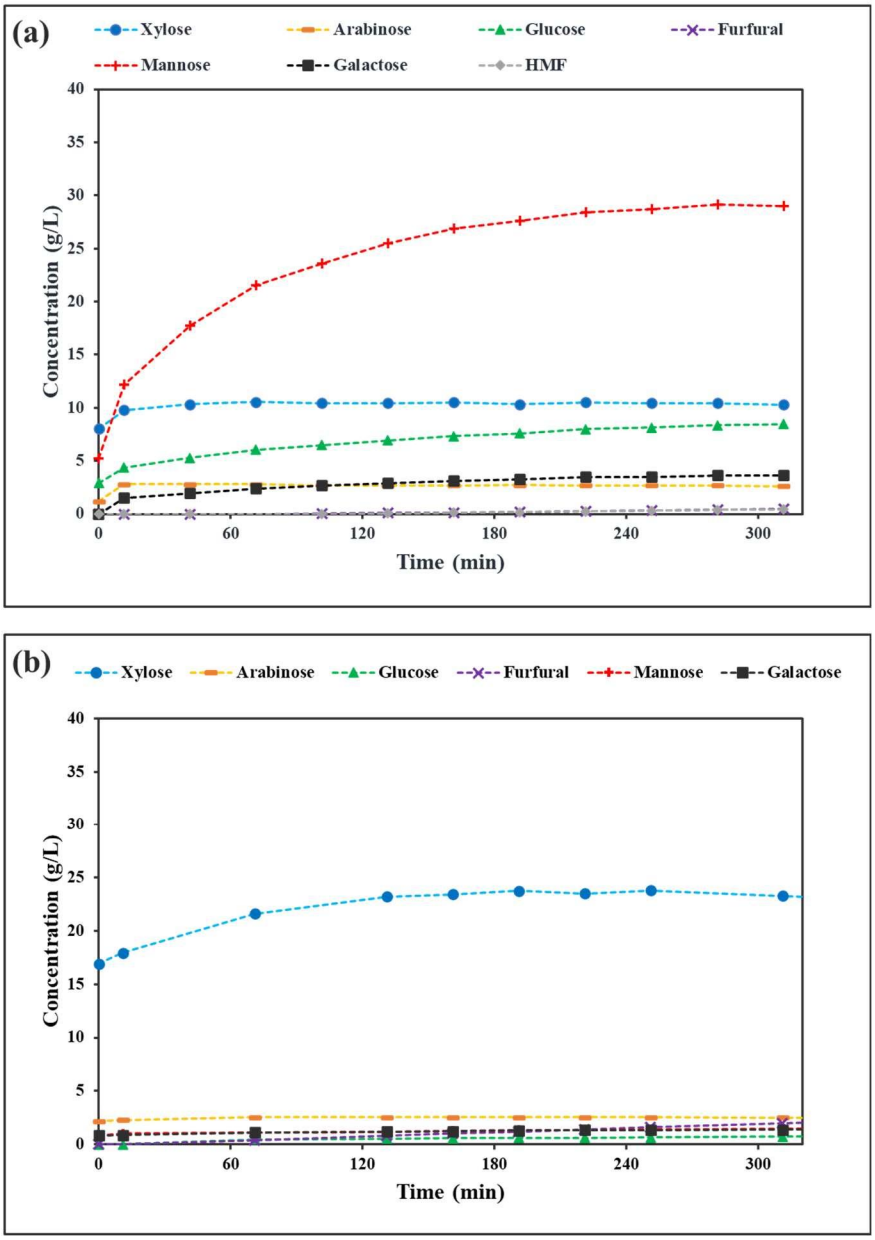

Figure V-1: The evolution of monosaccharide concentration over hydrolysis reaction. (a): hydrolysate from fir wood; (b) hydrolysate from OPEFB.
Op. Cond.: volume of the mixture = 150 mL; reaction temperature = 120 °C; hydrolysis time = 360 min.

As mentioned in the literature review, the concentration of released monosaccharides varies depending on the type of biomass. According to Table V-2, fir wood, categorized as a hardwood, exhibited a higher abundance of C_6 sugars (mannose, glucose, and galactose) compared to C_5 sugars (xylose and arabinose). Conversely, OPEFB, classified as residual biomass, contained a higher proportion of C_5 sugars than C_6 sugars. Under acidic and high-temperature conditions, C_5 sugars undergo conversion into furfural, while C_6 sugars are dehydrated into 5-HMF. Consequently, these differing proportions can impact the quality of

the end product, as discussed in chapter 3. Therefore, careful consideration of the choice of raw biomass is essential to optimize both the yield and quality of the desired end products.

V.1.1.3 Quantification inorganic elements in hydrolysates

In addition to monosaccharides, raw biomass hydrolysates may also contain inorganic elements such as Na^+, Ca^{2+}, Cl^-, among others. The presence of these elements has the potential to influence the reaction pathway of monosaccharide conversions and affect the yield of end products. As previously discussed, inorganic elements, particularly cations, can act as Lewis acids, facilitating the isomerization of monosaccharides. For example, xylose can be isomerized into xylulose, altering the reaction pathway of xylose dehydration into furfural. Furthermore, in biphasic solvent systems, these inorganic elements contribute to the salting-out effect, enhancing furfural separation and ultimately leading to a higher yield. For instance, Zhang et al. (2012) observed a substantial increase in furfural yield from 37.06% to 47.82% with the addition of NaCl to the 1-butanol/water system for furfural production catalyzed by MCM-41. According to the authors, NaCl modifies the solvent properties while remaining chemically inert, thereby improving the extraction capability of 1-butanol. The various inorganic elements and their concentrations are listed in Table V-3.

Table V-3: Different inorganic elements and their concentration in hydrolysates.

Biomass		**Fir wood**		**OPEFB**	
Elements	**Unit**	**Cutter and McGinnes (1979)**	**This study**	**Lee et al. (2020)**	**This study**
Na	ppm	44	7308	-	16,448
K	ppm	n.d	145	11,930	2343
Mg	ppm	41	56	790	214
Ca	ppm	295	256	2170	203
Fe	ppm	-	24,714	2680	46,920
Al	ppm	13	7217	1760	5024
P	ppm	-	12,773	750	9843
S	ppm	-	80,505	-	57,070
Si	ppm	-	1.3	760	1
Cl	ppm	67	30	-	450

n.d = non detected

When comparing the values obtained in this study with those reported in the literature, it becomes evident that the concentrations of nearly all inorganic elements in the hydrolysates, particularly sodium, sulfur, and iron, were significantly higher compared to literature values. This discrepancy could be attributed to the process utilized for biomass depolymerization, including the specific chemical reagents employed in the process. It's important to note that the composition of biomass can be influenced by various factors such as season-dependent supply, geographical diversity, variability, and sparse distribution, which may also contribute to the observed differences (Guo et al., 2019). Furthermore, upon comparing the two types of biomass, it was observed that the OPEFB hydrolysate contained substantially higher levels of inorganic elements than the hydrolysate derived from fir wood. This discrepancy could potentially account for the higher furfural yield observed in the OPEFB hydrolysate compared to the fir wood hydrolysate across all investigated systems.

V.1.2 Furfural production from xylan catalyzed by formic acid

As highlighted in the literature review, xylan emerges as a prominent heteropolymer within the hemicellulosic component. Its composition primarily comprises xylose as the monomeric unit, with additional traces of arabinose. Moreover, the backbone of xylan exhibits various substituents, including acetyl, arabinosyl, and glucuronysyl groups (Bajpai, 2014). In order to clarify the impact of the intricate structure of raw materials on furfural production, xylan was specifically used before conducting the furfural synthesis with raw biomass hydrolysate.

This study explores two distinct varieties of xylan: xylose sourced from Birchwood and xylan extracted from Oat spelts. The disparity between these xylans lies in the type of monomeric unit they contain. Birchwood-derived xylan consists solely of xylose, whereas xylan extracted from Oat spelts undergoes depolymerization, yielding primarily xylose alongside minor traces of arabinose and glucose.

V.1.2.1 Hydrolysis reaction of xylan

Before initiating the conversion of these xylans into furfural using formic acid as a catalyst, a hydrolysis reaction was conducted to determine the distinct monosaccharides present in each xylan. The experimental methodology for this procedure was detailed in Section II.4.1.3 and the temporal evolution of various monosaccharides within each xylan is depicted in Figure

V-2. The compositions of each xylan after hydrolysis at 120 °C for 240 min are presented in Table V-4.

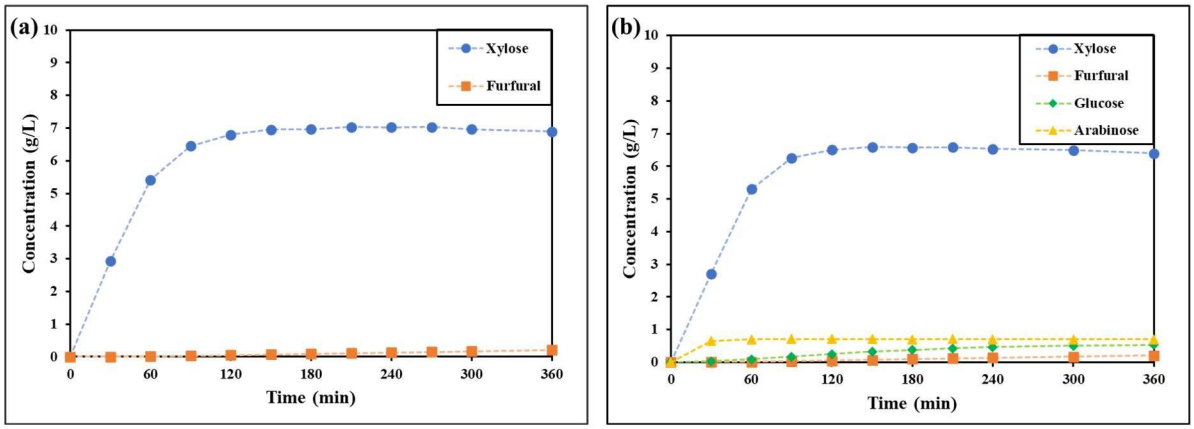

Figure V-2: Evolution of monosaccharide concentration over time. (a): xylan from Birchwood; (b): xylan from Oat Spelts
Op. Cond.: initial concentration = 10 g/L of xylan and 10 wt% of formic acid; volume of the mixture = 150 mL; temperature = 120 °C; hydrolysis time = 6h.

Table V-4: Xylans composition after hydrolysis at 120 °C for 240 min

Component	Unit	Xylan from Oat Spelts	Xylan from Birchwood
Ara	g/L	0.7	n.d
Glu	g/L	0.6	n.d
Xyl	g/L	6.6	7.0
Fur	g/L	0.3	0.1

n.d. = non detected

V.1.2.2 Dehydration of xylans into furfural catalyzed by formic acid

Table V-5: Experimental furfural yield from xylans using formic acid as a catalyst

Substance	Xyl conv (%)	Fur yield (%)	5-HMF yield (%)
Xyl	91	58	-
Xylan from Birch wood	91	68 (48)	-
Xylan from Oat Spelts*	94	60 (44)	33 (2)

The number in the bracket is the value calculated using number of moles of xylans.
**Conversion of arabinose and glucose are 89% and 67%, respectively.*
Op. Cond.: initial concentration = 10 g/L of xylose and xylans with 10 wt% of formic acid; volume of the mixture = 150 mL; temperature = 170 °C; residence time = 40 min.

Table V-5 presents the furfural yield derived from two types of xylans and pure xylose, employing formic acid as a catalyst under the optimized conditions established in the batch system. Remarkably, the results reveal that both xylans yielded higher furfural quantities compared to pure xylose, despite achieving similar levels of xylose conversion. This unexpected observation contradicts the findings commonly reported in the literature, where furfural production from xylan typically falls below that from pure xylose. For instance, Delbecq et al. (2016) achieved furfural yields of 76% from xylan and 80% from xylose, respectively, using a betaine and formic acid mixture in a CPME-water biphasic system under microwave irradiation. Similarly, Wang et al. (2017) investigated a bio-based sulfonated sporopollenin (SSP) catalyst in the presence of NaCl within a biphasic water-CPME system under microwave irradiation. They reported the highest furfural yield of 69% from xylose after 40 min at 190 °C, whereas xylan yielded furfural at a lower rate, reaching 37% after 50 min at the same temperature. The lower furfural yield observed from xylan can be attributed to a two-step mechanism. Initially, the polysaccharide backbone undergoes depolymerization into pentose monomer units before their subsequent dehydration. However, when calculating the furfural yield based on the number of moles of xylan, the furfural yield from xylan (yield in the bracket) in this case was lower than that from xylose, aligning with findings in the literature. Consequently, the interpretation of the results depends on whether xylose or xylan is used as the mole of substance for furfural production. Nonetheless, it's important to note that the furfural yield is basically dependent on the real concentration of xylose liberated during the process. From our perspective, the increased furfural yield may be attributed to the concurrent release of pentose monomers during the depolymerization process. This phenomenon, similar to the semi-batch system in which reactants are continuously added over the reaction time, appears to limit to some degree the loss reaction of cross-polymerization between xylose and the produced furfural.

When comparing the two investigated xylans, it was observed that the xylan derived from Birchwood yielded higher furfural quantities compared to the xylan sourced from Oat Spelts. This observation can be reasonably attributed to the composition of xylan from Oat Spelts, which includes glucose. Under the experimental conditions, glucose was converted into 5-HMF, rendering the mixture more complex (S. Xu et al., 2020). This complexity favored side-loss reactions, ultimately resulting in a lower furfural yield. This finding aligns with the study conducted by Agirrezabal-Telleria et al. (2012), wherein the combination of xylose and glucose resulted in reduced furfural production compared to using xylose alone. In their

research, they observed heightened secondary reactions due to interactions between the produced furfural and the increased glucose concentration when xylose and glucose were present in equal proportions (mass concentration ratio of xylose/glucose = 0.66).

When comparing the yields of furfural and 5-HMF obtained from xylan sourced from Oat Spelts, it was noted that the 5-HMF yield was lower than that of furfural. This observation is consistent with findings reported by Zhang et al. (2018), where a p-hydroxybenzenesulfonic acid-formaldehyde resin acid catalyst (MSPFR) was synthesized and utilized for furfural production from raw corn stover. Under optimized conditions (190 °C, 100 min), a higher furfural yield of 43.4% was achieved, with a 5-HMF yield of 30.7%. This difference can be attributed to the higher breakdown activation energy of hexose sugars, such as glucose, compared to pentose sugars, including xylose and arabinose. In a study by Wei et al. (2008), the degradation process of xylose and glucose using sulfuric acid as a catalyst in biomass hydrolysate was investigated. The results revealed that the activation energy required for the degradation of xylose was 114.4 kJ/mol, whereas for glucose, it was 136.8 kJ/mol. Consequently, the conversion of pentose sugars into furfural occurred at a faster rate compared to hexose sugars, resulting in a diminished production of 5-HMF (Istasse and Richel, 2020).

V.2 Kinetics of pentose dehydration into furfural catalyzed by formic acid and application to real biomass hydrolysates

The following results are presented as part of the scientific article entitled “Dehydration of Pentose to Furfural Catalyzed by Formic Acid – Kinetics and Application to Industrial Biomass Hydrolysates,” The *Journal of Environmental Chemical Engineering*, (2024) 113431.

In addition to investigating the impact of operating parameters, kinetic studies offer an alternative avenue for optimizing operational parameters in furfural production. Mechanistically, kinetic modeling offers comprehensive insights into the xylose conversion step to furfural including pathways and rate-limiting steps. Furthermore, this modeling approach facilitates the design and development of efficient processes, particularly in terms of scale-up considerations.

The purpose of this work is to develop a comprehensive kinetic model for furfural production that is universally applicable across various conditions within our range of study. Moreover, the model aims to be adaptable to more complex medium, enhancing its utility and versatility. The kinetic models utilized in this study were derived from previous research by

Lamminpää et al. (2012) and Dussan et al. (2015). Xylose was chosen as the model compound because of its prevalence in hemicellulose, the main component of lignocellulosic materials. The key parameters influencing furfural yield were assessed, such as reaction temperature ranging from 140 to 200 °C, xylose content between 0.067 and 0.2 mol/L, and formic acid concentration from 0 to 20 wt%. These amounts were representative of the hemicellulose hydrolysate generated during the breakdown of biomass in the LEEBio^{TM} process (Delmas, 2019). Three common reaction schemes were evaluated in terms of their ability to predict the effect of various operating conditions investigated on furfural yield. Finally, the kinetic models developed were used to optimize the conversion of xylans and raw biomass extracts into furfural.

V.2.1 Kinetic modeling of xylose dehydration into furfural

The kinetic modeling of xylose dehydration into furfural was split into two parts: the first part focuses on the kinetic modeling of furfural decomposition, as this reaction was represented by the three reaction mechanisms studied in this research. The second phase included modeling the decomposition of xylose and the formation of furfural. The kinetic parameters of the furfural degradation reaction remained constant and were the same as those determined in the first section.

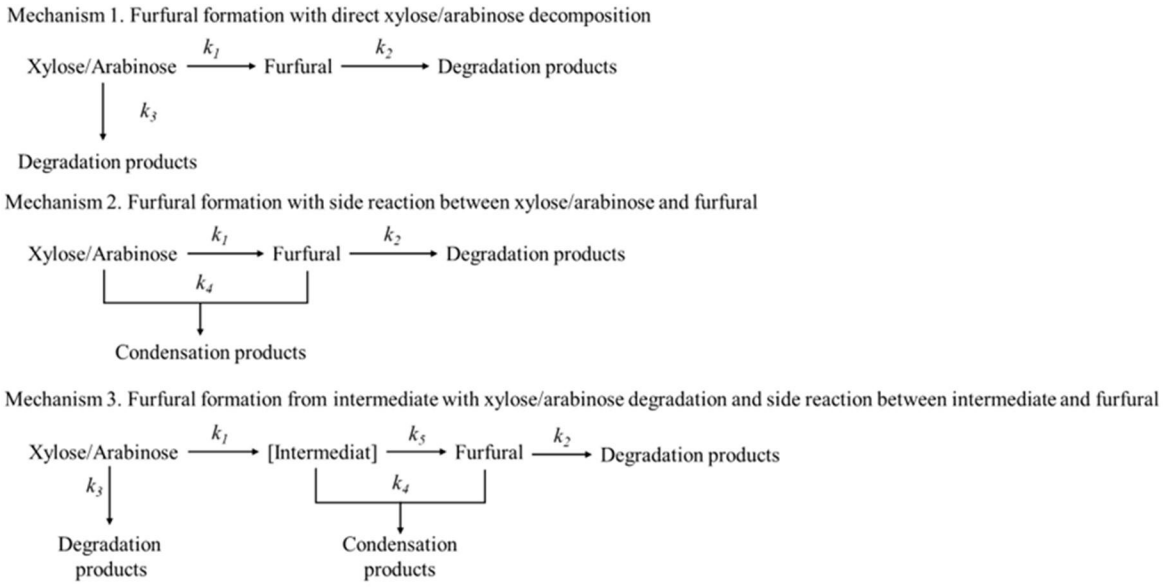

Figure V-3: Reaction mechanisms for kinetic study of acid-catalyzed dehydration of xylose/arabinose into furfural.

V.2.1.1 Kinetic modeling of furfural degradation

In addition to its formation, furfural is susceptible to be degraded through two loss reactions, particularly when exposed to high temperatures and acidic environments: (i) furfural resinification, where furfural reacts with itself to form polymeric resins; and (ii) fragmentation of furfural, where furfural breaks down into smaller molecules like formic acid (Zeitsch, 2000; Marcotullio and De Jong, 2010). Both reaction pathways are identified in this investigation as furfural degradation, denoted by k_2 in Figure V-3.

The reaction order was determined prior to estimating the rate constant of this reaction by graphing $\ln(C_{F,0}/C_F)$ against reaction time, as illustrated in Figure V-4. It is evident that the degradation of furfural follows a first-order reaction, as indicated by the linear relationship between time and $\ln(C_{F,0}/C_F)$. This result was consistent with the findings of Lamminpää et al. (2014), who examined the furfural degradation at temperatures varying from 160 to 200 °C using formic acid (2–30 wt%) as a catalyst. At high acid concentrations (30 wt%), the order of this reaction was greater than one; at low acid concentrations (2 wt%), it was less than one; and at acid concentrations ranging from 2 to 30 wt%, it was equal to one.

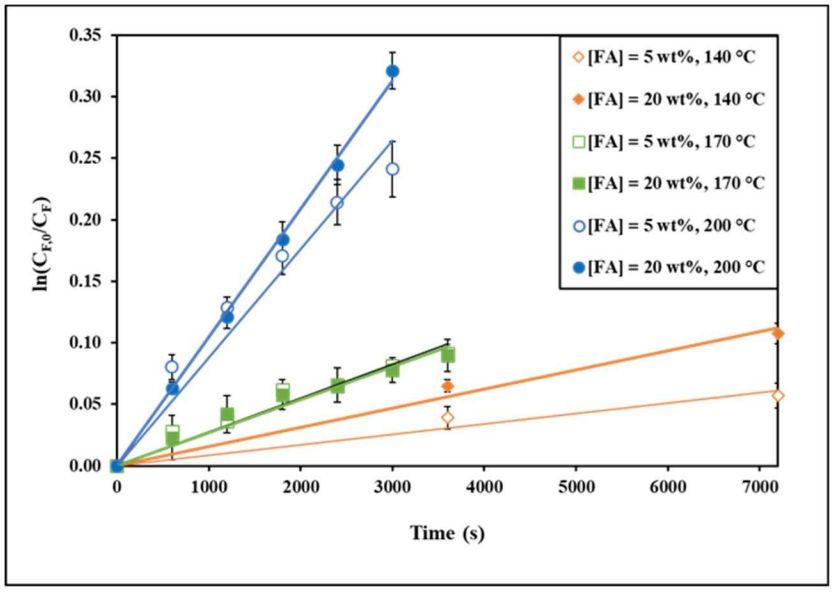

Figure V-4: Furfural concentration with time as $\ln(C_{F,0}/C_F)$ versus time.

Furthermore, as illustrated in Figure V-4, this reaction exhibited a dependence on acid concentration and temperature. The acid concentration had a more pronounced impact on the rate of the reaction as the temperature increased, a finding that was similarly reported by Lamminpää et al. (2012). Thus, the rate constant equation needed separate activation energies

for the acid-catalyzed and uncatalyzed parts. The rate constant equation (k_2) for this reaction was rewritten as shown in Eq. 14.

$$k_2 = k_{0,2}\, e^{-E0/R * (1/T - 1/T\text{mean})} + k_{H,2} C_H e^{-EH/R * (1/T - 1/T\text{mean})} \quad (14)$$

Table V-6: Determined kinetic parameters for furfural degradation reaction.

Reaction	k_0 (1/s)	k_H (L/mol/s)	E_0 (kJ/mol)	E_H (kJ/mol)	Fit to experimental data R^2
Fur degradation	$2.90 \times 10^{-5} \pm 3.17 \times 10^{-6}$	$2.72 \times 10^{-4} \pm 1.96 \times 10^{-4}$	65.17 ± 4.62	129.50 ± 0.0	0.9968

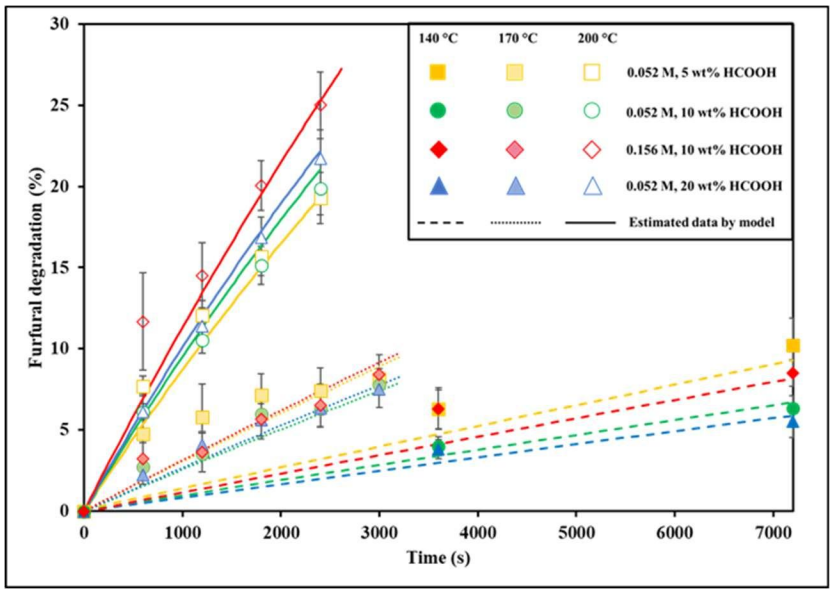

Figure V-5: Conversion profiles of furfural degradation.

The estimation of the rate constants and kinetic parameters for furfural degradation was performed utilizing the analytical solution of Eq. 14 and are given in Table V-6. The R^2 value of 99.68% indicates that the model accurately fit the experimental data. This accuracy was validated through the examination of Figure V-5, which illustrated the experimental and estimated conversion profiles of furfural at varying temperatures (140–200 °C), concentrations of formic acid (5–20 wt%), and initial concentrations of furfural (0.052–0.156 mol/L). Figure V-5 illustrates that the degradation of furfural exhibited a range of 0.2% to 28% under our conditions. Furthermore, it was observed that the degradation of furfural was highly influenced by temperature but not significantly affected by the concentration of formic acid or the initial

concentration of furfural, as reported in earlier research (Lamminpää et al., 2012; Köchermann et al., 2018).

The activation energies determined in this study closely align with those reported in literature utilizing formic acid as a catalyst. Moreover, these energies notably exceed those observed in other studies employing different acid types, with variances of up to threefold, as demonstrated in Table V-7. In comparison to studies using formic acid as a catalyst, Lamminpää et al. (2014) and Dussan et al. (2015) observed lower activation energy values of 81.7 kJ/mol and 110.3 kJ/mol, respectively. The discrepancy may be due to the temperature range studied, as it greatly influenced the breakdown of furfural and the incorporation of the initial furfural concentration's impact in the calculation. However, our calculated activation energy for the acid term (E_H = 129.5 kJ/mol) closely aligned with the values reported in studies by Lamminpää et al. (2012) (135 kJ/mol) and Marcotullio and De Jong (2010) (125.1 kJ/mol) that used formic acid and sulfuric acid, respectively, as a catalyst. Similarly, our calculated activation energy for the uncatalyzed term (E_0 = 65.2 kJ/mol) closely aligned with the values reported in experiments conducted by Jing and Lü (2007) (58.8 kJ/mol). The variation in reported activation energies may be due to factors such as catalyst type, concentration, operational parameters (i.e., T, t), as well as variances in modeling approaches.

V.2.1.2 Kinetic modeling of xylose decomposition and furfural formation

Apart from the furfural degradation reaction, the xylose decomposition and furfural production reactions were also examined for the purpose of validating the kinetic models and comparing the results with values found in the literature. As mentioned earlier, xylose was selected as the model compound representative of all pentoses in hemicellulose. It is noteworthy that the kinetic data for the conversion of arabinose to furfural was found to be comparable to the values obtained for xylose, as reported in studies by Jing and Lü (2007) and Gairola and Smirnova (2012). The solutions of xylose and formic acid utilized in this section were presented in Table II-15 in Chapter 2. Theirs concentration ranges were selected to replicate the concentrations found in the hydrolysate of biomasses obtained by LEEBio^{TM} process.

In order to determine the rate constants and kinetic parameters, Eqs. 17-22 were employed, utilizing the parameter values acquired from the preceding part (Section V.2.1.1) on furfural degradation. The rate constants and corresponding kinetic parameters for each reaction

model are provided in Table V-8. Figure V-6 displays the parity plots of xylose and furfural concentration, together with the coefficient of determination (R^2) for each model.

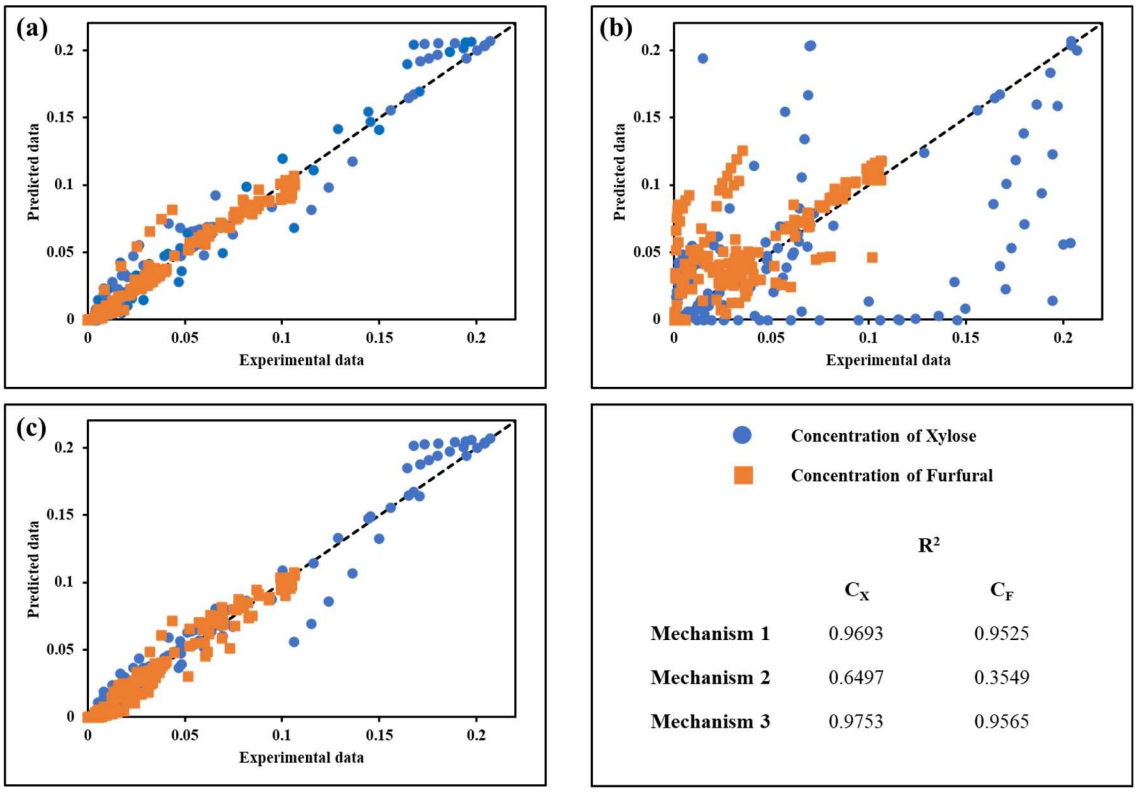

Figure V-6: Parity plot of xylose and furfural concentrations. (a): model 1, (b): model 2 and (c): model 3

Table V-7: Overview of activation energies (E_2) for furfural decomposition.

C_F (mol/L)	T (°C)	Catalyst (mol/L)	Solvent	Reactor	E (kJ/mol)	Ref.
0.01-0.02	150-210	0.1 (H_2SO_4)/0.05 (HCl)	H_2O	Sealed tubes	83.7	Williams and Dunlop (1948)
0.048	160-240	0.05-0.8 (H_2SO_4)	H_2O	Sealed tubes	92.4	Root (1956)
0.06-0.073	150-200	0.036-0.145 (H_2SO_4)	H_2O	PFR	125.1	Marcotullio and De Jong (2010)
0.1	160-200	0.025 (H_2SO_4)	H_2O	DSTR	44.2	Köchermann et al. (2018)
0.034	180-220	none	H_2O	DSTR	58.8	Jing and Lü (2007)
0.1	150-170	0.1 (HCl)	H_2O	DSTR	48.1	Rose et al. (2000)
0.156	140-160	0.1 (HCl)	H_2O	DSTR (microwave)	67.6	Weingarten et al. (2010)
0.05	160-200	0.05 (HCl)/ 0.5 NaCl	H_2O	DSTR	102.1	Danon et al. (2013)
0.051	160-200	1.86-7.95 (HCOOH)	H_2O	Sealed tubes	135	Lamminpää et al. (2012)
0.05-0.16	160-200	1.86-7.95 (HCOOH)	H_2O	Sealed tubes	110.3	Lamminpää et al. (2014)
0.1	130-170	7.81-16.46 (HCOOH)	H_2O	Sealed tubes	81.7	Dussan et al. (2015)
0.21	170-210	0.71 (CH_3COOH)	H_2O	DSTR	63.4	Chen et al. (2015)
0.052-0.156	140-200	none	H_2O	DSTR	65.17 ± 4.62	This work
0.052-0.156	140-200	1.32-5.3 (HCOOH)	H_2O	DSTR	129.5 ± 0.002	This work

DSTR: discontinuous stirred-tank reactor.

PFR: plug flow reactor.

Table V-8: Determined kinetic parameters for xylose decomposition and furfural formation reactions.

Mechanism	Reaction	k_0 (1/s)	k_H (L/mol/s)	E_a(kJ/mol)
Mechanism 1	1	$1.00 \times 10^{-5} \pm 3.88 \times 10^{-10}$	0.11 ± 0.005	174.43 ± 2.55
	3	$1.00 \times 10^{-5} \pm 2.43 \times 10^{-10}$	0.07 ± 0.004	190.00 ± 0.001
Mechanism 2	Reaction	k_0 (1/s))	k_H ($L/mol^1/s^1$)	E_a(kJ/mol)
	1	$7.17 \times 10^{-4} \pm 4.87 \times 10^{-5}$	0.04 ± 0.004	159.11 ± 1.65
	Reaction	k_0 (1/s))	k_H ($L^2/mol^2/s^1$)	E_a(kJ/mol)
	4	$3.25 \times 10^{-3} \pm 1.33 \times 10^{-4}$	$1.00 \times 10^{-4} \pm 7.01 \times 10^{-6}$	132.78 ± 2.32
Mechanism 3	Reaction	k_0 (1/s))	k_H ($L/mol^1/s^1$)	E_a(kJ/mol)
	1	$2.20 \times 10^{-5} \pm 4.80 \times 10^{-6}$	0.10 ± 0.003	156.04 ± 0.91
	3	$5.33 \times 10^{-6} \pm 3.00 \times 10^{-6}$	0.05 ± 0.003	180.06 ± 5.83
	5	$1.91 \times 10^{-4} \pm 6.25 \times 10^{-5}$	0.36 ± 0.01	170.37 ± 0.72
	Reaction	k_0 (1/s))	k_H ($L^2/mol^2/s^1$)	E_a(kJ/mol)
	4	$8.88 \times 10^{-4} \pm 4.85 \times 10^{-4}$	0.53 ± 0.04	200.80 ± 0.85

Regarding the parity plots of xylose and furfural concentration for the three study models, as well as the R^2 values, models 1 and 3 demonstrated accurate predictions for both xylose and furfural concentration. However, model 2 demonstrated the least precise predictions, exhibiting a higher degree of variability. This finding was consistent with earlier research, notably Lamminpää et al. (2012) and Dussan et al. (2015), which also used formic acid as a catalyst. Specifically, the model predicted a lower concentration of xylose compared to the experimental data when furfural was initially present in the reaction. This discrepancy implies substantial consumption of xylose through the condensation reaction with furfural. Previous studies have established that the conversion of xylose remains unaffected by the presence or concentration of furfural. This discovery clarified the reason why model 2 yielded less precise predictions. This supported to the hypothesis that furfural exclusively reacted with intermediates derived from xylose, resulting in the formation of the condensation product characterized by a kinetic constant k_4 in mechanism 3, which was significantly higher than that in mechanism 2.

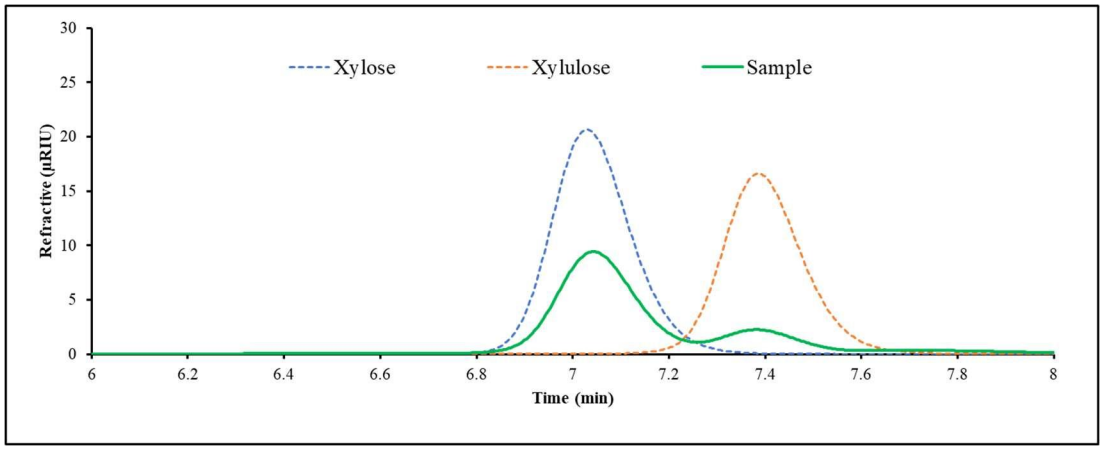

Figure V-7: HPLC chromatograms of the Bio-Rad Aminex HPX-87H column with a refractive index detector: standard of xylose (blue date), standard of xylulose (orange date) and sample at 10 min (green line).
Op. Cond. of sample: initial concentration = 0.067 mol/L of xylose and 10 wt% of formic acid; residence time = 10 min; temperature = 170 °C.

Upon detailed examination of parity curves and R^2 values between model 1 and 3, model 3 was found more accurately depicted the profile of xylose concentration compared to model 1. Concerning the progression of furfural concentration, both models 1 and 3 appeared to be in good agreement. It is important to highlight that mechanism 3 diverges from mechanism 1 in that it incorporated the intermediate compound, namely xylulose, and its subsequent decomposition. The formation of xylulose, a ketopentose, necessitates either functional group rearrangement or a configuration change around the carbon atom linked to the hydroxyl group of the xylose molecule, facilitated by Lewis acid or base (Ershova et al., 2015). In addition, Aida et al. (2010) stated that this intermediate can be generated through the conversion of xylose in water under elevated temperatures (350 and 400 °C) and pressures (40–100 MPa). This intermediate subsequently undergo rapid dehydration to furfural through Brønsted acid catalysis. By studying the xylulose dehydration kinetics catalyzed by HCl, Choudhary et al. (2012) reported that the furfural production from xylulose was faster than that from xylose. This is because the activation barrier for xylulose dehydration is lower (23.1 kcal/mol) than that of xylose (30-32 kcal/mol). Ershova et al. (2015) confirmed the same finding, illustrating that the process of furfural production from xylulose was almost six times quicker compared to that from xylose. This study highlighted this point through HPLC chromatogram analysis of the samples obtained throughout the reaction, as depicted in Figure V-7. The chromatogram confirmed the presence of xylulose, thereby validating the use of model 3 in this investigation. Based on this analysis, Mechanism 3 is therefore the best suitable model for describing the xylose dehydration reaction into furfural in a solution of formic acid under our investigated

conditions. This model will also be used to optimize furfural production from raw biomass in the Section V.2.2.

Table V-9 displays a comparison of the activation energies with the information found in the literature. It was found that the activation energies were consistent globally across all three models examined. Nevertheless, the values observed in this study were greater than those reported in previous research. Based on model 1, Lamminpää et al. (2012) reported an activation energy of 152.0 kJ/mol for E_1 and 161.0 kJ/mol for E_3, which were lower than our estimates of 174.4 kJ/mol for E_1 and 190.0 kJ/mol for E_3. Dussan et al. (2015), who conducted the experiment with formic acid as a catalyst, has calculated the values of 136.0 kJ/mol and 140.3 kJ/mol for E_1 and E_3, respectively. Other research groups have reported activation energies that were even lower than ours. The difference can be reasonably attributed to the variation in the range of operating parameters studied in each research and/or the specific catalyst (nature and concentration) and/or reactor types used.

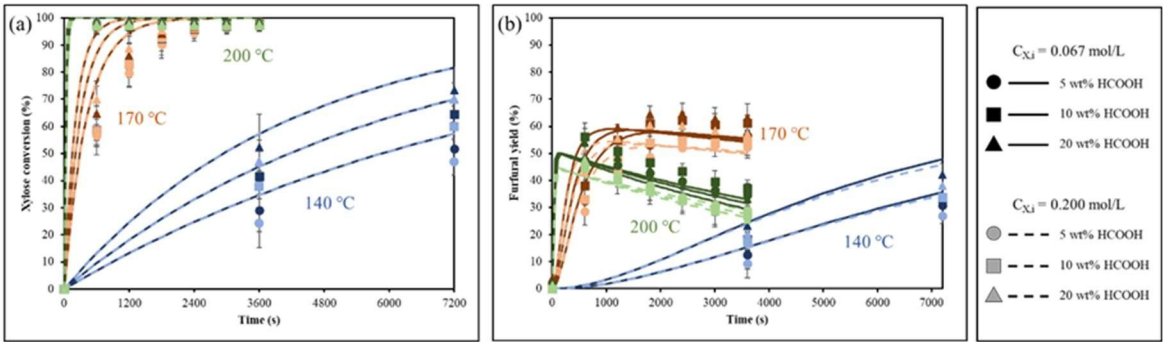

Figure V-8: Xylose conversion (a) and furfural yield (b) of the experimental and kinetic modeled data obtained from Model 3.

Upon comparing the kinetic parameters of various reactions, it was found that the kinetic constant of xylose decomposition (k_3) in accordance with model 1, and that of side reactions (k_4) in accordance with model 3, specifically the condensation reaction involving xylose or xylulose and furfural, were higher than the kinetic constant of the furfural formation reaction (k_1). This observation suggested that the rate at which the side reaction occurred was far faster than the rate at which furfural was formed. This provides a clear explanation for why a high yield of furfural is never achieved in a batch system. Figure V-8 illustrates xylose conversion (Figure V-8a) as well as furfural yield (Figure V-8b) versus reaction time. Analysis reveals that both reaction temperature and initial xylose concentration are key factors influencing furfural yield, whereas the concentration of formic acid appears to have minimal

impact, especially at high temperatures. Remarkably, furfural yield decreases notably at extremely high and low reaction temperatures despite identical reaction times, xylose and acid concentrations. Additionally, increasing the initial concentration of xylose results in a decrease in furfural yields across all tested temperatures. This phenomenon can be attributed to the accelerated reaction rate of furfural degradation, particularly the condensation reaction, under conditions of elevated temperature and xylose concentration. These observations align with the previously discussed high kinetic constants associated with the condensation reaction. According to the results of our investigation, the maximum furfural yield of 63% was obtained. In contrast, Dussan et al. (2015) reported a furfural yield ranging from 50% to 55% at a temperature of 190 °C. Köchermann et al. (2018) found that using H_2SO_4 as a catalyst resulted in a maximum furfural yield of 53.7%. In a separate study, Marcotullio and De Jong (2010) observed a maximum yield of 61.4% at a temperature of 200 °C.

In overall, our investigations have determined that the obtained results are consistent with the values reported in earlier studies. Different simulation methodologies and constant rate expressions can potentially yield distinct results. Moreover, the variations might also be ascribed to the examined ranges of operating conditions (i.e., temperature and reaction time), as previously stated

Table V-9: Overview of activation energies for xylose dehydration to furfural and side products.

Initial concentration (mol/L)			*T* (°C)	Solvent	Reactor	Activation energy: *E* (kJ/mol)				Ref.
Xyl	Fur	Catalyst				E_1	E_3	E_4	E_5	
0.072	0.034	none	180-220	H_2O	DSTR	111.5[a]	143.1[a]	/	/	Jing and Lü (2007)
0.002-0.25	0.156	0.1 (HCl)	130-170	H_2O	DSTR	123.9[b]	/	72.5[b]	/	Weingarten et al. (2010)
0.37	0.1	0.025 (H_2SO_4)	160-200	H_2O	DSTR	116.5[a]	61.4[a]	/	/	Köchermann et al. (2018)
0.37	0.1	0.025 (H_2SO_4)	160-200	H_2O	DSTR	94.8[b]	/	-12.7[b]	/	Köchermann et al. (2018)
0.067-0.2	0.05-0.16	1.86-7.95 (HCOOH)	130-200	H_2O	Sealed tubes	152.0[a]	161.0[a]	/	/	Lamminpää et al. (2012)
0.067-0.2	0.05-0.16	1.86-7.95 (HCOOH)	130-200	H_2O	Sealed tubes	155.0[c]	147.0[c]	235.0[c]	142.0[c]	Lamminpää et al. (2012)
0.1	0.1	2.65-16.96 (HCOOH)	130-170	H_2O	Sealed tubes	136.0[a]	140.3[a]	/	/	Dussan et al. (2015)
0.067-0.2	0.052-0.156	1.32-5.3 (HCOOH)	140-200	H_2O	DSTR	174.4[a]	190.0[a]	-	-	This work
0.067-0.2	0.052-0.156	1.32-5.3 (HCOOH)	140-200	H_2O	DSTR	159.1[b]	-	132.8[b]	-	This work
0.067-0.2	0.052-0.156	1.32-5.3 (HCOOH)	140-200	H_2O	DSTR	156.0[c]	180.1[c]	200.8[c]	170.4[c]	This work

[a]Based on model 1. [b]Based on model 2. [c]Based on model 3.

V.2.2 Application of kinetic model to furfural production

The aim of this section is to maximize furfural yield by applying the kinetic equations of the model 3. The selection of model 3 was based on its better ability to accurately represent the concentrations of xylose and furfural, as well as the furfural yield, compared to the other models investigated, as demonstrated in the previous section. The confirmation of the furfural yield was achieved through experimentation using xylose and xylan (the polysaccharide of xylose) as initial substances, followed by the optimization of the operational parameters. The method was subsequently applied to the transformation of hydrolysates derived from native biomass into furfural.

V.2.2.1 Optimal operating conditions

Table V-10: The range and step for each operating parameter used for the optimization in Matlab.

Parameter	Setting value		Step
	Min	Max	
T (K)	413	473	1
FA concentration (mol/L)	0.1	5.3	0.5
t (s)	0	∞	10

The important variables for xylose conversion and furfural production were determined to be temperature, reaction time, and formic acid concentration. In order to optimize these parameters, the kinetic equations of model 3 were implemented in a MATLAB software. The numerical optimization was performed using the *fminsearch* function. Table V-10 provides the specific range and step values for each operating parameter that were altered during the optimization process.

Figure V-9 depicts the correlation between temperature and concentration of formic acid for model 3. The high furfural yield (yellow area) is achievable at a moderate temperature (413–450 K) and a high formic acid concentration (> 15 wt%), as shown in this figure. Conversely, increased temperatures and reduced formic acid concentrations led to a diminished furfural yield. The observed phenomenon can be explained by the fact that high temperatures promote side reactions and the breakdown of furfural and xylose. The optimal conditions and highest furfural yield were determined by positioning in the yellow area of Figure V-9, as detailed in Table V-11.

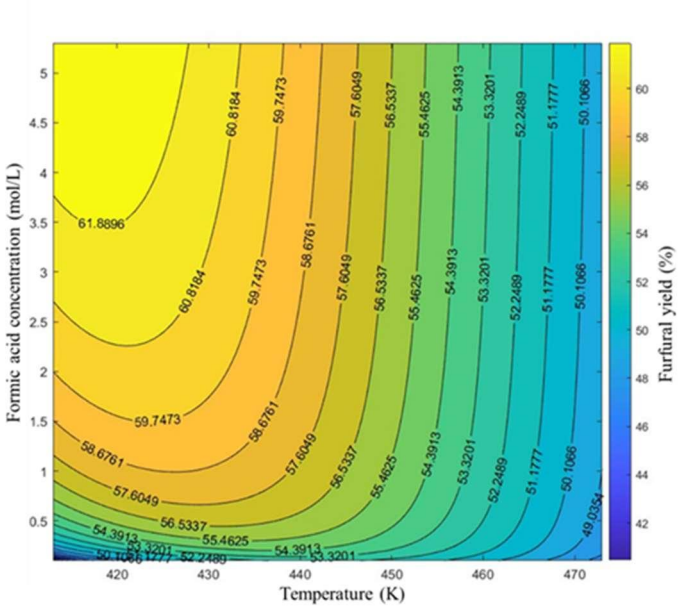

Figure V-9: Effect of temperature and formic acid concentration on furfural yield provided from model 3.

Table V-11: Optimum conditions and the corresponding furfural yield as well as the experimental furfural yield.

Case	Concentration (mol/L)		Optimum conditions by Model 3				
	C_5	C_6	T (K)	$C_{H,0}$ (mol/L)	t (s)	Fur yield (%)	5-HMF yield (%)
Model using Xyl	0.067	-	416	5.3	12720	63	-
Xyl*	0.067	-				58 ± 2	-
Xylan from Birchwood	0.047	-				63	-
Xylan from Oat Spelts	0.049	0.003				51	16

**The experiment was repeated three times.*

V.2.2.2 Furfural production from xylose and xylan

To confirm the optimum furfural yield determined by the optimization process for a xylose concentration of 0.067 mol/L, the experiments were conducted under optimum conditions (T = 416 K, $C_{H,0}$ = 5.3 mol/L, t = 12720 s and C_5 = 0.067 mol/L), and the results are presented in Table V-11. The experimental furfural yields closely approximated the anticipated value, with a relative deviation of less than 10%. The results clearly supported the previous

section's conclusion that our kinetic equations can reliably forecast the conversion of xylose into furfural, catalyzed by formic acid.

Upon comparing our furfural production to that of other investigations employing formic acid as a catalyst in batch systems, it was observed that the utilization of synthetic solutions led to a prolonged reaction time (212 min) and a lower furfural yield of 58%. As an illustration, the highest furfural concentration of 65.4% was attained by Lamminpää and Tanskanen (2009) using 30 wt% formic acid at 200 °C for 20 min. Similarly, Lopes et al. (2017) documented a furfural yield peak of 68% when a 0.4 M solution of $AlCl_3$ and 55 wt% formic acid was combined at 130 °C for 30 min. However, our methodology operated at a reduced temperature and lower formic acid concentration, potentially leading to a notable decrease in operational costs and mitigating the hazards associated with high formic acid concentrations utilized in prior investigations (Lamminpää and Tanskanen, 2009; Lopes et al., 2017) . Moreover, unlike the process described by Lopes et al. (2017), our study does not necessitate the separation or recovery of mineral salts since only formic acid was utilized without additional reactants. Consequently, this approach reduces expenses linked to post-treatment in downstream processing of the salt-saturated aqueous phase.

Prior to utilizing raw biomass hydrolysate, these conditions were also employed on two variants of xylan, a polysaccharide composed of xylose to clarify the impact of the intricate structure of raw materials on furfural production. The purpose of using two different xylan types—one composed solely of C_5 sugars (xylan from birchwood) and the other containing C_6 sugar (xylan from oat spelts)—is to examine the influence of C_6 sugars on furfural production. When comparing xylan to xylose, it was seen that xylan derived from Birchwood (63%) produced furfural at a similar level as xylose (58%) and the predicted value (63%). In contrast, xylan from Oat Spelts (51%) produced furfural with a significantly lower yield than both xylose and xylan from Birchwood, and even further from the predicted value. The results were consistent with the findings of Delbecq et al. (2016), who investigated the conversion of xylose and xylan into furfural through dehydration using betaine-formic acid as a catalyst in a water-CPME biphasic system. Under identical conditions, xylose produced the highest furfural yield of 80%, whereas Birchwood xylan only yielded 58%. In a study conducted by Zhang et al. (2014), comparable findings were reported when examining the synthesis of furfural from xylose and xylan derived from Birchwood in a deep eutectic solvent consisting of ChCl-oxalic acid. The use of xylan from Birchwood resulted in a reduced furfural yield of 34.9% compared to the 39.1% yield achieved with xylose. This can be reasonably explained by the high

concentration of pentose and hexose monomers that are released when the polysaccharide backbone in xylan is broken down, as further detailed in the following paragraph.

Table V-12: Xylans and biomass hydrolysate composition after hydrolysis at 120 °C for 240 min

Component	Unit	Xylan from Oat Spelts*	Xylan from Birchwood*	Fir wood	OPEFB
Ara	g/L	0.7	n.d	3.6 ± 0.8	2.8 ± 0.4
Galac	g/L	n.d	n.d	4.4 ± 0.8	1.6 ± 0.3
Glu	g/L	0.6	n.d	8.7 ± 0.5	0.8 ± 0.2
Mann	g/L	n.d	n.d	30.1 ± 1.2	1.5 ± 0.3
Xyl	g/L	6.6	7.0	10.8 ± 0.3	26.2 ± 3.3
FA	g/L	n.d	n.d	166.2 ± 17.4	141.1 ± 10.7
Fur	g/L	0.3	0.1	0.5 ± 0.2	2.1 ± 0.6
5-HMF	g/L	n.d	n.d	0.4 ± 0.1	n.d

n.d: non detected

** The mixture contains 1.5 g of xylan with 10 wt% formic acid*

Remarkably, unlike xylan from Birchwood, which consists solely of xylose, xylan extracted from Oat Spelts contains xylose, glucose, and arabinose, as indicated in Table V-12. Under conditions of high temperature and in an acidic medium, arabinose underwent conversion into furfural, while glucose was subjected to dehydration, resulting in the formation of 5-HMF (C. Xu et al., 2020). This increased the complexity of the mixture and promoted the occurrence of the side reaction, leading to a decrease in the furfural yield. Furthermore, the presence of xylo-oligomers with varying lengths and quantities within each xylan molecule could significantly influence overall furfural production. Indeed, Agirrezabal-Telleria et al. (2012) demonstrated that the combination of xylose and glucose resulted in decreased furfural production compared to using xylose alone. In their study, the presence of additional glucose, in equal proportions with xylose (mass concentration ratio of xylose/glucose = 0.66), heightened secondary reactions due to interactions between the produced furfural and elevated concentration of glucose.

V.2.2.3 Furfural production from biomass raw biomass hydrolysate

Table V-13: Optimum conditions and the corresponding highest furfural yield as well as the experimental furfural yield using raw biomass hydrolysates.

Biomass	Study	Concentration (mol/L)		Optimum conditions by Model 3				
		C_5	C_6	T (K)	$C_{H,0}$ (mol/L)	t (s)	Fur yield (%)	5-HMF yield (%)
Fir wood	Model	0.096	-	417	3.61	13440	61	-
	Experiment	0.096	0.240				57	32
OPEFB	Model	0.193	-	415	3.06	17040	57	-
	Experiment	0.193	0.022				62	32

After confirming the accuracy of the kinetic equations derived from the study's model through the optimization of operational parameters to enhance furfural yield, the approach was expanded to convert raw biomass hydrolysates into furfural. The biomass hydrolysate obtained from the LEEBio^{TM} process was used without the need for any supplementary chemicals. The study focused on two types of biomasses: residual biomass, namely OPEFB which has a high amount of C_5 sugars, and hardwood, represented by fir wood which is rich in C_6 sugars. As previously stated, the objective is to analyze the effect of C_6 sugars on the production of furfural. In this section, the concentrations of xylose and formic acid were the same for each experiment and were denoted by the values in hydrolysates that are provided in Table V-12. The xylose concentration represents the combined concentration of all pentose sugars, including xylose and arabinose, in the hydrolysates. The optimal conditions and corresponding maximum furfural yields predicted by Model 3, along with the experimental furfural yield obtained from raw biomass hydrolysates, are presented in Table V-13. As with the utilization of xylan as the starting material, there was no significant difference between the experimental furfural yield derived from both biomasses and the predicted value of model 3, with a relative gap of less than 10%.

As expected, the furfural yield obtained from fir wood (57%) was lower than the predicted yield (61%). This exhibited a comparable trend when xylan derived from Oat Spelts was utilized in comparison to a solution containing xylose. The rationale behind this observation can be attributed to the composition of fir wood, which primarily consists of C_6

sugars, exceeding the concentration of C_5 sugars by more than two-fold. As previously stated, the presence of C_6 sugars that convert to 5-HMF can intensify secondary loss reactions, ultimately leading to a reduced furfural yield.

Although C_6 sugars were present, the furfural yield (62%) produced from OPEFB was higher than that from fir wood (57%) and even surpassed the predicted yield (57%). Yemiş and Mazza (2011) also made a comparable observation. Under microwave-assisted conditions, the quantity of furfural generated from straw biomass exceeded the quantity generated from pure xylose and xylan. These authors suggest that the probability of a cross-polymerization reaction between furfural and xylose is higher in conversions that use pure xylose and xylan. Additionally, the presence of various metal ions (such as K^+, Ca^{2+}, Al^{3+}, etc.) in the biomass hydrolysate may contribute to this phenomenon by acting as Lewis acids, thereby enhancing the catalytic efficiency of formic acid in the conversion of pentose sugars into furfural (Yemiş and Mazza, 2011; Lopes et al., 2017). Furthermore, Lopes et al. (2017) reported a significant increase in furfural yield from 57% to 70% with the increase in Al^{3+} concentration from 0.2 mol/L to 0.8 mol/L in the presence of formic acid. Indeed, a comparison of the quantity of various inorganic elements in fir wood and OPEFB, as reported by Cutter and McGinnes (1979) and Lee et al. (2020) respectively, revealed that OPEFB contained significantly higher levels of metal ions. For example, in their studies, OPEFB contained 135 times more Al^{3+} and 7 times more Ca^{2+} compared to fir wood. These findings strongly support the hypothesis that furfural production is enhanced by the presence of metal ions along with formic acid, explaining why the furfural yield achieved from OPEFB surpassed that from fir wood and exceeded the predicted yield.

The furfural yield achieved in our study using the LEEBio^{TM} process notably surpassed that of other studies employing formic acid as a catalyst. For instance, Yong et al. (2016) obtained the highest furfural yield of 35.8% from Oil palm fronds (OPF) using a water-ethanol mixture at 240 °C. Huang et al. (2019), on the other hand, combined formic acid with solid acid SO_4^{2-}/SnO_2 montmorillonite to attain a maximum furfural yield of 40.2% from corncob at 180°C for 10 min under microwave irradiation (600W). Recently, Qiao et al. (2022) reported achieving the highest furfural yield of 49.3% from corn cobs at 160 °C for 60 min with the assistance of $AlCl_3$. These findings demonstrate the superior efficiency of our approach and catalytic activity of formic acid, which not only offered higher furfural yields but also could be performed without the need for additional chemicals

In addition to furfural, both biomass hydrolysates generated 5-HMF (32%) as a result of the existence of hexose sugars, including glucose, mannose, and galactose (Yang et al., 2023; Zhu et al., 2023). The conversion of hexose to 5-HMF involves two distinct steps: firstly, the isomerization of hexose sugars to fructose, followed by the dehydration of fructose to 5-HMF (Shao et al., 2022). The chemical composition of 5-HMF, characterized by a furan ring with an aldehyde group and an alcohol group, makes it highly suitable for the synthesis of various chemicals such as 5-hydroxymethyl furfural acid, levulinic acid, furfuryl alcohol, etc. through reactions such as oxidation, hydrogenation, hydration, decarbonylation and etherification (Tao et al., 2023). Moreover, 5-HMF has been recognized for its significance in biomass conversion, earning a spot alongside furfural in the "Top 10" list of chemicals derived from biomass, as reported by the U.S. Department of Energy (Wozniak et al., 2019). However, the yield of 5-HMF from these sugars was significantly lower compared to furfural, which had a yield of approximately 60%. This can be attributed to the greater breakdown activation energy of hexose sugars compared to pentose sugars. In a study conducted by Wei et al. (2008), the process of breaking down xylose and glucose using sulfuric acid as a catalyst in biomass hydrolysate was examined. The results showed that the activation energy required for the degradation of xylose was 114.4 kJ/mol, while for glucose it was 136.8 kJ/mol. The pre-exponential factor (k_0) of xylose and glucose were 2.38×10^{11} and 4.83×10^{13}, respectively. Consequently, the conversion of pentose sugars into furfural occurred at a higher rate compared to hexose sugars, leading to a reduced production of 5-HMF (Istasse and Richel, 2020).

When considering the findings reported in other literature, the 5-HMF yield (32%) obtained in this study was found to be comparable. For instance, Scapin et al. (2020) developed a sustainable process for furfural and 5-HMF production from lignocellulosic biomass using an ionic liquid. Operating at 120 °C for 3h, they attained the best furfural yield of 59% and maximum 5-HMF yield of 8.7% from rice husks. Hoang and Cuong (2021), employing porous HSO_3-ZSM-5 as a catalyst in water, reported the highest furfural yield of 40% with a 5-HMF yield of 19% from corncob biomass. In another study, $AlCl_3.6H_2O$ was utilized in a biphasic medium of water/tetrahydrofuran (THF) to convert various lignocellulosic biomass types (corn stover, pine wood, grass, and poplar) into furanic compounds. While the yields of HMF were modest (20–35%), high concurrent yields of furfural were observed (51-66%). This comparison underscores the efficacy of the formic acid utilized in the LEEBio^{TM} process as a catalyst for converting biomass into furfural and 5-HMF. Furthermore, it highlights the effectiveness of

kinetic equations in optimizing the process parameters, demonstrating the potential for enhanced efficiency in biomass conversion.

However, furfural can be effectively generated from the real biomass hydrolysate acquired by the LEEBio^{TM} method. It was discovered to be present in the combination along with by-products, particularly 5-HMF. It is observed that the amount of 5-HMF collected varies depending on the type of biomass. For instance, the hydrolysate from fir wood yielded 5.71 g/L of furfural (57%) and 8.96 g/L of 5-HMF (32%). On the other hand, the hydrolysate from OPEFB produced 10.43 g/L of furfural (62%) and 0.45 g/L of 5-HMF (32%). The results demonstrated that the selection of raw biomass is essential in determining the final output. Therefore, to achieve a large amount of furfural with the best possible purity, it may be preferable to use biomass that is abundant in C_5 sugars, such as OPEFB in this study. To enhance the quality of the produced furfural, one can employ separation techniques like distillation, liquid-liquid extraction, etc. In a study conducted by Wang et al. (2021), it was found that furfural may be extracted with selectivity from furfural-HMF combinations using dichloromethane or toluene. The extraction process resulted in a yield of 79% for furfural, while only 11% of 5-HMF was extracted at 150 °C. Fele Žilnik et al. (2023) conducted a study on the extraction of furfural from the furfural-5-HMF mixture using a combination of an extractor and a distillation column. When tetrahydrofuran (THF) was used as the extracting solvent, the recovery efficiency for 5-HMF was 98.5% with a purity of 90.1 wt%, and for furfural it was 99.7% with a purity of 96.2 wt%. Zhao et al. (2020) demonstrated that the process of separating furfural and 5-HMF could be achieved by dynamic column adsorption. Upon utilizing a MAF-5 packed column to separate furfural/5-HMF (2/2 wt%), it was observed that the eluent included negligible amounts of 5-HMF, while the furfural component could be enriched up to a maximum of 21.4 wt%. The results indicated that by employing the separation technique during the downstream purification process, along with the utilization of raw biomass containing a significant amount of C_5 sugars, it is possible to achieve a solution of furfural with a high level of purity. Nevertheless, it is essential to conduct a thorough energy assessment in order to design the complete process, including downstream separation and purification, along with the reaction step, within the context of sustainable development and the economic feasibility of the process.

V.3 Complementary study: Furfural production from raw biomass hydrolysates with low formic acid concentration.

As delineated in Section II.4.1.2, the formic acid present in the raw biomass hydrolysates was recovered by undergoing an additional evaporation process to meet the principles of green chemistry and sustainable processes. This part focused only on hydrolysates originating from fir wood due to constraints posed by the availability of hydrolysates from OPEFB. The experimental results of furfural production from fir wood hydrolysates, varying in formic acid concentrations, are presented in Table V-14.

Table V-14: Furfural production from fir wood hydrolysates with different formic acid concentrations.

Hydrolysate	FA Conc (g/L)	Xyl conv (%)	Ara conv (%)	Glu conv (%)	Mann conv (%)	Galac conv (%)	Fur yield (%)	5-HMF yield (%)
Fir wood	168.5	97	91	33	91	77	55	34
Fir wood 4/4	63.4	91	59	12	44	30	52	25
Fir wood 9/9	28.7	43	40	1	22	7	42	22

Op. Cond.: volume of the mixture = 150 mL; reaction temperature = 170 °C; residence time = 40 min.

According to the findings presented in Table V-14, the optimal method for recovering formic acid involved evaporating until the final volume was reduced by a factor of 4, leading to a decrease in formic acid concentration to 63.4 g/L. This recovered formic acid can be reused in the biomass fractionation process through the LEEBio^{TM} method, aligning with the principles of sustainable chemistry. Furthermore, the reaction was successfully conducted using lower concentrations of formic acid while still achieving comparable furfural yields, thus demonstrating progress towards the goals of green chemistry. However, further recovery of formic acid with a factor of 9, resulting in a concentration of 28.5 g/L, significantly diminished both furfural and 5-HMF yields. This decline is attributed to the insufficient quantity of formic acid to facilitate the depolymerization of polysaccharides and the subsequent dehydration reaction of monosaccharides, as evidenced by the notable decrease in monosaccharide conversion. Despite the high quantity of recovered formic acid solution, extending the reaction duration at elevated temperatures is necessary to attain higher furfural and 5-HMF yields. Nonetheless, this finding presents an opportunity for the incorporation of heterogeneous

catalysts, particularly Lewis acid heterogeneous catalysts, which can enhance the catalytic activity of formic acid. Finally, conducting an energy balance analysis could distinguish between the three cases outlined in Table V-14, providing insight into their alignment with the principles of sustainable development.

V.4 Conclusion chapter

Before employing real biomass hydrolysates, xylans derived from Birchwood and Oat Spelts were utilized to investigate the influence of the complex structure of raw materials on furfural production. Surprisingly, it was observed that xylans yielded higher furfural yields compared to pure xylose solutions (58%), based on the number of moles of xylose. This phenomenon could be attributed to the simultaneous liberation of pentose monomers during the depolymerization process, which may limit the cross-side reaction between xylose and furfural, resulting in a higher yield. Specifically, xylan from Birchwood, consisting solely of xylose, yielded a furfural yield of 68%, higher than that from Oat Spelts, which contains various sugar types (i.e., xylose, arabinose, and glucose), yielding 60%. Additionally, the presence of 5-HMF, a dehydration product of glucose, was observed when using xylan from Oat Spelts as a starting material, thereby reducing the purity of furfural compared to when xylan from Birchwood was employed.

The study also involved synthesizing furfural from raw biomass hydrolysates with a lower concentration of formic acid. This aimed to recover formic acid from the hydrolysate obtained via hydrolysis for reuse. The optimal condition was achieved by reducing the volume by a factor of 4 through evaporation, resulting in a formic acid concentration of 63.4 g/L. Further decreasing the concentration of formic acid significantly reduced furfural formation, likely due to insufficient formic acid to break down polysaccharides and convert monosaccharides into furfural through dehydration.

Regarding the kinetic modeling, statistical analysis and validation with further experimental data indicated that the most appropriate kinetic model was model 3. The mechanism of this model encompasses first-order reaction kinetics, where a part of xylose/arabinose undergoes reaction to form a degradation product, while another part converts into an intermediate. This intermediate subsequently undergoes dehydration to produce furfural. Furthermore, furfural degrades through self-polymerization and cross-polymerization with the xylose/arabinose intermediate, constituting a second-order reaction process. Model 3 was employed to optimize parameters for furfural production. The applicability of this model

across a wide range of operating parameters underscores the novelty of this study compared to existing literature. Through the optimization of operational parameters using kinetic equations derived from model 3, it was demonstrated that a high furfural yield (up to 63%) could be attained with a higher formic acid concentration (> 15 wt%) within a moderate temperature range (413–450 K) and over a reaction duration of 3.5 h. The robustness of the developed kinetic model was further evidenced by its successful application in studies concerning furfural production from raw materials such as xylans and hemicellulose-rich hydrolysates obtained through fractionation processes. The results demonstrated that the developed model accurately predicted maximum achievable yields with a precision exceeding 90%. These raw materials exhibited remarkable performance, yielding furfural in the range of 57% to 62%. However, the study also identified limitations of the model, particularly regarding the presence of additional compounds, such as inorganic elements and hexose sugars, which could potentially compromise the accuracy of predicted values.

V.5 References

Agirrezabal-Telleria, I., Requies, J., Güemez, M.B., Arias, P.L., 2012a. Furfural production from xylose + glucose feedings and simultaneous N2-stripping. Green Chem. 14, 3132–3140. https://doi.org/10.1039/c2gc36092f

Agirrezabal-Telleria, I., Requies, J., Güemez, M.B., Arias, P.L., 2012b. Furfural production from xylose + glucose feedings and simultaneous N2-stripping. Green Chem. 14, 3132–3140. https://doi.org/10.1039/c2gc36092f

Aida, T.M., Shiraishi, N., Kubo, M., Watanabe, M., Smith, R.L., 2010. Reaction kinetics of d-xylose in sub- and supercritical water. J. Supercrit. Fluids 55, 208–216. https://doi.org/10.1016/j.supflu.2010.08.013

Chang, S.H., 2014. An overview of empty fruit bunch from oil palm as feedstock for bio-oil production. Biomass Bioenergy 62, 174–181. https://doi.org/10.1016/j.biombioe.2014.01.002

Chen, Z., Zhang, W., Xu, J., Li, P., 2015. Kinetics of xylose dehydration into furfural in acetic acid. Chin. J. Chem. Eng. 23, 659–666. https://doi.org/10.1016/j.cjche.2013.08.003

Choudhary, V., Sandler, S.I., Vlachos, D.G., 2012. Conversion of Xylose to Furfural Using Lewis and Brønsted Acid Catalysts in Aqueous Media. ACS Catal. 2, 2022–2028. https://doi.org/10.1021/cs300265d

Cutter, B.E., McGinnes, E.A., 1979. Inorganic concentrations in selected woods and charcoals measured using naa. WOOD FIBER 12, 72–79.

Danon, B., Van Der Aa, L., De Jong, W., 2013. Furfural degradation in a dilute acidic and saline solution in the presence of glucose. Carbohydr. Res. 375, 145–152. https://doi.org/10.1016/j.carres.2013.04.030

Delbecq, F., Wang, Y., Len, C., 2016. Conversion of xylose, xylan and rice husk into furfural via betaine and formic acid mixture as novel homogeneous catalyst in biphasic system by microwave-assisted dehydration. J. Mol. Catal. Chem. 423, 520–525. https://doi.org/10.1016/j.molcata.2016.07.003

Delmas, M., 2019. A lignocellulosic biomass based process for production of lignins and syngas, and electricity production efficient syngas. EP3527531A1.

Dias, A.S., Pillinger, M., Valente, A.A., 2005. Liquid phase dehydration of d-xylose in the presence of Keggin-type heteropolyacids. Appl. Catal. Gen. 285, 126–131. https://doi.org/10.1016/j.apcata.2005.02.016

Dussan, K., Girisuta, B., Lopes, M., Leahy, J.J., Hayes, M.H.B., 2015. Conversion of Hemicellulose Sugars Catalyzed by Formic Acid: Kinetics of the Dehydration of D -Xylose, L -Arabinose, and D -Glucose. ChemSusChem 8, 1411–1428. https://doi.org/10.1002/cssc.201403328

Ershova, O., Kanervo, J., Hellsten, S., Sixta, H., 2015. The role of xylulose as an intermediate in xylose conversion to furfural: insights via experiments and kinetic modelling. RSC Adv. 5, 66727–66737. https://doi.org/10.1039/C5RA10855A

Fele Žilnik, L., Crnomarkovic, M., Novak, U., Grilc, M., Likozar, B., 2023. Modelling, optimal solvent screening and separation of 5-hydroxymethylfurfural or furfural from catalytic conversion reactor stream in downstream purification process. Chem. Eng. Res. Des. 194, 376–387. https://doi.org/10.1016/j.cherd.2023.04.062

Gairola, K., Smirnova, I., 2012. Hydrothermal pentose to furfural conversion and simultaneous extraction with SC-CO2 – Kinetics and application to biomass hydrolysates. Bioresour. Technol. 123, 592–598. https://doi.org/10.1016/j.biortech.2012.07.031

Guo, Z., Yan, N., Lapkin, A.A., 2019. Towards circular economy: integration of bio-waste into chemical supply chain. Curr. Opin. Chem. Eng. 26, 148–156. https://doi.org/10.1016/j.coche.2019.09.010

Hoang, P.H., Cuong, T.D., 2021. Simultaneous Direct Production of 5-Hydroxymethylfurfural (HMF) and Furfural from Corncob Biomass Using Porous HSO_3-ZSM-5 Zeolite Catalyst. Energy Fuels 35, 546–551. https://doi.org/10.1021/acs.energyfuels.0c03431

Huang, Y., Liao, X., Deng, Y., He, Y., 2019. Co-catalysis of corncob with dilute formic acid plus solid acid SO42−/SnO2-montmorillonite under the microwave for enhancing the biosynthesis of furfuralcohol. Catal. Commun. 120, 38–41. https://doi.org/10.1016/j.catcom.2018.10.021

Isroi, Ishola, M., Millati, R., Syamsiah, S., Cahyanto, M., Niklasson, C., Taherzadeh, M., 2012. Structural Changes of Oil Palm Empty Fruit Bunch (OPEFB) after Fungal and Phosphoric Acid Pretreatment. Molecules 17, 14995–15012. https://doi.org/10.3390/molecules171214995

Istasse, T., Richel, A., 2020. Mechanistic aspects of saccharide dehydration to furan derivatives for reaction media design. RSC Adv. 10, 23720–23742. https://doi.org/10.1039/D0RA03892J

Jing, Q., Lü, X., 2007. Kinetics of Non-catalyzed Decomposition of D-xylose in High Temperature Liquid Water. Chin. J. Chem. Eng. 15, 666–669. https://doi.org/10.1016/S1004-9541(07)60143-8

Köchermann, J., Mühlenberg, J., Klemm, M., 2018. Kinetics of Hydrothermal Furfural Production from Organosolv Hemicellulose and D -Xylose. Ind. Eng. Chem. Res. 57, 14417–14427. https://doi.org/10.1021/acs.iecr.8b03402

Lamminpää, K., Ahola, J., Tanskanen, J., 2014. Kinetics of furfural destruction in a formic acid medium. RSC Adv 4, 60243–60248. https://doi.org/10.1039/C4RA09276G

Lamminpää, K., Ahola, J., Tanskanen, J., 2012. Kinetics of Xylose Dehydration into Furfural in Formic Acid. Ind. Eng. Chem. Res. 51, 6297–6303. https://doi.org/10.1021/ie2018367

Lamminpää, K., Tanskanen, J., 2009. Study of furfural formation using formic acid. 8th World Congr. Chem. Eng. 7.

Lee, J.H., Ahmed, M.A., Choi, I.-G., Choi, J.W., 2020. Fractionation of Cellulose-Rich Products from an Empty Fruit Bunch (EFB) by Means of Steam Explosion Followed by Organosolv Treatment. Appl. Sci. 10, 2–11. https://doi.org/10.3390/app10030835

Lopes, M., Dussan, K., Leahy, J.J., 2017. Enhancing the conversion of D-xylose into furfural at low temperatures using chloride salts as co-catalysts: Catalytic combination of AlCl 3 and formic acid. Chem. Eng. J. 323, 278–286. https://doi.org/10.1016/j.cej.2017.04.114

Lu, Y., Mosier, N.S., 2007. Biomimetic Catalysis for Hemicellulose Hydrolysis in Corn Stover. Biotechnol. Prog. 23, 116–123. https://doi.org/10.1021/bp060223e

Marcotullio, G., De Jong, W., 2010. Chloride ions enhance furfural formation from d-xylose in dilute aqueous acidic solutions. Green Chem. 12, 1739–1746. https://doi.org/10.1039/b927424c

Morinelly, J.E., Jensen, J.R., Browne, M., Co, T.B., Shonnard, D.R., 2009. Kinetic Characterization of Xylose Monomer and Oligomer Concentrations during Dilute Acid Pretreatment of Lignocellulosic Biomass from Forests and Switchgrass. Ind. Eng. Chem. Res. 48, 9877–9884. https://doi.org/10.1021/ie900793p

O'Neill, R., Ahmad, M.N., Vanoye, L., Aiouache, F., 2009. Kinetics of Aqueous Phase Dehydration of Xylose into Furfural Catalyzed by ZSM-5 Zeolite. Ind. Eng. Chem. Res. 48, 4300–4306. https://doi.org/10.1021/ie801599k

Putri, D.N., Perdani, M.S., Yohda, M., Utami, T.S., Sahlan, M., Hermansyah, H., 2021. Effect of Ultrasound-Assisted on Sequential Peracetic Acid and Alkaline Peroxide Pretreatment to The Enzymatic Hydrolysis of Oil Palm Empty Fruit Bunch. https://doi.org/10.21203/rs.3.rs-284744/v1

Qiao, H., Han, M., Ouyang, S., Zheng, Z., Ouyang, J., 2022. An integrated lignocellulose biorefinery process: Two-step sequential treatment with formic acid for efficiently producing ethanol and furfural from corn cobs. Renew. Energy 191, 775–784. https://doi.org/10.1016/j.renene.2022.04.027

Root, D.F., 1956. Kinetics of the acid catalyzed conversion of xylose to furfural 9, 158–165.

Rose, I.C., Epstein, N., Watkinson, A.P., 2000. Acid-Catalyzed 2-Furaldehyde (Furfural) Decomposition Kinetics. Ind. Eng. Chem. Res. 39, 843–845. https://doi.org/10.1021/ie990550+

Scapin, E., Rambo, M.K.D., Viana, G.C.C., Marasca, N., Lacerda, G.E., Rambo, M.C.D., Fernandes, R.D.M.N., 2020. Sustainable production of furfural and 5-hidroximetilfurfural from rice husks and soybean peel by using ionic liquid. Food Sci. Technol. 40, 83–87. https://doi.org/10.1590/fst.04419

Shao, Y., Chen, J., Ding, X., Lu, W., Shen, D., Long, Y., 2022. Valorization of hexoses into 5-hydroxymethylfurfural and levulinic acid in acidic seawater under microwave hydrothermal conditions. Environ. Technol. 1–10. https://doi.org/10.1080/09593330.2022.2143294

Tao, J., Pan, Y., Zhou, H., Tang, Y., Ren, G., Yu, Z., Li, J., Zhang, R., Li, X., Qiao, Y., Lu, X., Xiong, J., 2023. Catalytic Systems for 5-Hydroxymethylfurfural Preparation from Different Biomass Feedstocks: A Review. Catalysts 14, 1–14. https://doi.org/10.3390/catal14010030

Wang, Y., Len, T., Huang, Y., Diego Taboada, A., Boa, A.N., Ceballos, C., Delbecq, F., Mackenzie, G., Len, C., 2017. Sulfonated Sporopollenin as an Efficient and Recyclable Heterogeneous Catalyst for Dehydration of D -Xylose and Xylan into Furfural. ACS Sustain. Chem. Eng. 5, 392–398. https://doi.org/10.1021/acssuschemeng.6b01780

Wang, Z., Bhattacharyya, S., Vlachos, D.G., 2021. Extraction of Furfural and Furfural/5-Hydroxymethylfurfural from Mixed Lignocellulosic Biomass-Derived Feedstocks. ACS Sustain. Chem. Eng. 9, 7489–7498. https://doi.org/10.1021/acssuschemeng.1c00982

Wei, Q., Zheng-wei, R., Yong-jie, Y., 2008. Degradation Kinetics of Xylose and Glucose in Hydrolysate Containing Dilute Sulfuric Acid. TheChineseJournalofProcessEngineering 8, 1132–1137.

Weingarten, R., Cho, J., Conner, Jr., Wm.C., Huber, G.W., 2010. Kinetics of furfural production by dehydration of xylose in a biphasic reactor with microwave heating. Green Chem. 12, 1423–1429. https://doi.org/10.1039/c003459b

Williams, D.L., Dunlop, A.P., 1948. Kinetics of Furfural Destruction in Acidic Aqueous Media. Ind. Eng. Chem. 40, 239–241. https://doi.org/10.1021/ie50458a012

Wozniak, B., Tin, S., De Vries, J.G., 2019. Bio-based building blocks from 5-hydroxymethylfurfural *via* 1-hydroxyhexane-2,5-dione as intermediate. Chem. Sci. 10, 6024–6034. https://doi.org/10.1039/C9SC01309A

Xu, C., Paone, E., Rodríguez-Padrón, D., Luque, R., Mauriello, F., 2020. Recent catalytic routes for the preparation and the upgrading of biomass derived furfural and 5-

hydroxymethylfurfural. Chem. Soc. Rev. 49, 4273–4306. https://doi.org/10.1039/D0CS00041H

Xu, S., Wu, N., Yuan, H., Chen, Y., Pan, D., Wu, Y., Fan, J., Gao, L., Xiao, G., 2020. An Effective and Stable HfP/SiO2 Catalyst for the Production of Furfural from Xylan. Catal. Lett. 150, 1121–1127. https://doi.org/10.1007/s10562-019-02994-2

Yang, Q., Tang, W., Ma, C., He, Y.-C., 2023. Efficient co-production of xylooligosaccharides, furfural and reducing sugars from yellow bamboo via the pretreatment with biochar-based catalyst. Bioresour. Technol. 387, 1–12. https://doi.org/10.1016/j.biortech.2023.129637

Yemiş, O., Mazza, G., 2011. Acid-catalyzed conversion of xylose, xylan and straw into furfural by microwave-assisted reaction. Bioresour. Technol. 102, 7371–7378. https://doi.org/10.1016/j.biortech.2011.04.050

Yong, T.L.-K., Mohamad, N., Yusof, N.N.M., 2016. Furfural Production from Oil Palm Biomass Using a Biomass-derived Supercritical Ethanol Solvent and Formic Acid Catalyst. Procedia Eng. 148, 392–400. https://doi.org/10.1016/j.proeng.2016.06.495

Zeitsch, K.J., 2000. The Chemistry and Technology of Furfural and its Many By-Products. Elsevier.

Zhang, J., Lin, L., Liu, S., 2012. Efficient Production of Furan Derivatives from a Sugar Mixture by Catalytic Process. Energy Fuels 26, 4560–4567. https://doi.org/10.1021/ef300606v

Zhang, L.-X., Yu, H., Yu, H.-B., Chen, Z., Yang, L., 2014. Conversion of xylose and xylan into furfural in biorenewable choline chloride–oxalic acid deep eutectic solvent with the addition of metal chloride. Chin. Chem. Lett. 25, 1132–1136. https://doi.org/10.1016/j.cclet.2014.03.029

Zhang, T., Li, W., An, S., Huang, F., Li, X., Liu, J., Pei, G., Liu, Q., 2018. Efficient transformation of corn stover to furfural using p-hydroxybenzenesulfonic acid-formaldehyde resin solid acid. Bioresour. Technol. 264, 261–267. https://doi.org/10.1016/j.biortech.2018.05.081

Zhao, Y., Xu, J., Wang, J., Wu, J., Gao, M., Zheng, B., Xu, H., Shi, Q., Dong, J., 2020. Adsorptive Separation of Furfural/5-Hydroxymethylfurfural in MAF-5 with Ellipsoidal Pores. Ind. Eng. Chem. Res. 59, 11734–11742. https://doi.org/10.1021/acs.iecr.0c01415

Zhu, L., Tang, W., Ma, C., He, Y.-C., 2023. Efficient co-production of reducing sugars and xylooligosaccharides via clean hydrothermal pretreatment of rape straw. Bioresour. Technol. 388, 1–10. https://doi.org/10.1016/j.biortech.2023.129727

General conclusions

The current state of the art highlights that lignocellulosic biomass recovery is emerging as a key solution to various societal issues. One way to upgrade biomass is to convert it into valuable products. Lignocellulosic material mainly consists of cellulose, hemicellulose, and lignin. Notably, hemicellulose can be converted into furfural, a versatile platform molecule essential for synthesizing numerous value-added products, including fuels and additives. However, few industrial processes have been established due to limited furfural yield, primarily caused by undesirable reactions between generated furfural and other molecules in the aqueous phase. Research indicates that while catalysts like homogeneous acids (such as sulfuric acid) and heterogeneous catalysts (such as zeolites) are used for synthesis from pure raw materials, formic acid is gaining attention. Formic acid offers a solution to the corrosiveness issues associated with mineral acid catalysts traditionally used in industrial furfural production. It also addresses challenges such as the deactivation of solid catalysts in aqueous media and the limited acidity of acids generated by water at high temperatures. Moreover, formic acid is successfully applied in biorefining processes, acting as a medium for treating lignocellulosic biomass. This treatment extracts a hemicellulose/pentose fraction free of lignin and cellulose, enabling furfural production without additional chemicals.

The objective of this thesis was to establish the viability of formic acid's dual role: as a solvent for lignocellulosic biomass depolymerization and as an efficient catalyst for pentose sugar dehydration into furfural. The study initially focused on optimizing furfural production using xylose and real biomass hydrolysate, employing extraction methods to prevent furfural degradation. Various operating parameters were investigated, including reaction temperature (100–200 °C), residence time (0–60 minutes), initial xylose concentration (2–30 g/L), and formic acid concentration (5–30 wt%), to determine the optimal conditions for the process. Xylose dehydration into furfural was conducted under different conditions: either at atmospheric pressure (boiling point of the mixture) or under pressure at high temperatures (>140 °C).

Under the atmospheric pressure and boiling temperature of the mixture, the furfural formation in both monophasic and biphasic solvent systems was not optimal. This was due to the low catalytic activity of formic acid in dehydrating xylose to furfural under these conditions. However, a significant increase in furfural yield was observed when the reaction was conducted at higher temperatures (> 140 °C). Analysis of the influence of operating parameters under pressure revealed that furfural production was highly dependent on

temperature, which correlates with residence time. Higher reaction temperatures necessitated shorter residence times, and vice versa. Interestingly, the concentration of formic acid had a lesser impact on furfural production, possibly due to its excess quantity compared to xylose. Optimal conditions were determined to be 170 °C, 40 min, 10 g/L xylose, and 10 wt% formic acid, resulting in a 58% furfural yield. Regarding simultaneous extraction, both steam stripping and the use of organic solvents in a biphasic system exhibited significant advantages in furfural production. The highest furfural yields of 80% and 70% were achieved by steam stripping and the water/cyclopentyl methyl ether biphasic system, respectively, at 170 °C for 40 min using 30 g/L xylose and 10 wt% formic acid. This surpasses the 54% yield achieved in batch processing under identical conditions.

The furfural yield obtained from real biomass hydrolysates exceeded that of a pure xylose solution. Specifically, under optimized conditions (170 °C for 40 min), fir wood hydrolysate yielded 50%, 72%, and 76% furfural in batch, semi-batch, and biphasic systems, respectively. Similarly, hydrolysate derived from OPEFB yielded 70%, 79%, and 83% furfural in the corresponding systems. This higher furfural yield may be attributed to the presence of inorganic elements such as Na^+, Al^{3+}, Cl^-, etc., acting as Lewis acids. These elements facilitate the conversion of xylose into furfural by isomerizing xylose into a reactive intermediate known as xylulose. Furthermore, these inorganic elements contribute to the salting-out effect, thereby enhancing furfural separation and ultimately resulting in a higher yield in a biphasic solvent system. Additionally, the presence of 5-HMF, a dehydration product of hexose sugars in the hemicellulose fraction, was observed when using real biomass hydrolysate as a starting material. However, the 5-HMF yield (38%–62%) was lower than the furfural yield (55%–83%) due to the higher activation energy required for the breakdown of hexose sugars compared to pentose sugars.

In the second part, the process was further developed to be more environmentally friendly by incorporating simultaneous extraction of furfural through supercritical CO_2 (Sc-CO_2) and using heterogeneous catalysts such as Amberlyst-15, Al_2O_3, H-ZSM-5, and H-mordenite. The findings revealed that under our experimental conditions, Sc-CO_2 not only served as an extracting agent but also exhibited Lewis acid properties, catalyzing the isomerization of xylose into a reactive intermediate termed “xylulose”. In the presence of Sc-CO_2, this mechanism involved a secondary reaction pathway comprising two steps: first, the Sc-CO_2-catalyzed isomerization of xylose into xylulose, followed by furfural production from xylulose, catalyzed by formic acid. Dehydration of xylose with Sc-CO_2 in both batch and semi-

batch systems resulted in higher furfural yield and selectivity compared to systems without Sc-CO_2. However, the efficiency of Sc-CO_2 extraction in the semi-batch system was influenced by the CO_2 flow rate, leading to a competition between furfural formation and extraction rate. Furthermore, the solubility of formic acid might decrease furfural solubility in the CO_2 stream. Nevertheless, simultaneous Sc-CO_2 extraction enabled the recovery of all produced furfural in the extract, minimizing furfural degradation and maintaining high furfural productivity, even with a high initial xylose concentration. A maximum furfural yield of 68.5% (with 71.4% selectivity and 99% separation efficiency) was attained after 5 h at 140°C and 20 MPa, with a constant CO_2 flow rate of 5 g/min, and initial concentrations of 10 g/L xylose and 10 wt% formic acid. Regarding the addition of both Brønsted and Lewis acid heterogeneous catalysts, it was found that the combination of these catalysts with formic acid did not enhance furfural production. This outcome is possibly due to the excess formic acid masking the catalytic activity of the heterogeneous catalysts.

Finally, a comprehensive investigation was conducted on the kinetic modeling, encompassing all reactions, including the formation of furfural and side-loss reactions. The kinetic parameters were determined using synthetic solutions containing xylose (10–30 g/L), formic acid (5–20 wt%), and furfural (5–15 g/L). Three different schemes of xylose dehydration into furfural were investigated in this study. The kinetic parameters were determined through nonlinear regression analysis, utilizing the *Nelder-Mead* algorithm within Python's optimization function for estimation. Subsequently, the most suitable kinetic model was analyzed and applied to raw material of varying purity levels for furfural production using the *fminsearch* function in MATLAB software.

According to the statistical evaluation, kinetic model 3 emerged as the most suitable for predicting xylose and furfural concentrations, along with furfural yield, boasting an R^2 exceeding 95%. The mechanism underlying this model encompasses first-order reaction kinetics. Here, a part of pentose undergoes a reaction to form a degradation product (k_3), while another part converts into an intermediate (k_1). Subsequently, this intermediate undergoes dehydration to produce furfural (k_5). Moreover, furfural degrades through self-polymerization (k_2) and cross-polymerization with the pentose intermediate (k_4), constituting a second-order reaction process. This model was used to optimize parameters for furfural production using synthetic solutions, leading to the highest furfural yield of 58% at a xylose concentration of 10 g/L. Similarly, Birchwood and Oat Spelts xylans yielded maximum furfural yields of 63% and 51%, respectively, under identical conditions. Furthermore, hydrolysates from OPEFB and fir

wood exhibited the best furfural yields of 62% and 57%, respectively, alongside an equivalent 5-HMF yield of 32%. These results underscored the accuracy of the developed model in predicting maximum achievable yields, achieving a precision exceeding 90%. Nonetheless, the study also highlighted limitations of the model, particularly concerning the presence of additional compounds such as inorganic elements and hexose sugars, which could potentially compromise the accuracy of predicted values.

Perspectives

Some perspectives can be highlighted from this work:

Firstly, simultaneous extraction during the reaction allows to constrain side reactions and maintain a high furfural productivity, even with a high initial xylose concentration. Additionally, literature reports suggest that achieving a high furfural yield (>60%) is feasible from concentrated xylose solutions (40–120 g/L) with low formic acid concentrations (5–15 g/L) via steam stripping in a semi-batch system. Moreover, the high xylose concentration meets industrial requirements for economic furfural production. Therefore, adjusting the concentrations of pentose (xylose and arabinose) and formic acid in real biomass hydrolysates to match these levels would be advantageous. As previously mentioned, this adjustment could be achieved using the NF process. The strategy involves diluting the hydrolysate in the initial stage to decrease the formic acid concentration. Subsequently, concentration step is carried out using NF with a membrane exhibiting a molecular weight cutoff (MWCO) higher than that of formic acid but lower than that of pentose sugars. In this process, xylose is retained by the membrane while formic acid passes through, resulting in a mixture with high concentration of pentose, while maintaining constant formic acid concentration. This resulting mixture could potentially integrate a Lewis acid heterogeneous catalyst to enhance formic acid’s performance in pentose dehydration into furfural.

Utilizing xylans as a starting material for furfural production revealed a higher furfural yield compared to that from a pure xylose solution. This enhancement could be attributed to the simultaneous release of pentose monomers during the reaction, which effectively limits cross-side reactions between xylose and furfural. This phenomenon aligns with the semi-batch principle, wherein the reactant is introduced during the reaction. Therefore, exploring a continuous system where xylose is added during the reaction while furfural is simultaneously removed from the reaction medium to prevent its degradation would be intriguing. Such a

process holds promise for industrial applications, offering heightened productivity alongside consistent product quality and reduced operational expenses.

Regarding the extraction of furfural by Sc-CO_2, the study observed that the efficiency of Sc-CO_2 extraction was influenced by the CO_2 flow rate, resulting in a competition between furfural production and extraction rate. Furthermore, the solubility of formic acid may decrease furfural solubility in CO_2 steam. Investigating the phase behavior of the CO_2-water-furfural-formic acid system and the kinetics involved in simultaneous Sc-CO_2 extraction would yield valuable insights into identifying optimal operating conditions for furfural recovery while minimizing formic acid concentration. Once these optimal conditions are determined, they should be applied alongside real biomass hydrolysates obtained through the LEEBio^{TM} process to demonstrate the feasibility of scaling up the approach to a larger industrial setting.

Upon analyzing the raw biomass hydrolysates, it was consistently observed that a mixture comprising furfural, 5-HMF, and formic acid was obtained. This occurrence is attributed to the presence of hemicellulose, a polysaccharide that yields both pentose and hexose sugars. The concentration of these sugars influences the production of furfural and 5-HMF, thereby affecting the quality of each product. Given that these products hold significant value and serve as excellent starting materials for producing various molecules, it becomes imperative to devise separation methods for their recovery with high purity. Interestingly, during steam stripping, an unexpectedly high separation efficiency between 5-HMF and furfural was achieved. This prompts the need for further investigation into the phase behavior of the furfural-5-HMF-water-formic acid system to elucidate these phenomena and facilitate the design of an efficient separation process.

As last, the assessment of investment cost and energy for three systems with extraction including steam stripping in semi-batch system, the use of organic solvents in biphasic system and the use of Sc-CO_2 would be interesting to be realized for selecting the best process with cost effectiveness. This would be a useful data for the companies to design the whole process Also, the life cycle assessment (LCA) would be interesting, regarding the principle of sustainable development, for assessing environmental impacts associated with all the stages of furfural production staring from the biomass cultivation until the recovery of pure furfural. This assessment is required more and more to companies for greater corporate sustainability

Appendix 1

Setting up of reactor

Before carrying out preliminary furfural synthesis tests, reactor start-up tests are carried out. These tests consist of measuring the saturation vapor pressure of pure water for the temperature range of 100 to 200 °C with a step of 10 °C. The reactor has a set minimum volume of 32 mL (Top Industrie, FR) and 126 mL (Equilabo, FR), ensuring that the 5 cm of thermocouple is submerged in the solution. The curve of pressure measured as a function of temperature is then plotted and compared with the curve of the vapor pressure of water (according to the NIST database) as illustrated below:

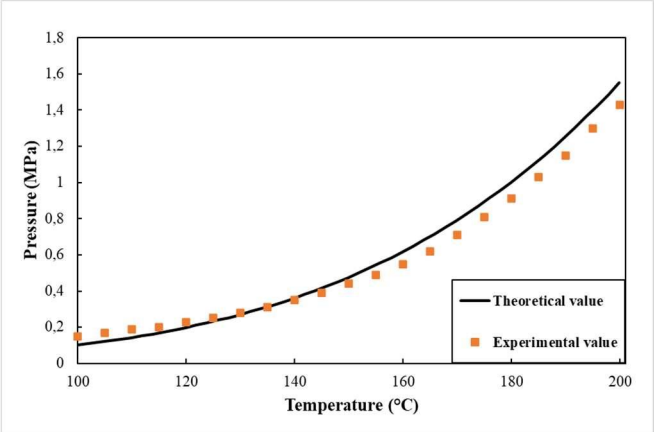

Water vapor pressure curve, comparison between the theoretical value provided by the NIST database and the experimental measurements.

The sample test is performed by default at 140 °C which is the first temperature studied. For the "Top Industrie" reactor, the V_1 valve is initially opened, followed by the subsequent opening of the V_2 valve. The sample is collected in the vial soaked in an ice bath. After the sample process, the V_1 valve is subsequently closed, followed by the closing of V_2. It is noted that when taking a sample, it is necessary to rinse the sampler before each new sample. Therefore, the first 0.5 mL of sample is discarded to avoid contamination with the previous sample. For the "Equilabo" reactor, sampling is performed via a liquid bleed valve (No. 9 in Figure II-3).

Concerning introduction of solution into the "Top Industrie" reactor via the sampling device, the V_1 valve is in a closed position while the V_2 valve is in an open position. The solution is taken by gently rotating the piston (P) while respecting the volume scale (2.5 mL max.). Subsequently, the V_2 valve is closed, and then the V_1 valve is opened. The solution is introduced into the reactor by placing the piston (P) in its initial state and thereafter closing the V_1 valve.

For the “Equilabo” reactor, in the injection of solution into the reactor is conducted by pump through liquid feed valve (N° 8 in Figure II-3).

Appendix 2

The vapor pressure of water (according to the NIST database)

Data NIST

T (°C)	P (MPa)
99.85	0.10088
101.85	0.1083
103.85	0.11617
105.85	0.1245
107.85	0.13333
109.85	0.14266
111.85	0.15252
113.85	0.16293
115.85	0.17393
117.85	0.18552
119.85	0.19773
121.85	0.2106
123.85	0.22414
125.85	0.23838
127.85	0.25335
129.85	0.26907
131.85	0.28558
133.85	0.30289
135.85	0.32105
137.85	0.34008
139.85	0.36001
141.85	0.38087
143.85	0.40269
145.85	0.42551
147.85	0.44935
149.85	0.47425
151.85	0.50025
153.85	0.52738
155.85	0.55567
157.85	0.58516
159.85	0.61588
161.85	0.64787
163.85	0.68118
165.85	0.71583
167.85	0.75186
169.85	0.78932
171.85	0.82824
173.85	0.86866
175.85	0.91063
177.85	0.95418
179.85	0.99936
181.85	1.0462
183.85	1.0948
185.85	1.1451
187.85	1.1972
189.85	1.2511
191.85	1.3069
193.85	1.3647
195.85	1.4245
197.85	1.4862
199.85	1.5501

Experimental data 17/03/2022

T (°C)	Pref (bar)	P (bar)	P (MPa)
100	0.5	1.5	0.15
105	0.7	1.7	0.17
110	0.9	1.9	0.19
115	1	2	0.2
120	1.3	2.3	0.23
125	1.5	2.5	0.25
130	1.8	2.8	0.28
135	2.1	3.1	0.31
140	2.5	3.5	0.35
145	2.9	3.9	0.39
150	3.4	4.4	0.44
155	3.9	4.9	0.49
160	4.5	5.5	0.55
165	5.2	6.2	0.62
170	6.1	7.1	0.71
175	7.1	8.1	0.81
180	8.1	9.1	0.91
185	9.3	10.3	1.03
190	10.5	11.5	1.15
195	12	13	1.3
200	13.3	14.3	1.43

Appendix 3

HPLC chromatograms

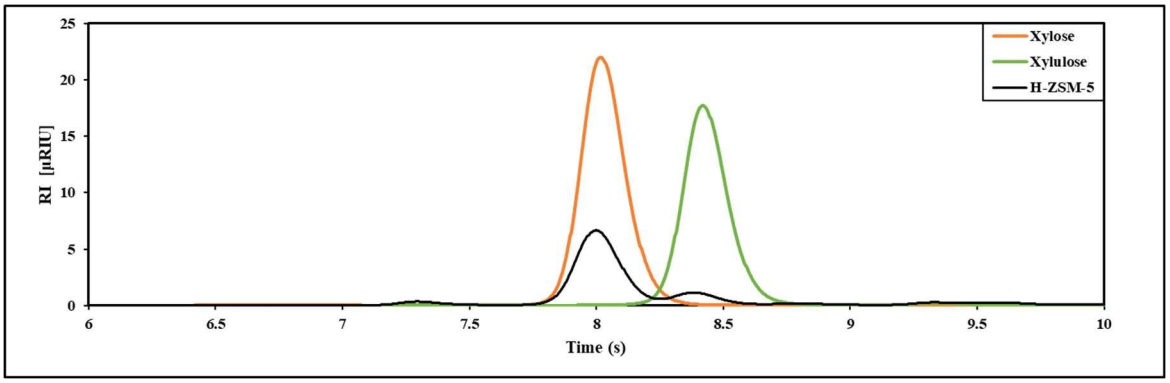

The sample after 1h of xylose dehydration into furfural catalyzed by H-ZSM-5, Biorad Aminex HPX-87H, 0.7 ml/min, 50 °C, 10 mM H_2SO_4.

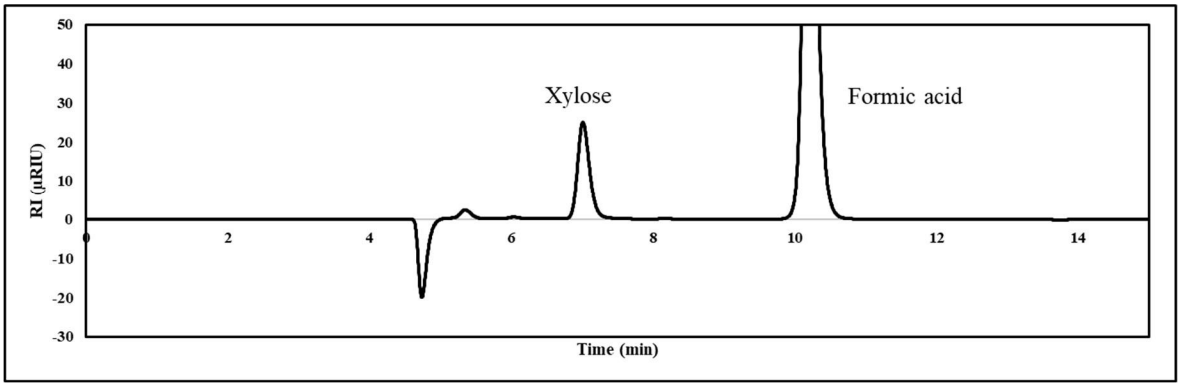

The xylan from Birchwood after 6h of acid hydrolysis, Biorad Aminex HPX-87H, 0.8 ml/min, 50 °C, 10 mM H_2SO_4.

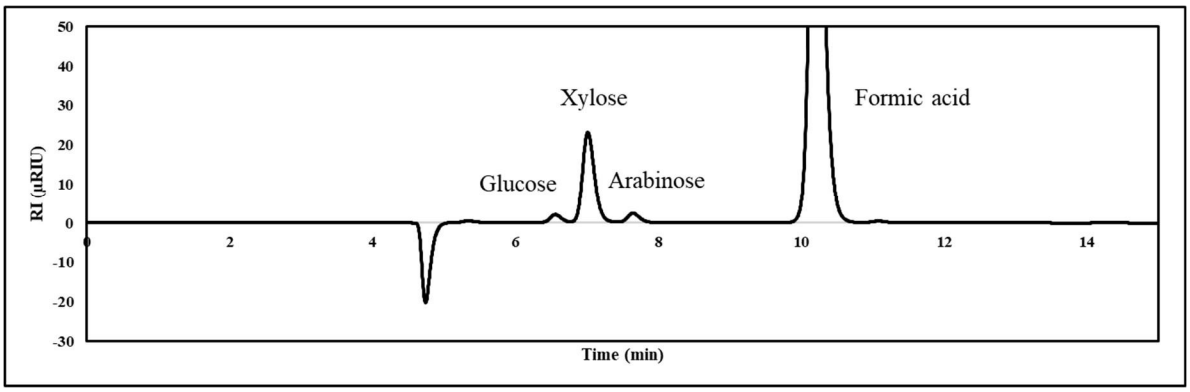

The xylan from Oat Spelts after 6h of acid hydrolysis, Biorad Aminex HPX-87H, 0.8 ml/min, 50 °C, 10 mM H_2SO_4.

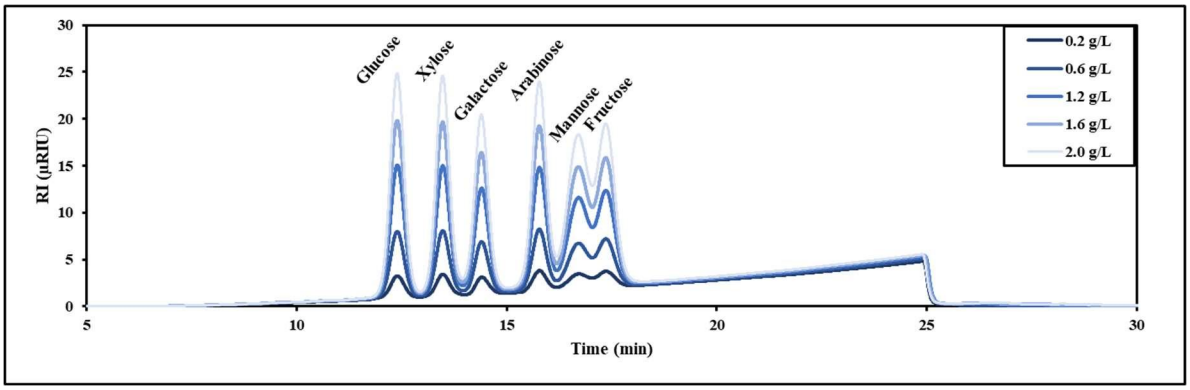

The standards of mixed sugars with formic acid, Biorad Aminex HPX-87P, 0.6 ml/min, 75 °C, deionized water.

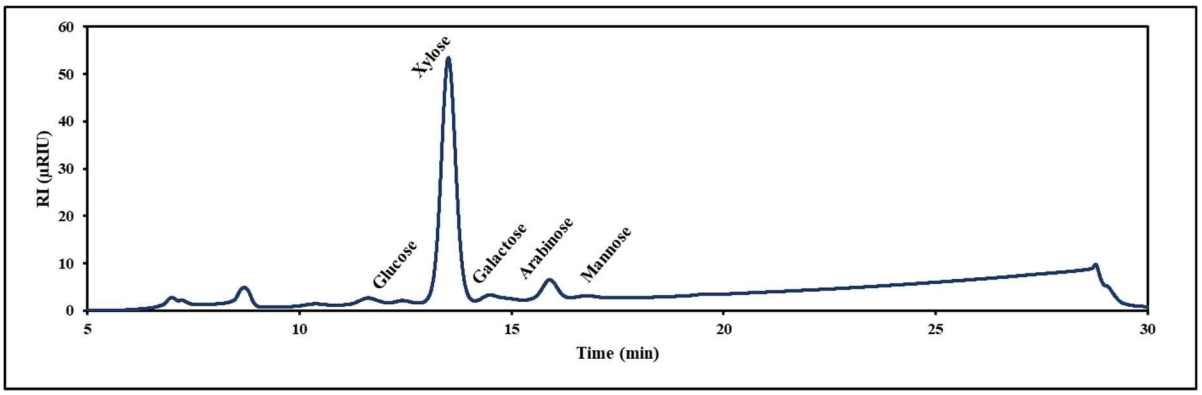

The OPEFB hydrolysate after 8h of acid hydrolysis, Biorad Aminex HPX-87P, 0.6 ml/min, 75 °C, deionized water.

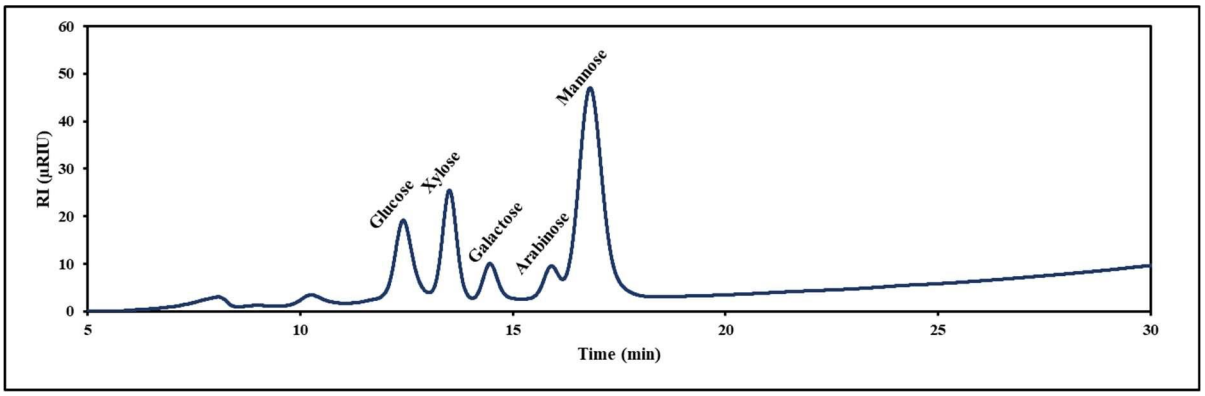

The fir wood hydrolysate after 8h of acid hydrolysis, Biorad Aminex HPX-87P, 0.6 ml/min, 75 °C, deionized water.

Appendix 4

Python code of kinetic modeling

Furfural degradation reaction

```
from lmfit import minimize, Parameters, fit_report
import matplotlib.pyplot as plt
import numpy as np
from scipy.integrate import odeint
from time import time

T_REF = 443  # K
R = 8.314  # J/mol/K


exp = {}

# exp173
exp['exp173'] = {
    'T': 413,  # K
    'Time': np.array([0, 3600, 7200, 10800, 14400, 18000, 21600]),
    'H+': np.array([0.00973453661855815, 0.00973453661855815, 0.00973453661855815, 0.00973453661855815, 0.00973453661855815, 0.00973453661855815, 0.00973453661855815]),
    'dH+/dt': lambda t: 0.00973453661855815* np.ones_like(t),
    'C0': 0.0536557,
    'FF': np.array([0.0536557, 0.0502805, 0.0481812, 0.0476235, 0.0463626, 0.0445180, 0.0443643]),
}
# exp177
exp['exp177'] = {
    'T': 413,  # K
    'Time': np.array([0, 3600, 7200, 10800, 14400, 18000, 21600]),
    'H+': np.array([0.0137815857064403, 0.0137815857064403, 0.0137815857064403, 0.0137815857064403, 0.0137815857064403, 0.0137815857064403, 0.0137815857064403]),
    'dH+/dt': lambda t: 0.0137815857064403* np.ones_like(t),
    'C0': 0.0538830,
    'FF': np.array([0.0538830, 0.0517252, 0.0504765, 0.0488335, 0.0478910, 0.0463099, 0.0453202]),
}
# exp175
exp['exp175'] = {
    'T': 413,  # K
    'Time': np.array([0, 3600, 7200, 10800, 14400, 18000, 21600]),
    'H+': np.array([0.0195049911630922, 0.0195049911630922, 0.0195049911630922, 0.0195049911630922, 0.0195049911630922, 0.0195049911630922, 0.0195049911630922]),
    'dH+/dt': lambda t: 0.0195049911630922* np.ones_like(t),
    'C0': 0.0555927,
    'FF': np.array([0.0555927, 0.0534714, 0.0525069, 0.0519274, 0.0508806, 0.0497562, 0.0482107]),
}
# exp174
exp['exp174'] = {
    'T': 443,  # K
    'Time': np.array([0, 600, 1200, 1800, 2400, 3000, 3600]),
    'H+': np.array([0.00787273281446994, 0.00787273281446994, 0.00787273281446994, 0.00787273281446994, 0.00787273281446994, 0.00787273281446994, 0.00787273281446994]),
    'dH+/dt': lambda t: 0.00787273281446994* np.ones_like(t),
    'C0': 0.0526842,
    'FF': np.array([0.0526842, 0.0501859, 0.0496206, 0.0489213, 0.0487729, 0.0484019, 0.04809]),
}
#exp178
exp['exp178'] = {
    'T': 443,  # K
    'Time': np.array([0, 600, 1200, 1800, 2400, 3000, 3600]),
    'H+': np.array([0.0111434448957653, 0.0111434448957653, 0.0111434448957653, 0.0111434448957653, 0.0111434448957653, 0.0111434448957653, 0.0111434448957653]),
    'dH+/dt': lambda t:  0.0111434448957653* np.ones_like(t),
    'C0': 0.0543176,
    'FF': np.array([0.0543176, 0.0528328, 0.0523958, 0.0510797, 0.0509000, 0.0500861, 0.0495585]),
}
#exp176
exp['exp176'] = {
    'T': 443,  # K
    'Time': np.array([0, 600, 1200, 1800, 2400, 3000, 3600]),
    'H+': np.array([0.0157689375371582, 0.0157689375371582, 0.0157689375371582, 0.0157689375371582, 0.0157689375371582, 0.0157689375371582, 0.0157689375371582]),
    'dH+/dt': lambda t: 0.0157689375371582* np.ones_like(t),
    'C0': 0.0549713,
    'FF': np.array([0.0549713, 0.0537313, 0.0527128, 0.0518866, 0.0514747, 0.0508487, 0.0502610]),
}
# exp 181
exp['exp181'] = {
    'T': 473,  # K
    'Time': np.array([0, 600, 1200, 1800, 2400, 3000, 3600]),
    'H+': np.array([0.00625216210439607, 0.00625216210439607, 0.00625216210439607, 0.00625216210439607, 0.00625216210439607, 0.00625216210439607, 0.00625216210439607]),
    'dH+/dt': lambda t: 0.00625216210439607* np.ones_like(t),
    'C0': 0.0483382272081584,
    'FF': np.array([0.0483382272081584, 0.0446098626853248, 0.0425147415114017, 0.0407526085224711, 0.0390172560340836, 0.0379830817062608, 0.0377679197413918]),
}
# exp 182
exp['exp182'] = {
    'T': 473,  # K
    'Time': np.array([0, 600, 1200, 1800, 2400, 3000, 3600]),
    'H+': np.array([0.00884801795290226, 0.00884801795290226, 0.00884801795290226, 0.00884801795290226, 0.00884801795290226, 0.00884801795290226, 0.00884801795290226]),
    'dH+/dt': lambda t:  0.00884801795290226* np.ones_like(t),
    'C0': 0.049260091061275,
    'FF': np.array([0.049260091061275, 0.0462470173442997, 0.0440668930257322, 0.041803385962404, 0.0394690682223795, 0.0375157041003617, 0.036018813809655 3]),
}
# exp 183
exp['exp183'] = {
    'T': 473,  # K
    'Time': np.array([0, 600, 1200, 1800, 2400, 3000, 3600]),
    'H+': np.array([0.0125191161280647, 0.0125191161280647, 0.0125191161280647, 0.0125191161280647, 0.0125191161280647, 0.0125191161280647, 0.0125191161280647]),
    'dH+/dt': lambda t: 0.0125191161280647* np.ones_like(t),
    'C0': 0.0521756454413998,
    'FF': np.array([0.0521756454413998, 0.048989013327016, 0.0462245233202967, 0.0433949299566688, 0.0408510697666432, 0.0378413086898245, 0.0359585955991945]),
}
# exp 208
exp['exp208'] = {
    'T': 413,  # K
    'Time': np.array([0, 3600, 7200, 10800, 14400, 18000, 21600]),
    'H+': np.array([0.0137815857064403, 0.0137815857064403, 0.0137815857064403, 0.0137815857064403, 0.0137815857064403, 0.0137815857064403, 0.0137815857064403]),
    'dH+/dt': lambda t: 0.0137815857064403* np.ones_like(t),
    'C0': 0.1344915429,
    'FF': np.array([0.1344915429, 0.1259975504, 0.1230493805, 0.1209234637, 0.1156933238, 0.1167678325, 0.1161345994]),
}
# exp211
exp['exp211'] = {
    'T': 443,  # K
    'Time': np.array([0, 600, 1200, 1800, 2400, 3000, 3600]),
    'H+': np.array([0.0111434448957653, 0.0111434448957653, 0.0111434448957653, 0.0111434448957653, 0.0111434448957653, 0.0111434448957653, 0.0111434448957653]),
    'dH+/dt': lambda t: 0.0111434448957653* np.ones_like(t),
    'C0': 0.129286004,
    'FF': np.array([0.129286004, 0.125118128, 0.124603384, 0.121958987, 0.120850857, 0.118405889, 0.116046284]),
}
```

Appendix

```
# exp 214
exp['exp214'] = {
    'T': 473,  # K
    'Time': np.array([0, 600, 1200, 1800, 2400, 3000, 3600]),
    'H+': np.array([0.00884801795290226, 0.00884801795290226, 0.00884801795290226, 0.00884801795290226, 0.00884801795290226, 0.00884801795290226, 0.00884801795290226]),
    'dH+/dt': lambda t:  0.00884801795290226* np.ones_like(t),
    'C0': 0.133040095,
    'FF': np.array([0.133040095, 0.117496023, 0.113731490, 0.106361960, 0.099787127, 0.092201612, 0.088268080]),
}


exp_names = [
             'exp173',
             'exp174',
             'exp175',
             'exp176',
             'exp177',
             'exp178',
             'exp181',
             'exp182',
             'exp183',
             'exp208',
             'exp211',
             'exp214',
             ]

## Définition des fonctions ----------------------------------------------------------------------------------------

def system_of_equations(t, cf, k02, kh2, e02, eH2, exp_name):

    CH = exp[exp_name]['H+'][0]
    T = exp[exp_name]['T']

#    return -(k02+kh2*CH)*np.exp((-e2/R)*(1/T - 1/T_REF))*cf

    return -((k02*np.exp((-e02/R)*(1/T - 1/T_REF))) +(kh2*CH*np.exp((-eH2/R)*(1/T - 1/T_REF))))*cf

def solve_ODE(params, t, exp_name):

    try:
        parvals = params.valuesdict()
        k02, kh2, e02, eH2 = list(params[par_val] for par_val in parvals)
    except:
        k02, kh2, e02, eH2 = params

    y0 = exp[exp_name]['C0']

    return odeint(system_of_equations, y0, t, args=(k02, kh2, e02, eH2, exp_name), tfirst=True)

def fun(params):

    diff = lambda exp_name: solve_ODE(params, exp[exp_name]['Time'], exp_name).reshape(-1) - exp[exp_name]['FF']

    return np.array([ diff(exp_name) for exp_name in exp_names])


## Cycle d'estimation ----------------------------------------------------------------------------------------------

vk02 = 1e-3
vkh2 = 1e-2
ve02 = 1e4
veH2 = 1e5

params = Parameters()
params.add('K02', value=vk02, min=0, max=1e-2)
params.add('KH2', value=vkh2, min=1e-6, max=4.8e-2)
params.add('E02', value=ve02, min=50e3, max=100e3)
params.add('EH2', value=veH2, min=100e3, max=129.5e3)


res1 = minimize(fun, params, method ='nelder')
print(fit_report(res1))

```

Appendix

Model 1

```python
from handle import *  ## module personnalisé créé pour une gestion agréable de tous les fichiers
from lmfit import minimize, Parameters, fit_report
import matplotlib.pyplot as plt
import numpy as np
from os import walk
from scipy.integrate import odeint
from time import time

path = '../Data/model_1' ## le chemin d'accès au dossier Data

T_REF = 443
R = 8.314
k02 = 2.8986e-05 #s^-1
kH2 = 2.7213e-04 #L mol^-1 s^-1
E02 = 65170.6917 # mJ Kmol^-1
EH2 = 129500.000 # mJ Kmol^-1

## Rassembler tous les fichiers expérimentaux ----------------------------------------------------------------------------------

exp = {}

exp_names = list(walk(path + '/'))[0][2] ## enregistrer tous les noms d'exp dans le dossier Data
exp_names = [name.split('.')[0] for name in exp_names] ## reformater pour se débarrasser de l'extension

exp = load_and_format(path, exp_names) ## charger tous les fichiers avec leurs données

## Définition des fonctions ----------------------------------------------------------------------------------

def system_of_equations(t, y, k01, k03, kH1, kH3, E1, E3, exp_name):

    CH = exp[exp_name]['H+'][0]
    T = exp[exp_name]['T'][0]

    Cx, Cf = y

    c1 = (k01+kH1*CH)*np.exp((-E1/R)*(1/T - 1/T_REF))
    c2 = (k02*np.exp((-E02/R)*(1/T - 1/T_REF))) +(kH2*CH*np.exp((-EH2/R)*(1/T - 1/T_REF)))
    c3 = (k03+kH3*CH)*np.exp((-E3/R)*(1/T - 1/T_REF))

    return -c1*Cx-c3*Cx, c1*Cx-c2*Cf

def solve_ODE(params, t, exp_name):

    parvals = params.valuesdict()
    k01, k03, kH1, kH3, E1, E3 = list(params[par_val] for par_val in parvals)

    y0 = exp[exp_name]['CxCF'][0, :]  ## initial condition

    return odeint(system_of_equations, y0, t, args=(k01, k03, kH1, kH3, E1, E3, exp_name), tfirst=True)

def fun(params):

    diff = lambda exp_name: solve_ODE(params, exp[exp_name]['Time'], exp_name) - exp[exp_name]['CxCF']

    return np.array([ diff(exp_name) for exp_name in exp_names])

## Cycle d'estimation ----------------------------------------------------------------------------------

vk01 = 1e-4
vk03 = 1e-4
vkh1 = 1e-2
vkh3 = 1e-2
ve1 = 150000.
ve3 = 150000.

params = Parameters()
params.add('K01', value=vk01, min=1e-5, max=0.001)
params.add('K03', value=vk03, min=1e-5, max=0.001)
params.add('KH1', value=vkh1, min=1e-4, max=1)
params.add('KH3', value=vkh3, min=1e-4, max=1)
params.add('E1', value=ve1, min=100e3, max=250e3)
params.add('E3', value=ve3, min=190e3, max=250e3)


res1 = minimize(fun, params, method='nelder') # https://lmfit.github.io/lmfit-py/fitting.html

print(fit_report(res1))

```

Appendix

Model 2

```python
from handle import *  ## module personnalisé créé pour une gestion agréable de tous les fichiers
from lmfit import minimize, Parameters, fit_report
import matplotlib.pyplot as plt
import numpy as np
from os import walk
from scipy.integrate import odeint
from time import monotonic
import sys

path = '../Data/model_2' ## le chemin d'accès au dossier Data

T_REF = 443
R = 8.314 #J/mol K
k02 = 2.8986e-05 #s^-1
kH2 = 2.7213e-04 #L mol^-1 s^-1
E02 = 65170.6917 # mJ Kmol^-1
EH2 = 129500.000 # mJ Kmol^-1

## Rassembler tous les fichiers expérimentaux ----------------------------------------------------------------------------------

exp = {}

exp_names = list(walk(path + '/'))[0][2] ## enregistrer tous les noms d'exp dans le dossier Data
exp_names = [name.split('.')[0] for name in exp_names] ## reformater pour se débarrasser de l'extension

exp = load_and_format(path, exp_names) ## charger tous les fichiers avec leurs données

## Définition des fonctions ----------------------------------------------------------------------------------

def system_of_equations(t, y, k01, k04, kH1, kH4, E1, E4, exp_name):

    CH = exp[exp_name]['H+'][0]
    T = exp[exp_name]['T'][0]

    Cx, Cf = y

    c1 = (k01+kH1*CH)*np.exp((-E1/R)*(1/T - 1/T_REF))

    c2 = (k02*np.exp((-E02/R)*(1/T - 1/T_REF))) +(kH2*CH*np.exp((-EH2/R)*(1/T - 1/T_REF)))
    c4 = (k04+kH4*CH)*np.exp((-E4/R)*(1/T - 1/T_REF))

    return -c1*Cx-c4*Cx*Cf, c1*Cx-c4*Cx*Cf-c2*Cf

def solve_ODE(params, t, exp_name):

    parvals = params.valuesdict()
    k01, k04, kH1, kH4, E1, E4 = list(params[par_val] for par_val in parvals)

    y0 = exp[exp_name]['CxCF'][0, :]  ## initial condition

    return odeint(system_of_equations, y0, t, args=(k01, k04, kH1, kH4, E1, E4, exp_name), tfirst=True)

def fun(params):

    diff = lambda exp_name: solve_ODE(params, exp[exp_name]['Time'], exp_name) - exp[exp_name]['CxCF']

    return np.array([ diff(exp_name) for exp_name in exp_names])

## Cycle d'estimation ----------------------------------------------------------------------------------

vk01 = 1e-3
vk04 = 1e-3
vkh1 = 1e-2
vkh4 = 1e-4  #ancienne valeur 1e-3
ve1 = 160000
ve4 = 160000

params = Parameters()
params.add('K01', value=vk01, min=1e-6, max=1e-2)
params.add('K04', value=vk04, min=1e-6, max=1e-2)
params.add('KH1', value=vkh1, min=1e-4, max=1e-1)
params.add('KH4', value=vkh4, min=1e-4, max=1e-2)
params.add('E1', value=ve1, min=100e3, max=250e3)
params.add('E4', value=ve4, min=100e3, max=250e3)

start = monotonic()

res1 = minimize(fun, params, method='nelder') # https://lmfit.github.io/lmfit-py/fitting.html

print(f'Total time: {monotonic() - start}')
print(fit_report(res1))

```

Appendix

Model 3

```python
from handle import *  ## module personnalisé créé pour une gestion agréable de tous les fichiers
from lmfit import minimize, Parameters, fit_report
import matplotlib.pyplot as plt
import numpy as np
from os import walk
from scipy.integrate import odeint
from scipy.interpolate import interp1d
from time import monotonic
import sys

path = 'Data/model_3' ## le chemin d'accès au dossier Data

T_REF = 443 #K
R = 8.314 #mJ Kmol^-1 K^-1
k02 = 2.8986e-05 #s^-1
kH2 = 2.7213e-04 #L mol^-1 s^-1
E02 = 65170.6917 # mJ Kmol^-1
EH2 = 129500.000 # mJ Kmol^-1

## Rassembler tous les fichiers expérimentaux ----------------------------------------------------------------------------

exp = {}

exp_names = list(walk(path + '/'))[0][2] ## enregistrer tous les noms d'exp dans le dossier Data
exp_names = [name.split('.')[0] for name in exp_names] ## reformater pour se débarrasser de l'extension

exp = load_and_format(path, exp_names) ## charger tous les fichiers avec leurs données

## Définition des fonctions ----------------------------------------------------------------------------------------------

def system_of_equations(t, y, k01, k03, k04, k05, kH1, kH3, kH4, kH5, E1, E3, E4, E5, exp_name):

    CH = exp[exp_name]['H+'][0] # mol L^-1
    T = exp[exp_name]['T'][0]

    Cx, Cf, CI = y

    c1 = (k01+kH1*CH)*np.exp((-E1/R)*(1/T - 1/T_REF))
    c2 = (k02*np.exp((-E02/R)*(1/T - 1/T_REF))) +(kH2*CH*np.exp((-EH2/R)*(1/T - 1/T_REF)))
    c3 = (k03+kH3*CH)*np.exp((-E3/R)*(1/T - 1/T_REF))
    c4 = (k04+kH4*CH)*np.exp((-E4/R)*(1/T - 1/T_REF))
    c5 = (k05+kH5*CH)*np.exp((-E5/R)*(1/T - 1/T_REF))

    return -(c1+c3)*Cx, c5*CI-c2*Cf-c4*CI*Cf, c1*Cx-c5*CI-c4*CI*Cf

def solve_ODE(params, t, exp_name):

    parvals = params.valuesdict()
    k01, k03, k04, k05, kH1, kH3, kH4, kH5, E1, E3, E4, E5 = list(params[par_val] for par_val in parvals)

    y0 = np.hstack((exp[exp_name]['CxCF'][0, :], exp[exp_name]['CI'][0]))## initial condition

    return odeint(system_of_equations, y0, t, args=(k01, k03, k04, k05, kH1, kH3, kH4, kH5, E1, E3, E4, E5, exp_name), tfirst=True)

def fun(params):

    diff = lambda exp_name: solve_ODE(params, exp[exp_name]['Time'], exp_name) - np.hstack((exp[exp_name]['CxCF'], exp[exp_name]['CI'].reshape(-1, 1)))

    return np.array([ diff(exp_name) for exp_name in exp_names])


## Cycle d'estimation ----------------------------------------------------------------------------------------------------

vk01 = 2e-5
vk03 = 2e-5
vk04 = 2e-2
vk05 = 2e-3
vkh1 = 0.36
vkh3 = 0.36
vkh4 = 1.5
vkh5 = 1.5
ve1 = 160000
ve3 = 160000
ve4 = 210000
ve5 = 140000

params = Parameters()
params.add('K01', value=vk01, min=0)#, max=1e-3)
params.add('K03', value=vk03, min=0)#, max=1e-2)
params.add('K04', value=vk04, min=0)#, max=1e-2)
params.add('K05', value=vk05, min=0)#, max=1e-1)
params.add('KH1', value=vkh1, min=0)#, max=1)
params.add('KH3', value=vkh3, min=0)#, max=1)
params.add('KH4', value=vkh4, min=0)#, max=1)
params.add('KH5', value=vkh5, min=0)#, max=2)
params.add('E1', value=ve1, min=100e3, max=200e3)
params.add('E3', value=ve3, min=100e3, max=200e3)
params.add('E4', value=ve4, min=200e3, max=250e3)
params.add('E5', value=ve5, min=100e3, max=200e3)

start = monotonic()

#res1 = minimize(fun, params, method=sys.argv[1]) # https://lmfit.github.io/lmfit-py/fitting.html
res1 = minimize(fun, params, method='nelder')

print(f'Total time: {monotonic() - start}')
print(fit_report(res1))

```

Appendix

Parity curve of model 1

```
from handle import *  ## module personnalisé créé pour une gestion agréable de tous les fichiers
import numpy as np
import matplotlib.pyplot as plt
from scipy.integrate import odeint
from os import walk
from textwrap import wrap
import pandas as pd

path = 'Data Model 1' ## le chemin d'accès au dossier Data

T_REF = 443 #K
R = 8.314 #J mol^-1 K^-1
k02 = 2.8986e-05 #s^-1
kH2 = 2.7213e-04 #L mol^-1 s^-1
E02 = 65170.6917 # J mol^-1
EH2 = 129500.000 # J mol^-1

## Rassembler tous les fichiers expérimentaux ----------------------------------------------------------------------------------

exp = {}

exp_names = list(walk(path + '/'))[0][2] ## enregistrer tous les noms d'exp dans le dossier Data
exp_names = [name.split('.')[0] for name in exp_names] ## reformater pour se débarrasser de l'extension

exp = load_and_format(path, exp_names) ## charger tous les fichiers avec leurs données

## Définition des fonctions ----------------------------------------------------------------------------------------------
k01 = 1.0e-05 # fix valeur 1.2164e-05
k03 = 1.0e-05 # fix valeur 1.1598e-05
kH1 = 0.10729208 # fix valeur 0.08574804
kH3 = 0.07196120 # fix valeur 0.07597053
E1 = 174427.382 # fix valeur 163948.735
E3 = 190000.0 # fix valeur 178386.982

def system_of_equations(t, y, k01, k03, kH1, kH3, E1, E3, exp_name):

    CH = exp[exp_name]['H+'][0]
    T = exp[exp_name]['T'][0]

    Cx, Cf = y

    c1 = (k01+kH1*CH)*np.exp((-E1/R)*(1/T - 1/T_REF))
    c2 = (k02*np.exp((-E02/R)*(1/T - 1/T_REF))) +(kH2*CH*np.exp((-EH2/R)*(1/T - 1/T_REF)))
    c3 = (k03+kH3*CH)*np.exp((-E3/R)*(1/T - 1/T_REF))

    return -c1*Cx-c3*Cx, c1*Cx-c2*Cf

def solve_ODE(t, exp_name):

    y0 = exp[exp_name]['CxCF'][0, :]  ## initial condition

    return odeint(system_of_equations, y0, t, args=(k01, k03, kH1, kH3, E1, E3, exp_name), tfirst=True)

exp_plot_10 = {
    '413': ['exp162', 'exp164', 'exp165', 'exp166'],
    '443': ['exp56', 'exp55', 'exp61', 'exp160'],
    '473': ['exp179', 'exp184', 'exp185', 'exp186']
}

exp_plot_30 = {
    '413': ['exp163', 'exp167', 'exp168', 'exp169'],
    '443': ['exp161', 'exp170', 'exp171', 'exp172'],
    '473': ['exp180', 'exp187', 'exp188', 'exp189']
}

exp_plots = {key: exp_plot_10[key] + exp_plot_30[key] for key in exp_plot_10.keys()}

mse_cx = []
mae_cx = []
mse_cf = []
mae_cf = []

computations_Cx = []
computations_CF = []

maxes = []

experimental_data_Cx = []
experimental_data_Cf = []
model_predictions_Cx = []
model_predictions_Cf = []

i = 0
for key in exp_plots.keys():
    prev_maxes = []
    for EXP in exp_plots[key]:
        t_1 = exp[EXP]['Time']
        computation = solve_ODE(t_1, EXP)
        computations_Cx.append(computation[:, 0])
        computations_CF.append(computation[:, 1])
```

Appendix

```
91
92          square_cx = (exp[EXP]['CxCF'][:, 0] - computations_Cx[i])**2
93          mse_cx.append( square_cx )
94          square_cf = (exp[EXP]['CxCF'][:, 1] - computations_CF[i])**2
95          mse_cf.append( square_cf )
96
97          mae_cx.append( abs(exp[EXP]['CxCF'][:, 0] - computations_Cx[i])  )
98          mae_cf.append( abs(exp[EXP]['CxCF'][:, 1] - computations_CF[i])  )
99
100         prev_maxes.append(max(computations_Cx[i]))
101         prev_maxes.append(max(computations_CF[i]))
102
103         experimental_data_Cx.append(exp[EXP]['CxCF'][:, 0])
104         experimental_data_Cf.append(exp[EXP]['CxCF'][:, 1])
105         model_predictions_Cx.append(computation[:, 0])
106         model_predictions_Cf.append(computation[:, 1])
107
108         i += 1
109
110     maxes.append(max(prev_maxes))
111
112 # Save experimental data and model predictions to Excel files
113 df_exp_Cx = pd.DataFrame(experimental_data_Cx)
114 df_exp_Cf = pd.DataFrame(experimental_data_Cf)
115 df_pred_Cx = pd.DataFrame(model_predictions_Cx)
116 df_pred_Cf = pd.DataFrame(model_predictions_Cf)
117
118 df_exp_Cx.to_excel("experimental_data_Cx.xlsx", index=False)
119 df_exp_Cf.to_excel("experimental_data_Cf.xlsx", index=False)
120 df_pred_Cx.to_excel("model_predictions_Cx.xlsx", index=False)
121 df_pred_Cf.to_excel("model_predictions_Cf.xlsx", index=False)
122
123 plt.figure(figsize=(8, 6))
124 for key in exp_plots.keys():
125     plt.plot([0, 100_000], [0, 100_000], linestyle='--', color='gray')
126     for EXP in exp_plots[key]:
127         t_1 = exp[EXP]['Time']
128         if i == 0:
129             plt.scatter(exp[EXP]['CxCF'][:, 0], computations_Cx[i],  marker='o', color='blue', label='Xylose')
130             plt.scatter(exp[EXP]['CxCF'][:, 1], computations_CF[i],  marker='s', color='orange', label='Furfural')
131         else:
132             plt.scatter(exp[EXP]['CxCF'][:, 0], computations_Cx[i],  marker='o', color='blue')
133             plt.scatter(exp[EXP]['CxCF'][:, 1], computations_CF[i],  marker='s', color='orange')
134
135         i += 1
136
137 plt.xlim(0, 1.1*max(maxes))
138 plt.ylim(0, 1.1*max(maxes))
139
140 plt.title('\n'.join(wrap(f"Parity plot of Xylose and Furfural concentrations", 60)), fontsize=15)
141 plt.xlabel("Experimental", fontsize=15)
142 plt.ylabel("Model 1", fontsize=15)
143 plt.legend()
144
145 print('Cx:')
146 print(f'RMSE: {np.sqrt(np.mean(mse_cx))}')
147 print(f'MAE: {np.mean(mae_cx)}')
148 print(f'R^2: {1 - (np.sum(mse_cx)/R2_den_cx)}')
149 print('--------------------')
150 print('Cf:')
151 print(f'RMSE: {np.sqrt(np.mean(mse_cf))}')
152 print(f'MAE: {np.mean(mae_cf)}')
153 print(f'R^2: {1 - (np.sum(mse_cf)/R2_den_cf)}')
154 print('--------------------')
155 print('Total:')
156 print(f'RMSE: {np.sqrt(np.mean([mse_cx, mse_cf]))}')
157 print(f'MAE: {np.mean([mae_cx, mae_cf])}')
158 print(f'R^2: {1 - (np.sum([mse_cx, mse_cf])/R2_den_glob)}')
159
160 plt.show()
161
```

Parity curve of model 2

```python
from handle import *  ## module personnalisé créé pour une gestion agréable de tous les fichiers
import numpy as np
import matplotlib.pyplot as plt
from scipy.integrate import odeint
from os import walk
from textwrap import wrap

path = 'Data Model 1' ## le chemin d'accès au dossier Data

T_REF = 443 #K
R = 8.314 #mJ Kmol^-1 K^-1
k02 = 2.8986e-05 #s^-1
kH2 = 2.7213e-04 #L mol^-1 s^-1
E02 = 65170.6917 # mJ Kmol^-1
EH2 = 129500.000 # mJ Kmol^-1

## Rassembler tous les fichiers expérimentaux ----------------------------------------------------------------------------------------

exp = {}

exp_names = list(walk(path + '/'))[0][2] ## enregistrer tous les noms d'exp dans le dossier Data
exp_names = [name.split('.')[0] for name in exp_names] ## reformater pour se débarrasser de l'extension

exp = load_and_format(path, exp_names) ## charger tous les fichiers avec leurs données

## Définition des fonctions ----------------------------------------------------------------------------------------
k01 = 7.1653e-04 # fix valeur 9.3392e-04
k04 = 0.00324739 # fix valeur 0.00542873
kH1 =  0.04735912 # fix valeur 0.04198121
kH4 = 1.0025e-04 # fix valeur 0.00999999
E1 =  159108.031 # fix valeur 163177.387
E4 = 132784.301 # fix valeur 163239.753

def system_of_equations(t, y, k01, k04, kH1, kH4, E1, E4, exp_name):

    CH = exp[exp_name]['H+'][0]
    T = exp[exp_name]['T'][0]

    Cx, Cf = y

    c1 = (k01+kH1*CH)*np.exp((-E1/R)*(1/T - 1/T_REF))

    c2 = (k02*np.exp((-E02/R)*(1/T - 1/T_REF))) +(kH2*CH*np.exp((-EH2/R)*(1/T - 1/T_REF)))
    c4 = (k04+kH4*CH)*np.exp((-E4/R)*(1/T - 1/T_REF))

    return -c1*Cx-c4*Cx*Cf, c1*Cx-c4*Cx*Cf-c2*Cf

def solve_ODE(t, exp_name):

    y0 = exp[exp_name]['CxCF'][0, :]  ## initial condition

    return odeint(system_of_equations, y0, t, args=(k01, k04, kH1, kH4, E1, E4, exp_name), tfirst=True)

exp_plot_10 = {'413': ['exp162', 'exp164', 'exp165', 'exp166'],
               '443': ['exp56', 'exp55', 'exp61', 'exp160'],
               '473': ['exp179', 'exp184', 'exp185', 'exp186']}

exp_plot_30 = {'413': ['exp163', 'exp167', 'exp168', 'exp169'],
               '443': ['exp161', 'exp170', 'exp171', 'exp172'],
               '473': ['exp180', 'exp187', 'exp188', 'exp189']}

exp_plots = {key: exp_plot_10[key] + exp_plot_30[key] for key in exp_plot_10.keys()}

mse_cx = []
mae_cx = []
mse_cf = []
mae_cf = []
R2_nom_cx = []
R2_den_cx = []
R2_nom_cf = []
R2_den_cf = []

computations_Cx = []
computations_CF = []

maxes = []

i = 0
for key in exp_plots.keys():
    prev_maxes = []
    for EXP in exp_plots[key]:
        t_1 = exp[EXP]['Time']
        computation = solve_ODE(t_1, EXP)
        computations_Cx.append(computation[:, 0])
        computations_CF.append(computation[:, 1])

        square_cx = (exp[EXP]['CxCF'][:, 0] - computations_Cx[i])**2
        mse_cx.append( square_cx )
        square_cf = (exp[EXP]['CxCF'][:, 1] - computations_CF[i])**2
        mse_cf.append( square_cf )

        mae_cx.append( abs(exp[EXP]['CxCF'][:, 0] - computations_Cx[i])  )
        mae_cf.append( abs(exp[EXP]['CxCF'][:, 1] - computations_CF[i])  )
```

Appendix

```
94
95          prev_maxes.append(max(computations_Cx[i]))
96          prev_maxes.append(max(computations_CF[i]))
97
98          i += 1
99
100     maxes.append(max(prev_maxes))
101
102 glob_mean_cx = np.mean([exp[EXP]['CxCF'][:, 0] for key in exp_plots.keys() for EXP in exp_plots[key]])
103 glob_mean_cf = np.mean([exp[EXP]['CxCF'][:, 1] for key in exp_plots.keys() for EXP in exp_plots[key]])
104 glob_mean = np.mean([exp[EXP]['CxCF'][:, :] for key in exp_plots.keys() for EXP in exp_plots[key]])
105
106 R2_den_cx = np.sum([(exp[EXP]['CxCF'][:, 0] - glob_mean_cx)**2 for key in exp_plots.keys() for EXP in exp_plots[key]])
107 R2_den_cf = np.sum([(exp[EXP]['CxCF'][:, 1] - glob_mean_cf)**2 for key in exp_plots.keys() for EXP in exp_plots[key]])
108 R2_den_glob = np.sum([(exp[EXP]['CxCF'][:, :] - glob_mean)**2 for key in exp_plots.keys() for EXP in exp_plots[key]])
109
110 i = 0
111 plt.figure(figsize=(8, 6))
112 for key in exp_plots.keys():
113     plt.plot([0, 100_000], [0, 100_000], linestyle='--', color='gray')
114     for EXP in exp_plots[key]:
115         t_1 = exp[EXP]['Time']
116         if i == 0:
117             plt.scatter(exp[EXP]['CxCF'][:, 0], computations_Cx[i],  marker='o', color='blue', label='Xylose')
118             plt.scatter(exp[EXP]['CxCF'][:, 1], computations_CF[i],  marker='s', color='orange', label='Furfural')
119         else:
120             plt.scatter(exp[EXP]['CxCF'][:, 0], computations_Cx[i],  marker='o', color='blue')
121             plt.scatter(exp[EXP]['CxCF'][:, 1], computations_CF[i],  marker='s', color='orange')
122
123         i += 1
124
125 plt.xlim(0, 1.1*max(maxes))
126 plt.ylim(0, 1.1*max(maxes))
127
128 plt.title('\n'.join(wrap(f"Parity plot of Xylose and Furfural concentrations", 60)), fontsize=15)
129 plt.xlabel("Experimental", fontsize=15)
130 plt.ylabel("Model 2", fontsize=15)
131 plt.legend()
132
133 print('Cx:')
134 print(f'RMSE: {np.sqrt(np.mean(mse_cx))}')
135 print(f'MAE: {np.mean(mae_cx)}')
136 print(f'R^2: {1 - (np.sum(mse_cx)/R2_den_cx)}')
137 print('--------------------')
138 print('Cf:')
139 print(f'RMSE: {np.sqrt(np.mean(mse_cf))}')
140 print(f'MAE: {np.mean(mae_cf)}')
141 print(f'R^2: {1 - (np.sum(mse_cf)/R2_den_cf)}')
142 print('--------------------')
143 print('Total:')
144 print(f'RMSE: {np.sqrt(np.mean([mse_cx, mse_cf]))}')
145 print(f'MAE: {np.mean([mae_cx, mae_cf])}')
146 print(f'R^2: {1 - (np.sum([mse_cx, mse_cf])/R2_den_glob)}')
147
148
149 plt.show()
150
```

Parity curve of model 3

```python
from handle import *  ## module personnalisé créé pour une gestion agréable de tous les fichiers
import numpy as np
import matplotlib.pyplot as plt
from scipy.integrate import odeint
from os import walk
from textwrap import wrap

path = 'Data' ## le chemin d'accès au dossier Data

T_REF = 443 #K
R = 8.314 #J mol^-1 K^-1
k02 = 2.8986e-05 #s^-1
kH2 = 2.7213e-04 #L mol^-1 s^-1
E02 = 65170.6917 # J mol^-1
EH2 = 129500.000 # J mol^-1

## Rassembler tous les fichiers expérimentaux ----------------------------------------------------------------------------------

exp = {}

exp_names = list(walk(path + '/'))[0][2] ## enregistrer tous les noms d'exp dans le dossier Data
exp_names = [name.split('.')[0] for name in exp_names] ## reformater pour se débarrasser de l'extension

exp = load_and_format(path, exp_names) ## charger tous les fichiers avec leurs données

## Définition des fonctions ----------------------------------------------------------------------------------
k01 = 2.2002e-05#1.2904e-05 # fix valeur 2.4668e-05
k03 = 5.3301e-06#7.1594e-06
k04 = 8.8881e-04#7.3780e-04 # fix valeur 2.6798e-04
k05 = 1.9118e-04#0.00124622 # fix valeur 0.00272208
kH1 = 0.09731914#0.10237935 # fix valeur 0.16282247
kH3 = 0.05318912#0.07441892
kH4 = 0.52876070#0.19855546 # fix valeur 0.41338844
kH5 = 0.35759123#0.13367635 # fix valeur 1.63562028
E1 = 156037.112#160883.547 # fix valeur 168384.133
E3 = 180057.759#200057.335
E4 = 200799.902#201293.073 # fix valeur 173465.219
E5 = 170366.180#142671.168 # fix valeur 188334.356

def system_of_equations(t, y, k01, k03, k04, k05, kH1, kH3, kH4, kH5, E1, E3, E4, E5, exp_name):

    CH = exp[exp_name]['H+'][0] # mol L^-1
    T = exp[exp_name]['T'][0]

    Cx, Cf, CI = y

    c1 = (k01+kH1*CH)*np.exp((-E1/R)*(1/T - 1/T_REF))
    c2 = (k02*np.exp((-E02/R)*(1/T - 1/T_REF))) +(kH2*CH*np.exp((-EH2/R)*(1/T - 1/T_REF)))
    c3 = (k03+kH3*CH)*np.exp((-E3/R)*(1/T - 1/T_REF))
    c4 = (k04+kH4*CH)*np.exp((-E4/R)*(1/T - 1/T_REF))
    c5 = (k05+kH5*CH)*np.exp((-E5/R)*(1/T - 1/T_REF))

    return -(c1+c3)*Cx, c5*CI-c2*Cf-c4*CI*Cf, c1*Cx-c5*CI-c4*CI*Cf

def solve_ODE(t, exp_name):

    y0 = np.hstack((exp[exp_name]['CxCF'][0, :], exp[exp_name]['CI'][0]))## initial condition

    return odeint(system_of_equations, y0, t, args=(k01, k03, k04, k05, kH1, kH3, kH4, kH5, E1, E3, E4, E5, exp_name), tfirst=True)

exp_plot_10 = {'413': ['exp162', 'exp164', 'exp165', 'exp166'],
               '443': ['exp56', 'exp55', 'exp61', 'exp160'],
               '473': ['exp179', 'exp184', 'exp185', 'exp186']}

exp_plot_30 = {'413': ['exp163', 'exp167', 'exp168', 'exp169'],
               '443': ['exp161', 'exp170', 'exp171', 'exp172'],
               '473': ['exp180', 'exp187', 'exp188', 'exp189']}

exp_plots = {key: exp_plot_10[key] + exp_plot_30[key] for key in exp_plot_10.keys()}

mse_cx = []
mae_cx = []
mse_cf = []
mae_cf = []
R2_nom_cx = []
R2_den_cx = []
R2_nom_cf = []
R2_den_cf = []

computations_Cx = []
computations_CF = []

maxes = []

i = 0
for key in exp_plots.keys():
    prev_maxes = []
    for EXP in exp_plots[key]:
        t_1 = exp[EXP]['Time']
        computation = solve_ODE(t_1, EXP)
        computations_Cx.append(computation[:, 0])
        computations_CF.append(computation[:, 1])
```

Appendix

```
93
94          square_cx = (exp[EXP]['CxCF'][:, 0] - computations_Cx[i])**2
95          mse_cx.append( square_cx )
96          square_cf = (exp[EXP]['CxCF'][:, 1] - computations_CF[i])**2
97          mse_cf.append( square_cf )
98
99          mae_cx.append( abs(exp[EXP]['CxCF'][:, 0] - computations_Cx[i])  )
100         mae_cf.append( abs(exp[EXP]['CxCF'][:, 1] - computations_CF[i])  )
101
102         prev_maxes.append(max(computations_Cx[i]))
103         prev_maxes.append(max(computations_CF[i]))
104
105         i += 1
106
107     maxes.append(max(prev_maxes))
108
109 glob_mean_cx = np.mean([exp[EXP]['CxCF'][:, 0] for key in exp_plots.keys() for EXP in exp_plots[key]])
110 glob_mean_cf = np.mean([exp[EXP]['CxCF'][:, 1] for key in exp_plots.keys() for EXP in exp_plots[key]])
111 glob_mean = np.mean([exp[EXP]['CxCF'][:, :] for key in exp_plots.keys() for EXP in exp_plots[key]])
112 R2_den_cx = np.sum([(exp[EXP]['CxCF'][:, 0] - glob_mean_cx)**2 for key in exp_plots.keys() for EXP in exp_plots[key]])
113 R2_den_cf = np.sum([(exp[EXP]['CxCF'][:, 1] - glob_mean_cf)**2 for key in exp_plots.keys() for EXP in exp_plots[key]])
114 R2_den_glob = np.sum([(exp[EXP]['CxCF'][:, :] - glob_mean)**2 for key in exp_plots.keys() for EXP in exp_plots[key]])
115
116 i = 0
117 plt.figure(figsize=(8, 6))
118 for key in exp_plots.keys():
119     plt.plot([0, 100_000], [0, 100_000], linestyle='--', color='gray')
120     for EXP in exp_plots[key]:
121         t_1 = exp[EXP]['Time']
122         if i == 0:
123             plt.scatter(exp[EXP]['CxCF'][:, 0], computations_Cx[i],  marker='o', color='blue', label='Xylose')
124             plt.scatter(exp[EXP]['CxCF'][:, 1], computations_CF[i],  marker='s', color='orange', label='Furfural')
125         else:
126             plt.scatter(exp[EXP]['CxCF'][:, 0], computations_Cx[i],  marker='o', color='blue')
127             plt.scatter(exp[EXP]['CxCF'][:, 1], computations_CF[i],  marker='s', color='orange')
128
129         i += 1
130
131 plt.xlim(0, 1.1*max(maxes))
132 plt.ylim(0, 1.1*max(maxes))
133 plt.title('\n'.join(wrap(f"Parity plot of Xylose and Furfural concentrations", 60)), fontsize=15)
134 plt.xlabel("Experimental", fontsize=15)
135 plt.ylabel("Model 3", fontsize=15)
136 plt.legend()
137
138 print('Cx:')
139 print(f'RMSE: {np.sqrt(np.mean(mse_cx))}')
140 print(f'MAE: {np.mean(mae_cx)}')
141 print(f'R^2: {1 - (np.sum(mse_cx)/R2_den_cx)}')
142 print('--------------------')
143 print('Cf:')
144 print(f'RMSE: {np.sqrt(np.mean(mse_cf))}')
145 print(f'MAE: {np.mean(mae_cf)}')
146 print(f'R^2: {1 - (np.sum(mse_cf)/R2_den_cf)}')
147 print('--------------------')
148 print('Total:')
149 print(f'RMSE: {np.sqrt(np.mean([mse_cx, mse_cf]))}')
150 print(f'MAE: {np.mean([mae_cx, mae_cf])}')
151 print(f'R^2: {1 - (np.sum([mse_cx, mse_cf])/R2_den_glob)}')
152
153 plt.savefig('parity-3.png')
154 plt.show()
```

Appendix 6

Matlab code: optimization by model 3

```
function maxYfurf = objectif_modele3(tf,T,Cform_bond,Cinit,par,up_Cform)

Cform = up_Cform/(1 + Cform_bond^2);

pKa = -57.528 + 2773.9/T + 9.1232 * log(T);
CH  = -10^-pKa + sqrt( (10^-pKa)^2 + 4 * Cform * 10^-pKa );

deltat = 10;
t = transpose(0:deltat:tf);

f = @(t,C) reaction_xylose_3(C,par,T,CH);
[t,C] = ode15s(f,t,Cinit);

maxYfurf = -100 * C(length(t),3) / Cinit(1,1);

end
```

```
function dC = reaction_xylose_3(C,par,T,CH)

dC = zeros(6,1);

k01 = par.k01;
kH1 = par.kH1;
k02 = par.k02;
kH2 = par.kH2;
k03 = par.k03;
kH3 = par.kH3;
k04 = par.k04;
kH4 = par.kH4;
k05 = par.k05;
kH5 = par.kH5;
E1  = par.E1;
E02 = par.E02;
EH2 = par.EH2;
E3  = par.E3;
E4 = par.E4;
E5 = par.E5;

Tref = par.Tref;

r1 = (k01 + kH1*CH) * exp(-(E1/8.314) * ((1/T) - (1/Tref))) * C(1);
r2 = (k02 * exp(-(E02/8.314) * ((1/T) - (1/Tref))) + ...
     kH2 * exp(-(EH2/8.314) * ((1/T) - (1/Tref))) * CH) * C(3);
r3 = (k03 + kH3*CH) * exp(-(E3/8.314) * ((1/T) - (1/Tref))) * C(1);
r4 = (k04 + kH4*CH) * exp(-(E4/8.314) * ((1/T) - (1/Tref))) * C(3) * C(2);
r5 = (k05 + kH5*CH) * exp(-(E5/8.314) * ((1/T) - (1/Tref))) * C(2);

dC(1) = - r1 - r3; % Xylose
dC(2) = r1 - r5 - r4; % Intermédiaire
dC(3) = r5 - r2 - r4; % Furfural
dC(4) = r3; % Sous-p. xylose
dC(5) = r2; % Sous-p. furfural
dC(6) = 2*r4; % Sous-p. condensation

end
```

```
% Concentrations initiales [mol/l]
Cinit = zeros(6,1); % Lignes : produits, colones : conditions de concentration
Cinit(1) = 0.06667;   % Xylose (à changer)
Cinit(2) = 0;         % Intermédiaire
Cinit(3) = 0;         % Furfural
Cinit(4) = 0;         % Sous-produits xylose
Cinit(5) = 0;         % Sous-produits furfural
Cinit(6) = 0;         % Sous-produits condensation

% Volume du réacteur [l]
V = 0.150;

% Paramètres cinétiques
par.k01 = 1.2907*10^-5;          % s^-1
par.kH1 = 0.10237668;       % L.mol^-1.s^-1

par.k02 = 2.8986*10^-5;     % s^-1
par.kH2 = 2.7213*10^-4;     % L.mol^-1.s^-1

par.k03 = 7.1580*10^-6;          % s^-1
par.kH3 = 0.07441137;       % L.mol^-1.s^-1

par.k04 = 7.3922*10^-4;          % s^-1
par.kH4 = 0.19850481;       % L.mol^-1.s^-1

par.k05 = 0.00124656;          % s^-1
par.kH5 = 0.13366125;       % L.mol^-1.s^-1

par.E1 = 160880.322;        % J/mol
par.E02 = 65170.6917;       % J/mol
par.EH2 = 129500;           % J/mol
par.E3 = 200057.225;            % J/mol
par.E4 = 201279.619;            % J/mol
par.E5 = 142667.492;            % J/mol


% Température de référence [K]
par.Tref = 443;

% Visualisation du rendement en furfural en fonction de la température et
% de la concentration en acide formique

T_inf       = 413; % Limite inférieure de température [K]
T_sup       = 473; % Limite supérieure de température [K]
intervalle_T = 1; %

Cform_inf   = 0.1; % Limite inférieure de concentration en acide formique [mol/l]
Cform_sup   = 5.3; % Limite supérieure de concentration en acide formique [mol/l]
intervalle_Cform = 0.05;

[X,Y] = meshgrid(T_inf:intervalle_T:T_sup,Cform_inf:intervalle_Cform:Cform_sup);

% Temps final d'intégration [s]
tf = 50000;

% Pas de temps [s]
deltat = 10;
```

```
% Calcul des profils au cours du temps
t = transpose(0:deltat:tf);

Y_fur = zeros(length(t),1);
Z = zeros(size(X));

for i = 1:size(X,1)

    for j = 1:size(X,2)

        pKa = -57.528 + 2773.9/X(1,j) + 9.1232 * log(X(1,j));
        CH  = -10^-pKa + sqrt( (10^-pKa)^2 + 4 * Y(i,1) * 10^-pKa );

        f = @(t,C) reaction_xylose_3(C,par,X(1,j),CH);
        [t,C] = ode15s(f,t,Cinit(:,1));

        % Rendement en furfural [%]
        Y_fur = 100 .* C(:,3) / Cinit(1,1);

        % Rendement maximum
        Z(i,j) = max(Y_fur);

        % % Trouver le temps correspondant au rendement maximum
        % idx_max = find(Y_fur == max(Y_fur));
        % t_max = t(idx_max);
        %
        % % Afficher le temps correspondant au rendement maximum
        % fprintf('Pour T=%d K, Cform=%0.2f mol/L, Y_fur max atteint à t=%d s\n', X(i,j), Y(i,1), t_max);

    end

end

surf(X,Y,Z)
title 'Rendement en furfural ([Xylose] = 30 g/L)'
xlabel('Temperature [K]')
ylabel('Concentration acide formique [mol/l]')
zlabel('Rendement en furfural [%]')
colorbar
```

RÉPUBLIQUE FRANÇAISE
Liberté
Égalité
Fraternité

Université de Toulouse

Titre : Étude d'un procédé durable de production de furfural à partir des résidus hémicellulosiques issus de la biomasse

Mots clés : Biomasse, Furfural, Membrane, Procédé durable, Réacteur, Catalyse

Résumé : Avec l'épuisement des réserves fossiles et les préoccupations environnementales, l'utilisation de la biomasse lignocellulosique renouvelable apparaît comme une voie prometteuse pour la production de produits chimiques non dérivés du pétrole. L'un de ces produits chimiques intéressants est le furfural, qui constitue un substitut viable aux biocarburants et aux additifs. Le furfural peut être généré efficacement par la déshydratation acide des sucres C5 présents dans les hémicelluloses des biomass lignocellulosiques. L'objectif principal de cette étude est de développer un procédé durable de conversion des sucres C5, présents dans les hydrolysats de la biomasse (via le procédé LEEBioTM), en furfural en utilisant l'acide formique comme catalyseur. L'acide formique est très prometteur en raison de sa double fonctionnalité : il sert à la fois de solvant dans l'hydrolyse de la biomasse, produisant des hydrolysats riches en sucre, et de catalyseur efficace pour la déshydratation des sucres C5 en furfural. L'étude a examiné l'impact de divers paramètres opératoires sur la production de furfural, afin d'identifier les conditions optimales par le biais d'expériences en système discontinu utilisant des solutions synthétiques. Trois méthodes d'extraction - stripping à la vapeur, solvants organiques dans le système biphasiques et extraction au dioxyde de carbone supercritique (Sc-CO2) - ont été exploitées pour extraire le furfural du milieu réactionnel, empêchant ainsi sa dégradation et améliorant à la fois le rendement et la sélectivité. Ces procédés d'extraction ont facilité la récupération de tout le furfural produit dans l'extrait, tout en minimisant les concentrations de xylose et de furfural dans le réacteur. En outre, le potentiel de l'acide formique en tant que solvant de fractionnement et catalyseur pour la conversion des sucres C5 en furfural a été exploré en utilisant des hydrolysats obtenus à partir du fractionnement de la biomasse via le procédé LEEBioTM. Dans des conditions optimisées, les rendements en furfural obtenus à partir d'hydrolysats de biomasse réelle ont dépassé ceux rapportés dans la littérature pour tous les systèmes étudiés. De plus, un modèle cinétique a été mis au point pour fournir des informations détaillées sur la conversion des sucres C5 en furfural catalysée par l'acide formique. Ce modèle s'est avéré très précis, prédisant les rendements maximaux réalisables avec une précision de plus de 90 %. Cependant, la présence de composés supplémentaires, tels que des éléments inorganiques et des sucres hexosés, a affecté la précision du modèle. Néanmoins, le modèle est resté applicable pour optimiser la production de furfural à partir de matières premières telles que les xylanes et les hydrolysats de biomasse réels.

Title: Study of a green process for the production of furfural from hemicellulosic residues of biomass

Key words: Biomass, Green process, Furfural, Reactor, Catalysis, Membrane

Abstract: Along with the depletion of fossil reserves and environmental concerns, the utilization of renewable lignocellulosic biomass stands out as a promising avenue for the production of non-petroleum-derived chemicals. One such chemical of interest is furfural, which serves as a viable substitute for biofuels and additives. Furfural can be efficiently generated through the acid dehydration of C5 sugars found in hemicelluloses within lignocellulosic materials. The primary objective of this study is to develop a sustainable process for converting C5 sugars, present in hydrolysates from biomass hydrolysis (via the LEEBioTM process), into furfural using formic acid as a catalyst. Formic acid exhibits considerable promise due to its dual functionality: serving as both a solvent in biomass hydrolysis, yielding sugar-rich hydrolysates, and as an effective catalyst for the dehydration of C5 sugars into furfural. The study investigated the impact of various operating parameters on furfural production, aiming to identify optimal conditions through batch system experiments utilizing synthetic solutions. Three extraction methods - steam stripping, biphasic organic solvent systems, and supercritical carbon dioxide (Sc-CO2) extraction - were employed to extract furfural from the reaction medium, thereby preventing furfural degradation and enhancing both yield and selectivity. These extraction processes facilitated the recovery of all produced furfural in the extract, while minimizing concentrations of xylose and furfural in the reactor. Furthermore, the potential of formic acid as a fractionation solvent and catalyst for the conversion of C5 sugars into furfural was explored using hydrolysates obtained from biomass fractionation via the LEEBioTM process. Under optimized conditions, furfural yields from real biomass hydrolysates surpassed those reported in the literature for all investigated systems. Additionally, a kinetic model was developed to offer detailed insights into the conversion of C5 sugars into furfural catalyzed by formic acid. This model proved highly accurate, predicting maximum achievable yields with over 90% precision. However, the presence of additional compounds, such as inorganic elements and hexose sugars, did affect the model's accuracy. Nonetheless, the model remained instrumental in optimizing furfural production from raw materials like xylans and real biomass hydrolysates.